TECTONIC CONTROLS ON ALLUVIAL ARCHITECTURE IN THE UPPER CRETACEOUS JOHN HENRY MEMBER, STRAIGHT CLIFFS FORMATION, SOUTHERN UTAH

by

Luke Andrew Pettinga

A thesis submitted to the faculty of
The University of Utah
in partial fulfillment of the requirements for the degree of

Master of Science

in

Geology

Department of Geology and Geophysics

The University of Utah

May 2013

Copyright © Luke Andrew Pettinga 2013

All Rights Reserved

The University of Utah Graduate School

STATEMENT OF THESIS APPROVAL

The thesis of **Luke Andrew Pettinga**

has been approved by the following supervisory committee members:

Cari L. Johnson	, Chair	**11/15/2012** Date Approved
Lauren P. Birgenheier	, Member	**11/19/2012** Date Approved
Lisa E. Stright	, Member	**11/16/2012** Date Approved

and by **D. Kip Solomon** , Chair of

the Department of **Geology and Geophysics**

and by Donna M. White, Interim Dean of The Graduate School.

ABSTRACT

A detailed understanding of spatial and temporal changes in alluvial architecture is essential in deciphering the mechanisms controlling stratigraphic trends, and their relative influence throughout a sedimentary basin. In this study, nonmarine exposures of the John Henry Member (Upper Cretaceous Straight Cliffs Formation) are characterized by measured stratigraphic sections, paleocurrent measurements, lateral facies mapping, and channel belt dimension measurements along a three km wide by ~200 m tall outcrop in Bull Canyon of the southwest Kaiparowits Plateau, Utah. Seven depositional units (DU) are interpreted, which define intervals with distinct alluvial architecture. The DUs are grouped into three stratigraphic intervals, each of which represents a large-scale trend in alluvial architecture. The lower stratigraphic interval includes a trend of upward decreasing grain size and channel belt width, thickness, and amalgamation, with isolated tidal influence. The middle stratigraphic interval is composed of consistently thick floodplain and coal mire deposits with laterally restricted channel belts. The upper stratigraphic interval includes vertical trends of increasing grain size, channel belt widths and amalgamation.

These data are combined with previously published sections to produce a ~60 km long, dip-oriented correlation of the stratigraphic intervals, which is used to investigate variability within the depositional system. Paleomorphodynamic parameters are calculated from measurements made in fluvial strata at Bull Canyon and Rock House

Cove, located ~20 km to the west (paleo-landward). The regional stratigraphy and paleomorphodynamic parameters indicate that the impact of tectonic activity is the primary driver of preserved alluvial architecture. Although some effect of sea level change, climate, and fluvial autogenic processes may be identifiable, they exert lower order control on the preserved system. In the proposed depositional model, changes in alluvial architecture represent the dynamic responses of fluvial fan systems (or distributive fluvial systems) to changes in accommodation and sediment supply resulting from episodic tectonic activity. This study contributes to the evolving paradigm that is transiting from an emphasis on downstream controls on fluvial systems (i.e., accommodation due to relative sea level changes) to more accurately account for hinterland controls (i.e., the interaction of accommodation and sediment supply due factors such as tectonic activity). These concepts are more broadly applicable to the understanding of depositional cyclicity in terrestrial (fluvial) deposits and are particularly relevant to foreland basin systems, which are common in the Cretaceous strata of western North America.

TABLE OF CONTENTS

ABSTRACT iii

ACKNOWLEDGEMENTS vii

INTRODUCTION 1

REGIONAL GEOLOGY 4

- Tectonic and Paleogeographic Setting 4
- Stratigraphy 5
- Genetic Stratigraphy 6

RESEARCH GOALS 22

METHODS 24

DESCRIPTIVE CLASSIFICATION SCHEME 45

- Fluvial Terminology 45
- Channel Classification 46
- Descriptive Hierarchy 46

RESULTS 54

- Lithofacies 54
- Facies Associations 55
- Channel Belt Dimensions and Stacking Patterns 61
- Depositional Units and Bounding Members 63
- Paleomorphodynamics 76
- Sedimentary Petrology 81

INTERPRETATION AND DISCUSSION 130

- Stratigraphic Intervals 130
- Correlation of Fluvial to Paralic Facies 132
- Relationship Between Fluvial Architecture and Shoreline Successions 134
- Controls on Fluvial Sequences 136

Depositional Model 139

CONCLUSIONS 160

APPENDICES

A. MEASURED STRATIGRAPHIC SECTIONS 163

B. INTERPRETED PHOTOMOSAICS 188

C. PALEOCURRENT AND ACCRETION DATA 216

D. PALEOMORPHODYNAMIC SPREADSHEET 242

E. SAMPLES LIST 243

F. PETROGRAPHIC DATA 246

G. GPS DATASET 248

REFERENCES 278

ACKNOWLEDGEMENTS

I would like to express gratitude to my advisor, Dr. Cari Johnson, for guidance throughout this project. Thanks to Dr. Lisa Stright and Dr. Lauren Birgenheier for agreeing to participate as members of my thesis committee. Thanks to everyone who assisted me in the field: Patrick Dooling, Ian Semple, Alex Turner, Tyler Szwarc, and Brenton Chentnik. This project was made possible by funding through donors to the American Chemical Society - Petroleum Research Fund (grant to Cari Johnson), and support through University of Utah Rocks to Models research group from Chevron, ConocoPhillips, Hess, Shell, and Statoil. Thanks to ConocoPhillips for providing a research fellowship for my studies. Thanks to the Bureau of Land Management and Grand Staircase-Escalante National Monument for granting me permission to conduct research on federal land. I am extremely grateful to all of my family, friends, and colleagues who have helped support and guide me through this process.

INTRODUCTION

Knowledge of the spatial and temporal changes in terrigenous-clastic deposits within foreland basin systems can yield insight into the mechanisms controlling deposition (Paola et al., 1992; Dreyer et al., 1993; Blum and Törnqvist, 2000; Holbrook et al., 2006) and has implications for subsurface reservoir characterization (Tye, 2004; Pranter and Sommer, 2011). Alluvial architecture can be influenced by autogenic controls, like avulsion, progradation, and scouring (Mackey and Bridge, 1995; Sheets et al., 2007; Hajek et al., 2010), and allogenic controls, such as relative sea level, climate, hinterland tectonics, and basin subsidence (Fisk, 1944; Ouchi, 1985; Shanley and McCabe, 1994; Holbrook, 2006; Hampson et al., 2012). Large-scale alluvial architecture is the product of some combination of autogenic and allogenic controls, and their complex interaction. Many of the current predictive models of alluvial architecture and geometry focus on variations in downstream base level (commonly sea level) as the primary allogeneic control (Shanley and McCabe, 1993; Wright and Marriott, 1993; Richards, 1996; Currie, 1997; van Heijst and Postma, 2001). These models likely have relevance in the lower reaches of fluvial systems, but do not account for variations in allogenic controls that may exist within a basin (Slingerland and Snow, 1988; Mackey and Bridge, 1995; Blum and Törnqvist, 2000; Bridge, 2003; Holbrook et al., 2006). Sedimentary cycles present in the upper reaches of fluvial systems are more likely to be influenced by factors such as tectonics, climate, and autogenic processes than

downstream base level (Olsen et al., 1995, Legarreta and Uliana, 1998; Kjemperud et al., 2008; Hampson et al., 2012). Quantitative modeling and studies of modern and recent (Pleistocene) fluvial deposits have emphasized some of the complexity within the interaction of upstream and downstream controls (Blum and Aslan, 2006; Martin et al., 2010; Gibling et al., 2011). The datasets from numerous large-scale, outcrop-based studies are required to account for the spatial variability of these controls on fluvial systems preserved in the sedimentary record; however, relatively few studies of this scope exist (Hirst, 1991; Dreyer et al., 1993; Shanley & McCabe, 1993; Burns et al., 1997; Currie, 1997; Holbrook et al., 2006; Corbett et al., 2011; Hampson et al., 2012). This study incorporates what we are beginning to understand about the modern depositional systems in order to re-evaluate the ancient; specifically, how fluvial depositional models should be revised.

The John Henry Member of the Straight Cliffs Formation contains one of several cyclical stratigraphic sequences present within the Upper Cretaceous strata of the Kaiparowits Plateau, southern Utah (Peterson, 1969a; Ryer, 1993). The John Henry Member in this area is particularly well suited for a detailed study of alluvial architecture and basin scale controlling mechanisms because of nearly continuous exposures from fluvial strata in the west to marginal marine strata in the east. A commonly cited predictive model of alluvial architecture was based on sequence stratigraphic interpretations of outcrops of the John Henry Member (Shanley, 1991; Shanley and McCabe, 1991, 1993). This model focuses on downstream relative sea level controls on deposition. Some aspects of these interpretations have been called into question by several more recent studies (Little, 1995; Gallin et al., 2010; Gooley, 2010; Allen and

Johnson, 2011). In order to resolve the primary controls on alluvial architecture, the spatial and temporal variability present within the John Henry Member must be better understood.

This study builds on previous research in advancing toward a comprehensive understanding of the relationship between coeval fluvial and marginal marine strata, and the mechanisms that controlled deposition within the Kaiparowits Basin. The specific goals of this study are to investigate primary controls in deposition by documenting the alluvial architecture and paleomorphodynamic characteristics in a previously unstudied exposure of the John Henry Member, creating a dip oriented correlation from fluvial to marine strata, and refining the depositional model. The results of this study have implications for a number of terrigenous-clastic depositional systems including analogous foreland basin and passive margin systems.

REGIONAL GEOLOGY

Tectonic and Paleogeographic Setting

The Kaiparowits Plateau of southern Utah contains expansive exposures of the Upper Cretaceous Straight Cliffs Formation (Figure 1). Located near the western margin of the Colorado Plateau physiographic province, the plateau is bounded by the Escalante River valley to the east, erosional features of the Colorado River to the south, and the Cockscomb (the physiographic expression of the East Kaibab Monocline) to the west. The strata of the plateau dip gently to the north and are locally deformed by a series of north-south trending anticlines, synclines, and normal faults (Peterson, 1969a; Doelling et al., 2000).

In the Late Cretaceous, isostatic adjustment due to the east-west shortening along the Sevier orogenic belt and dynamic subsidence associated with subduction of the Farallan plate led to the development of a foreland basin system along the western edge of Western Interior Seaway (Figure 2) (Kauffman, 1977; Kauffman and Caldwell, 1993; DeCelles and Coogan, 2006; Liu et al., 2011). The Upper Cretaceous strata of the Kaiparowits Plateau are composed of siliciclastic sediments that were transported eastward from the Sevier orogenic belt and northeastward from the Mogollon Highlands (Peterson, 1969a, 1969b; Eaton, 1991; Hettinger et al., 1993; Lawton et al., 2003). The paleoshoreline in this area was generally oriented northwest-southeast, and paleocurrent

indicators and facies transitions indicate that the fluvial systems mainly flowed to the east-northeast (Peterson, 1969a; Ryer, 1977, 1993; Bobb, 1991; Shanley and McCabe, 1991, 1995; Roberts and Kirschbaum, 1995; Christensen, 2002; Lawton et al., 2003).

Stratigraphy

Gregory and Moore (1931) conducted an initial geologic investigation of the Kaiparowits Plateau. These authors identified a thick, sandstone dominated section overlying the Tropic Shale, which they named the Straight Cliffs Sandstone after the large marine sandstone exposures along the Straight Cliffs escarpment (i.e., Fifty Mile Mountain) south of Escalante, Utah. Peterson and Waldrop (1965) redefined it as the Straight Cliffs Formation after finding that away from the type area it was composed of interbedded sandstone, smectitic mudstone, carbonaceous mudstone, and coal. They also proposed three informal members (Lower, Middle, and Upper).

Peterson (1969a, 1969b) conducted the first detailed stratigraphic correlation of the Straight Cliffs Formation on the Kaiparowits Plateau. This work along the southern margin of the plateau led to the division of the formation into four members that were formally named, in ascending order: Tibbet Canyon, Smoky Hollow, John Henry, and Drip Tank (Peterson, 1969b). Additionally, seven shoreface units, named A through G, and four coal zones, name Lower, Christenson, Rees, and Alvey, were identified within the John Henry Member (Figure 3) (Peterson, 1969a).

The John Henry Member is the thickest member of the Straight Cliffs Formation and preserves a fluvial-marine transition; with continental deposits in the southwest that grade into paralic and marine deposits to the northeast (Peterson, 1969a, 1969b). Preservation of these transitional facies makes the plateau an ideal location to investigate

the relationship between marine and terrestrial sequence stratigraphy. The John Henry Member is believed to have been deposited over ~6.2 my from the Early Coniacian to Late Santonian (89.8 to 83.6 Ma) (Eaton 1987, 1991; Eaton and Nations, 1991; Kauffman et al., 1993; Gradstein et al., 2012); however, the dates are primarily based on biozones identified within the marine strata, which are poorly constrained. The presence of the inoceramid *Volviceramus involutus* at the base of the John Henry Member indicates that deposition began in the Early Coniacian (Eaton, 1987, 1991). The upper part of the John Henry Member is assumed to be no younger than Late Santonian based on the assemblage of inoceramid bivalves and the presence of the ammonite *Desmoscaphites* (Eaton 1987, 1991; Peterson, 1969a; Kauffman et al., 1993).

A number of early studies focused on the distribution and nature of coal-bearing facies (Robison 1963, 1964, 1966; Doelling, 1967, 1968; Doelling and Graham, 1972). More recently, studies by Vaninetti (1979), Hettinger (1995, 2000), and Hettinger et al. (1996) investigated the distribution and westward thinning of coal zones in the southwestern portion of the plateau. Vaninetti (1979) investigated the relationship between fluvial channel systems and peat-forming (swamp) conditions along the southern border of the plateau. Hettinger (1995, 2000) and Hettinger et al. (1996) used outcrop, cored wells, and well logs to document the distribution of coal throughout the plateau and its relationship with shoreline facies.

Genetic Stratigraphy

Shanley (1991) and Shanley and McCabe (1991, 1993) developed the first sequence stratigraphic framework for the Straight Cliffs Formation, which included four unconformity-bound sequences. The sequence boundaries were identified by a distinct

basinward shift in facies and included (Figure 3): (1) Tibbet Canyon sequence boundary, located at the top of the Tibbet Canyon Member; (2) Calico sequence boundary, located near the top of the Smoky Hollow Member at the base of the Calico bed; (3) the "A-sequence boundary," in the lower John Henry Member near the top of the A-shoreface; and (4) Drip Tank sequence Boundary, located at the base of the Drip Tank Member.

Shanley and McCabe (1991) attempted to trace the sequence stratigraphic surfaces from marine into terrestrial strata. For example, the "A-sequence boundary" was traced from the top of the A-shoreface into fluvial strata of the lower John Henry Member, where the unconformity is represented by the transition to amalgamated sandstones of incised valley fill and overlying estuarine and tidally-influenced fluvial strata. Subsequent studies have also reported incised valley candidates, which may be associated with the "A-sequence boundary" (Hettinger et al., 1993; Stephen and Dalrymple, 2002).

Correlation of sequence stratigraphic surfaces into terrestrial deposits resulted in development of a frequently-cited sequence stratigraphic model of alluvial architecture (Figure 4a) (Shanley and McCabe, 1991, 1993, 1994, 1995). This model identifies four stages based on distinctive patterns of alluvial architecture, each of which has been tied to changes in base level: (1) early lowstand systems tract, erosion and incised valleys development during base level fall; (2) late lowstand systems tract, coarse-grained, vertically and laterally amalgamated braided fluvial channels that backfilled the valleys during slow base level rise; (3) transgressive systems tract, heterolithic strata and tidally-influenced fluvial channel-fill deposited during marine transgression; and (4) highstand

systems tract, fine-grained, isolated meandering fluvial channels in thick floodplain alluvium deposited during high rates of base level rise.

Little (1995, 1997) investigated Upper Cretaceous strata of the Kaiparowits Plateau, and speculated on the relative role of tectonic and eustatic controls in the development of the cyclical fluvial depositional patterns. Cyclicity within alluvial stratigraphy was interpreted using the concept of thrust propagation (Figure 4b), a modified version of the two-phase tectonic deposition proposed by Heller et al. (1988). In this interpretation, each cycle begins with the onset of active tectonism in the Sevier fold and thrust belt causing subsidence and highly aggradational fluvial systems with thick floodplain deposits. Subsequent decreasing tectonism, and a corresponding decrease in subsidence, allow the basin to fill, producing an upward-coarsening fluvial succession. Tectonic quiescence results in the formation of a coarse-grained sheet, which caps each cycle. These sheets develop due to the combination of denudation and isostatic rebound that cause the redistribution of the coarse sediments that had been deposited adjacent to the thrust belts during initial rapid subsidence. Little (1997) concluded that hinterland tectonics was the main factor controlling the depositional architecture with the basin, but acknowledged that eustatic sea level may have contributed to depositional cycles during the early stages of basin development, including deposition of the Straight Cliffs Formation.

Conditions typical of the early stages of foreland basin development, including low-lying sediment source area and a relatively wide and shallow basin, may have allowed eustatic sea level to influence alluvial architecture during deposition of the John Henry Member. However, in later stages of the foredeep the eustatic signal was completely overpowered by tectonic control due to continued eastward movement of the Sevier

thrust belt. Similar cyclicity in fluvial deposits has been interpreted as tectonically driven (Dreyer et al., 1993; Legarreta and Uliana, 1998; Horton and DeCelles, 2001; Weissmann et al., 2010).

Several studies have noted that the coarse clastic sheets within the Straight Cliffs Formation (Calico bed and Drip Tank Member) are conformable and interfinger with underlying strata (Peterson, 1969b; Vaninetti, 1979; Eaton, 1991; Tilton, 1991; Little, 1995; Lawton et al. 2003). However, Shanley and McCabe (1995) described the bases of these clastic sheets as sharp erosional surfaces, which were used as evidence that they represent sequence boundaries. Lawton et al. (2003) described the base of the Drip Tank Member to be a gradational contact, but still concluded that a drop in sea level caused the formation of a sequence boundary.

Allen (2009) and Allen and Johnson (2010) investigated the stratigraphy of marine deposits in the John Henry Member in Rogers Canyon. These studies advocate the use of transgressive-regressive cycles (T-R cycles) to describe the marine stratigraphic architecture. Seven T-R cycles, named 0 through 6, were identified to form three large-scale trends: net progradation in cycles 0 through 2; net retrogradation in cycles 3 through 5; and net aggradation in cycles 5 to 6 (Figure 3). Allen (2009) did not identify any sequence boundaries in this part of the plateau, but noted that the transition between the B and C sandstones records the greatest basinward shift in facies and is the best candidate for a sequence boundary.

Gallin (2010) and Gallin et al. (2010) investigated paralic facies within the John Henry Member of the south-central Kaiparowits Plateau and their correlation with marine strata to the east. Gallin (2010) identified three facies associations within the John Henry

Member, in ascending order (Figure 5b): Facies association 1 includes tidally influenced, laterally restricted fluvial channel belts, coastal mires and shoreface sandstones, which correlate with the lower, net progradational marine packages. Facies association 2 includes laterally restricted, highly sinuous fluvial channel belts, lagoonal and estuarine coastal plain mires, bay-head deltas, isolated distributary and tidal channels, which correlate with the middle, net retrogradational marine packages. Facies association 3 includes laterally extensive, low sinuosity fluvial channel belts, and vertically amalgamated fluvial channel belt complexes, and floodplain deposits, which correlate with the upper, net progradational marine packages. Gallin et al. (2010) noted the absence of an unconformable surface that would correlate with the A-sequence boundary. Rather, the section was characterized by fairly consistent vertical trends of increasing grain size, channel belt amalgamation, and downstream accretion, and a vertical trend of decreasing tidal influence.

In the southwestern corner of the Kaiparowits Plateau, Gooley (2010) divided the proximal fluvial strata of John Henry Member into seven depositional units, named DU-0 through DU-6 (Figure 5a), in ascending order: DU-0 is composed of tidally-influenced channel belts. DU-1 overlies an unconformable surface and is composed of highly amalgamated, laterally accreting channel belts with tidally-influenced channel belts in the upper section. DU-2 is composed of laterally extensive, laterally accreting channel belts. DU-3 is composed of isolated channel belts embedded within thick floodplain muds. DU-4 through DU-6 grade from laterally restricted laterally accreting channel belts with low vertical amalgamation, to highly vertically amalgamating downstream accreting channels. It is important to note that the use of the term depositional units by Gooley (2010) and the

current study is equivalent to the use of facies associations in Gallin (2010). Gooley (2010) documented two characteristic, large-scale trends within the John Henry Member: First, there is an upward decrease in grain size, decrease in channel belt frequency and lateral extent, and episodic increase in tidal influence in DU-1 through DU-3. Second, there is an upward increase in grain size, increased channel belt frequency and lateral extent, and a shift from lateral to downstream accretion in DU-3 through DU-6 and continues into the Drip Tank Member.

Additionally, Gooley (2010) correlated Rock House Cove depositional units and stratigraphic trends across the plateau, incorporating the measured sections and interpretations of previous studies (Vaninetti, 1979; Allen, 2009, Gallen, 2010). One conclusion from this work was that additional inquiry was required to adequately document the stratigraphic changes between the Rock House Cove and Kelly Grade areas. Bull Canyon, the focus of this study, is located approximately half way between these two locations.

The Straight Cliffs Formation has been used in outcrop analogue studies for subsurface reservoirs. Two studies used exposures of the lower John Henry Member in the Blue Cove area as a reservoir outcrop analog to calculate statistics and construct reservoir models (Dalrymple, 2001; Stephen and Dalrymple, 2002). Gooley (2010) evaluated the reservoir potential of nonmarine outcrops in Rock House Cove.

Figure 1 – Map of the Kaiparowits Plateau showing the locations of measured stratigraphic sections and logged cores from this study and those of relevant previous studies. The Kaiparowits Plateau is shaded in light gray. Outcrops of the members of the Straight Cliffs Formation are shown (modified from Doelling and Willis, 1999, 2006). The transect A-A'-A" marks the locations used to construct stratigraphic correlations through the plateau (Figures 37 and 38). The inset map of Utah shows the location of the Kaiparowits Plateau and the approximate locations of the Sevier orogenic belt and the Western Interior Seaway during the middle Santonian, ~85 Ma (DeCelles, 2004).

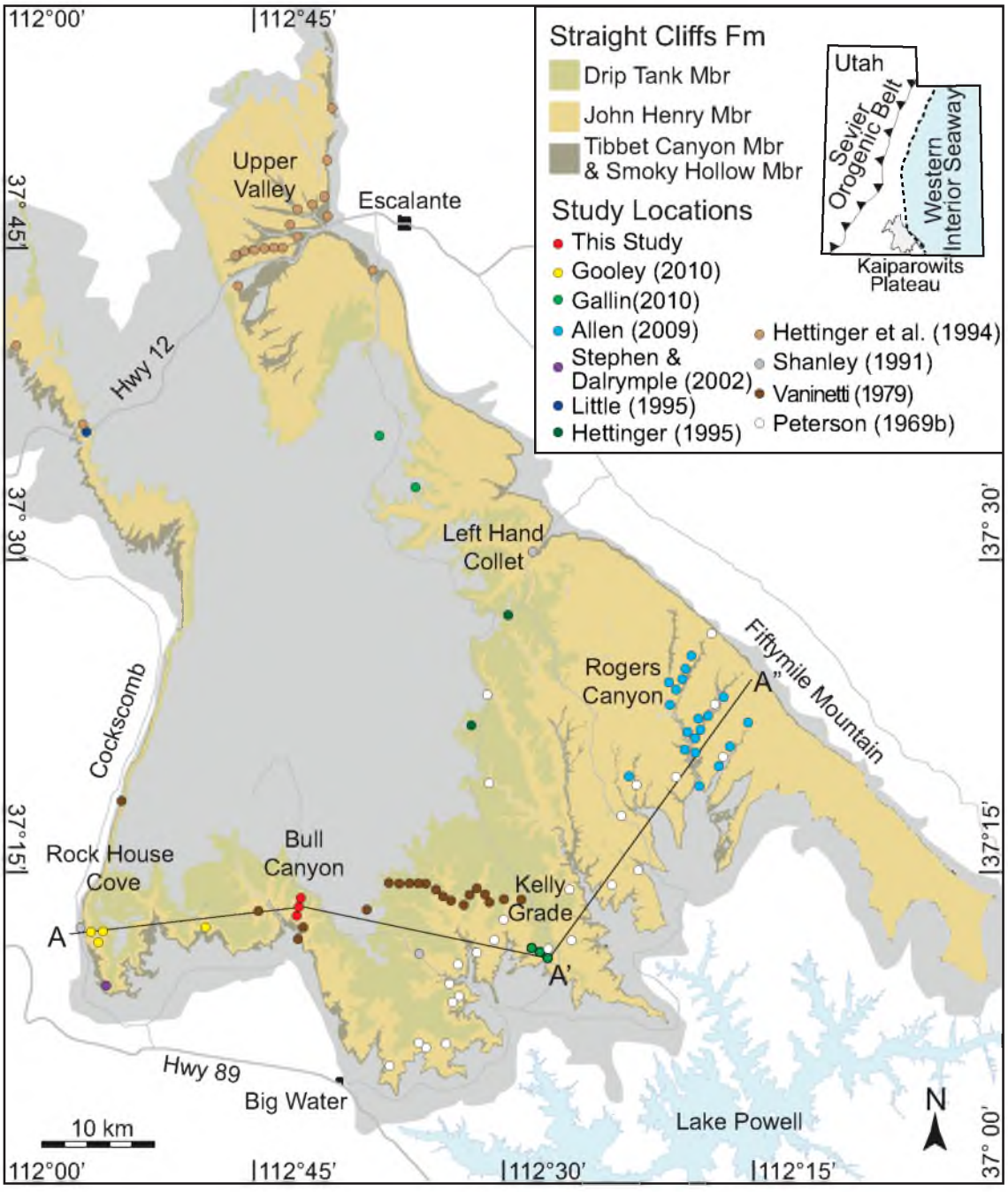
112°00'
112°45'
112°30'
112°15'
37° 45'
37° 30'
37°15'
37° 00'
Straight Cliffs Fm
Drip Tank Mbr
John Henry Mbr
Tibbet Canyon Mbr
& Smoky Hollow Mbr
Study Locations
This Study
Gooley (2010)
Gallin(2010)
Allen (2009)
Stephen &
Dalrymple (2002)
Little (1995)
Hettinger (1995)
Hettinger et al. (1994)
Shanley (1991)
Vaninetti (1979)
Peterson (1969b)
Utah
Sevier Orogenic Belt
Western Interior Seaway
Kaiparowits Plateau
Upper Valley
Escalante
Hwy 12
Left Hand Collet
Cockscomb
Fiftymile Mountain
Rogers Canyon
A"
Rock House Cove
Bull Canyon
Kelly Grade
A
A'
Hwy 89
Big Water
Lake Powell
10 km
N

Figure 2 – Paleogeography of southwestern North America in Coniacian-Santonian time (modified from Roberts and Kirschbaum, 1995). The location of Kaiparowits Plateau (KP) is outlined in black.

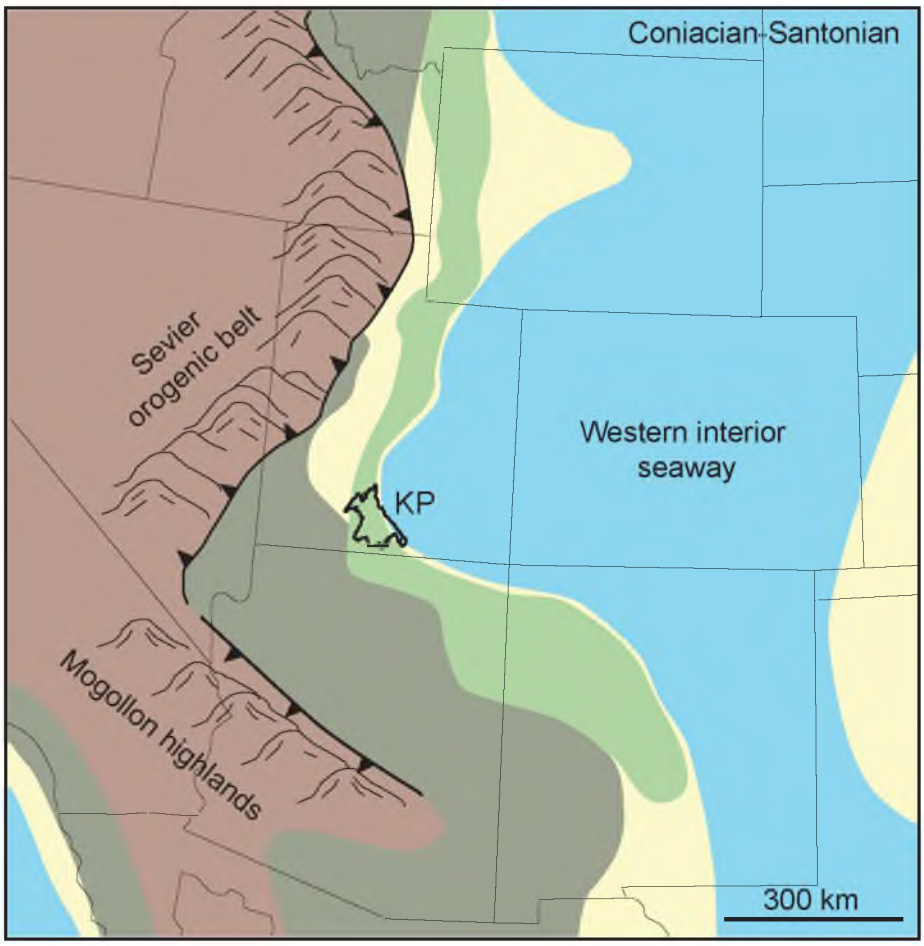
Coniacian-Santonian
Sevier orogenic belt
Western interior seaway
KP
Mogollon highlands
300 km
Highlands
Alluvial plain
Coastal plain
Mires (coal beds)
Offshore marine
Fold and thrust front

Figure 3 – Upper Cretaceous stratigraphy of south-central Utah. A) Regional stratigraphy. B) Lithostratigraphy of the Straight Cliffs Formation showing the fluvial to marginal marine strata. The coastal onlap curve of Allen and Johnson (2010) and sequence stratigraphic interpretation of Shanley and McCabe (1991) are shown alongside the lithostratigraphic divisions for locations along a SW-NE transect of the Kaiparowits Plateau: Rock House Cove (Gooley, 2010), Bull Canyon (this study), Kelly Grade (Gallin, 2010), and Rogers Canyon (Peterson, 1969b; Allen, 2009). The labels on the left side of the Rogers canyon section are the shoreface sandstone names from Peterson (1969b) and on the right are the T-R cycle labels from Allen (2009).

A. Regional Stratigraphy

B. Straight Cliffs Formation, Kaiparowits Plateau

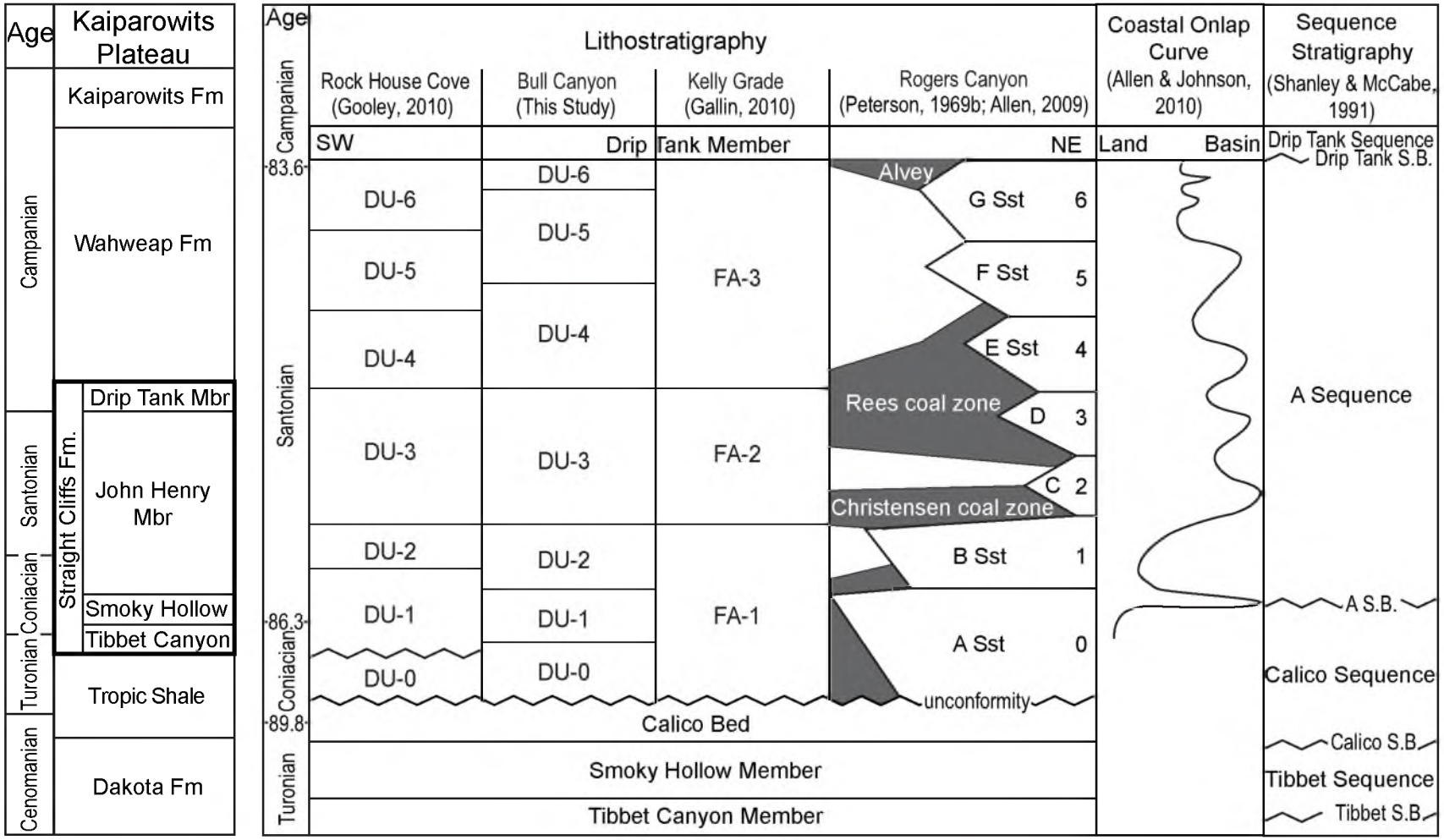

Figure 4 – Predictive models for alluvial stratigraphy. A) Eustatic model of alluvial stratigraphy (Shanley and McCabe, 1993). B) Tectonic model of alluvial stratigraphy (Little, 1997). Both models are based on observations made in Kaiparowits basin strata.

A. Eustatic Model (Shanley and McCabe, 1993)

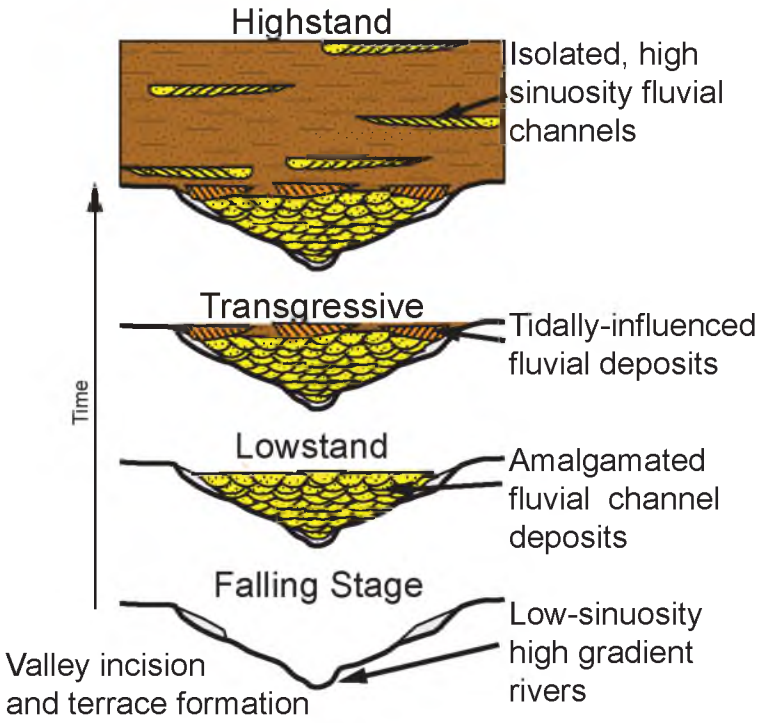

B. Tectonic Model (Little, 1997)

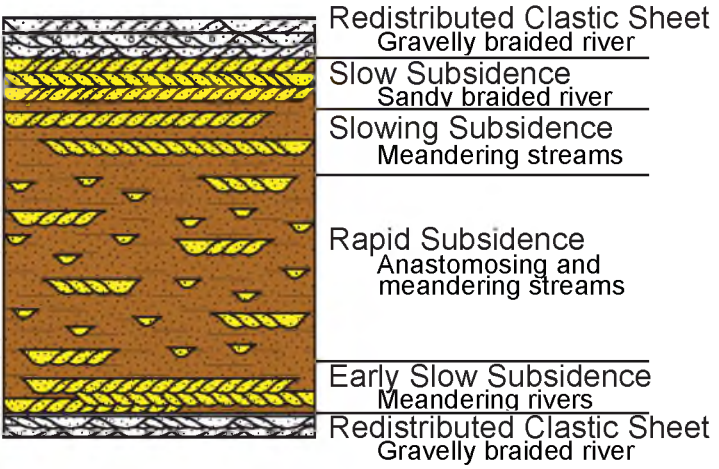

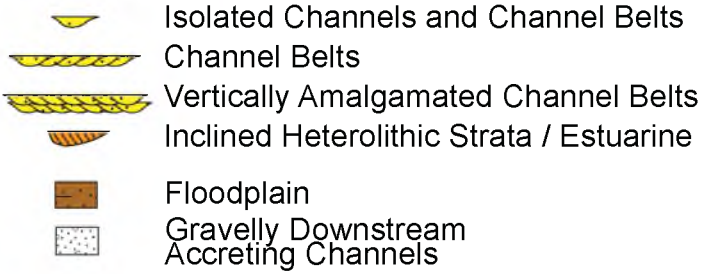

Figure 5 – Simplified stratigraphic diagrams of the John Henry Member at (A) Kelly Grade (Gallin, 2010) and (B) Rock House Cove (Gooley, 2010). The locations of these study areas are shown on Figure 1.

A) Rock House Cove

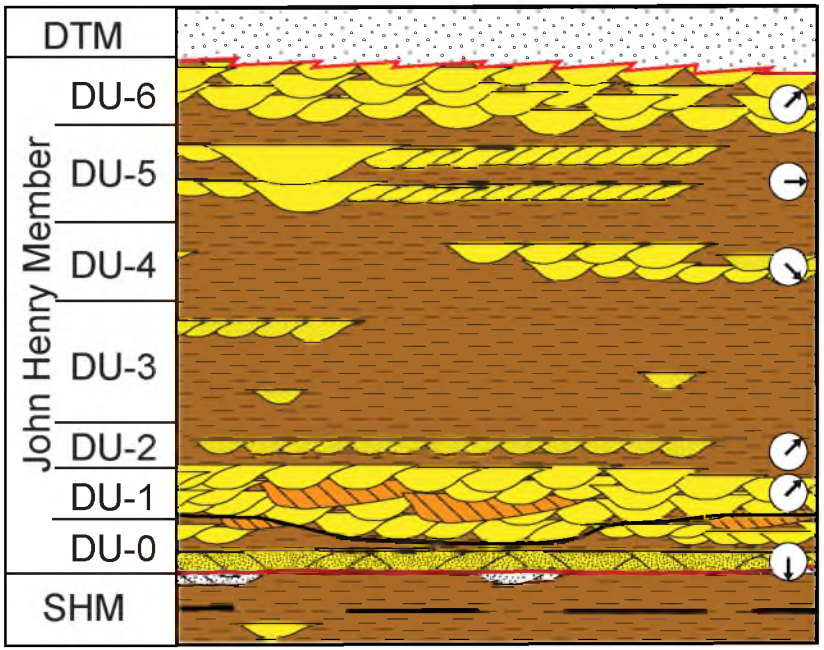

B) Kelly Grade

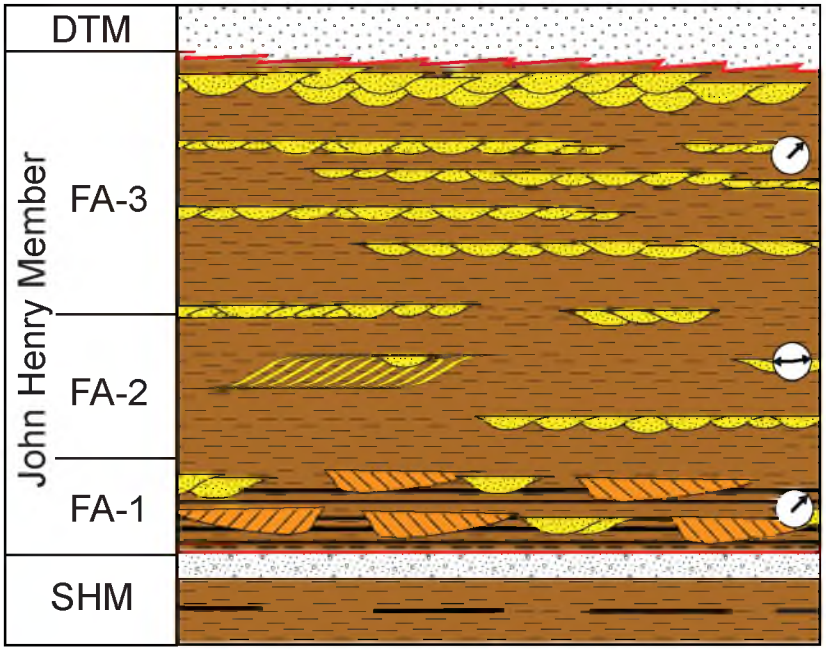

Floodplain
Coarse-grained braided river
Coal / coal mire
Isolated channels
Channel belts
Vertically amalgamated channel belts
Inclined heterolithic strata / estuarine
Paleocurrent direction
Member contact
Unconformity

RESEARCH GOALS

Preservation of the fluvial-marine transition within the John Henry Member in the Kaiparowits Plateau makes it an ideal case study to investigate an ancient sediment-routing system (i.e., the transfer zone) (Castelltort and Van Den Driessche, 2003, Goodbred, 2003; Armitage et al., 2011). In this system sediment shed from the Sevier thrust belt was transported through the coastal plain, with some degree of storage occurring enroute, and ultimately deposited along the shore of the Western Interior Seaway. Unlike depositional systems connecting to ocean basins, the shorelines may be the ultimate sink for much of the coarser sediment (i.e., sand sized sediment) in this system, particularly due to the limited presence of this material in age-equivalent deepwater turbidite systems to the east. Within the current body of research involving the interpretation, stratigraphic correlation, and depositional models of the John Henry Member, there is a relative lack of detailed inquiry into the nature of the transition from purely fluvial deposition on the west side of the plateau to paralic deposition in the central portion of the plateau and marine successions to the east. This study attempts to provide insight into many of the questions associated with this gap in the current literature by conducting a detailed stratigraphic study of the Bull Canyon region, located approximately halfway between the previously studied areas of proximal fluvial strata at Rock House Cove and fluvial/paralic strata at Kelly Grade (Figure 1).

The outstanding questions include: What is the nature of the fluvial architecture in this portion of the system, and how do the trends in fluvial architecture correlate with previously studied areas throughout the plateau? Do the trends in fluvial architecture fit the existing depositional and sequence stratigraphic models, and if not, what modifications should be made to these models? What implications does this area have on changes in geographic and temporal shift in the depositional environment (e.g., changes in provenance)? What are the broader implications of this study for depositional cycles present in the terrestrial (fluvial) deposits?

METHODS

The stratigraphy of Bull Canyon was initially characterized using a series of logged stratigraphic sections measured along the east side of the canyon (Figures 6 and 7; Appendix A). Two of the measured sections (SXN1 and SXN4) cumulatively covered the entire section exposed at Bull Canyon and were used to delineate the Tibbet Canyon, Smoky Hollow, John Henry, and Drip Tank Members. A total of three sections (SXN1, SXN2, and SXN3) were measured through the John Henry Member along the eastern side of the canyon at ~0.5 km spacing (Figure 6). Each section began at the lowest exposure of the John Henry Member and extended the top of the canyon.

Stratigraphic sections were described using the methods outlined in Miall (2000), which include documenting lithology, grain size, sedimentary structures, and body and trace fossils. While measuring sections, straight 'vertical' paths were maintained whenever possible; however, offsets were occasionally necessary due to topography and outcrop accessibility. The use of trenching along sloped portions of the outcrop allowed for nearly continuous section documentation. The measured sections were used to determine the percent distribution of lithofacies within each depositional unit. These distributions were used to determine the ratio of net sandstone to gross sediment within each depositional unit (i.e., net-to-gross ratio).

Two high-resolution composite photographs (Gigapans: Appendix B) of the east side of Bull Canyon, which cover approximately 2.5 km of lateral outcrop, were used to

map facies distributions and channel stacking patterns in the John Henry Member (Figure 8a,b). A composite photo of the west side of Bull Canyon was used to confirm observations made on the east side of the canyon (Figure 8c). An additional composite photograph was used to document lower portion of the canyon, which was poorly represented in the previously mentioned composite photographs (Figure 9).

Paleocurrent and barform accretion measurements were taken along sandstone beds from the base of the John Henry Member through the Drip Tank Member in order to document the paleotransport direction and mode of accretion (Appendix C). Paleocurrent measurements were taken on trough cross-stratification, ripple cross-lamination, and tabular cross sets (Allen, 1966; Selley, 1968; Miall, 1974). The orientation of barform accretion sets were measured and evaluated in relation to the paleocurrent direction to identify the dominant mode of accretion (i.e., lateral or downstream accretion) for the seven depositional units using an approach similar to McLaurin and Steel (2007). Rose diagrams of accretion set directions were each overlain with the corresponding mean paleocurrent direction, a blue colored wedge marking orientations within 45° of the mean paleocurrent direction, and two yellow wedges marking orientations within 45° of being perpendicular to paleocurrent (Figure 10). Accretion sets measurements that fall within the yellow wedges are considered to be generally lateral accreting and those with the blue wedges are considered to be generally downstream accreting.

The dimensions and distribution of sandstone bodies were documented using a differential GPS unit paired with a laser rangefinder. A series of base stations were established on the west side of Bull Canyon, and their locations were recorded with sub-meter accuracy (99% of points with 5-15 cm accuracy) using a Trimble® GeoExplorer®

6000 GPS unit equipped with a Tempest™ antenna. The locations of sandstone bodies were documented using a series of points that were recorded as offsets from the base station using a TruPulse 306b rangefinder. The most effective method for documenting the sandstone bodies was to collect points at their furthest lateral extents to the left and right and a series of paired points to record their thickness, which consisted of vertically aligned measurements of the base and top of the bed. The paired measurements were generally evenly spaced at ~10 m or less, but additional points were collected where changes in thickness or significant topographic relief along the cliff face. Differential corrections were made with GPS Pathfinder® Office software using the reference station in Page, Arizona. Petrel™ software (by Schlumberger) was used to display the data in 3D, which allowed for the thickness, apparent width and orientation of the sandstone bodies to be measured (Figure 11; Appendix G).

The apparent channel belt widths were corrected to true channel widths using the methods of Fabuel-Rerez et al. (2009). In this method, the paleocurrent, outcrop orientation, and apparent channel width are used to trigonometrically solve for true (cross channel) widths (Figure 12).

Fluvial morphodynamics relate to the coevolution of flow hydrodynamics and surface morphology (Paola et al., 2009; Kleinhans, 2010). Various methods can be used to calculate paleomorphodynamic parameters using measurements of bankfull depths and the d50 (median grain size) of bedload material (Paola and Mohrig, 1996; Bridge and Tye, 2000; Leclair and Bridge, 2001; Hajek and Wolinsky, 2012). These calculations were developed for, and are commonly used in, Quaternary research. In this study, a workflow was developed that incorporates a number of paleomorphodynamic parameters,

which was used to investigate Upper Cretaceous fluvial strata in the John Henry Member (Appendix D). The workflow was applied to each depositional unit within the John Henry Member in Bull Canyon and those identified by Gooley (2010) in Rock House Cove. The parameters that were investigated include: bankfull depth, slope, Froude number (and Froude squared), and backwater length. These parameters are explained more fully in the Results section.

Thin sections were prepared from 20 medium-grained sandstone samples, which were collected from channels at roughly even spacing vertically through the section (Figure 7; Appendices E and F). A modified version of the Gazzi-Dickinson method was used to point count the thin sections (Ingersoll et al., 1984; Dickinson, 1985; Zuffa, 1985). The results were examined for trends throughout the section in Bull Canyon and compared to similar work conducted in Rock House Cove and Kelly Grade.

Figure 6 – Map of Bull Canyon with the locations of the four measured sections (SXN 1-4) and the camera locations and areas included in the three panoramic photographs (lower east Bull Canyon, upper east Bull Canyon, and west Bull Canyon).

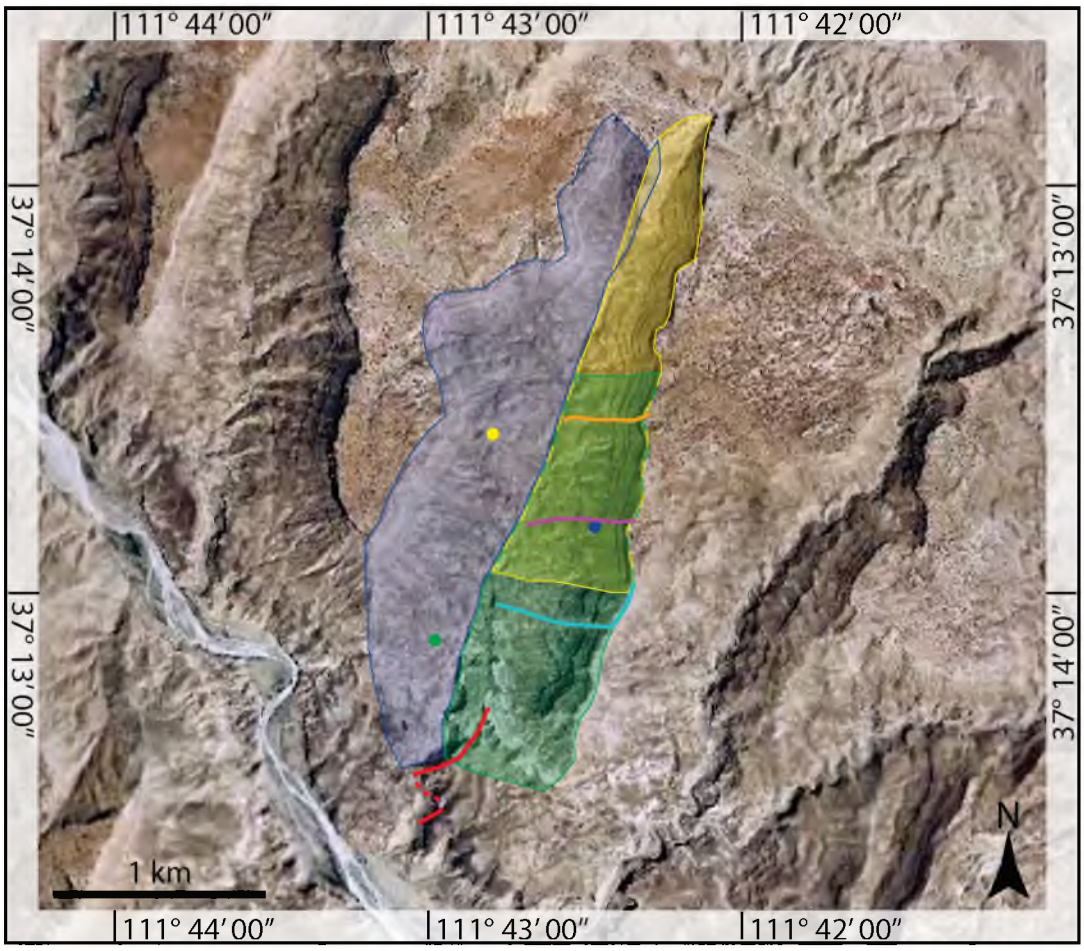

Measured Sections

- SXN1
- SXN2
- SXN3
- SXN4

Areas in Panoramic Photos/Camera Locations

- Lower East Bull Canyon
- Upper East Bull Canyon
- West Bull Canyon

Figure 7 – Measured stratigraphic sections. A) Stratigraphic sections legend. B) Measured stratigraphic sections of the Straight Cliffs Formation from the east side of Bull Canyon. Section locations are shown on Figure 5. Blue lines mark the contacts between the Smoky Hollow Member (SHM), John Henry Member (JHM) and Drip Tank Member (DTM). Boundaries between the seven depositional units (DU-0 through DU-6) are marked with grey dashed lines. A black line marks the location of a fault with ~15 m of normal displacement.

A) Stratigraphic Sections Legend

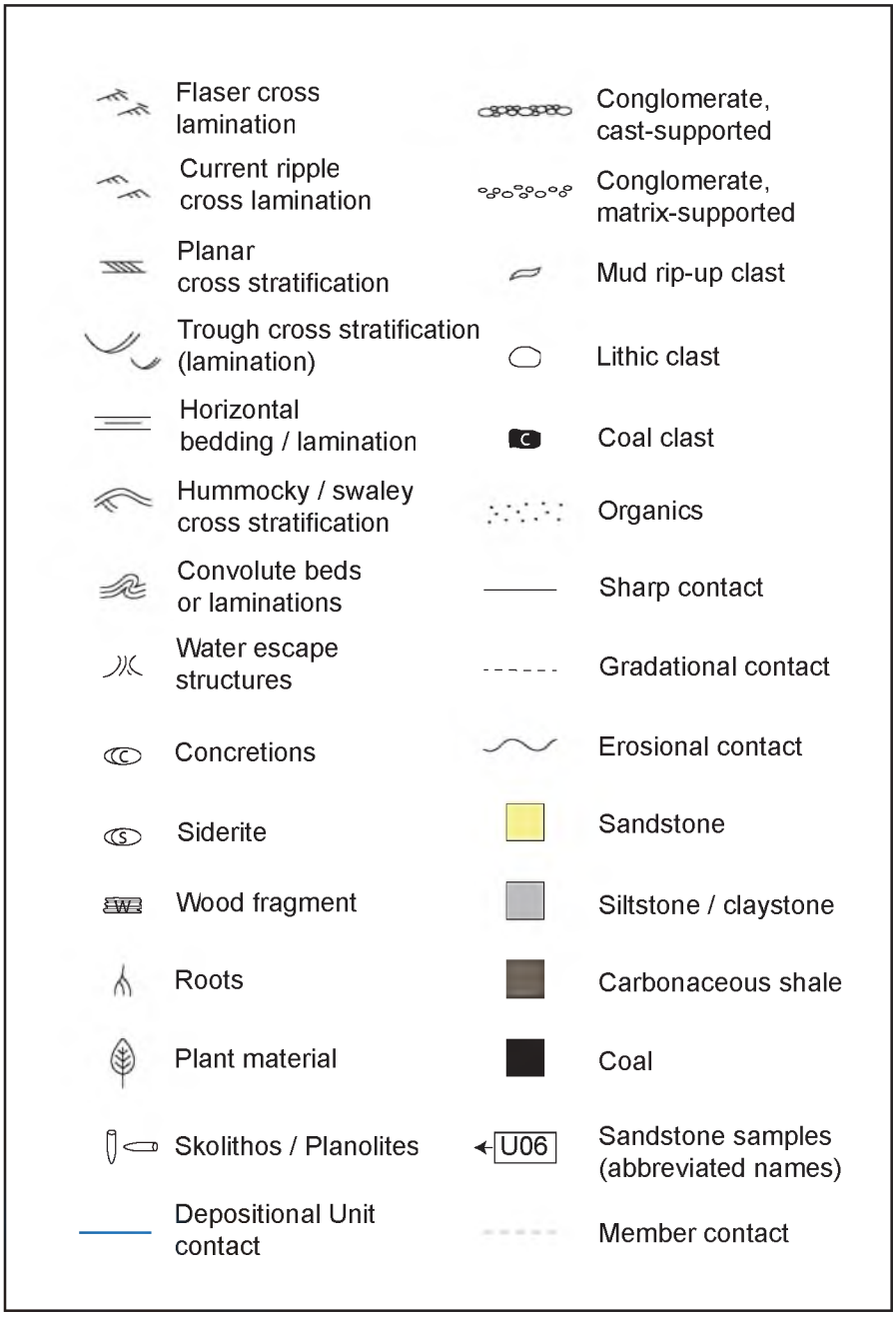

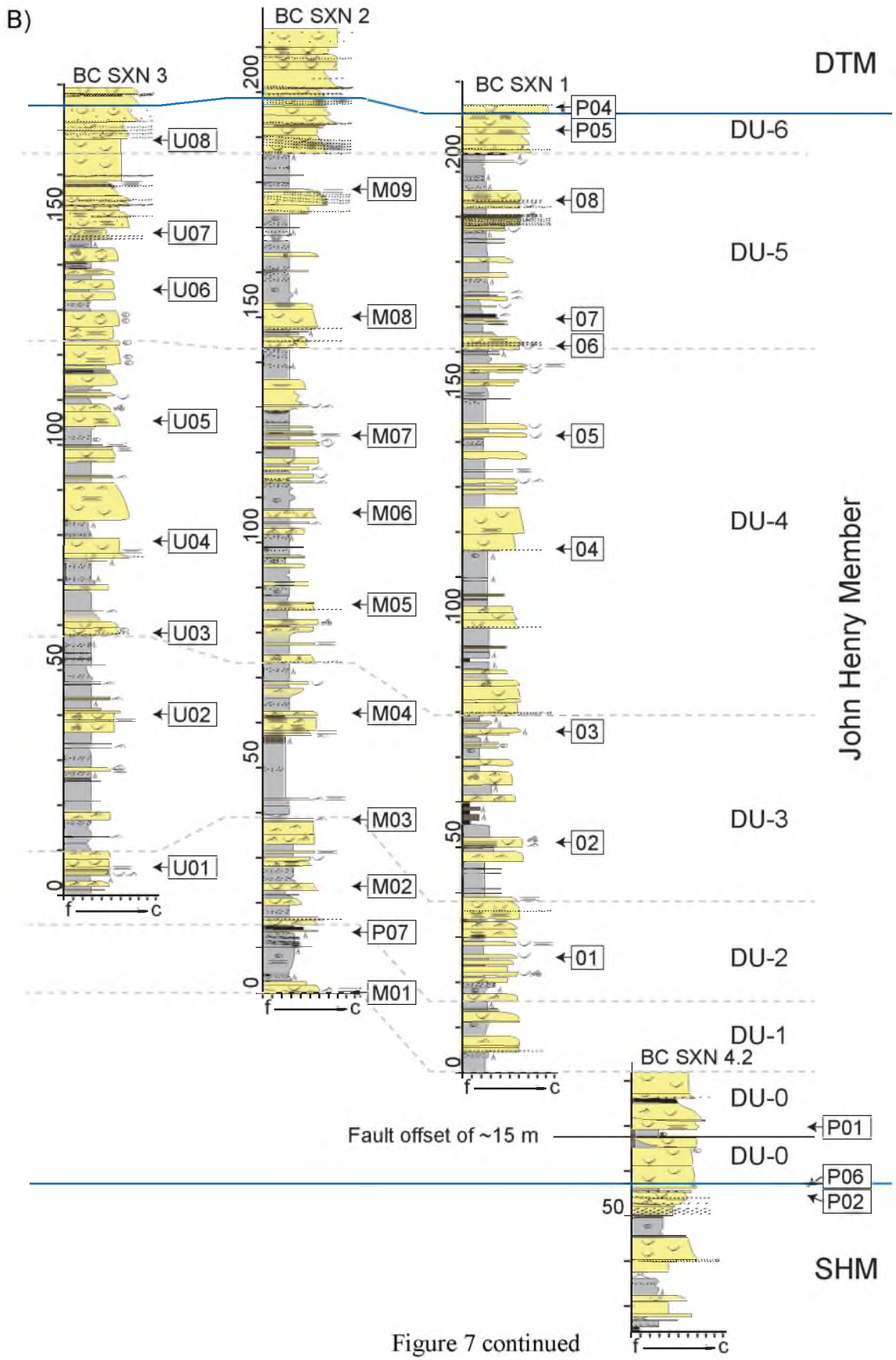

Figure 7 continued

Figure 8 – Three photomosaics and interpretations of the John Henry Member in lower east Bull Canyon (A), upper east Bull Canyon (B) and west Bull Canyon (C). The field of view and camera locations for each of the photomosaics are shown in Figure 3.

A) Photomosaic and Interpretation of Lower East Bull Canyon

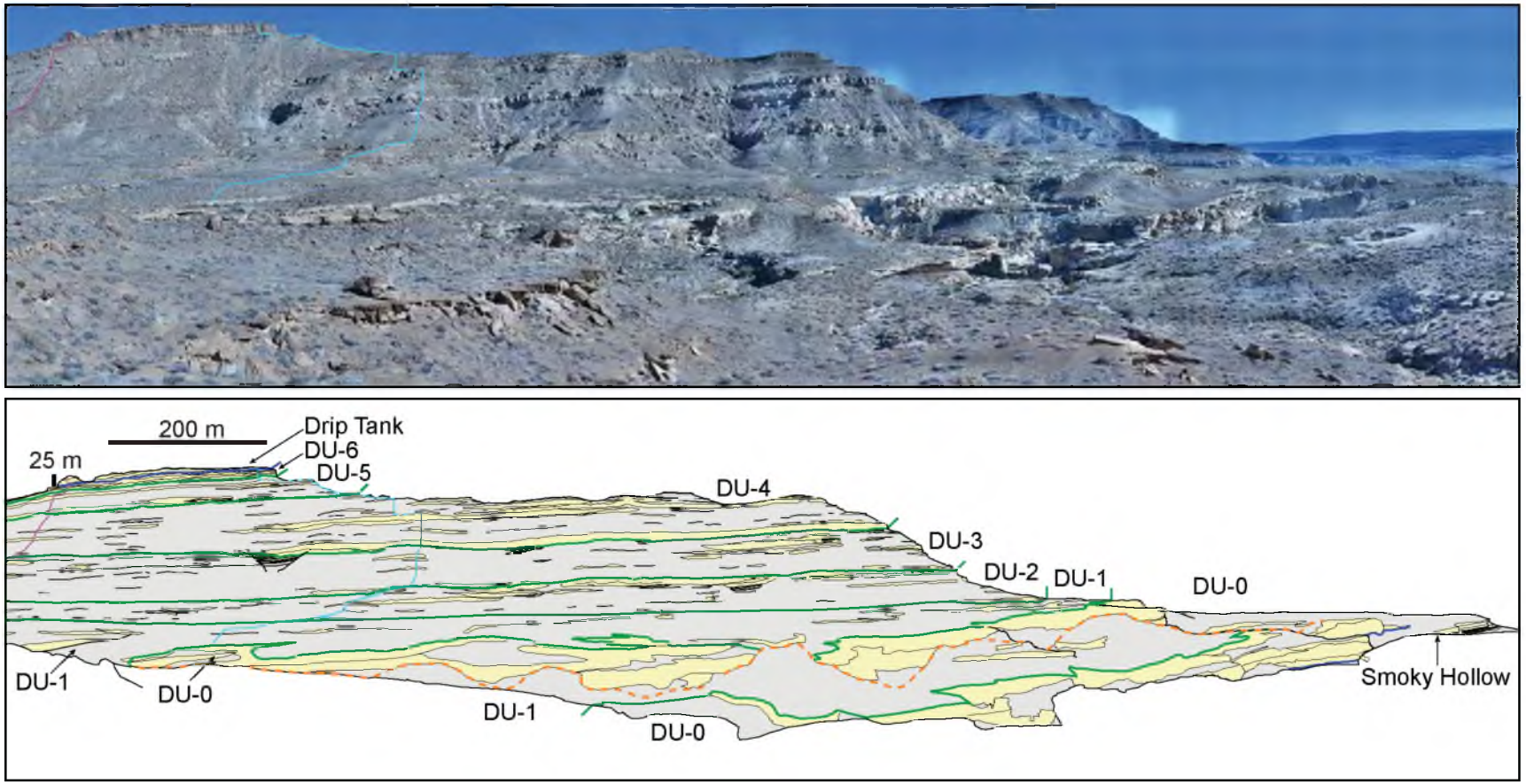

B) Photomosaic and Interpretation of Upper East Bull Canyon

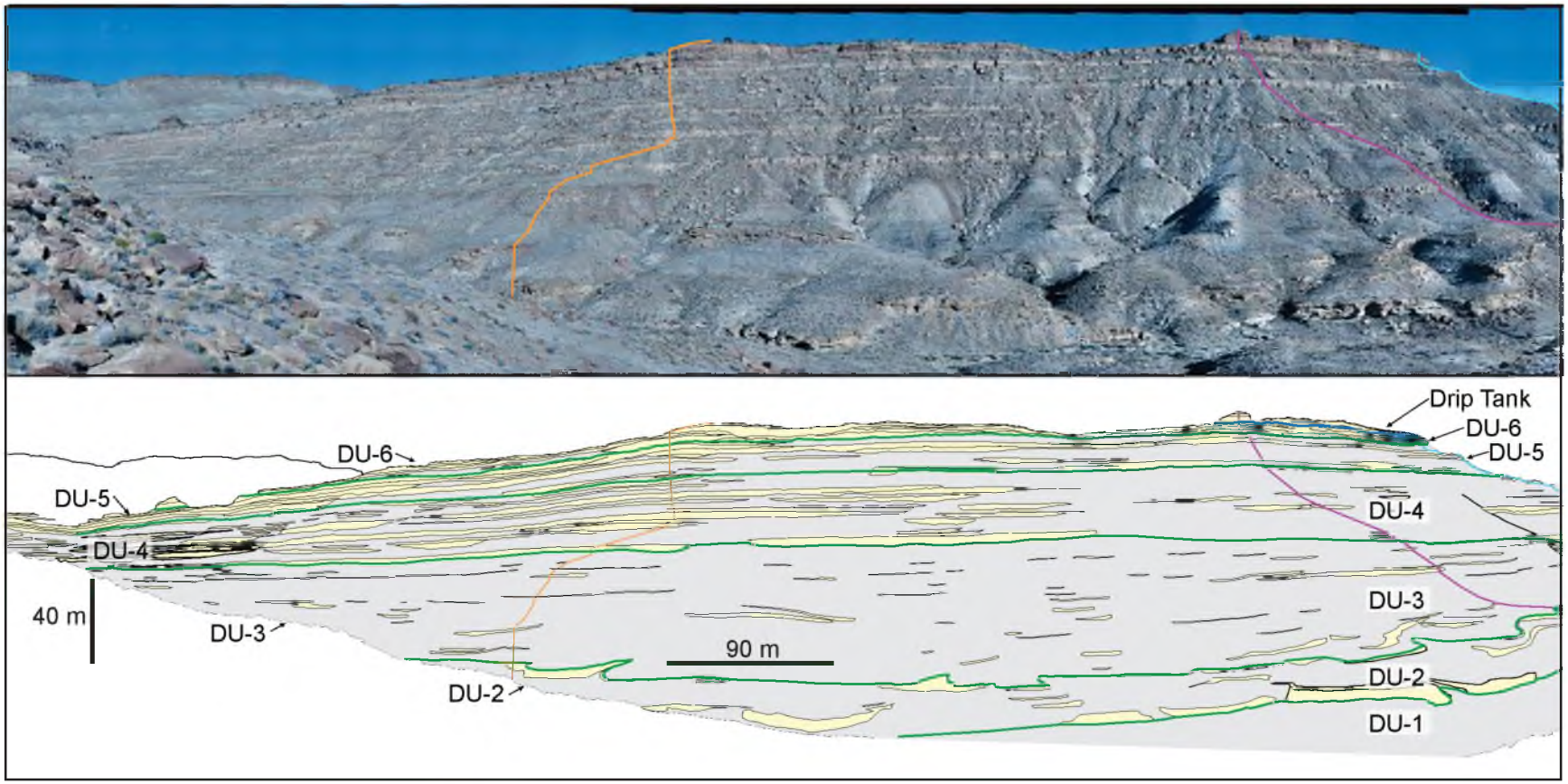

Figure 8 continued

C) Photomosaic and Interpretation of West Bull Canyon

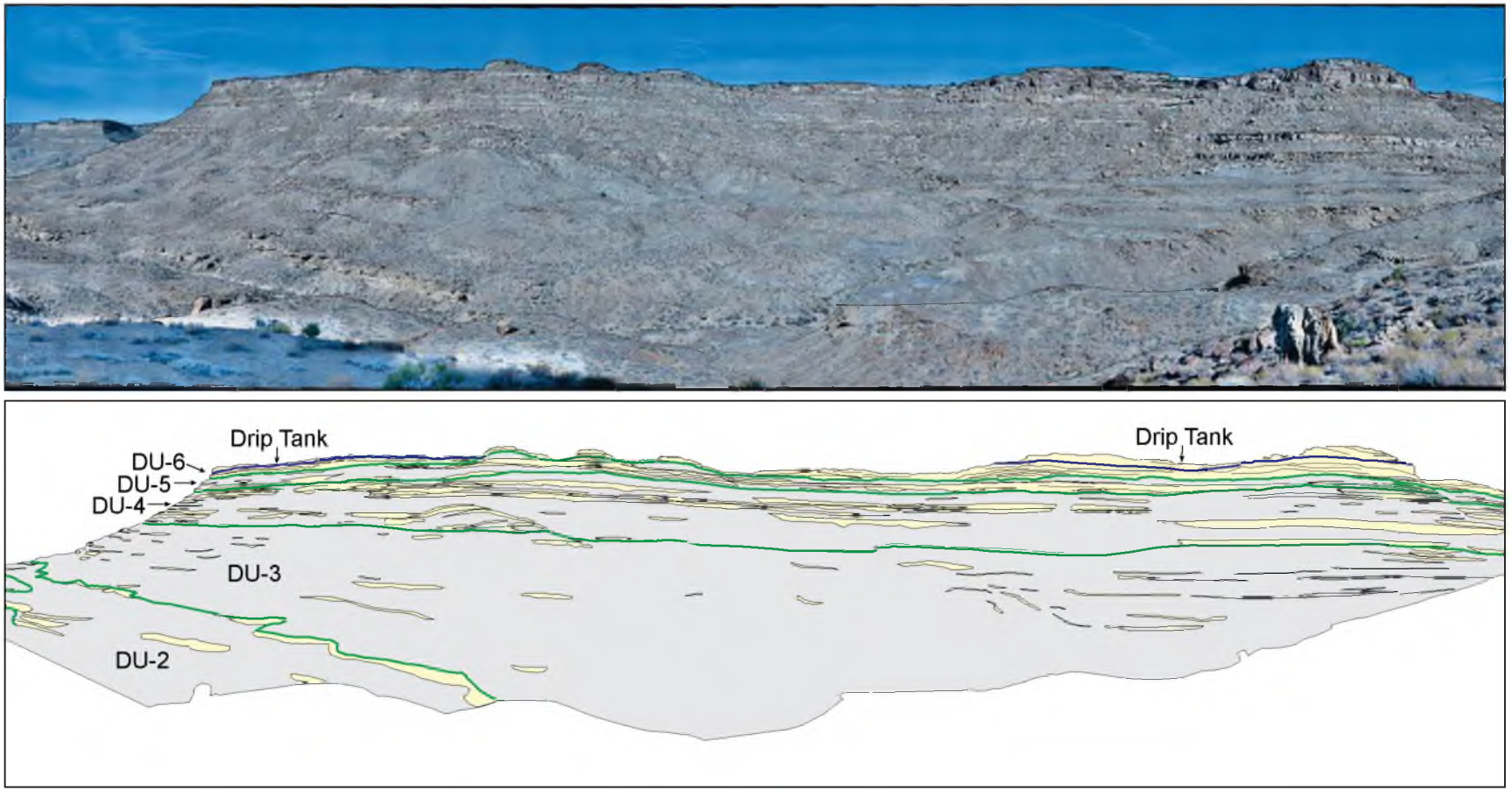

Figure 8 continued

Figure 9 – Photomosaic and interpretation of the Smoky Hollow Member (Calico bed) and DU-0 of the John Henry Member near the mouth of Bull Canyon facing northwest. The interpretations show the distribution of sandstone (yellow) and floodplain fines (gray). Blue lines mark formation member boundaries. Green lines mark the boundaries of depositional units, which are stratigraphic intervals that contain distinct fluvial architecture.

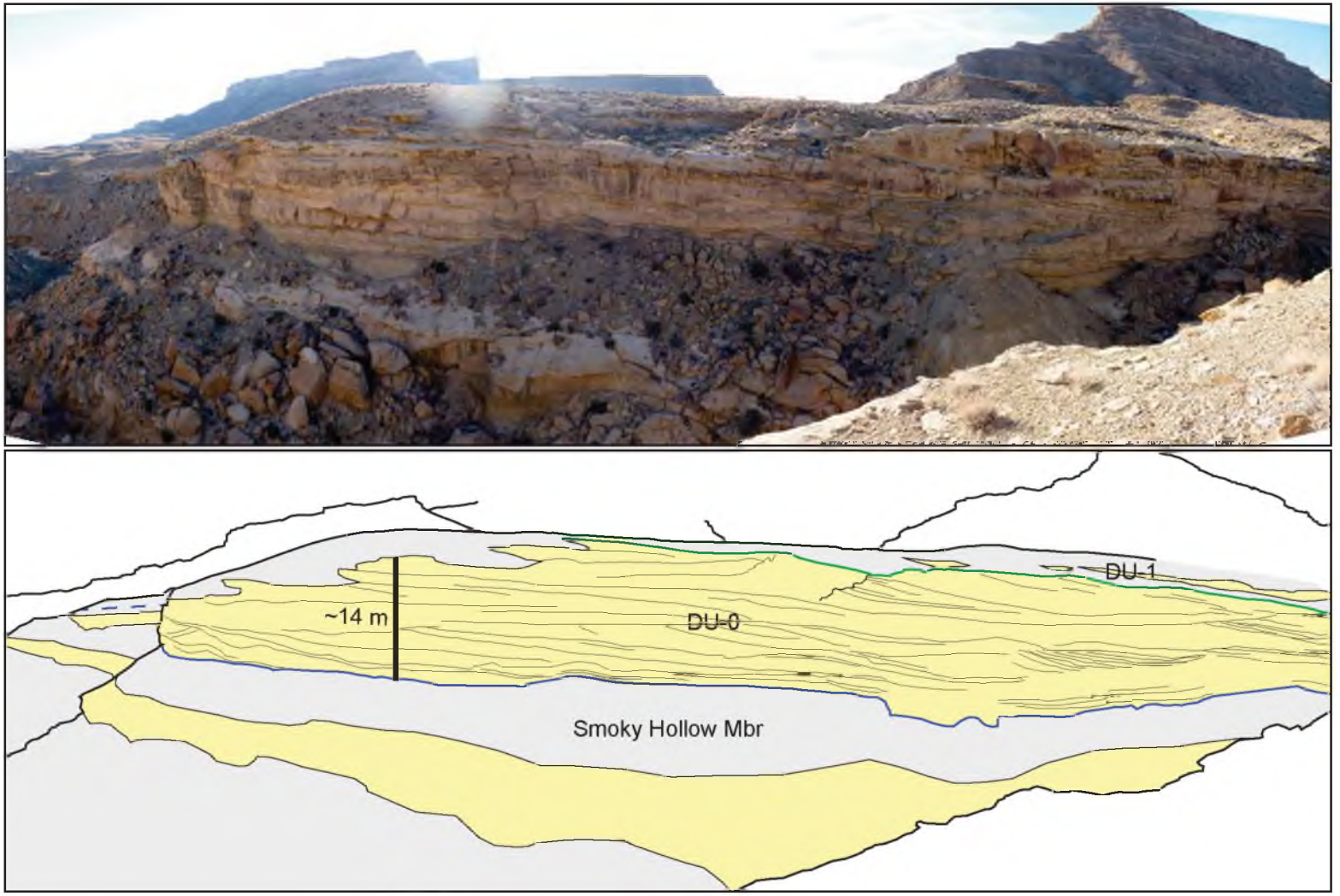
~14 m
DU-0
DU-1
Smoky Hollow Mbr
Siltstone/mudstone
Sandstone
Depositional unit boundary
Member boundary

Figure 10 – Documentation of paleocurrent and accretion measurements. A) A key to the paired paleocurrent and accretion diagrams that were constructed for each depositional unit (Figure 18). The rose diagrams are oriented so that north is up. The blue colored zone includes 45° on either side of the mean paleocurrent direction. Accretion measurements within the blue zone are considered to be downstream accreting. The yellow zones each included 90° areas with their centers oriented perpendicular to the mean paleocurrent. Accretion measurements within the yellow zones are considered to be laterally accreting. B) An example of dominantly downstream accreting DU-0. C) An example of dominantly lateral accretion in DU-4.

A. Paleocurrent and accretion diagram key

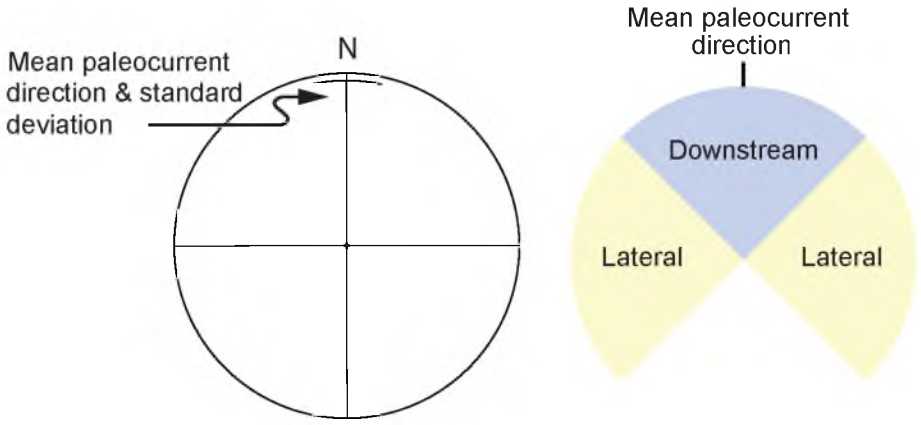

B. Dominant downstream accretion (ex. DU-0)

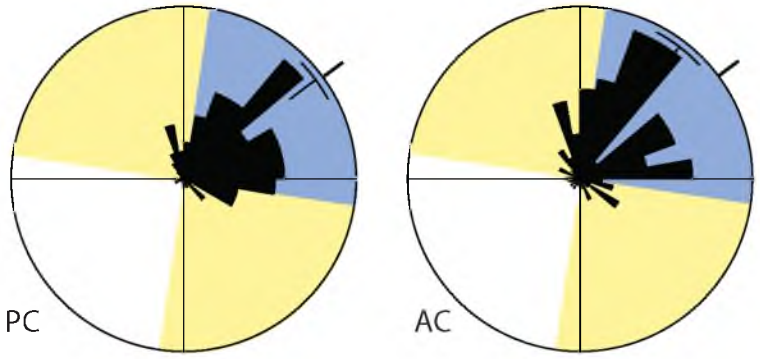

C. Dominant lateral accretion (ex. DU-4)

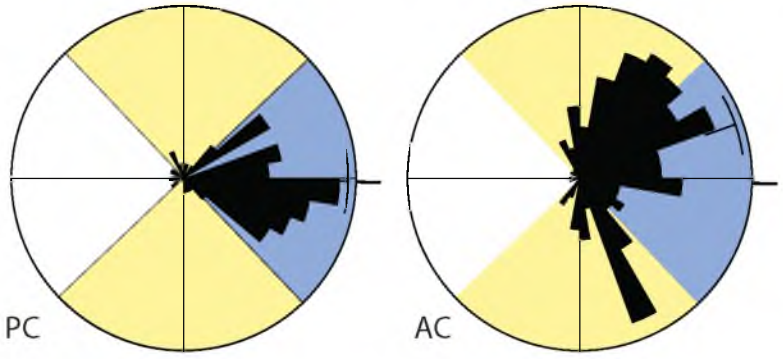

Figure 11 – GPS point cloud and digital elevation model (DEM) of the east side of Bull Canyon displayed using Petrel™ (by Schlumberger). Northing and easting are shown in UTM coordinates (zone 12N) and elevation is shown in meters above sea level. The DEM is marked with 20 m contour lines. Groups of colored spheres represent the channel belt boundaries (left, right, and paired points from the base and top). Channel centers are displayed as white boxes.

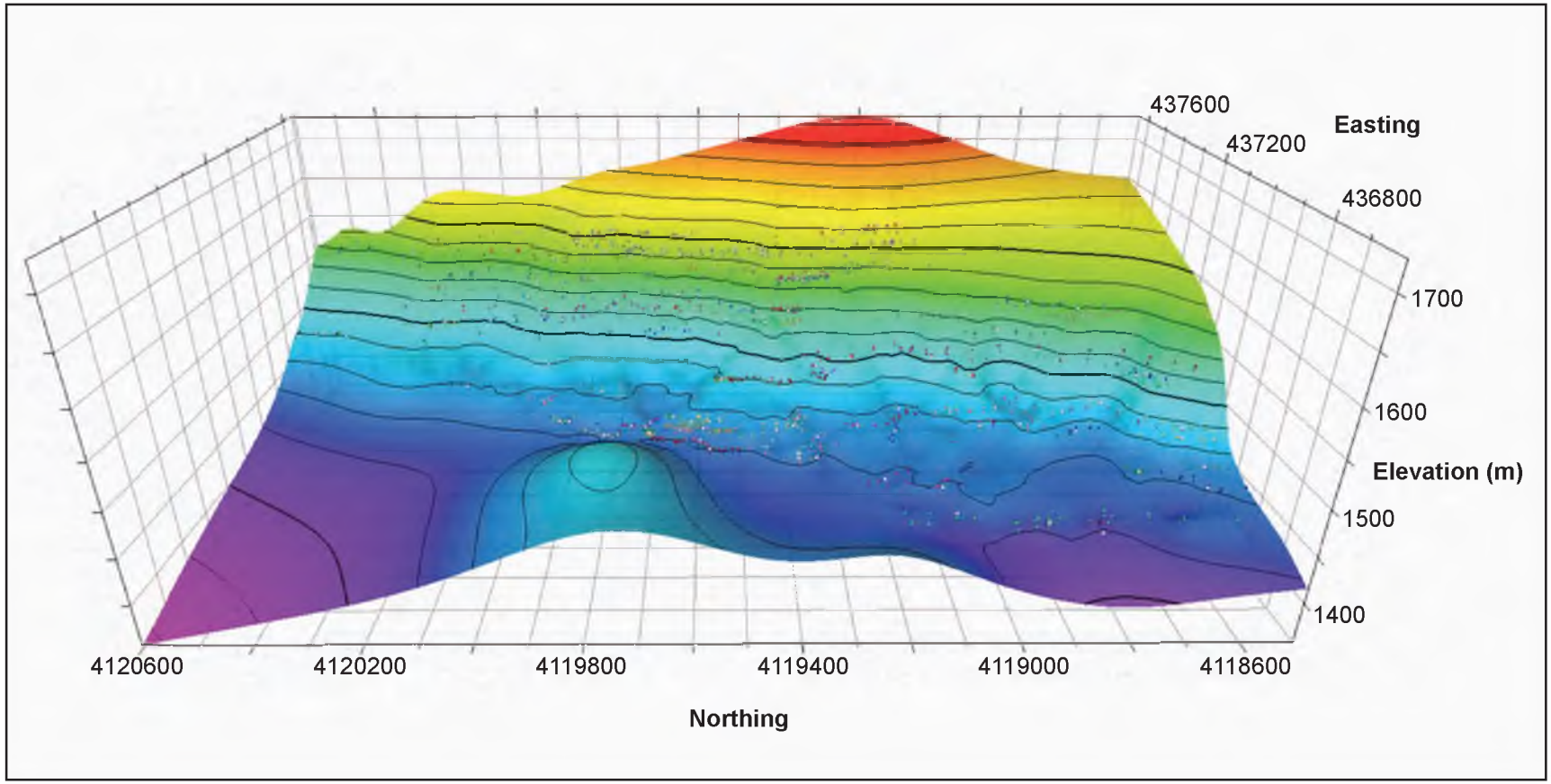
437600
437200
436800
Easting
1700
1600
1500
1400
Elevation (m)
4120600
4120200
4119800
4119400
4119000
4118600
Northing

Figure 12 – True channel belt width correction. The diagram shows how paleocurrent direction was used to correct apparent channel belt widths (measured on outcrops) to true channel belt widths (i.e., actual width of the channel belt) (modified from Fabuel-Perez et al., 2009).

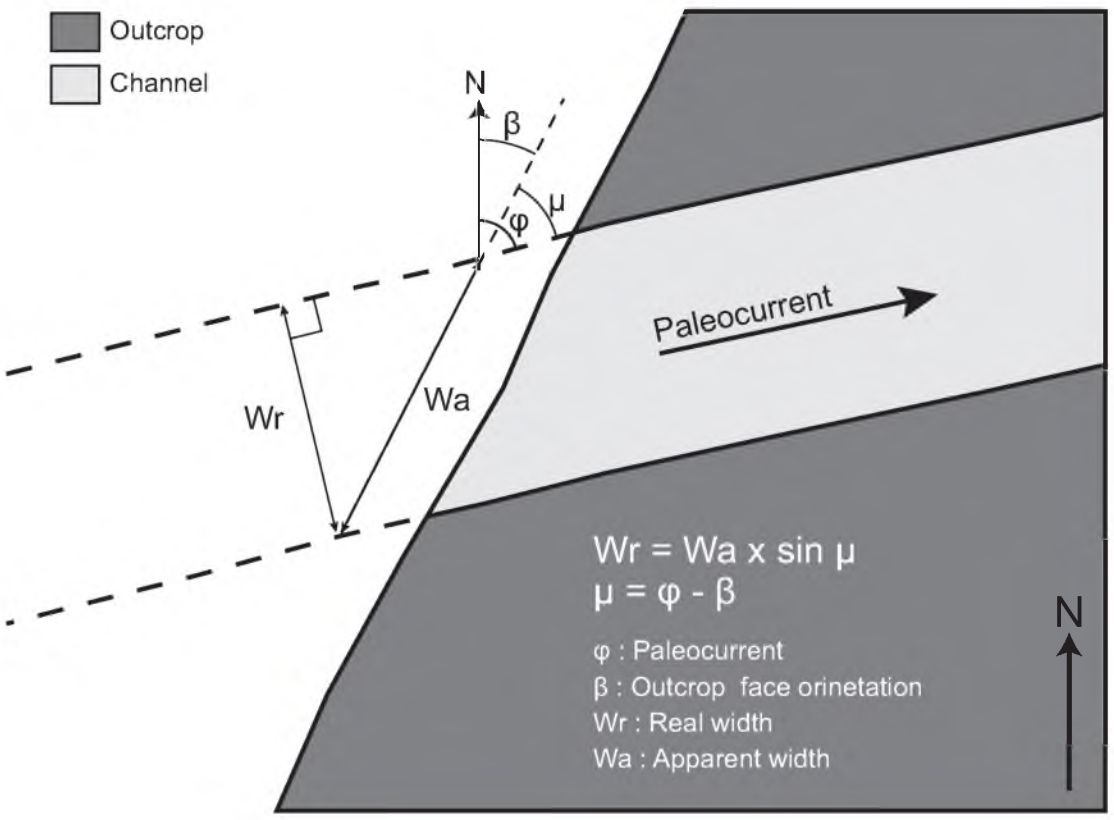
Outcrop
Channel
N
β
φ
μ
Paleocurrent
Wr
Wa
Wr = Wa x sin μ
μ = φ - β
φ : Paleocurrent
β : Outcrop face orinetation
Wr : Real width
Wa : Apparent width
N

DESCRIPTIVE CLASSIFICATION SCHEME

Fluvial Terminology

This study addresses the descriptive hierarchy of alluvial architecture and architectural elements using an approach similar to previous studies in the John Henry Member (Gallin, 2010; Gooley, 2010). Alluvial architecture, the largest scale of fluvial description, is the distribution, proportion, and geometry of alluvial deposits with a sedimentary basin (Allen, 1978). Thus, alluvial architecture relates to the long-term, large-scale aspects of alluvial deposition and erosion. Fluvial architecture, though sometimes used synonymously with alluvial architecture, more appropriately refers to smaller scale three-dimensional arrangement of architectural elements (Mackey and Bridge, 1995; Heller and Paola, 1996; Bridge, 2003; Ethridge, 2011). Architectural elements range from channel scale down to lamination scale features, which include: channels, gravel bars and bedforms, sandy bedforms, foreset macroforms, lateral accretion deposits, sediment gravity flow deposits, laminated sand sheets and overbank fines (Miall, 1985).

The hierarchy of channel descriptions includes, in increasing scale, channel stories, channel belts, and channel belt complexes. Channel stories are composed of amalgamated barforms that are bound by scour surfaces and represent a single channel migration. Channel belts consist of a series of related channel stories that represent continued migration of a channel across the floodplain (Bridge, 2003). Channel belt

complexes (or amalgamated complexes) are composed of a series of amalgamated channel belts that were deposited at separate points in time on the same position on the floodplain (Hirst, 1991).

Channel Classification

There are numerous problems associated with relating the fluvial sedimentary record to modern streams, which have been the topic of much debate (see Bridge, 2003 and authors therein). As a result, the application of the traditional classification, which uses planform geometry to identify paleo-rivers as straight, meandering, anastomosing, or braided, in outcrop studies is particularly controversial (Ethridge, 2011). In this study, the criteria for classifying channels was based on the sediment type, architectural elements, sedimentary structures, and cross-section form typical of these channel types (detailed descriptions are included in the facies association section below).

Descriptive Hierarchy

This study implemented a descriptive classification hierarchy that includes, in increasing scale, lithofacies, facies associations, and depositional units. This descriptive hierarchy is based on standard methods of fluvial description outlined by Miall (1996) and was modified in a similar fashion to those used by other researchers on outcrop studies in the Straight Cliffs Formation (Gallen, 2010; Gooley, 2010; Semple, 2011).

Lithofacies are defined using bedding, grain size, texture, and sedimentary structures. This study employs a modified version of the lithofacies classification scheme proposed and refined by Miall (1977, 1978, 1985, 1996) that uses two or three letter facies codes in which the first capital letter indicates the dominant grain size (G = gravel,

S = sand, F = fine grained facies, including very fine sand, silt and mud) and the accompanying lower case letters indicate bedding, sedimentary structures, and texture. The lithofacies used in this study are listed and defined in Table 1.

Facies associations are groups of genetically related facies that have an environmental significance (Collinson, 1969). The facies associations identified in this study include: coal mire, floodplain, meandering and anastomosing fluvial, braided fluvial, and tidally-influenced fluvial (Table 2).

Depositional units (DU) are defined as stratigraphic intervals that possess a distinct alluvial architecture (i.e. the nature and arrangement of various facies associations) (Gooley, 2010). The depositional units identified in this study are summarized in Table 3. Transitions between depositional units are commonly gradational, and as a result, it is not always possible to place their boundaries along discrete surfaces. The depositional units are defined in Bull Canyon, but they are more broadly applicable; some can be correlated more than 40 km across the surrounding region of the southern Kaiparowits Plateau.

Table 1

Descriptions of Lithofacies

Facies Code	Facies	Description	Interpretation
Gcm, Gct	Clast-supported conglomerate, massive and trough cross-stratified	Structureless and trough cross-stratified matrix supported conglomerate; the grain size of the sandstone matrix was fine to very course and clasts varied from 0.2 to >4 cm; sometimes graded; typically 10 to 50 cm thick.	Gravel bedforms, lag deposits
Gmm, Gmt	Matrix-supported conglomerate, massive and trough cross-stratified	Subangular to well rounded pebbles and gravel supported in a sandstone matrix; grain size of sandstone matrix grain size varied from fine to very course and clasts varied from 0.2 to >4 cm; typically 10 to 30 cm thick.	Barforms and channel bedforms
Smrc	Mud-rip up clast conglomerate	Angular to subrounded, granule to pebble size clasts of mud and silt in a sandstone matrix; commonly located at the base of channels and barforms; coal and wood fragments are often present; typically 15 to 30 cm thick.	Initial deposition during a flooding event
Sm	Massive sandstone	Very fine to course sand that lacks distinguishable sedimentary structures, convolute bedding, and bioturbation.	High sedimentation rate
St	Trough cross-bedded sandstone	Trough sets ranging from 0.05 to 0.5 m tick and cosets up to 4 m thick; grain size varied from fine to very course.	Migration of sinuous-crested and linguoid dunes (3D bedforms)

Table 1 Continued

Facies Code	Facies	Descriptions	Interpretation
Sp	Planar cross-bedded sandstone	Planar sets are generally 0.05 to 0.15 m thick; grain size varied from fine to very course.	Migration of transverse and liguoid dunes (2D bedforms)
Sc	Convoluted sandstone	Distorted bedding within fine to medium grain sandstones; features included dewatering, oversteepened, and erratic structures.	High sedimentation rate or slumping
Sb	Bioturbated sandstone	Fine- to medium- grain sandstone bodies in which bioturbation has modified the primary depositional structures; ichnogenera include *Skolithos, Rhizocorallium, Teredolites, Thalassinoides*, and *Planolites*.	Biogenic activity
Sr	Ripple cross-laminated sandstone	Current ripples, including climbing ripples, in very fine to medium sandstone; less than 5 cm in height.	Deposition during lower flow regime flow
Sh	Horizontally laminated sandstone	Horizontally laminated fine to medium grain sandstone dipping <5°	Deposition during critical flow
Sf	Flaser bedded sandstone	Fine to medium grain sandstone crossbeds draped with carbonaceous mud or micas.	Deposits representing fluctuations in flow
Fm, Fl	Massive and laminated siltstone/mudstone	Structureless or horizontally laminated clay and silt; often interbedded with coals and very fine to medium grain sandstone; may contain plant material, wood fragments and leaf impressions; occasionally siderite nodules and lenses are present.	Floodplain deposits from suspension, weak traction currents, and floodplain ponds.

Table 1 Continued

Facies Code	Facies	Descriptions	Interpretation
Fr	Rooted mud and silt	Layers of incipient soils are found within sections of floodplain mud and silt; roots and plant material are abundant; bioturbation and siderite nodules are occasionally present.	Vegetated floodplain
Fc	Carbonaceous mud	Black to dark grey clay and silt; contains abundant organic material, plant and coal fragments; often laminated, but occasionally massive; commonly found grading up into coal or below channel scours.	High organic content floodplain or silt diluted mire
C	Coal	Lignite and sub-bituminous coal; black, occasionally displaying vitrinite reflectance; beds range from a few cm to 0.5 m thick; commonly underlain by carbonaceous mud that grades vertically into coal and overlain gradationally by carbonaceous shale or, more commonly, by a sharp contact with sandstone.	Mire peat development

Table 2

Descriptions of Facies Associations

Facies Associations	**Architectural Elements**	**Lithofacies**	**Avg. Grain Size**	**Biogenic Sed. Structures**	**Macrofossils**
Coal Mire	Horizontal-tabular beds	C, Fc	silt-coal	*Planolites and Rooting*	Leaf impressions and wood fragments
Floodplain	Horizontal-tabular beds	C, Fc, Fr, Fl, Fm, Sr, Sb, Sm	mud-silt	*Planolites and Rooting*	Leaf impressions and wood fragments
Braided Fluvial	Downstream accretion sets, gravel beds, and gravel barforms	Sr, Sh, St, Sp, Sc, Smrc, Gmm, Gmt, Gcm, Gct	cs-vcs	*Teredolites, Planolites, and Thalassinoides*	Wood fragments
Meandering Fluvial (Braided Fluvial)	Lenticular and tabular sandstone bodies with lateral accretion sets	Sf, Sr, Sh, St, Sp, Sm, Smrc	ms	*Skolithos, Teredolites, Rhizocorallium, and Planolites*	Wood fragments, logs, leaf impressions
Tidally-Influenced Fluvial	Inclined heterolithic strata, and lateral accretion sets	Fl, Fm, Sf, Sr, Sh, St, Sp, Sb, Sc	fs	*Teredolites, Planolites, Thalassinoides, and Skolithos*	Shells and wood fragments

Table 3

Descriptions of Depositional Units and Bounding Members

DU	Facies Accociation	Avg. Grain Size	Channel Description	Avg. Thickness	Net to Gross
DTM	1. Braided fluvial	vcs; granule-pebble	Highly amalgamated; laterally extensive channel belt complex	NA	1.00
DU-6	1. Braided fluvial 2. Meandering fluvial	ms-vcs; granule lenses	Multi-story, highly amalgamated channel belt complexes; moderately extensive; laterally accreting; low horizontal offset	11 m	1.00
DU-5	1. Meandering Fluvial	ms-vcs; granule lenses	Multi-story, thick and laterally extensive, sheet-like channel belts; laterally accreting; moderate horizontal offset; channel belt complexes	43 m	0.51
DU-4	1. Meandering Fluvial	fs-ms	Multi-story, thick, laterally accreting, and laterally extensive channel belts; large lateral offset; locally amalgamated	71 m	0.42
DU-3	1. Floodplain 2. Meandering to anastomosing fluvial	silt-fs	Single story; thin; laterally accreting; laterally isolated channels in thick floodplain deposits; very low amalgamation	46 m	0.30

Table 3 Continued

DU	Facies Accociation	Avg. Grain Size	Channel Description	Avg. Thickness	Net to Gross
DU-2	1. Meandeing fluvial 2. Floodplain	fs-ms	Single and multi-story channels; lateral accretion; isolated to moderately laterally extensive; low to moderate amalgamation	17 m	0.58
DU-1	1. Tidally-influenced fluvial 2. floodplain 3. Coal mire	ms	Single story; downstream and laterally accreting; laterally isolated; high lateral offset; little to no amalgamation	14 m	0.42
DU-0	1. Braided fluvial 2. Tidally-influenced fluvial	cs-ms	Highly amalgamated, downstream accreting, channels that compose a laterally extensive channel belt complex	13 m	0.89
SHM	1. Floodplain 2. Braided fluvial	vfs-fs; cs (Calico Bed)	Single story, isolated channels and multi-story channel belt (highly amalgamated fluvial sheet)	50 m	0.56

RESULTS

Lithofacies

Distribution of lithofacies (Figure 13; Table 1) varies vertically through the section (Figure 14). The most common lithofacies present in the measured sections were trough cross-stratified sandstone (St) and massive and laminated mudstone (Fm, Fl) (Figure 13h). Siltstone and mudstone facies (Fm, Fl, Fr) are nearly to completely absent from the lowermost and uppermost portions of the John Henry Member and the Drip Tank Member, but are the dominant lithofacies in the middle of the John Henry Member. Carbonaceous shale (Fc) and organic-rich siltstone/mudstone are most abundant in the lower portion of the John Henry Member, in an interval that begins directly above the amalgamated sand at the base of the section and extends about half way to the top of the member (Figure 7). This interval also contains the greatest occurrence of coal beds, which are most abundant lower in the interval and decrease vertically in abundance and thickness (Figure 14).

The abundance and lateral distribution of sandstone facies varies throughout the section. The base and top of the John Henry Member, as well as the Drip Tank Member, are primarily composed of sandstone channels that are amalgamated into extensive sheets, whereas the middle of the John Henry Member is composed of isolated channel sandstone and laterally restricted sandstone channel belts.

Trough cross-stratified sandstone (St) and massive sandstone (Sm) are the dominant lithofacies within channel deposits (Figure 13c,e). Convolute bedded sandstone (Sc) is also commonly located in channel sandstones, and is most abundant in DU-2 and the large channel sandstones located near the top of the John Henry Member (Figure 13d). Planar and ripple cross-laminated sandstone (Sp and Sr) are commonly located at the top of channel deposits, but at times compose entire beds (Figure 13a). Bioturbated sandstone (Sb) is commonly located in fine and medium grained sandstone at the bases and tops of channels (Figure 13b). Flaser bedded sandstone (Sf) is abundant in the lower John Henry Member and is absent higher in the section.

Gravel lithofacies (Gcm, Gct, Gmm, and Gmt) are primarily limited to the Drip Tank Member and the uppermost channels of the John Henry Member (Figure 13g,f). These lithofacies are only sparsely present within the uppermost channel deposits in the John Henry Member and occur in greater abundance (Figure 13g), at times forming an entire bed, within Drip Tank Member.

Facies Associations

Five facies associations, which link assemblages of lithofacies with specific depositional environments, are identified within Bull Canyon. They include coal mire, floodplain, meandering and anastomosing fluvial, braided fluvial, and tidally-influenced fluvial (Figure 15; Table 2).

Coal Mire Facies Association

The coal mire facies association (Figure 15a) is composed of coal (C), carbonaceous shale (Fc), and organic rich siltstone/mudstone with abundant coal spar,

rooting, wood, and leaf impressions (Figure 16a,e). Occurrences of mire facies range in thickness from less than 1 m to greater than 8 m and extend laterally for tens of meters. Individual coal beds vary in thickness from 5 to 120 cm, with an average thickness of 35 cm. Mire facies laterally interfinger with floodplain facies, or are truncated by post depositional scouring, and are commonly capped by a sandstone fluvial channel. The coal mire facies association is present in the lower half of the John Henry Member, above the highly amalgamated sandstone at its base (DU-0), and almost completely absent in the upper half (Figure 14).

The term mire generally applies to any of a number of non-saline peat-forming environments (McCabe and Parrish, 1992). Coal mires can develop in floodplain, coastal plain, delta plain, and back-barrier environments (Horne et al., 1978; Thornton, 1979; Thomas, 2002). The coals at Bull Canyon are interpreted as coastal plain mires that developed in swamps, small ponds, or lakes adjacent to fluvial channels.

The distribution of coastal plain mires can be used as an indicator of changes in base level. Variations in the ratio of accommodation/peat accumulation, which dictates peat preservation, are mainly attributed to oscillations in base level (Deissel et al., 2000; Wadsworth et al., 2002; Davies et al., 2006). The groundwater table, which is one of the factors controlling peat development, can be impacted by sea-level (base-level) changes up to 150 km landward (Koster and Suter, 1993; Törnqvist, 1993). The lateral shifts in paralic coal distribution resulting from base-level influenced changes in the groundwater table correspond to progradational and retrogradational parasequences in sequence stratigraphy (Deissel et al., 2000).

Floodplain Facies Association

The floodplain facies association (Figure 13b) is predominantly composed of massive and laminated siltstone and mudstone (Fm, Fl). Layers of abundant rooting (Fr) and organic material are common within the floodplain fine-grained deposits, and poorly developed soil horizons are occasionally present. Siderite nodules, either isolated or concentrated along distinct horizons, commonly occur within the floodplain fines. Siderite nodules develop in reducing environments below the water table during the early stages of diagenesis (Driese et al., 2010; Surez et al., 2010). Carbonaceous shales (Fc) are frequently present at the base of channels and at times grade vertically into coal (C). Tabular beds of very fine- to fine-grained massive, planar, and rippled sandstones (Sm, Sp, Sr), interpreted as crevasse splays, occur throughout this facies association, but are most abundant below and adjacent to channel sandstones bodies. Series of inclined (dipping ~10°), tapering downward medium-grained sandstone (Sm, Sl) beds that interfinger with the floodplain siltstones and mudstone are occasionally present at the edges of channel sandstones. These deposits are interpreted as levee deposits or floodplain deposits that were deposited in close proximity to a channel. The architectural elements (Table 2; Figure 15b) that comprise this facies association include: levee deposits, crevasse-splay deposits, floodplain fines, and incipient soil horizons (Miall, 1996; Bridge, 2003).

Meandering and Anastomosing Fluvial Facies Association

The meandering and anastomosing fluvial facies association is dominated by medium grain-size sandstone facies (Sm, St, Sp, Sc, Sr, Sh) that form lenticular or tabular bodies with a large width to depth ratio (Figure 15c). These sandstone bodies consist of a

single or multiple channel stories, which are composed of amalgamated barforms and fine upward. At their base is a sharp, erosive contact with the underlying floodplain and coal mire facies associations or an older channel sandstone. The channel facies laterally interfinger with crevasse splay and levee sandstone bodies of the floodplain facies association. Lag deposits composed of mud rip-up clasts (Smrc) (Figure 13e), gravel (Gmm, Gcm) (Figure 13g), wood, coal, bone fragments, and shell material (Figure 16h) are occasionally present at the bases of channel stories and along omission surfaces. Wood and coal are sporadically distributed throughout this facies association (Figure 16b). Trace fossils are sparse, but when present, they are often in dense concentrations of a single ichnospecies. *Planolities, Rhizocorallium*, and *Teredolites* are often located near the bases of beds and *Skolithos* and root traces are present in the fine grain sandstones near the tops of some sandstone bodies (Figure 17c,d,g,f). Accretion-set measurements indicate a wide range of accretion directions, a high proportion of which are oriented sub-lateral and lateral to the paleocurrent directions (DU-3 through DU-5 in Figure 18).

This facies association is interpreted as channel deposits with characteristics that are indicative of low gradient, low discharge fluvial systems with moderate sediment load and infrequent channel avulsions. The arrangement of facies and the dominant lateral accretion in most of this facies association indicates a meandering fluvial system (Bridge, 2003). However, intervals dominated by coal mire and overbank deposits (interpreted as crevasse-splay, swamp, pond and lake deposits) with infrequent and laterally isolated channel sandstone bodies (DU-3) are consistent with the facies model for anastomosing fluvial deposits (Nadon, 1994). It is important to note that it is not possible to identify whether multiple channels were active at the same time, which is necessary to have

anastomosing channels (Schumm, 1968; Bridge, 2003). The preservation of coal is more likely in an anastomosing than meandering river environment, because the floodplain is not reworked through channel migration and frequent avulsions and abundant vegetation can develop in interfluvial wetlands (Smith and Smith, 1980). Anastomosing fluvial deposits are common in foreland basin systems and develop due to the combination of high-suspended load, seasonal water flow, and low depositional gradient (Nadon, 1994).

Braided Fluvial Facies Association

The braided fluvial facies association (Figure 15d) is primarily composed of coarse-grained sandstone (Sm, St, Sp, Sc, Sr, Sh) and gravel facies (Gcm, Gct, Gmm, Gmc). The median grain size is coarse to very coarse sand, but gravel beds (Gcm) ranging from 5 to 100 cm thick are common and fine-grain sediments are almost completely absent. Large-scale dune foresets (up to 2 m tall) composed of coarse-grained sand and gravel, are pervasive within this facies association. Undulating scour surfaces with up to several meters of relief are abundant and often intersect one another. Paleocurrent and accretion set measurements indicate that downstream accretion is more dominant than in the meandering and anastomosing facies association (DU-0 and DU-6 in Figure 18).

This facies association is indicative of a higher gradient, higher discharge, bedload dominated fluvial system that experiences frequent avulsions and thalweg shifts. These characteristics fit the depositional model for a braided fluvial system (Schumm and Kahn, 1972; Chitale, 1973).

Tidally-Influenced Fluvial Facies Association

Tidally-influenced fluvial facies association (Figure 15e) primarily consists of very fine to lower-medium grain sandstone (Sr, Sp, Sb) and siltstone (Fl, Fr). This association contains flaser bedding, wavy bedding, lenticular bedding, and inclined heterolithic strata (IHS), which is rhythmically interbedded sandstone and siltstone facies that are dipping at angles of 5° to 20°. Interlaminated sandstone/mudstone within a few channel bodies were identified as possible double mud drapes, which are a good indicator of tidal influence (Visser, 1980). This facies association is commonly adjacent to coal mire facies and capped by the meandering fluvial facies association. In addition to *Skolithos* and *Planolites* (Figure 17g,c), the traces fossil assemblage of this association includes *Thalassinoides* (Figure 17a,b), most commonly present in marine to brackish salinities (Kern and Warme, 1974), and *Teredolites* (Figure 17f), a brackish water indicator (Bromley et al., 1984). Paleocurrent and accretion set measurements indicate a slight tendency towards lateral barform accretion (DU-1 in Figure 18).

The IHS and rhythmic mudstone/organic drapes present in this facies association are formed under conditions of fluctuating current energy (Thomas et al., 1987; Shanley et al., 1992). These types of bedding have been documented in distinctly non-marine influenced fluvial environments (Jackson, 1981; Page et al., 2003); however, the presence of brackish/marine trace fossils at this location makes an exclusive fluvial influence unlikely, and supports a mixed fluvial and tidal depositional environment. Therefore, the IHS and rhythmic drapes are interpreted as representing periodic fine-grained sediment fallout that occurred when fluvial currents slowed due to influence of the tidal cycle (Thomas et al., 1987; Kvale and Mastalerz, 1998; Dalrymple and Choi, 2007). In other

parts of the Kaiparowits Plateau, previous studies of the John Henry Member have also interpreted tidal influence within a portion of the fluvial deposits (Gallen, 2010; Gooley, 2010) or the entire fluvial section (Shanley et al., 1992; Shanley and McCabe, 1995).

Channel Belt Dimensions and Stacking Patterns

The true channel belt dimensions (Figure 12) for 136 channel belts on the east side of Bull Canyon were calculated using the GPS point cloud and paleocurrent measurements (Figure 18; Table 4). Due to the large variance in channel dimensions and the range of stacking patterns within Bull Canyon, a number of measurements were used to quantitatively document the variability. Channel belt widths are highly variable (from 15 to 733 m), and show trends of reducing widths from the base of the member to the middle and increasing widths from the middle to the top of the member (Figure 19a). The patterns in average channel belt thicknesses range from ~1 to 7 m and match the trends in channel belt widths (Figure 19b). The cross plots of channel belt width to thickness ratio (W/T) vs. stratigraphic order show an increase in the maximum W/T ratio higher in the section (Figure 20a). The W/T ratios for meandering channel belt are commonly 30-100 and braided systems are commonly 50-1000 (Gibling, 2006). In Bull Canyon, W/T ratios generally fit within the typical range of meandering channel belts. However, some studies would consider the fully amalgamated channel belts at the base and top of the section as a single unit (i.e., a fluvial sheet) and would document the dimensions of the entire amalgamated complex (Cotter, 1978). If this approach were used these intervals would have widths of over a km and much higher W/T ratios. The plot of channel belt width vs. thickness shows a possible linear relationship between these two variables (Figure 20b).

Vertical and lateral offsets describe the spatial relationship between channel belts. Channel belt offset measurements were made by projecting the channel belt midpoints (documented in the GPS point cloud) onto a vertical plane perpendicular to the mean paleocurrent and recording their relative positions. Figure 21 contains a graph and statistics of the lateral and vertical offset of channel belts based on the stratigraphic order assigned within each depositional unit. The moving average (with a range of five) for the lateral channel belt offsets is also plotted, which shows the larger trends in channel belt locations. The average magnitude of lateral offsets (dx) increases vertically from DU-1 (dx = 134 m) through DU-3 (dx = 531 m) and remains in fairly constant (dy = 523-556 m) from DU-3 through DU-6. Groups of channel belts separated from one another by large lateral offsets (as seen in DU-4) may indicate clustering and/or compensational stacking (Straub et al., 2009). The average magnitude of the vertical offset decreases vertically from DU-1 (dy = 10.1 m) through DU-4 (dy = 1.8 m) and then remains fairly consistent from DU-4 through DU-6 (dy = 1.4-1.8 m). DU-0 and DU-1 have small sample numbers due to lack of exposure, and thus, offset data for from these depositional units are less reliable than those higher in the section.

Channel belt complex geometries are highly variable and range from groups of partially amalgamated channel belts, local clusters of high amalgamation, and extensive fully amalgamated intervals (or fluvial sheets). The degree of vertical and lateral amalgamation was quantified using an amalgamation index, in which, each channel belt was assigned a number for both vertical and lateral amalgamation: 0 = not amalgamated, 1 = amalgamated on one side, or on either the top or base, 2 = amalgamated on both sides, or the top and the base. These numbers were averaged for each depositional unit

and are displayed in Figure 22. Depositional units with very little amalgamation have index numbers ≈0, and those with very high amalgamation have index numbers ≈2.

The degree of amalgamation does not appear to be related to changes in lateral channel belt offset in this outcrop, though there is a slight correlation between reducing vertical offset and increasing amalgamation. The degree of amalgamation appears to be related to channel belt dimensions, where larger channel belts are coincident with higher amalgamation index (Figures 19 and 22).

Depositional Units and Bounding Members

This section includes detailed descriptions of the Smoky Hollow Member, seven depositional units within the John Henry Member, and the Drip Tank Member, including: stratigraphic thickness, distribution of facies associations, channel belt dimensions, paleocurrent and accretion directions, and trace fossil assemblages.

Smoky Hollow Member

The Smoky Hollow Member underlies the John Henry Member, and is 33.5 m thick where it crops out near the mouth of Bull Canyon. A measured section and photos showing the extent of the Smoky Hollow Member are in Figure 23a,b. The Smoky Hollow Member was informally divided into three units (Peterson, 1969b), in ascending order: the coal zone, the barren zone, and the Calico bed. The coal zone consists of the lowermost 3.5 m of the Member and is composed of carbonaceous mudstone and coal beds (Figure 23g,h). Overlying the coal zone, the barren zone is 12 m thick and composed of mudstones and fine- to medium-grained horizontally and cross-stratified sandstones (Sh, St). The barren zone contains plant fossils, but no coal or carbonaceous

shale. The uppermost portion of the member, the Calico bed, is up to 16 m thick and consists of white and very light grey, fine- to very coarse-grained cross-stratified sandstone (St). The sandstones are poorly sorted and contain conglomerate lenses and isolated quartz and chert pebbles (Figure 23c,d). In this location, the Calico bed is composed of a series of sandstone bodies that are either separated by mudstones or are amalgamated into a large channel belt complex (Figure 23b). *Teredolites* was identified near the base of the Calico bed, which indicates a tidal influence (Figure 23e). The base of the Calico bed interfingers with the barren zone.

Interpretation - Fluvial sandstone bodies at the base of the Smoky Hollow have incised into the underlying shorefaces of the Tibbet Canyon Member. The coal and carbonaceous mudstone of the coal zone were deposited in a coastal plain environment. The overlying isolated channel sandstones and floodplain deposits of the barren zone (which lack coal) represent an increase in sedimentation and fluvial influence (McCabe and Parish, 1992). At the top of the Smoky Hollow Member, the Calico bed is composed of tabular channelized deposits of the braided fluvial facies association with minor amounts of floodplain facies. The Calico bed has been interpreted as a braided fluvial system that formed during high sediment supply and low accommodation (Bobb, 1991; Semple, 2011), and associated with an unconformity and possible sequence boundary (Shanley and McCabe, 1991, 1995). The abrupt increased grain size in the Calico bed reflects a distinct change in the system at this time, which caused an increase in its carrying capacity.

Depositional Unit 0 (DU-0): Laterally Extensive, Braided Channel Belts

Depositional Unit 0, the lowermost depositional unit in the John Henry Member, has an average thickness of 13 m and forms a prominent cliff (Figure 24a,b). The base of DU-0 is erosive, with over 2 m of relief, and directly overlies coarse-grained sandstones or a few meters of floodplain fines of the Calico bed of the Smoky Hollow Member. There is a recessive bench at the top of DU-0 (Figure 24a,c), which likely developed due to the presence of fine-grained floodplain and coal mire facies associations at the base of DU-1. Near the mouth of the canyon, a fault has caused a portion of the DU-0 section to be repeated in the measured section (Figure 6).

The thick (~6 m) and laterally extensive (ave. 316 m) channel belts that comprise this unit contain many internal erosive surfaces and macroform accretion sets showing both downstream (Figure 24c,d) and lateral accretion (Figure 18f,g). These beds are composed of upper-medium to very-coarse grain sandstones of the braided fluvial facies association (Figure 24h). Overbank and floodplain deposits are generally absent from this depositional unit. Small, isolated zones composed of IHS and flaser bedding within the upper half of DU-0 weakly fit the tidally influenced fluvial facies association (Figure 24e), but this is a minor component of the unit. DU-0 has a high net-to-gross ratio (0.89), is highly laterally and vertically amalgamated (Figure 22), and has low lateral offset. The paleocurrent direction is to the northeast and barform accretion is dominantly downstream, with some sublateral accretion (Figure 18). Large-scale, up to several meters tall, high-angle dune foresets are distinctive features of DU-0 (Figure 24d). No trace fossils were identified within this depositional unit.

Interpretation - DU-0 is interpreted as a sand-dominated, low-sinuosity braided fluvial deposit composed of multiple, superimposed channel belts. Channel belts contain both bank attached bars and in channel, downstream accreting bars. The large dune foresets are oriented in the downstream direction and are interpreted as part of mid-channel, downstream accreting bars. Internal scours represent frequent avulsions and thalweg shifts, and larger scours may represent channel confluences.

Depositional Unit 1 (DU-1): Tidally-Influenced Channel Belts

Depositional Unit 1 has an average thickness of 14 m and is composed of floodplain and coal mire facies surrounding isolated, single story fluvial channels. A measured section and photographs of distinctive features are in Figure 25. Channel belts are thin (ave. <2 m), tabular, laterally isolated (ave. 75 m), have a low degree of amalgamation (amalgamation index = 0.40; Figure 22), and moderate lateral offset (Figure 19). There is a dramatic reduction in the net-to-gross ratio from 0.89 in DU-0 to 0.42 in DU-1. The average paleocurrent is to the east, with both downstream and lateral barform accretion (Figure 18).

Floodplain and coal mire facies associations are commonly interbedded. Coal beds comprise ~2% of the unit and are located in clusters distributed irregularly throughout the unit (Figure 25c). Coal spar is commonly present within sandstones. Rooting and siderite nodules, indicative of poorly drained soils, are common in floodplain deposits.

Rhythmically laminated flaser, wavy, and lenticular bedding, which are indicative of fluctuations in flow, occur within channel deposits (Figure 25d,e). IHS and sigmoidal heterolithic deposits occur both in and around channel deposits (Figure 25b,f). Due to the

limited number and isolated nature of the sigmoidal structures, they are not definitively identified as tidally derived (Kreisa and Moiola, 1986; Shanley et al., 1992). This unit contains the most diverse suite of trace fossils, which includes *Thalassinoides*, *Teredolites*, *Skolithos*, and *Planolities,* and the greatest presence of shell material (Figure 25g,h). The top of DU-1 was placed above the last layer showing prominent "tidal" indicators, commonly the stratigraphically highest IHS deposit.

Interpretation - The depositional environment is interpreted as distal coastal plain located downstream from the bayline, where tidal cycles cause fluctuations in flow and brackish water may be present. This interpretation is supported by the presence of IHS, rhythmically laminated beds (possible double mud drapes) and marine/brackish trace fossils in channels that have a unidirectional flow; which indicate a dominant fluvial current that experienced fluctuation, likely due to tidal influence. The wide range of paleocurrent directions indicate that channels were highly sinuous, a trait common to the distal coastal plain (Dalrymple and Choi, 2007). The multiple adjacent channels could be part of a distributary system, though it is not possible to identify from outcrop whether channels are coeval and part of the same branching fluvial system. The presence of coal mires fits with this interpretation, as they are common to interdistributary locations in the lower coastal plain (Thomas, 2002).

Depositional Unit 2 (DU-2): Laterally Restricted Channel Belts

Depositional Unit 2 has an average thickness of 17 m, and is composed meandering fluvial and floodplain facies associations. Sandstone bodies form a series of back stepping ledges, up to 6 m tall, separated by slope forming floodplain deposits. The

net-to-gross ratio (0.58) for DU-2 is somewhat higher than DU-1. Figure 26 contains a typical measured section and photographs of the typical sedimentary features from DU-2.

Fluvial channels are an average of 2.4 m thick, and isolated to laterally restricted (ave. 92 m). Some channels are multistoried, but the amalgamation index for DU-2 is low (Figure 20). Paleoflow is to the east with moderate sinuosity and sub-lateral barform accretion (Figure 26g). Planar, trough, and ripple cross-laminated sandstone (Fp, Ft, Fr) are common within channels (Figure 26b,c). In comparison with DU-1, this depositional unit contains very little evidence of any tidal influence; some flaser bedding is present (Figure 26f), but IHS is completely absent. Trace fossils are limited to those typical to fluvial setting, *Skolithos* and *Planolities*.

Averages from the measured sections indicate that floodplain fines comprise 42% of this depositional unit, while the rest is composed of sandstone (Figure 14). Floodplain deposits are locally rooted and contain some carbonaceous content, but no coal was identified in this unit (Figure 26d,e).

Near the mouth of the canyon, DU-2 is composed of a series of tabular sandstone beds that are successively thicker and show evidence of rapid sedimentation, including climbing ripples and convolute bedding. These sandstone bodies are separated by fine-grained floodplain deposits, thicker higher in the depositional unit, and eroded into and are capped by a series of meandering fluvial channel belts (Figure 26a).

Interpretation - This unit is interpreted to contain meandering fluvial channels that developed in the distal portion of the coastal plain, though slightly less distal than DU-1. This environment could be near or just upstream of where distributary channels develop, which could explain why the channel belts are slightly larger than those in DU-1 (ave.

width: DU-1 = 75 m and DU-2 = 91 m). Being deposited further from the coeval shoreline than DU-1 could also explain the relative lack of tidal indicators.

The succession near the mouth of the canyon is interpreted as a crevasse delta (Figure 26a) that was developed as a series of crevasse splay deposits that prograded into a body of water (Flores, 1983; Fielding, 1984). These deposits represent repeated overbank flows that eventually caused the main channel to avulse over these deposits, which produced the channel belts that scour into the splay deposits.

Depositional Unit 3 (DU-3): Isolated Channel Belts in Thick Floodplain Deposits

Depositional Unit 3 has an average thickness of 46 m and is composed of floodplain, coal mire, and meandering or anastomosing fluvial facies associations. DU-3 has the lowest net-to-gross ratio (0.30), least amount of amalgamation, and greatest abundance of coal of any depositional unit. The dominant feature of this DU-3 is the abundance of floodplain and coal mire facies associations (Figure 27a,b), which cumulatively compose ~70% of the deposit (Figure 14).

Coal mire facies are present throughout DU-3, but occur in much greater abundance in the lower portions of the unit. The thickest coal beds (up to 1.2 m thick) within the John Henry Member are located in DU-3 and are encased in thick carbonaceous shale deposits. The presence of cover made it difficult to measure the lateral extent of the coals, but some extend laterally for 10s of meter. The top of this unit generally marks the vertical limit of the distribution of the coal mire facies association; a limited amount of coal was identified near the base of DU-4.

The floodplain deposits are primarily composed of siltstones (Fm, Fl) containing abundant rooting and siderite nodules (Figure 27c,d), which indicate poorly drained environments. Root haloes are common in both channel and floodplain material. Incipient soils were identified based on evidence of the early stages of horizon development and presence of blocky pedogenic structures. Floodplain fines are commonly red-brown, and the sandstones adjacent to them show signs of diagenetic red (hematite?) staining, which was most prominent along the tops of sandstone beds.

Channel belts are typically single storied, thin (ave. thickness of 1.5 m), laterally isolated (ave. width 60 m), and have the lowest degree of amalgamation of all the depositional units (Figure 22). Well-defined channels are uncommon, and when present, composed of fine- to medium-grained sandstone with trough-cross stratification (St) (Figure 27f). Paleotransport was to the east with dominant lateral barform accretion (Figure 18). Many of the sandstone bodes of this DU-3 are poorly channelized, fine grained, and dominated by soft sediment deformation, planar bedding, and ripple cross laminations, commonly climbing ripples (Sc, Sp, Sr) (Figure 27g,h).

Interpretation - The channels in DU-3 are interpreted as low sinuosity, slightly laterally accreting fluvial system with stabilized banks, which resulted in infrequent channel avulsion. The limitations of outcrop studies preclude the ability to determine if groups of these channels were coeval and interconnected to form an anastomosing fluvial system; however, this depositional unit generally fits the criteria established by Nadon (1994) for ancient anastamosed systems in the sedimentary record. Frequent flooding events could have caused deposition of thin tabular sandstone bodies, which are interpreted as avulsion deposits and crevasse splays/channels (Gibling, 2006). The

increased clastic input higher in the depositional unit likely caused the coincident reduction in the abundance of coal mire facies (McCabe and Parrish, 1992).

Depositional Unit 4 (DU-4): Laterally Extensive, Meandering Channel Belts

Depositional Unit 4 has an average thickness of 71 m, and is composed of meandering fluvial and floodplain facies associations. Figure 28 contains a typical measured section and photographs of sedimentary features of DU-4. The base of this depositional unit was placed where there is a marked increases in channel belt size, abundance, and degree of amalgamation.

The percentage of coarse-grained sediment in DU-4 (net-to-gross ratio of 0.42) is greater that the underlying depositional unit. Floodplain facies are generally light yellow to light olive gray, massive siltstones (Fm) that are devoid of organics and siderite nodules. These deposits can be relatively thick (up to 10 m) and contain occasional crevasse splay deposits.

Channel belts are composed of medium grained sandstone, typically thick (ave. 3.3 m) and laterally restricted to laterally extensive (ave. 180 m). However, a number of channel belts are laterally extensive (exceeding 300 m in width, Figure 19). There is moderate amalgamation among channels (Figure 22); some channel belts are locally amalgamated into groups, forming channel belt complexes. Paleotransport is to the east with dominant lateral barform accretion (Figure 18). Channels contain trough-cross stratification, planar lamination, and some ripple lamination (Figure 28b,c,d). *Skolithos* burrows were common at the tops of channel deposits (Figure 25 d,e). Some lag deposits contain shell and bone fragments (Figure 28g).

Interpretation - DU-4 is interpreted as a meandering fluvial system that is laterally accreting and moderately sinuous. Frequent avulsions likely resulted from less stabilized channel banks and caused the depositional unit to have a higher net-to-gross ratio than DU-3. Multiple avulsions that occurred in close proximity to one another produced the channel belt complexes. The lack of siderite nodules indicates that there was a transition from poorly drained floodplain in DU-3 to a well-drained floodplain in DU-4.

Depositional Unit 5 (DU-5): Moderately Amalgamated, Meandering Channel Belts

Depositional Unit 5 has an average thickness of 43 m, and is composed of meandering fluvial and floodplain facies associations. Figure 29 contains a typical measured section and photographs of sedimentary features from DU-5. The base of DU-5 is located below the first channel that contains granule and gravel lag deposits (Figure 27g).

Fine grained sediments compose less than 50% of this depositional unit (Figure 14). The percentage of fine-grained sediment is less than the underlying depositional unit, continuing the trend that is present in DU-4. Floodplain deposits are similar to those of DU-3 and consist of light yellow to light olive gray, massive siltstones (Fm) that are devoid of organics and siderite nodules. The occurrences of overbank deposits are relatively limited.

Channels belts are composed of medium to lower coarse sandstones, with a steady vertical increase in the presence of gravel lags and average grain-size. The average channel belts thickness is 3.9 m and average width is 225 m (Figure 19). Channel belts are commonly amalgamated into channel belt complexes (moderate amalgamation index,

Figure 22). Channel belt complexes are much larger in size and are comprised of a larger number of channel belts than those of DU-4. Paleotransport is to the east, with dominant lateral accretion (Figure 18). The top of DU-5 is located along the stratigraphic level, above which the channel belts are completely amalgamated.

In DU-5, trace fossils are more abundant and the assemblage is more diverse than DU-2, DU-3, and DU4, and includes *Rhizocorallium, Thalassinoides,* and *Skolithos. Rhizocorallium* is typically considered a marine trace produced in firmgrounds (Figure 27e); however, there is one documented occurrence of non-marine *Rhizocorallium* (Fursich and Mayr, 1981).

Interpretation - DU-5 is interpreted as a meandering fluvial system due to its channel characteristics and facies associations. The presence of gravel within channel deposits demonstrated an increase in the carrying capacity of the fluvial system. The trace fossil assemblage may indicate an increase in marine influence; a similar trend was documented in Rock House Cove (Gooley, 2010).

Depositional Unit 6 (DU-6): Highly Amalgamated Channel Belts

Depositional Unit 6 has an average thickness of 11 m and is composed of the meandering and braided fluvial facies associations. Figure 30 contains a typical measured section and photographs of sedimentary features from DU-6. This depositional unit is cliff-forming, composed of medium sandstone through gravel clasts, with no silt or fine-grained sandstone (net-to-gross ratio = 1.0), and contained occasional mud rip-up clasts (Figure 30b,c). Sandstone bodies typically contain trough cross-stratification and low angle bedding (Figure 30d,f). The mean grain size increases stratigraphically higher

within the DU. *Teredolites* traces were the only trace fossils present with DU-6 (Figure 30e).

Channel belts have an average thickness of 3.5 m and average width of 190 m (Figure 18). The smaller channel belt widths compared to DU-5 are likely due to the increase in channel amalgamation (amalgamation index: vertical = 1.93 and lateral = 1.83), which caused truncation of channel belts. Low lateral offset and high amalgamation of channel belts resulted in a sheet-like unit with abundant internal scour surfaces, up to several meters deep, which frequently crosscut one another (Figure 30a). Paleoflow is to the east, with intermediate lateral accretion (Figure 18).

Interpretation - The channel belts of DU-6 are transitional from more meandering fluvial at the base to sandy braided fluvial at the top. The paleocurrent and accretion measurements were taken at a limited number of locations due to the inaccessibility of the cliff forming exposures, and as a result, it was not possible to document any vertical changes in paleocurrent or accretion through the depositional unit. However, the fluvial system experienced frequent avulsions and no floodplain or overbank deposits are preserved, which are more characteristic of a braided fluvial system. The presence of *Teredolites* in DU-6, in combination the trace fossil assemblage in DU-5, indicates a possible marine influence near the top of the John Henry Member.

Drip Tank Member

A few meters of the Drip Tank Member are preserved along the rim of Bull Canyon, which is composed of coarse-grained sandstone (Sm, St, Sl) through gravels (Gmm, Gmt, Gct, Gcm) of the braided fluvial facies association (Figure 31). No floodplain deposits are preserved among the channel deposits (Figure 14). In addition to

forming beds (up to ~1 m thick) and lag deposits, pebbles and granules are located in isolated areas throughout many of the sandstone beds (Figure 31d,e). No trace fossils, except *Teredolites* in float material, were identified within the Drip Tank Member.

As documented in other locations, the top of the John Henry Member (DU-6) interfingers with the Drip Tank Member (Peterson, 1969a,b; Bobb, 1991; Gooley, 2010), and because of this, the member contact is considered to be gradational. The contact between these members was placed along a series of scour surfaces, above which there is a distinct increase in mean grain-size, from upper medium sandstone to very coarse sandstone or gravel (Figure 31a,f,g).

Large dune foresets, up to several meters tall, and abundant scour surfaces with gravel lags are prominent sedimentary features (Figure 31b). The paleocurrent direction was highly variable, with an average orientation to the east-southeast (Figure 18). Barform accretion was also highly variable, with both downstream and sub-lateral accretion; however, the most common accretion direction is downstream. Due to the limited exposure of the Drip Tank Member at Bull Canyon, the dimensions of channel belts were not documented.

Interpretation - The Drip Tank Member is interpreted as mixed sand and gravel, downstream accreting braided fluvial system; a continuation of the trend of increasing braided fluvial characteristics that began in DU-6. The base of the Drip Tank Member, where there is an increase in grain size, marks the onset of an increase in stream competence. This fluvial system experienced frequent avulsions and thalweg shifts that removed any of the fine-grain sediments that were present.

Paleomorphodynamics

The steps included in the paleomorphodynamic workflow are discussed in detail within this section. The workflow was applied to the depositional units in Bull Canyon and Rock House Cove, using data collected by Gooley (2010), which permits observations of temporal and spatial variations in paleomorphodynamic parameters. Graphs of the key paleomorphodynamic parameters (bankfull depth, slope, Froude squared, and backwater length) are in Figures 32 and 33.

The bankfull depth (H) is most reliably measured directly from non-truncated point bars, but various methods exist for calculating bankfull depth that can be used when direct measurements are not possible (Bridge and Tye, 2000; Leclair and Bridge, 2001). Due to the limited number and uneven distribution of nontruncated barforms identified within the field area, the bankfull depths were calculated using the method described by Leclair and Bridge (2001), which proved to be the most accurate when compared to direct barform measurements. In this method the bankfull depth is 6-10x the mean dune height (hm), which is calculated using the formula:

$$hm = (2.9 \pm 0.7) * Sm \quad (1)$$

where Sm is mean cross-set height in meters. Calculations of bankfull depth using 8x hm produced the most reliable estimates compared to story heights. Calculations using 6x and 10x hm were propagated through the rest of the workflow calculations and used to create the error bars, which document the uncertainty produced by initial uncertainty in bankfull depth (Figures 32 and 33).

The calculated bankfull depths at Bull Canyon show a relatively large range of flow depths, from 3 to 10 m, and a trend of decreasing flow depth vertically through the section (Figure 32a). The lower DUs have larger estimated flow depths (>4 m to 10 m), whereas, the upper DUs have smaller calculated flow depth (generally <4 m). Calculated bankfull depths for Rock House Cove vary from 2.4 to 5.1 m (Figure 33b). On average the Rock House Cove estimates are slightly smaller in magnitude than those of Bull Canyon (but generally within the error range), and they do not show a consistent decreasing trend through the section.

The paleoslope (S) calculation provides insight into the slope of the streambed at the time of sediment deposition. The formula used to calculate paleoslope was (Paola and Mohrig, 1996):

$$S = R\tau^{*}(d50/H) \tag{2}$$

where R is the submerged specific gravity quartz (1.65), τ^{*} is the shield stress (1.0 for sand bedload and 0.4 for gravel bedload – 1.0 was used for these calculations), and d50 is the median grain size of bedload material. The d50 was estimated for each DU based on the grain size in sandstone cross-sets near the base of channels, lag deposits were excluded. This estimation is very likely an under-represented source of uncertainty in the present dataset; more thorough d50 measurements would improve the results. This calculation produces a dimensionless quantity, but was converted to degrees for the graphs in Figures 32b and 33b. The dimensionless quantity was used in the following equations.

The calculated paleoslopes for Bull Canyon indicate that the system had a low gradient, slopes of 6 x 10^{-5} (0.003°) to 3 x 10^{-4} (0.02°) (Figure 32b). Typical toe-to-apex slopes in modern distributive fluvial systems are between 6 x 10^{-5} (0.003°) and 2.6 x 10^{-2} (1.5°) (Hartley et al., 2010). A distinct change in the calculated slope occurs in the middle of the John Henry Member. On average, the calculated paleoslopes for Rock House Cove are slightly higher than those at Bull Canyon (Figure 33b), which is typical of a more proximal location on a graded stream profile. At both Rock House Cove and Bull Canyon, the paleoslopes in the lower half (DU-0 through DU-3) are relatively low and fairly consistent (perhaps showing a slight vertically decreasing trend at Bull Canyon), whereas, paleoslopes in the upper half (DU-4 through DU-6) are larger by ~ 0.01 degrees and increase vertically.

The square of the Froude number, or Froude squared (Fr^2), and backwater length (Lw) parameters provide insight into the interaction of upstream normal flow and downstream base level. Froude squared is calculated from the drag (Cd) and depth averaged velocity (U) using:

$$Cd = (d50/H)^{1/6} \text{ (Hajek and Wolinsky, 2012) (3)}$$

$$U = \sqrt{t/Cd} \text{ (Hajek and Wolinsky, 2012) (4)}$$

$$Fr^2 = (U/\sqrt{g*H})^2 \text{ (Parker, E-book) (5)}$$

where t is the kinematic shear stress (= stress / fluid density; $(m/s)^2$) and g is gravitational acceleration (9.8 m/s). Far upstream $Fr^2 \approx 1$ and the flow depth is determined by the discharge and topography. Far downstream $Fr^2 \approx 0$ and the water surface is impacted by

the downstream base level (Sturm, 2001). In the transition zone, located between the two end members listed above, $Fr^2<<1$ and flow is influenced by upstream discharge, topography, and downstream base level (i.e., within the backwater curve) (Figure 34). This backwater transitional zone is the length of a channelized flow that is included in the backwater curve, where flow "feels" the impact of the base level causing the slope of the water surface to be less than the channel bed slope (Chanson, 2004).

The calculations of Fr^2 are all quite low in Bull Canyon (0.03 to 0.07) and Rock House Cove (0.05 to 0.09) (Figure 33c and 34c). Fr^2 numbers are much closer to 0 than 1, which indicates that these locations may be within the backwater transition zone. There is a trend of increasing Fr^2 numbers vertically through the section at Bull Canyon; the most dramatic increase occurs above DU-3. The Fr^2 numbers for Rock House Cove are relatively consistent with the exception of DU-3, which is slightly larger than the others (although error bars are large: Figure 33c).

The backwater length (Lw) scales with the backwater transition zone (backwater transition zone $\approx$ 3Lw) (Hajek and Wolinsky, 2012). The formula used to approximate the backwater length is (Paola and Mohrig, 1996):

$$Lw = H / S \tag{6}$$

where H is upstream "normal flow" depth. In order for this calculation to be accurate the input data must be from a location upstream from the bayline (or landward of the transition zone) (Strum, 2001; Chanson, 2004). This formula will overestimate the backwater length if H is taken from within the transition zone.

Calculations of Lw for Rock House Cove range from 10-36 km and show a trend of vertically decreasing backwater length, with the exception of DU-0 (Figure 33d). Lw calculations at Bull Canyon show a greater degree of variability. Calculated Lw of DU-4 through DU-6 at Bull Canyon (4-14 km) are roughly equivalent to the upper DUs at Rock House Cove (Figure 32d). However, Lw lengths for DU-0 through DU-3 at Bull Canyon (75-97 km) are dramatically larger than those of the upper half of Bull Canyon and the entirety of Rock House Cove.

Within the transition zone, bankfull channel depths should increase downstream as the surface gradient diverges from the channel bed slope (Strum, 2001; Petter, 2010), which causes the paleoslope calculation to predict increased Lw lengths downstream. This may explain the variations between calculations of Lw in the lower half of Rock House Cove and Bull Canyon. Assuming dominant eastward sediment transport, the distances from the John Henry Member at Rock House Cove and Bull Canyon to the landward pinchouts of correlative shorelines (i.e., the pinchout of the C sandstone) are ~55 km and ~35 km respectively (Allen, 2009; Dooling, in prep). The locations of shoreline pinchouts are variable within the John Henry Member, but the pinchouts are all within a ~15 km zone that is roughly parallel to Fiftymile Mountain (Allen, 2009). The distances from Rock House Cove and Bull Canyon to the shorelines are less than the transition zone predicted by Lw calculations from Rock House Cove; however, the measured distance to the shoreline is not necessarily equivalent to the actual distance to where the fluvial system interacted with the shoreline. The presence of tidal indicators in lower portions at both locations would support the interpretation that deposition occurred within the backwater transition zone, for at least some period of time (Gooley, 2010).

Sedimentary Petrology

Petrographic analysis consisted of point counting 20 samples that were collected, at roughly even spacing, from just below the base of the John Henry Member up to the base of the Drip Tank Member in medium grained sandstones. Point counts for each sample included a minimum of 500 grains consisting of monocrystalline quartz (Qm), polycrystalline quartz (Qp), chert (Cht), potassium feldspar (K), plagioclase (P), and miscellaneous grains. Subcategories of the miscellaneous grains category include lithic carbonate (Lc), sedimentary lithic fragment (Ls), volcanic lithic clasts (Lv), and metamorphic lithic clasts (Lm) (these data are included in Appendix F). The data were plotted on standard ternary diagrams (Figure 35), QmFLt diagram with provenance fields (Dickinson, 1985) and QtFLu diagram with sandstone classification fields (Pettijohn, 1975). The end members of the QmFLt diagram include Qm, F (feldspar, K+P), and Lt (total lithic fragments, Lc+Ls+Lm+Lv+Cht+Qp) and the end members of the QtFLu diagram are Qt (total quartz, Qp+Qm+Cht), F, and Lu (unstable grains; Lc+Ls+Lm+Lv).

The presence of detrital carbonates (Lc) is characteristic of many foreland basins (Dickinson, 1985); however, they are typically not recalculated with other lithic grains in QtFLu and QmFLt diagrams due to the difficulty in distinguishing between extrabasinal or intrabasinal origin and their different geochemical responses to weathering and diagenesis (Mack, 1984). In this study, lithic carbonates were included in lithic counts because intrabasinal carbonates are not a concern due to the location of the study area proximal to the orogenic belt in terrestrial (fluvial) strata. However, weathering and diagenesis may have an impacted their concentration.

The two samples from the Calico bed of the John Henry Member are quartz arenites (98-99% Qt) and plot within the craton interior field of the QtFLu diagram (Figure 35b). Samples from the John Henry Member are generally sublithic arenites or lithic arenites and fall within the recycled orogen field of the QtFLu diagram (Figure 35a). The compositions of John Henry Member samples are typical of fold-thrust systems (Dickinson and Suczek, 1979; Dickinson, 1985). The Calico samples are more Qt rich and poor in Lu and F than expected in this tectonic setting, although interstratified petrofacies with highly variable and contrasting Qm/Lt and Qt/Lu ratios have been documented in foreland basins sequences (Putnam, 1982). The differences in composition between the Calico bed and the John Henry Member may be attributed to either different proportions of recycled quartzose sand derived from the orogenic terranes or contrasting climatic/weathering influences.

The percentage of lithic grains increases from the base to the middle of the John Henry Member (DU-0 to DU-3), and then gradually decreases vertically through the rest of the member. This trend is primarily due to the abundance of Lc (up to 28%) in the middle of the member (DU-3 and DU-4) compared to the upper and lower sections (0-14% Lc). A similar, though more pronounced, trend was documented in Rock House Cove (Gooley, 2010). The increase in lithic carbonates in the middle of the John Henry Member may have been caused by the exposure of Paleozoic rocks in the upper plate of the Blue Mountain thrust sheet of the Sevier orogenic belt (Fillmore, 1991; Goldstrand, 1992) or by differences in preservation potential in the middle depositional units.

Figure 13 – Lithofacies photos. A) Ripple cross-laminated sandstone (Sr) and massive siltstone/mudstone. B) Bioturbated sandstone (Sb), coal (C), and horizontally laminated sandstone (Sh). C) Trough cross-stratified sandstone (St). D) Convolute sandstone. E) Massive sandstone (Sm) and massive grain supported mud rip-up clast conglomerate. F) Grain and matrix supported cross-stratified conglomerate. G) Matrix and grain supported conglomerate (Gmm and Gcm). H) Massive siltstone/claystone (Fm), carbonaceous shale (Fc), and coal (C).

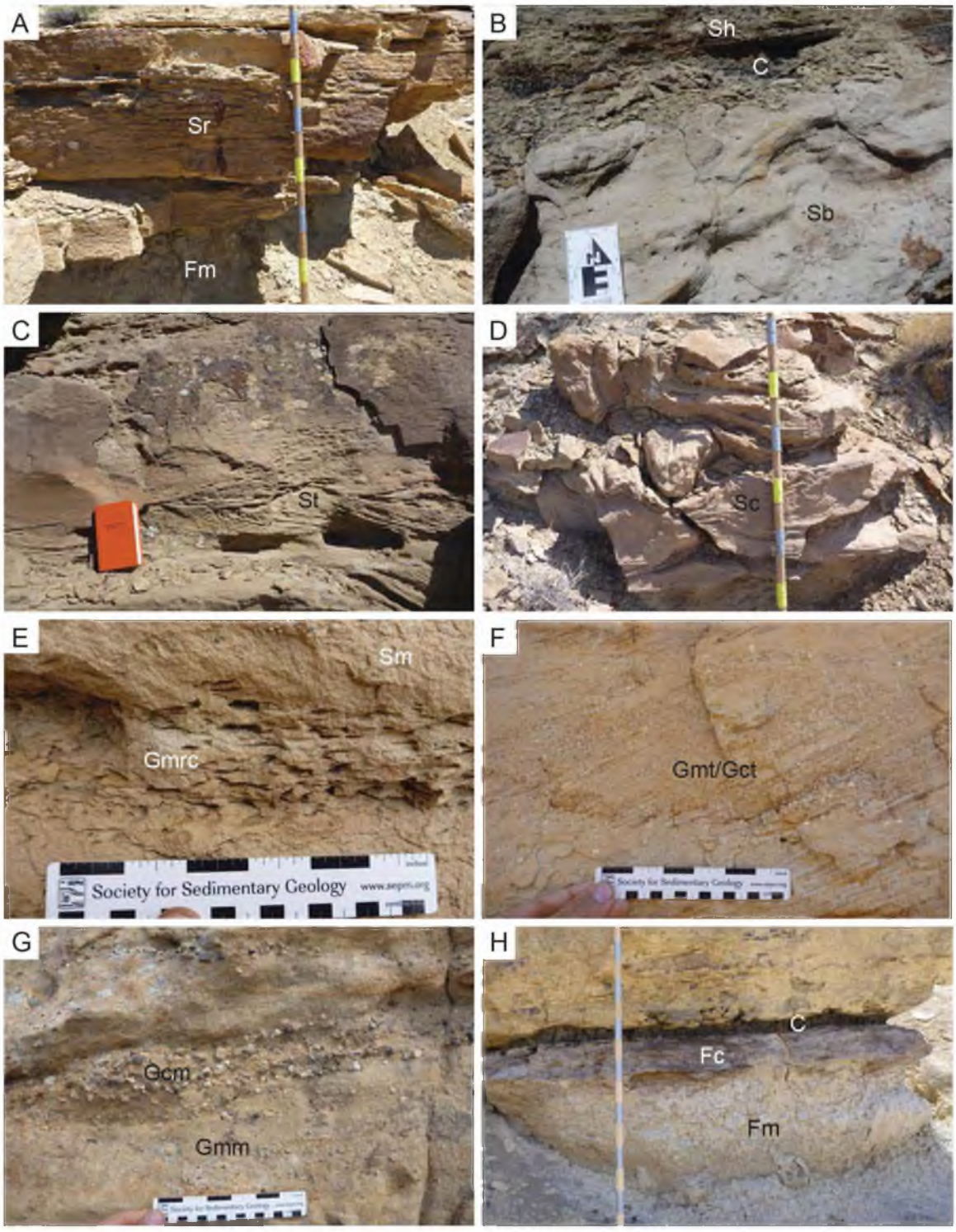
A
Sr
Fm
B
Sh
C
Sb
C
St
D
Sc
E
Sm
Gmrc
Society for Sedimentary Geology
F
Gmt/Gct
G
Gcm
Gmm
H
C
Fc
Fm

Figure 14 – Distribution of lithologies within depositional units (DU-0 through DU-6) and members (SHM = Smoky Hollow Member; DTM = Drip Tank Member). The lithologic information documented in the measured sections (Figure 7) was divided into five categories based on grain size: sandstone, interbedded sandstone and siltstone, siltstone/mudstone, coal, and covered (undefined lithology). The thicknesses of the columns are scaled to the average thickness of each depositional unit.

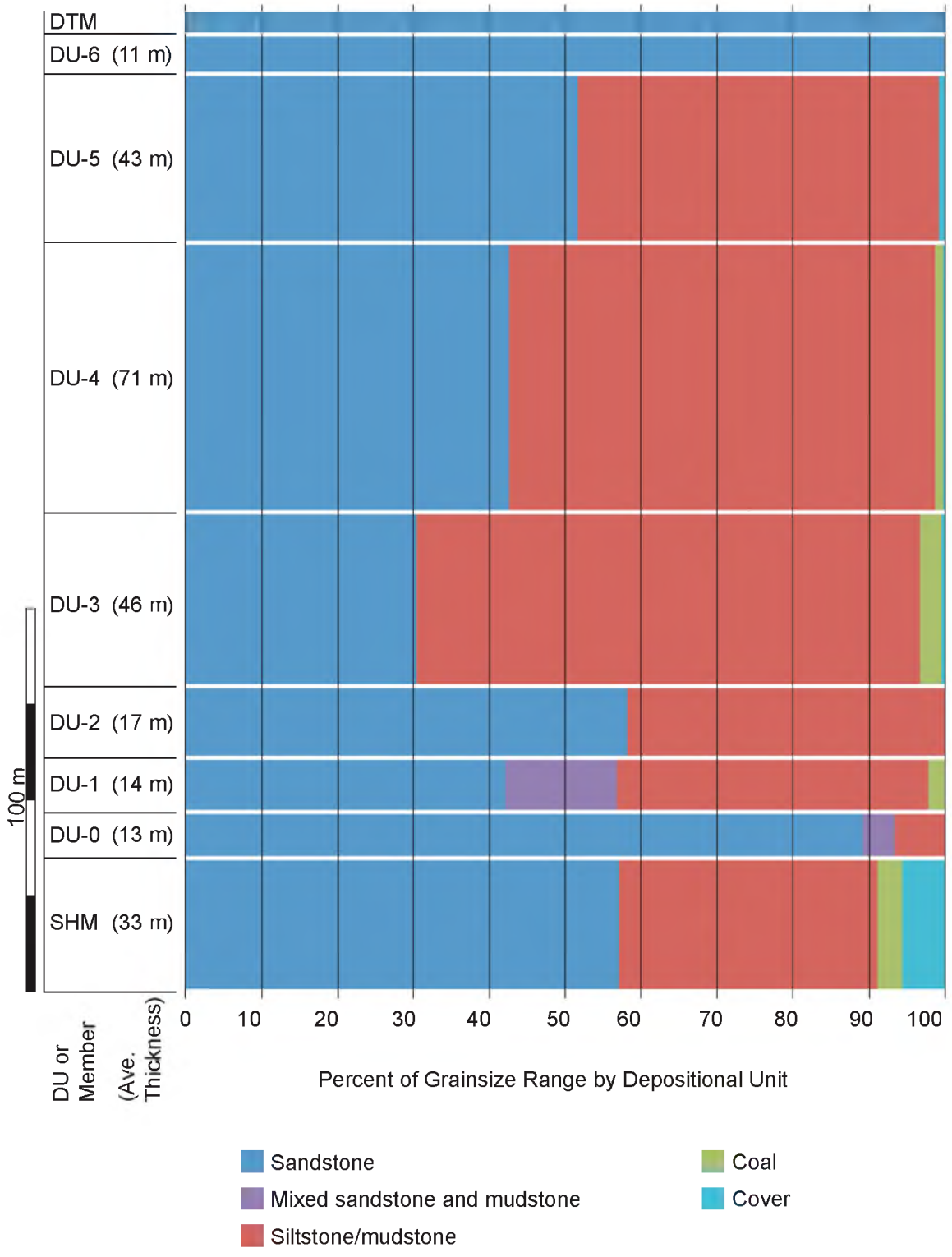
DTM
DU-6 (11 m)
DU-5 (43 m)
DU-4 (71 m)
DU-3 (46 m)
DU-2 (17 m)
DU-1 (14 m)
DU-0 (13 m)
SHM (33 m)
100 m
DU or Member (Ave. Thickness)
0
10
20
30
40
50
60
70
80
90
100
Percent of Grainsize Range by Depositional Unit
Sandstone
Mixed sandstone and mudstone
Siltstone/mudstone
Coal
Cover

Figure 15 – Photos of the facies associations. A) Coal mire facies association. B) Floodplain facies association. C) Meandering (and anastomosing) fluvial facies association. D) Braided fluvial facies association. E) Tidally-influenced fluvial facies association.

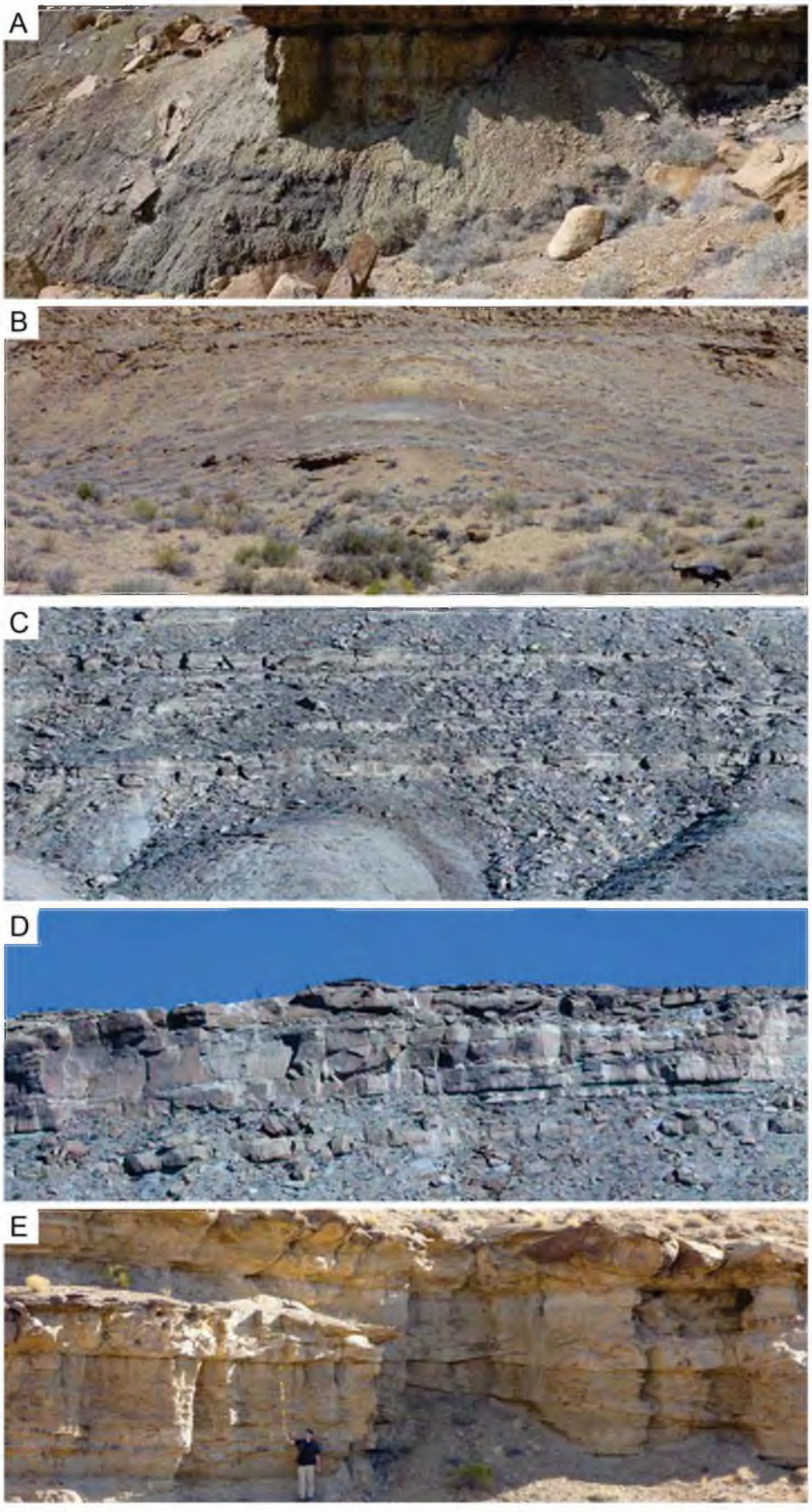
A
B
C
D
E

Figure 16 – Body fossils and biologic structures. A) Gymnosperm needles and unidentified plant fragments. B) Petrified wood. C) Root traces in channel sandstone. D) Root traces in siltstone. E) Angiosperm leaf in carbonaceous shale. F) Angiosperm leaf in siltstone; G) Bivalve shell fragments. H) Shell and bone fragments in a sandstone channel lag deposit.

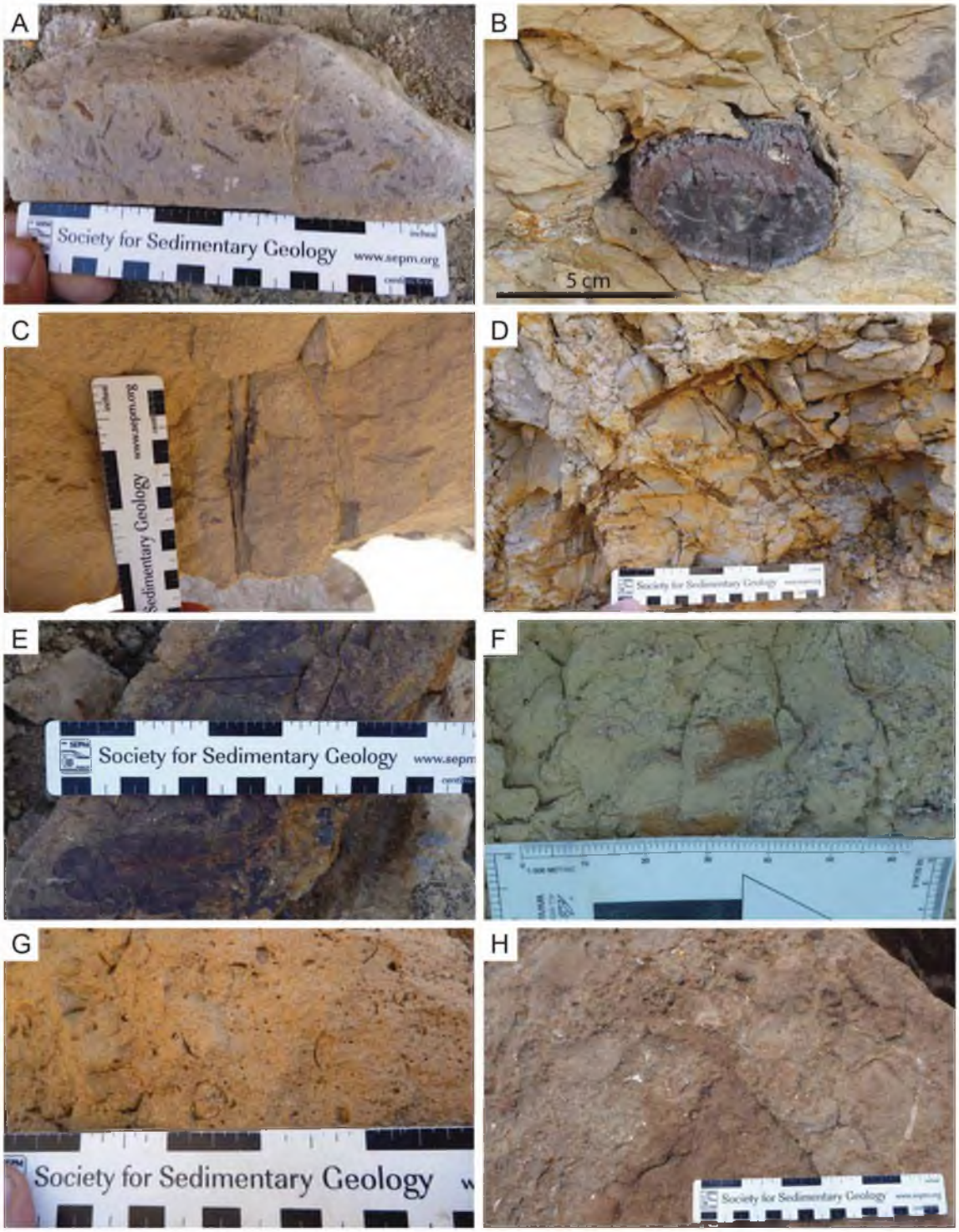
A
Society for Sedimentary Geology
www.sepm.org
B
5 cm
C
Sedimentary Geology
D
E
Society for Sedimentary Geology
F
G
Society for Sedimentary Geology
H

Figure 17 – Trace fossils. A) Large *Thalassinoides*. B) small *Thalassinoides*. C) *Planolites*. D) *Rhizocorallium*? E) highly bioturbated sandstone (bioturbation index 5). F) *Teredolites*. G) Lined *Skolithos* and *Planolites*. H) *Skolithos*.

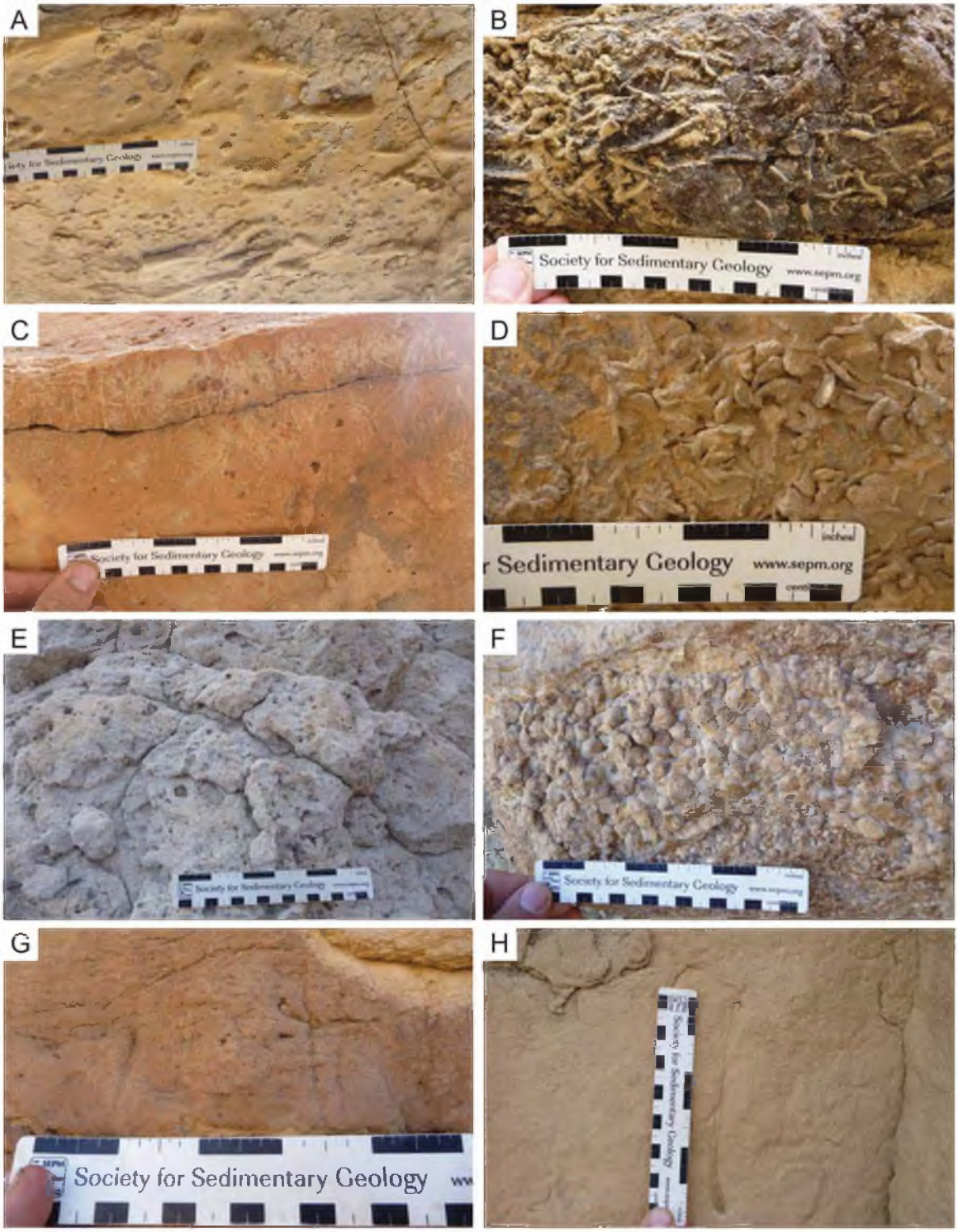
A
B
Society for Sedimentary Geology
C
Society for Sedimentary Geology
D
Sedimentary Geology
www.sepm.org
E
F
Society for Sedimentary Geology
G
Society for Sedimentary Geology
H

Figure 18 – Paleocurrent and barform accretion direction measurements from Bull Canyon grouped by depositional unit and member. Figure 10 includes a description of these graphs.

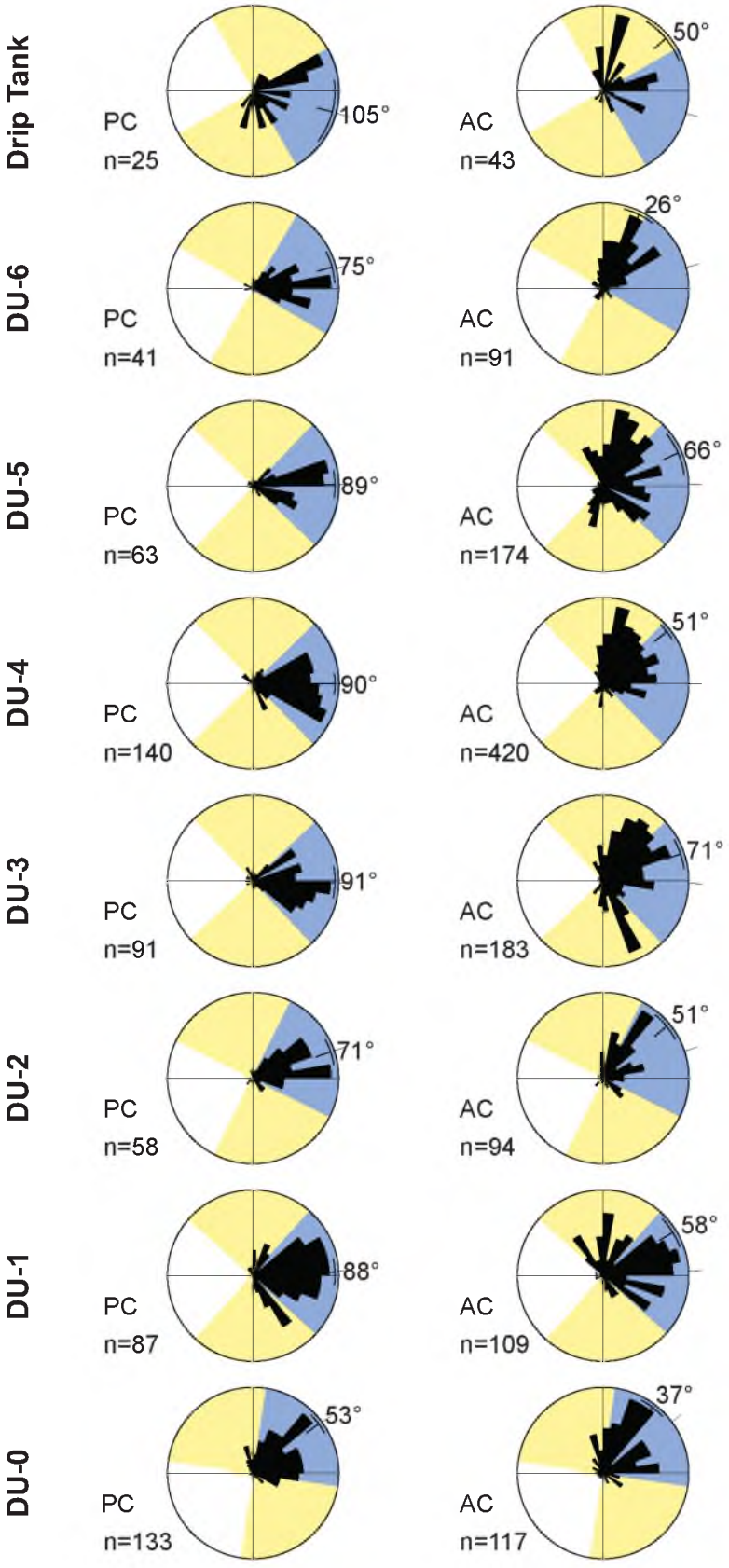
Drip Tank
PC
n=25
105°
AC
n=43
50°
DU-6
PC
n=41
75°
AC
n=91
26°
DU-5
PC
n=63
89°
AC
n=174
66°
DU-4
PC
n=140
90°
AC
n=420
51°
DU-3
PC
n=91
91°
AC
n=183
71°
DU-2
PC
n=58
71°
AC
n=94
51°
DU-1
PC
n=87
88°
AC
n=109
58°
DU-0
PC
n=133
53°
AC
n=117
37°

Figure 19 - Channel belt width and thickness. The average (ave), standard deviation (SD), and number of measurements are listed for each DU. Colored boxes represent the averages for each depositional unit (DU). The blue lines represent moving averages (with a range of five). A) True (corrected) channel belt widths in stratigraphic order (see Figure 12). B) Channel belt thicknesses in stratigraphic order.

A) Channel Belt Widths

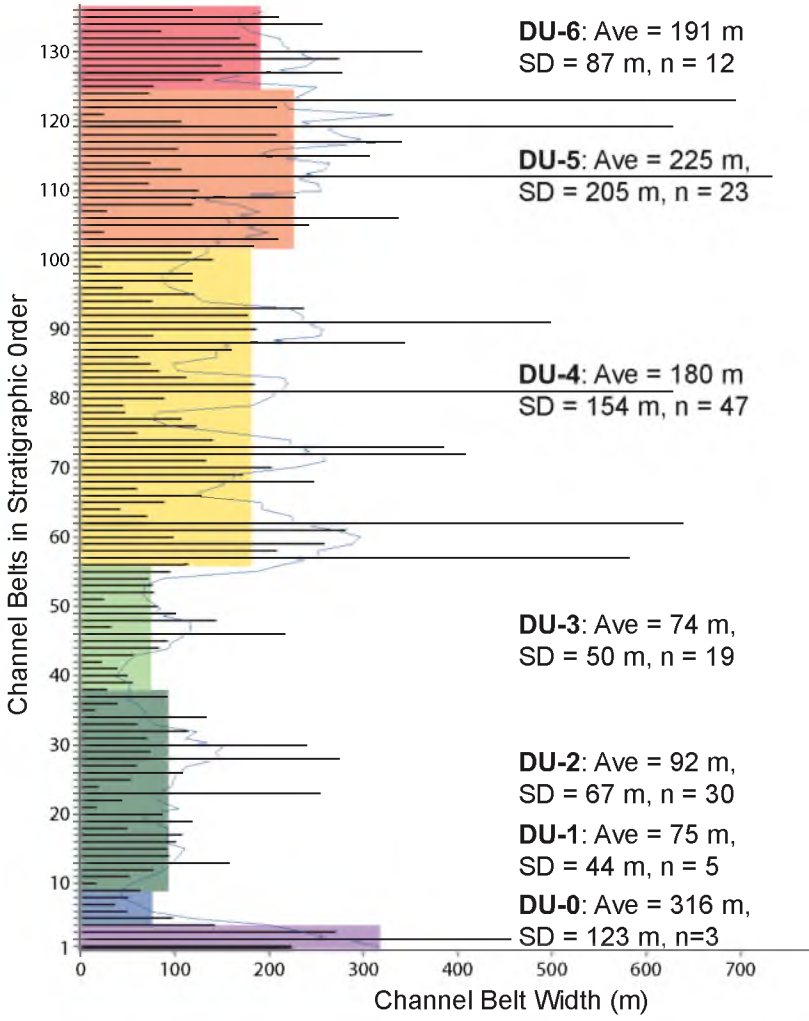

B) Channel Belt Thicknesses

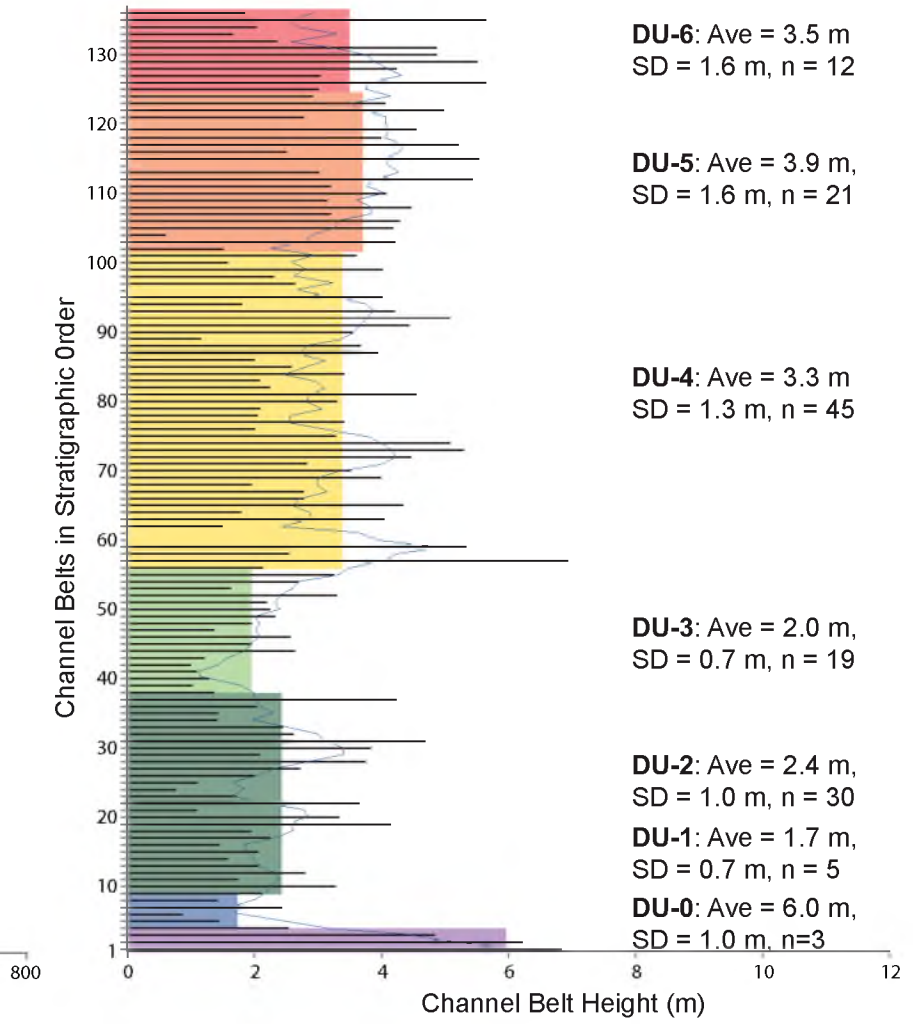

Figure 20 – Cross plots of channel belt dimensions. A) Width-to-thickness ratios (W/T) of channel belts are displayed in stratigraphic order. The W/T ratios were calculated, using the measurements from the GPS dataset, and dividing the width by the thickness (channel belt width/channel belt thickness). B) Cross plot of channel belt widths and thicknesses. Measurements of channel belt width and thickness are from the GPS dataset.

A)

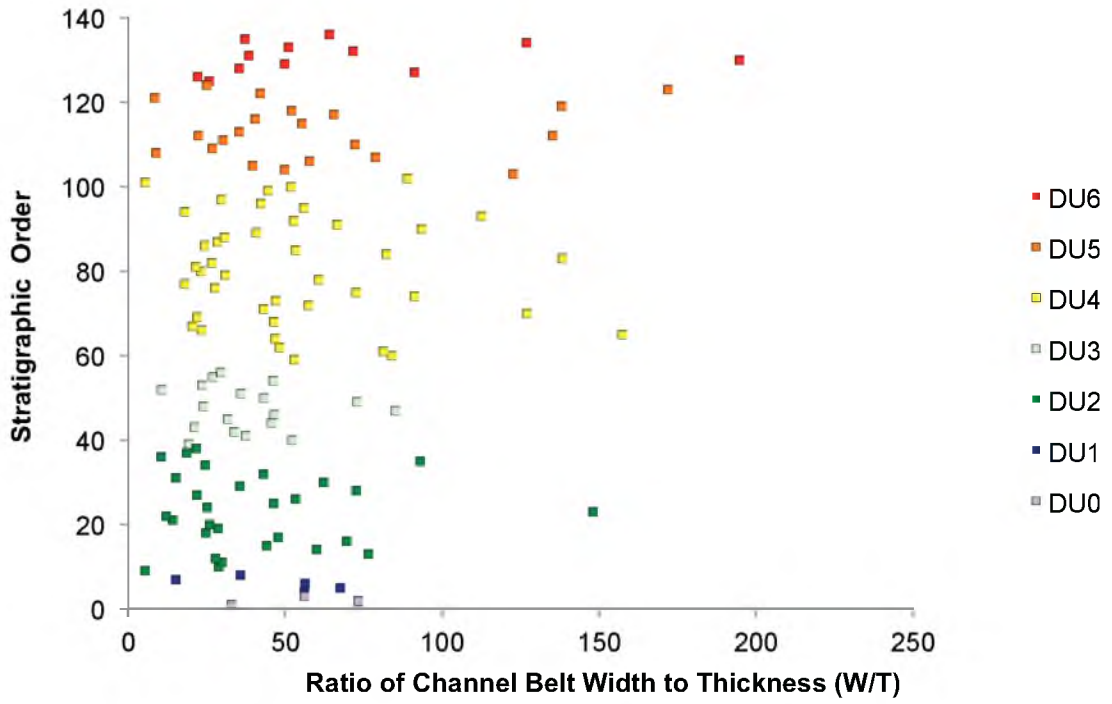
Stratigraphic Order
0
20
40
60
80
100
120
140
0
50
100
150
200
250
Ratio of Channel Belt Width to Thickness (W/T)
DU6
DU5
DU4
DU3
DU2
DU1
DU0

B)

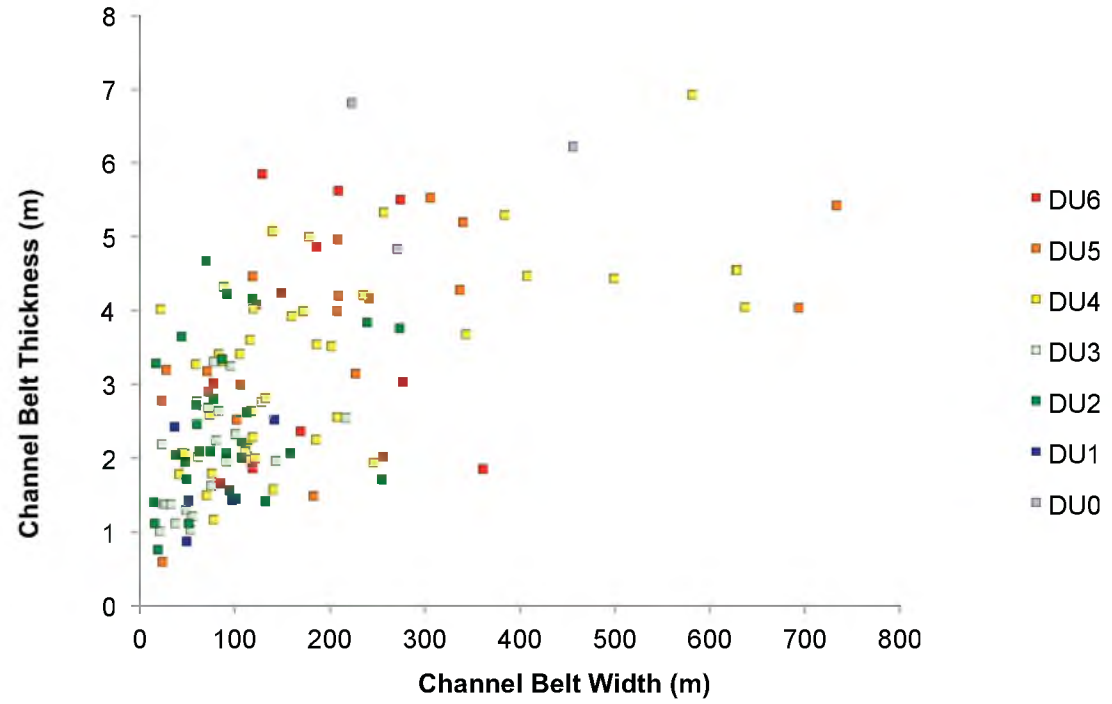
Channel Belt Thickness (m)
0
1
2
3
4
5
6
7
8
0
100
200
300
400
500
600
700
800
Channel Belt Width (m)
DU6
DU5
DU4
DU3
DU2
DU1
DU0

Figure 21 – Vertical and lateral channel belt offsets. A) Graph of the vertical and lateral offsets between channel belt centers in the stratigraphic order assigned within each depositional unit. A moving average of horizontal offsets with a range of five (MA Horizontal) is also included. B) List of the average (ave), median (med), and standard deviation (STDEV) for the change in vertical (dy) and lateral (dx) offsets between channel belts.

A) Vertical and lateral offset of channel belts

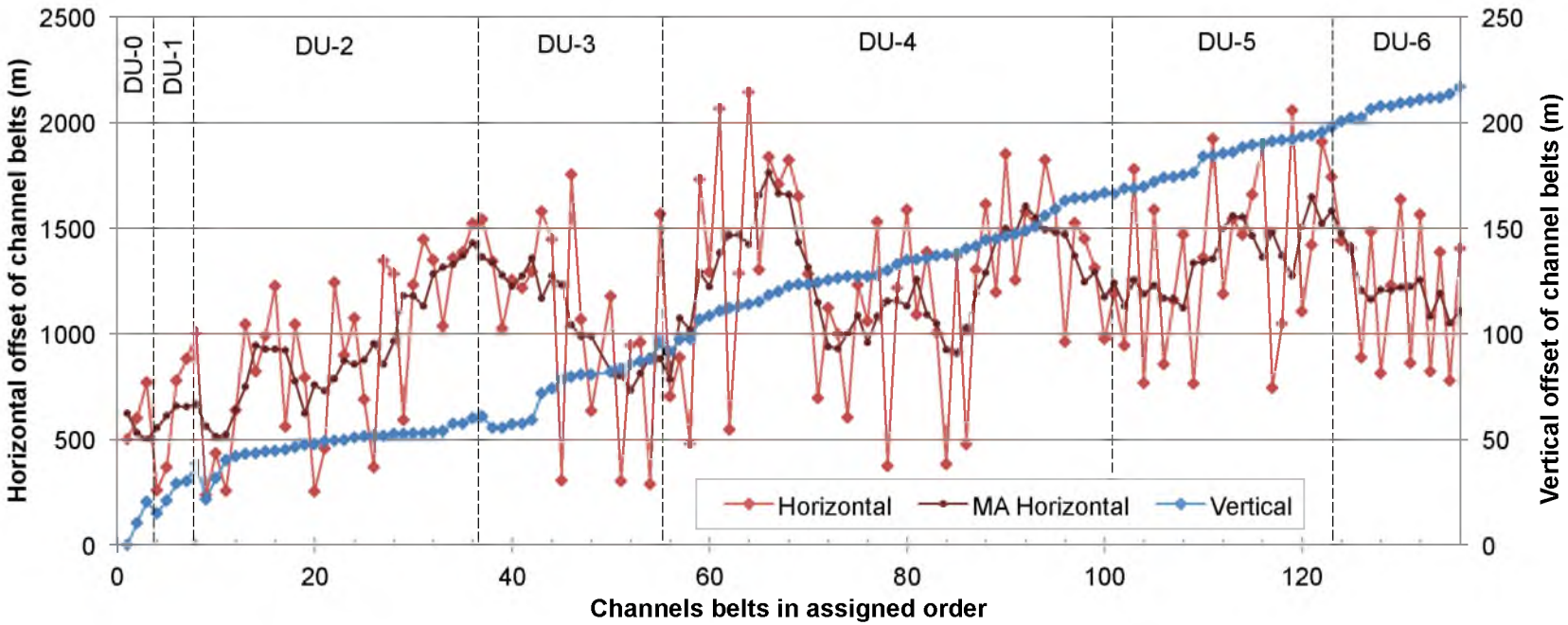

B) Average vertical (y) and lateral (x) offset of channel belts

DU	n=	Ave dx	Med dx	SDEV dx	Ave dy	Med dy	STDEV dy
DU-6	12	555.7	603.9	200.0	1.4	1.3	1.3
DU-5	24	525.5	421.0	318.3	1.4	1.2	1.6
DU-4	45	522.6	439.0	330.2	1.8	1.2	1.8
DU-3	17	530.2	433.1	442.5	2.7	1.6	3.2
DU-2	30	344.8	283.5	247.3	2.1	0.7	3.8
DU-1	5	251.4	122.4	194.5	5.7	5.9	2.8
DU-0	3	133.8	133.8	50.0	10.1	10.1	0.4

Figure 22 – Channel belt amalgamation index. Each channel belt was assigned a number for both vertical and lateral amalgamation: 0 = not amalgamated, 1 = amalgamated on one side, or on either the top or base, 2 = amalgamated on both sides, or the top and the base. The average vertical and lateral amalgamation index numbers for each depositional unit are displayed.

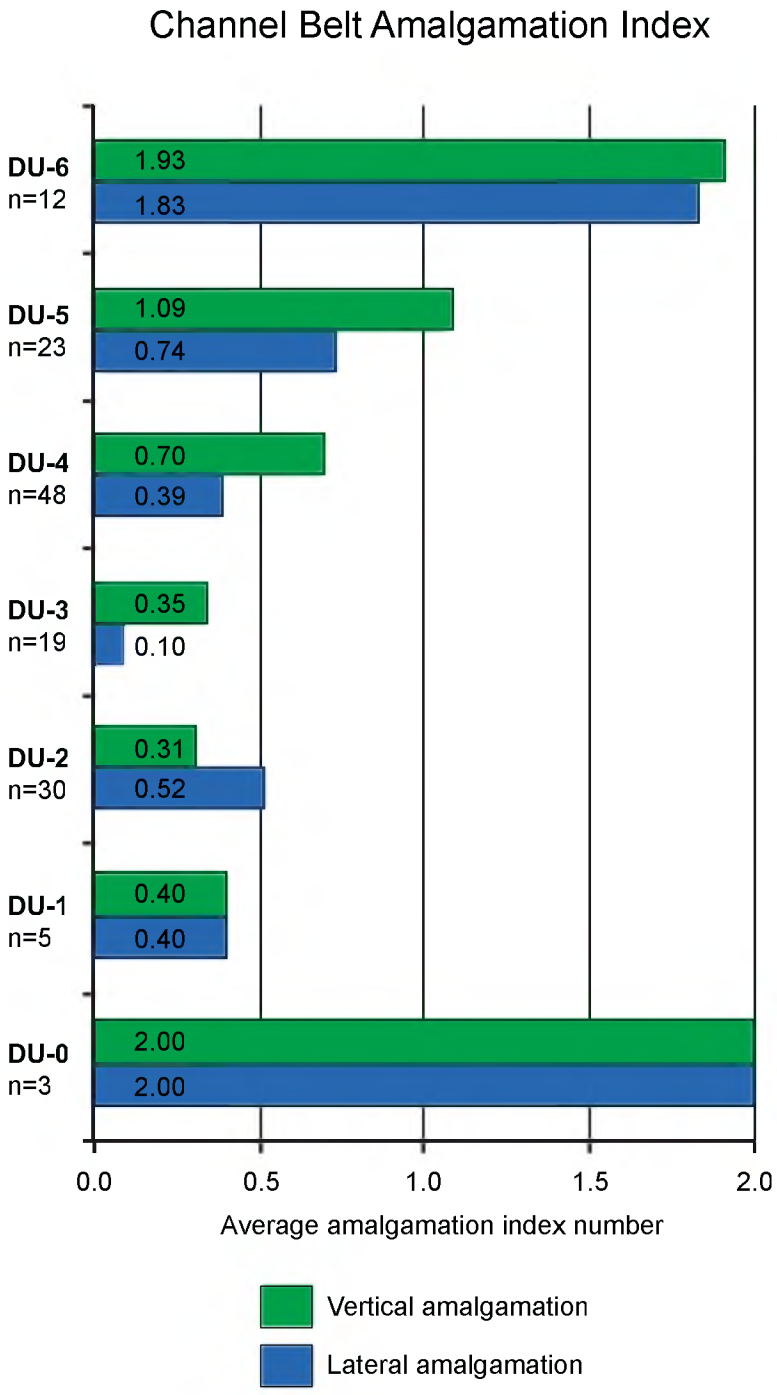
Channel Belt Amalgamation Index
DU-6
n=12
1.93
1.83
DU-5
n=23
1.09
0.74
DU-4
n=48
0.70
0.39
DU-3
n=19
0.35
0.10
DU-2
n=30
0.31
0.52
DU-1
n=5
0.40
0.40
DU-0
n=3
2.00
2.00
0.0
0.5
1.0
1.5
2.0
Average amalgamation index number
Vertical amalgamation
Lateral amalgamation

Figure 23 - Summary plate of the Smoky Hollow Member (SHM). On the left, an example section of the SHM that shows the base of the Calico bed in green. On the right, photos: A) The entire Smoky Hollow Member section is shown between the blue line and the green line, which marks the base of the Calico bed. B) The thickest exposure of the calico bed; located near the mouth of Bull Canyon. The blue line marks the top of the Smoky Hollow Member and the green line marks the base of the Calico bed. C) Bleached, very coarse- to medium-grained sandstone of the Calico bed with chert and quartzite gravel. D) Bleached, coarse-grained sandstone of the Calico bed. E) *Teredolites* from near the base of the Calico bed. The staff is marked with 10 cm increments. F) Ripple cross lamination (Sr) at the base of a sandstone bed near the base of the Calico bed. G) The top of the coal zone and transition to the barren zone at the base of the sandstone. The staff is marked with 10 cm increments. H) Angiosperm leaves in carbonaceous shale from the coal zone.

55
50
45
40
35
30
25
C,D
E,F
Calico
G,H
C
A
B
C
D
E
F
G
H
ociety for Sedimentary Geology
Society for Sedimentary

Figure 24 - Summary plate of DU-0. On the left, an example section through DU-0. On the right, photos: A) Contact between Smoky Hollow (Calico bed) and John Henry Member (DU-0) at the transition from bleached to caramel color sandstone. White arrows point to the member contact. B) Erosive contact between the Calico bed of the Smoky Hollow and DU-0 of the John Henry Member indicated by white arrows. C) Large downstream accreting bar. D) Steeply inclined forests and scours from a downstream accreting bar. E) Inclined heterolithic strata from a muddy bar located in the middle of the DU-0. F) Laterally accreting point bar. G) Two stories of lateral accreting point bars. H) Very-coarse sand and gravel from DU-0.

80
75
70
C, D
E
F, G
H
f
c
A
John Henry Member
Calico bed
B
C
D
E
F
G
H

Figure 25 - Summary plate of DU-1. On the left, an example section through DU-1. On the right, photos: A) Exposure of tidally influenced channel belts and laminated and carbonaceous shale, interpreted as lake/pond deposits. B) Inclined heterolithic strata from a muddy bar. C) Horizontally laminated and massive siltstone and carbonaceous shale capped by channelized sandstones. D) Carbonaceous shale drapes. E) Paired mud/sandstone couplets (double mud drapes?). F) Sigmoidal sandstone. G) *Thalassinoides* in a tidally influenced channel belt sandstone. H) Bivalve shells and small burrows in a channel sandstone.

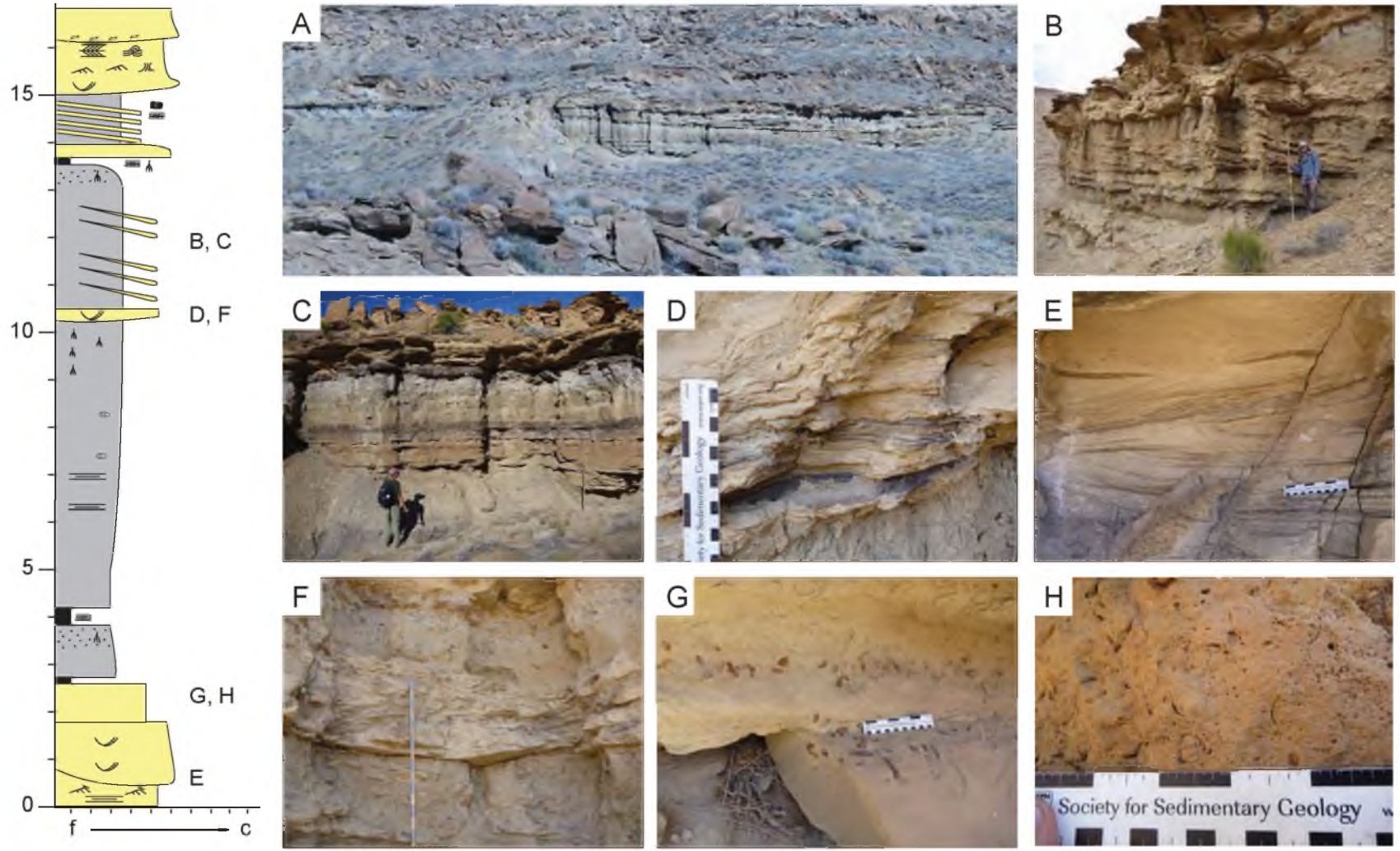
15
10
5
0
B, C
D, F
G, H
E
f
c
A
B
C
D
E
F
G
H
Society for Sedimentary Geology

Figure 26 - Summary plate of DU-2. On the left, an example section through DU-2. On the right, photos: A) Crevasse splay deposits capped by a channel belt complex, interpreted as a crevasse splay delta. B) Trough cross-stratified sandstone. C) Thick assemblage of ripple cross-stratification that includes climbing ripples. D) Carbonaceous shale under channelized sandstone. E) Carbonaceous shale. F) Flaser bedding. G) Lateral point-bar accretion.

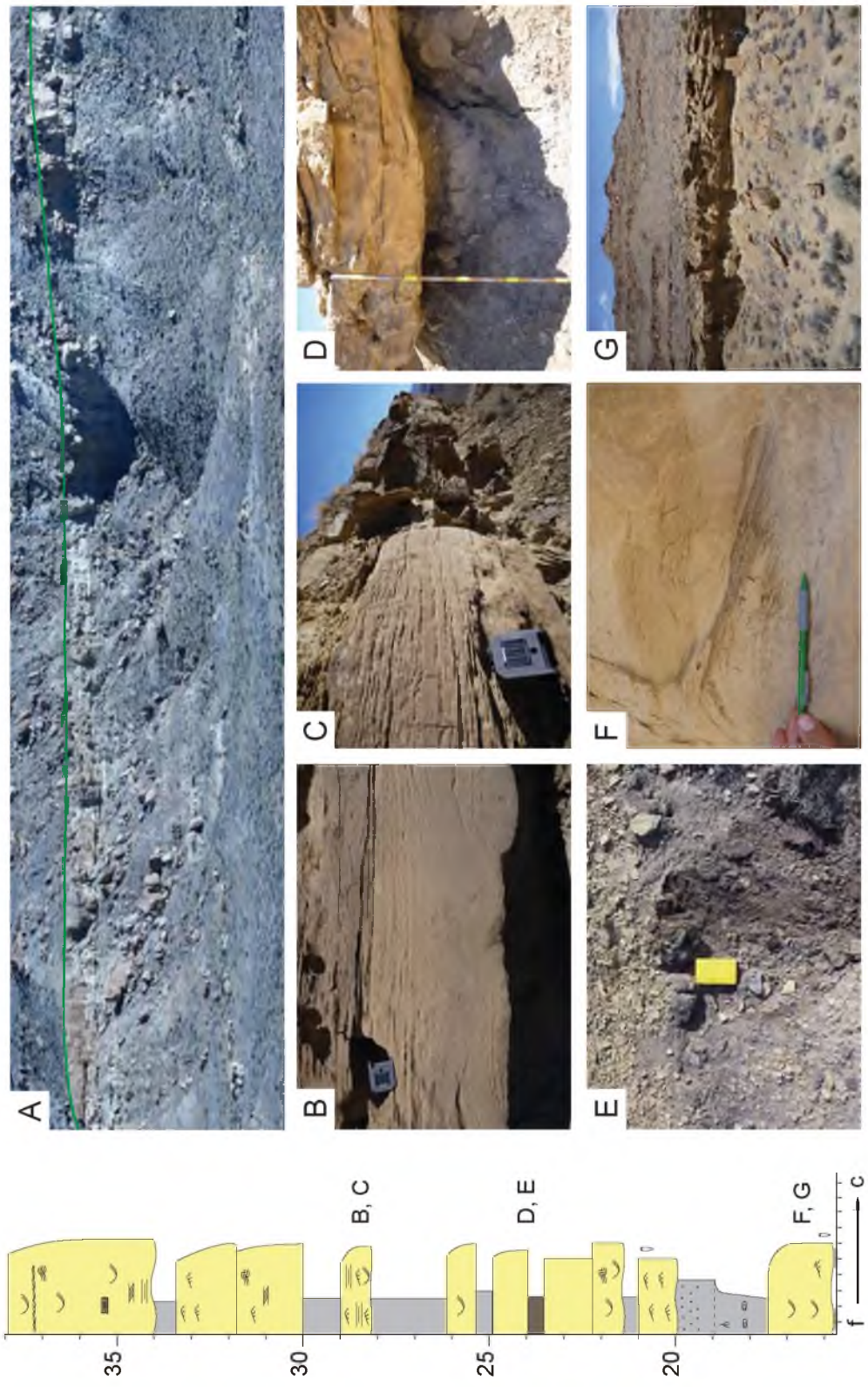
A
B
C
D
E
F
G
B, C
D, E
F, G
35
30
25
20
f
c

Figure 27 - Summary plate of DU-3. On the left, an example section through DU-3. On the right, photos: A) Thick accumulations of floodplain fines and coal mire facies, with few channelized deposits. The green line marks that top of DU-3. B) Variegated fine grain deposits with occasional thins crevasse play sandstones. C) Root haloes at the top of a crevasse splay deposit. D) Siderite nodule in siltstone/mudstone. E) Coal mire facies capped by channelized sandstone. F) Trough cross-stratified sandstone in a channel. G) Ripple and horizontally laminated sandstone. H) Asymmetric ripples (and climbing ripples) in a crevasse splay sandstone.

75
70
65
60
55
50
45
40
C
D
E
F
G
f
c
A
B
C
D
E
F
G
H

Figure 28 - Summary plate of the DU-4. On the left, an example section through DU-4. On the right, photos: A) Panoramic photograph showing the channel belts of DU-4, located between the green lines. B) Abundant trough cross-stratification. C) Planar laminated sandstone. D) Lined *Skolithos* in a channel sandstone. E) *Skolithos* at the top of a channel fill. F) Bioturbation in rippled sandstone. G) Lag deposit with shell and bone fragments.

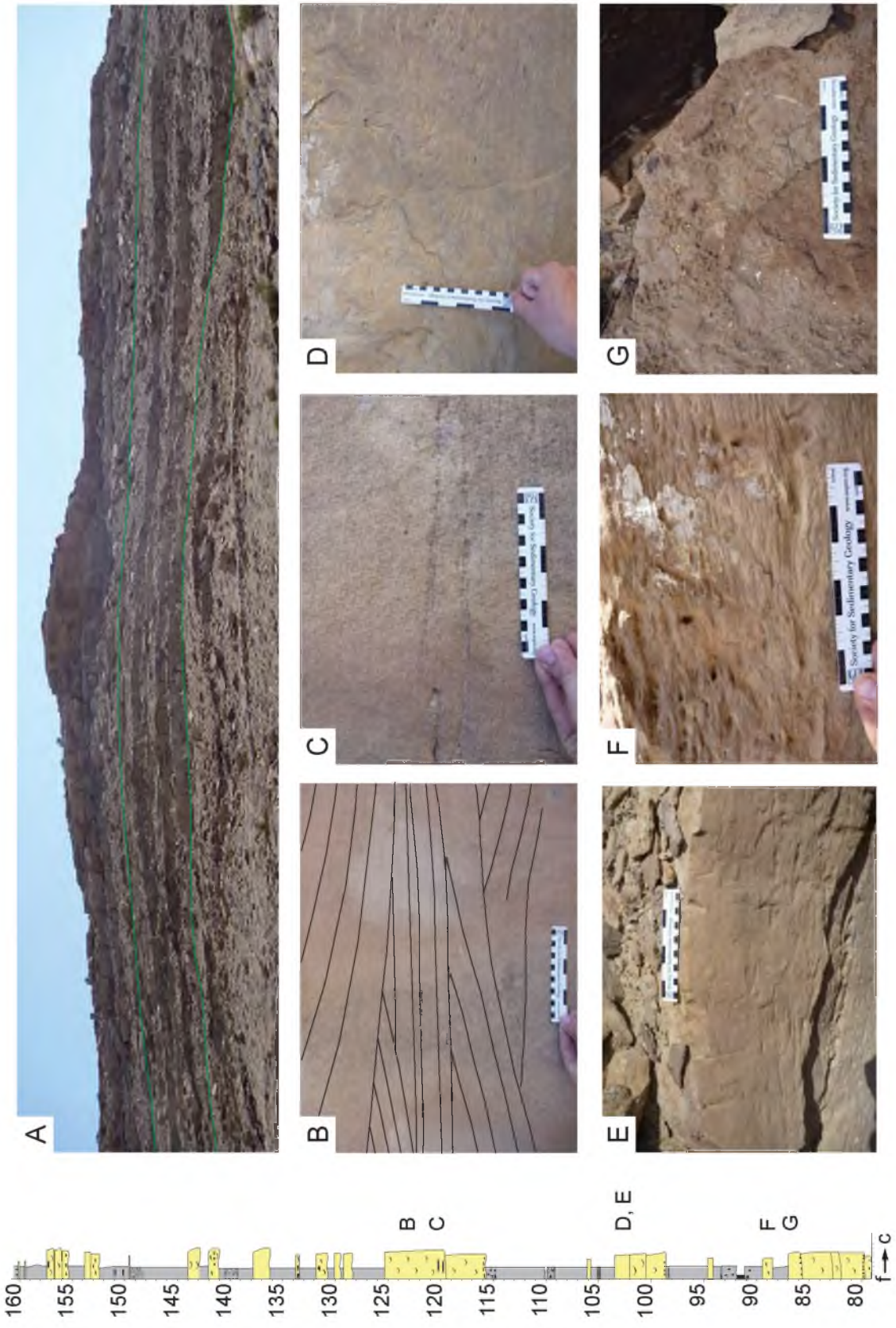
A
B
C
D
E
F
G
B
C
D, E
F
G
160
155
150
145
140
135
130
125
120
115
110
105
100
95
90
85
80
f→c

Figure 29 - Summary plate of the DU-5. On the left, an example section through DU-5. On the right, photos: A) Panoramic photograph showing the laterally extensive channel belts. B) Trough cross-stratified sandstone. C) Muddy toe sets of a bar, located at the base of a channel deposits. D) Convolute sandstone common at the bases of many of the channel belts. E) *Rhizocorallium*? located along the base of a channel sandstone. F) Climbing ripples in a splay deposit. G) Very coarse-grained sandstone and small pebbles in lags.

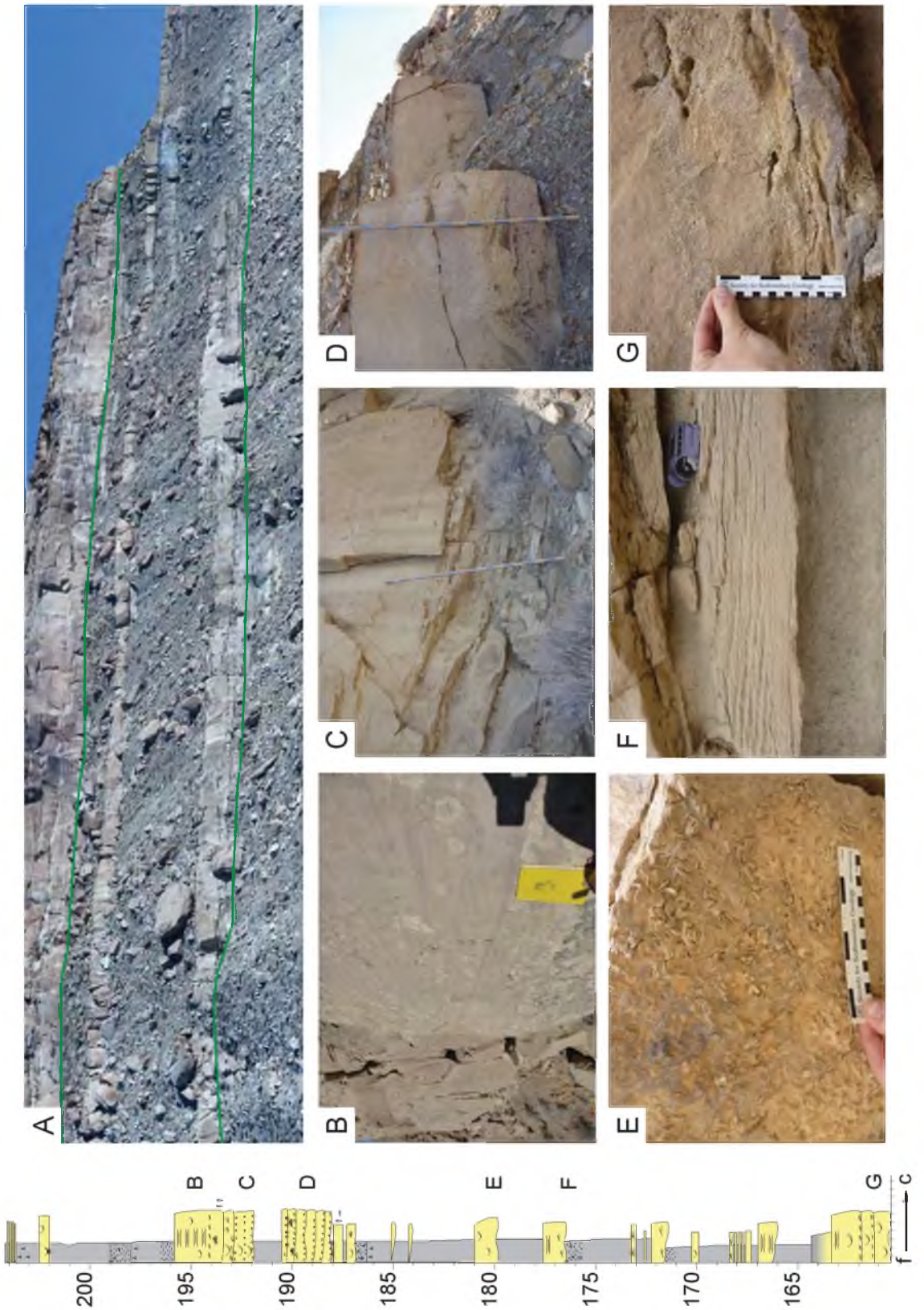
A
B
C
D
E
F
G
200
195
190
185
180
175
170
165
f
c

Figure 30 - Summary plate of the DU-6. On the left, an example section through DU-6. On the right, photos: A) Panoramic photograph of DU-6; the green line marks the based of DU-6 and the blue line marks the base of the Drip Tank Member. B) Amalgamated channel belts. One-meter increments marked in black and white. C) Matrix and grain supported conglomerates (Gmm and Gcm). D) Coarse-grained trough cross-stratification. E) *Teredolites*. F) Granules and mud rip-ups on large forests.

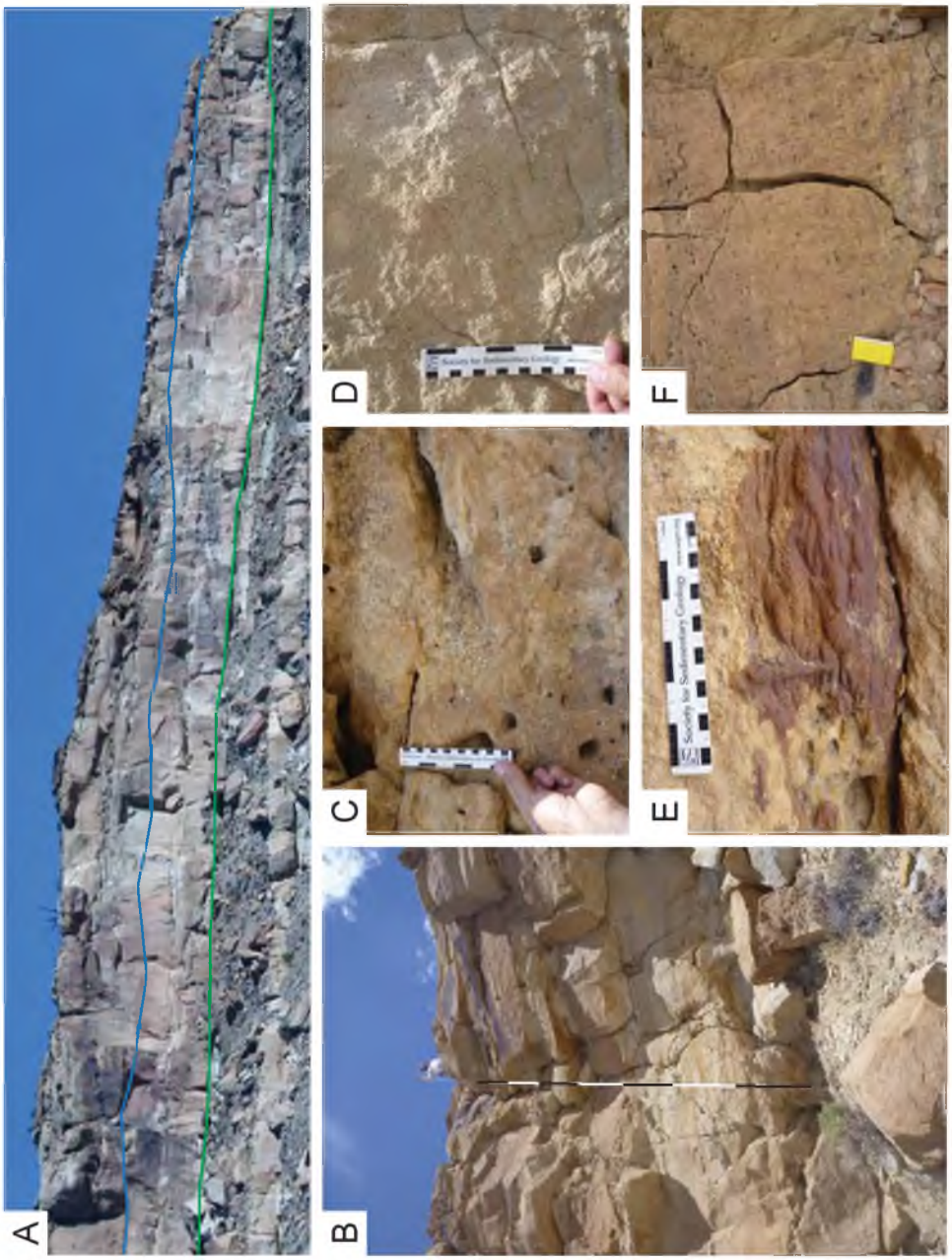
A
B
C
D
E
F

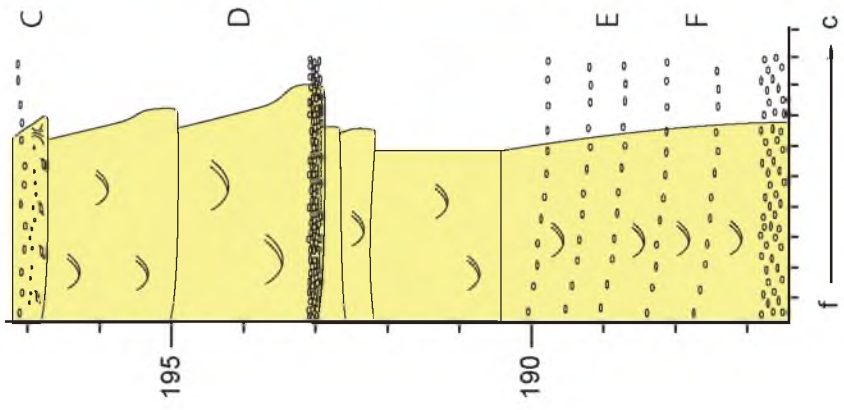
C
D
E
F
c
f
195
190

Figure 31 - Summary plate of the Drip Tank Member (DTM). On the left, an example section through the lower portion of the DTM. On the right, photos: A) Panoramic photo of the Drip Tank Member. White arrows point to the contact with the John Henry Member. B) Large dunes and downstream accreting barforms. C) Gravel bed about 0.5 m thick. D) Gravel lag (Gmm) at the base of the DTM. F) Coarse and very-coarse graded sandstone. G) ~2 m thick channel at the base of the DTM. G) The transition from lighter colored sandstones of DU-6 to caramel colored sandstones and gravels of the DTM (located above the notebook).

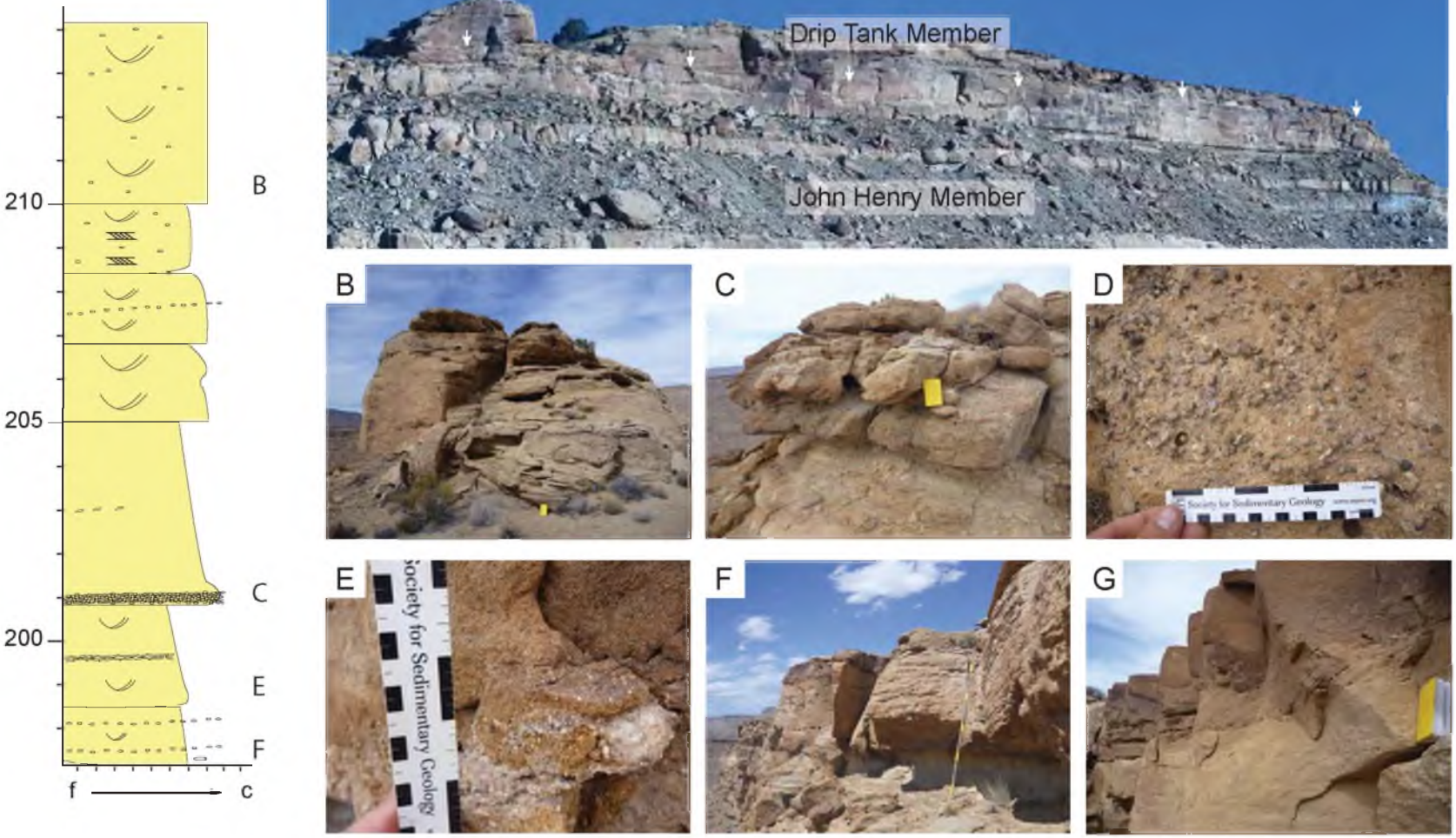
A
Drip Tank Member
John Henry Member
B
C
D
E
F
G
210
205
200
B
C
E
F
f
c
Society for Sedimentary Geology

Figure 32 – Paleomorphodynamic parameters calculated for Bull Canyon (BC). Graphs show parameters calculated for each depositional unit and include: A) BC - bankfull depth, B) BC – Paleoslope, C) BC - Froude squared, and D) BC - backwater length.

A) BC – Bankfull Depth (H)

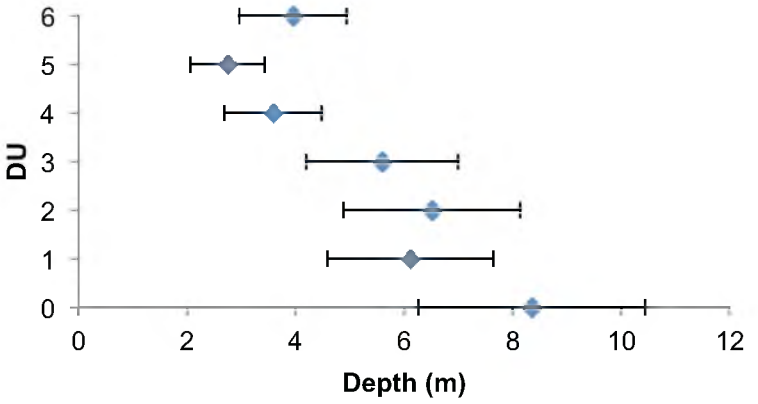

B) BC – Paleoslope (S)

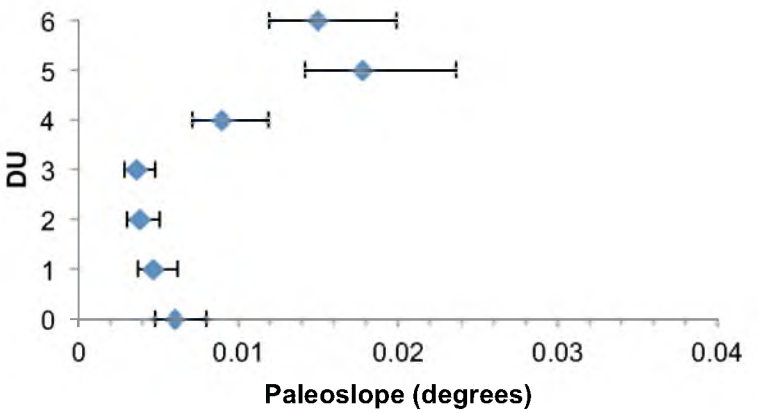

C) BC – Froude Squared (Fr^2)

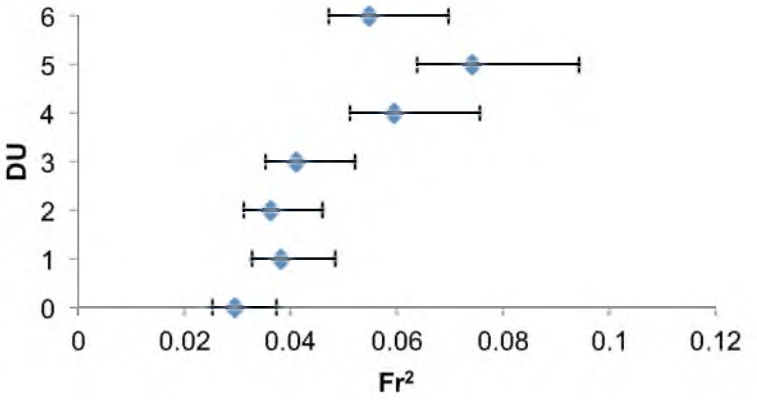

D) BC – Backwater Length (Lw)

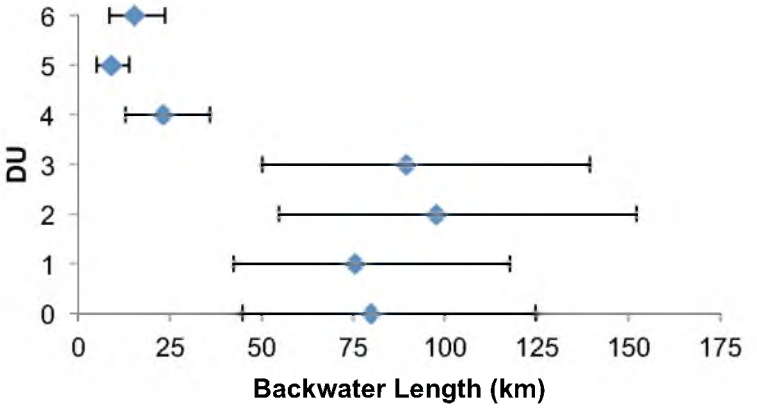

Figure 33 – Paleomorphodynamic parameters calculated for Rock House Cove (RHC), based on data collected by Gooley (2010). Graphs show parameters calculated for each depositional unit and include: A) RHC - bankfull depth, B) RHC – paleoslope, C) RHC - Froude squared, and D) RHC - backwater length.

A) RHC – Bankfull Depth (H)

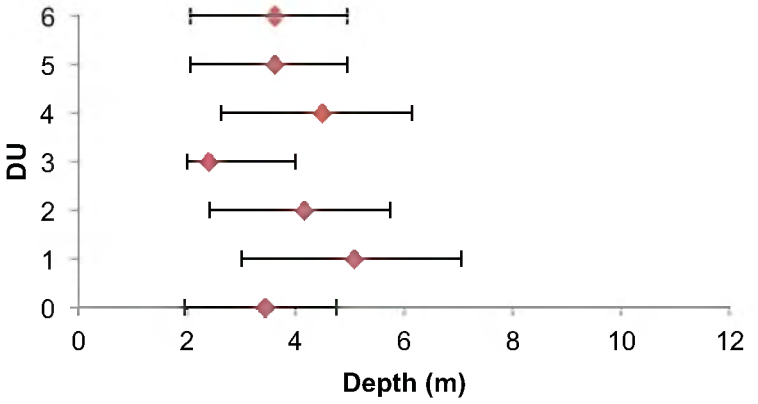

B) RHC – Paleoslope (S)

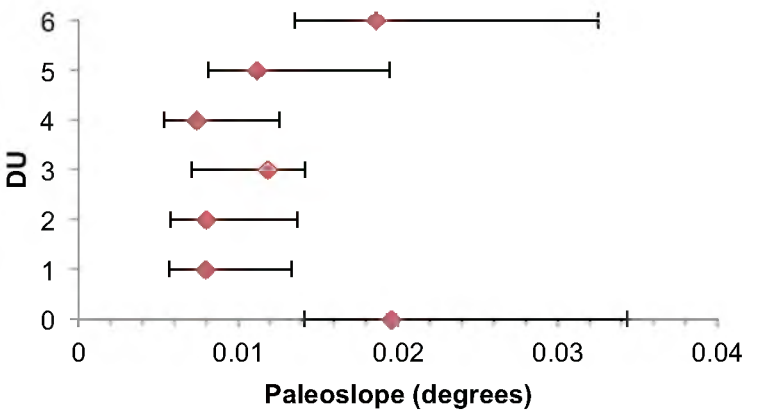

C) RHC – Froude Squared (Fr^2)

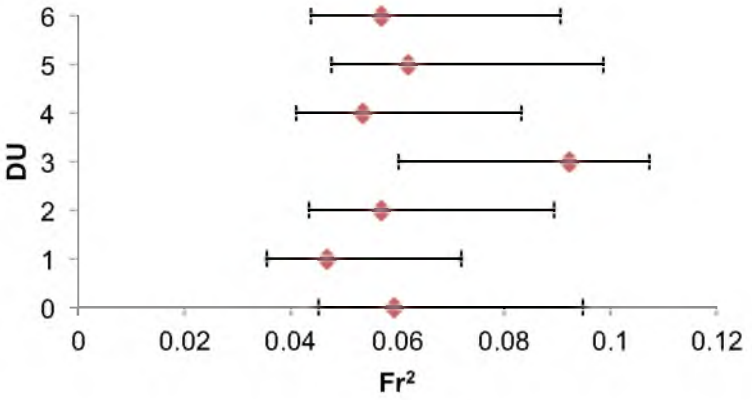

D) RHC – Backwater Length (Lw)

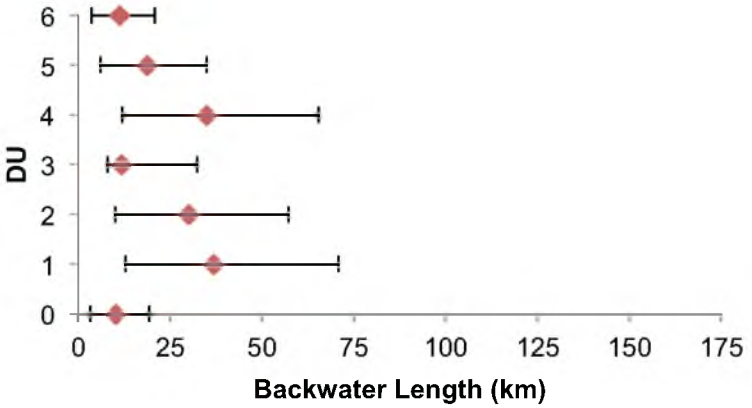

Figure 34 – Backwater and low-Froude flows (modified from Hajek and Wolinsky, 2012). A) The slope of the bed and water surface are typically equivalent in the upper reaches of a river, but in the lower reaches the slope of the water surface is often less than the bed slope. The area within the black box represents the backwater transition zone (i.e., the extent of the backwater curve). B) The backwater transition zone is where the influence of base level is felt upstream. This transition zone scales with the backwater length (Lw).

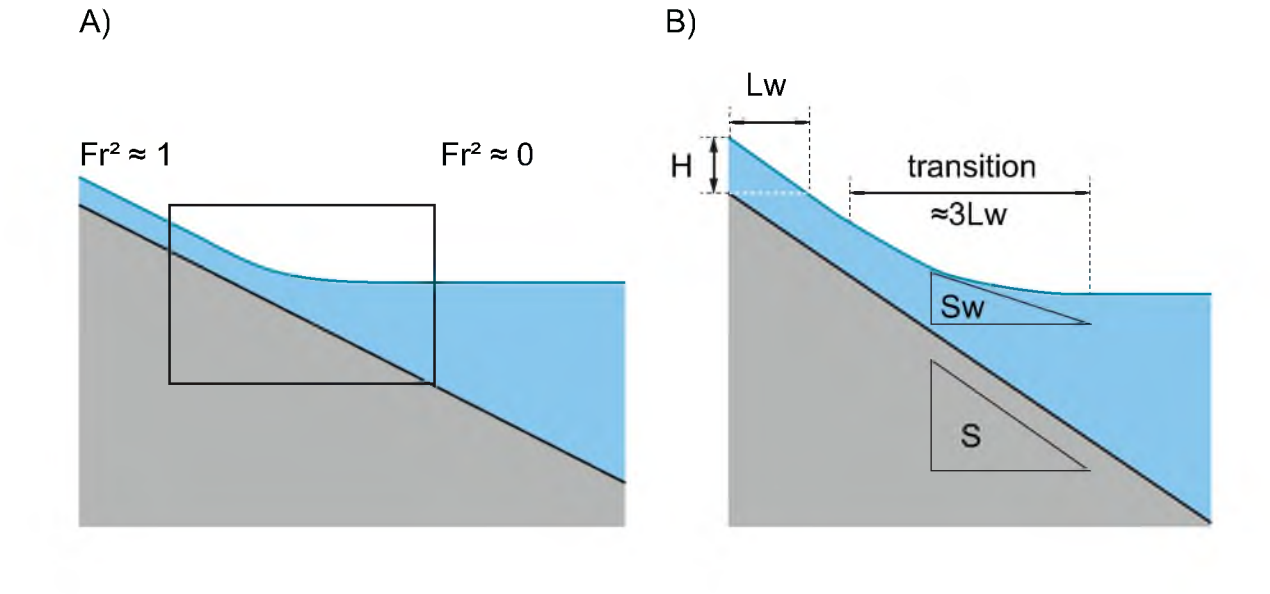
A)
Fr² ≈ 1
Fr² ≈ 0
B)
Lw
H
transition
≈3Lw
Sw
S

Figure 35 – Sandstone petrographic analysis from the John Henry Member at Bull Canyon. A) QmFLt diagram with sandstone classification fields from Pettijohn (1985). B) QtFLu diagram with provenance fields from Dickinson (1975).

Bull Canyon Samples
- DTM
- DU-6
- DU-5
- DU-4
- DU-3
- DU-2
- DU-1
- DU-0
- Calico

John Henry Mbr Average Compositions and Standard Deviations
- Bull Canyon
- Kelly Grade (Gallin, 2010)
- Rock House Cove (Gooley, 2010)

A)

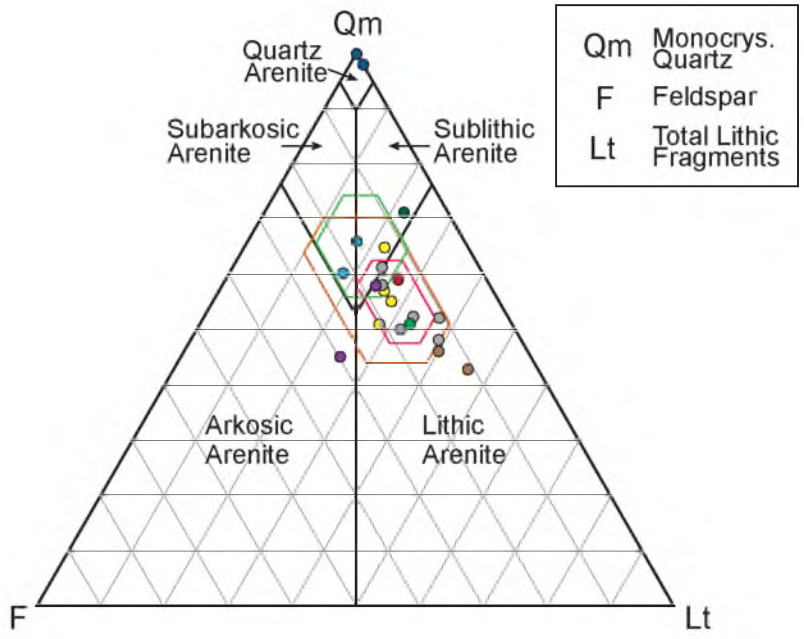

B)

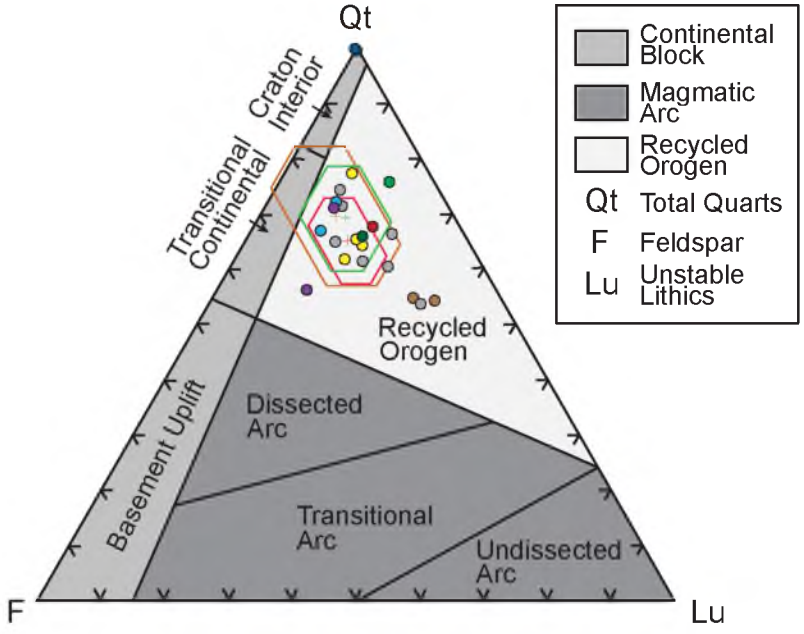

Table 4

Channel Belt Measurements from GPS Data and Stratigraphic Sections

Depositional Unit	Ave. Width*	STDEV Width*	Max Width*	Ave. Thickness*	STDEV Thickness*	Max Thickness*	Ave. W/T*	Ave. d50 Bedload[δ]	Ave. Cross-set Thickness[§]	Ave. Dune Height[+]
DU6	190.98	86.94	360.90	3.5	1.6	5.9	67.3	0.63	0.17	0.51
DU5	225.37	205.20	733.48	3.7	1.3	5.5	60.8	0.51	0.12	0.36
DU4	180.10	154.92	637.31	3.3	1.7	10.0	62.6	0.34	0.15	0.46
DU3	73.75	52.64	216.74	2.0	0.7	3.3	38.0	0.21	0.24	0.72
DU2	91.96	67.13	273.27	2.4	1.0	4.7	40.8	0.26	0.28	0.84
DU1	75.09	43.62	141.37	1.7	0.7	2.5	46.1	0.30	0.26	0.79
DU0	316.63	122.96	455.90	6.0	1.0	6.8	54.0	0.53	0.36	1.08

All measurements are recorded in meters except average d50 bedload, which is in mm.

* Measurements from GPS dataset

[δ] Estimated from grain size measurements in the stratigraphic sections

[§] Measurements from stratigraphic sections and paleocurrent dataset

[+] Estimated from average cross-set height using method from Leclair and Bridge (2001)

INTERPRETATION AND DISCUSSION

Stratigraphic Intervals

The depositional units were grouped into three stratigraphic intervals, which have implications for large-scale temporal changes in the depositional environment that resulted from changes in the relationship between sedimentation and accommodation. A summary of key attributes of the stratigraphic interval is included in Figures 36.

Lower Stratigraphic Interval

The lower stratigraphic interval includes DU-0 and DU-1, which show a general trend of decreasing net-to-gross, channel belt width, bankfull depth, and grain size (Figure 36). DU-0 is separated from the underlying Calico bed by an unconformity and potential sequence boundary. This boundary is irregular (with ~2 m of relief) and clasts of the Calico bed material are contained within lags near the base of DU-0. This unit contains medium- to coarse-grained sandstone and some of the thickest channels within the Bull Canyon section. The lower stratigraphic interval is interpreted as forming during low, but increasing, rates of accommodation relative to sediment supply. The distinct increase in fine-grained material (i.e., floodplain and coal mire facies) above the transition to DU-1 may have resulted from an abrupt increase in accommodation.

Middle Stratigraphic Interval

The middle stratigraphic interval includes DU-2 and DU-3, which has the highest amount of coal mire and floodplain facies and the narrowest channel belts. This interval lacks the abundance of tidal indicators that are present in the lower stratigraphic interval. Locally, within DU-2 there is an upward coarsening pattern over approximately 17 meters, which show evidence of rapid sedimentation, limited presence of carbonaceous shale, and does not include any coals. This portion is interpreted as resulting from a local increase in sediment supply relative to accommodation that caused the formation of a crevasse delta. DU-3 contains thick accumulations of floodplain (overbank) and coal mire facies with relatively few channels, and tidal indicators are completely absent. Due to the isolated nature of channel deposits in thick floodplain accumulations, the middle stratigraphic interval is interpreted to represent a period of high accommodation formation relative to sediment supply in which the channels were relatively stable and experienced infrequent avulsions. In general, this is a continuation of the trend present in the lower stratigraphic interval, but it is much more pronounced.

Upper Stratigraphic Interval

The upper stratigraphic interval includes DU-4, DU-5, DU-6 and continues into the Drip Tank Member. This interval contains trends of vertically increasing average channel belt width and amalgamation, and a steady increase in median and maximum grain size. There is one exception, the average channel belt widths in DU-6 are slightly less than DU-5 (Figure 18); however, this is likely due to the truncation of channel belts by one another, and therefore is not representative of the original deposited widths. The changes in character of channel belts can be attributed to an increase in the rate of

channel avulsion and/or a decrease in the sediment accommodation rate accompanied by progradation of a clastic wedge (cf., Ryer, 1993). The upper stratigraphic interval is interpreted as representing decreasing accommodation rate relative to sedimentation rate.

Correlation of Fluvial and Paralic Facies

A correlation along southern edge of the Kaiparowits Plateau was constructed (Figure 37), which incorporates the sections measured for this study with previously published stratigraphic sections and logged cores of Vaninetti (1979), Shanley (1991), Gallin (2010), and Gooley (2010) (A-A' in Figure 1). This correlation permits observations regarding how architectural trends in proximal fluvial facies are related to those present in more distal fluvial and paralic facies. The top of the Calico bed was used as the datum for correlation of sections. Correlations were driven by large-scale trends in outcrop architecture for published sections, and when this information was not available (i.e., logged cores), outcrop architecture was inferred from the distribution of lithologies. The three stratigraphic intervals (lower, middle, and upper) identified within the John Henry Member at Bull Canyon were correlated to roughly equivalent intervals in the proximal fluvial and paralic facies.

Correlation of the Lower Stratigraphic Interval

The lower depositional units in Bull Canyon correlates landward to DU-0 and DU-1 in Rock House Cove, defined by Gooley (2010), and basinward to the lower facies associations (FA-1) in Kelly Grade, defined by Gallin (2010). Gallin (2010) and Gooley (2010) also interpreted this interval as representing a period of increased accommodation relative to sediment input, but there is no evidence of an incised valley in Bull Canyon

(cf., Rock House Cove, DU-1). Despite the lack of an observable incised valley, this interval does generally fit the stratigraphic patterns predicted for incised valley fill (Shanley and McCabe, 1993, Figure 4a). This pattern includes, in ascending order: amalgamated channel deposits that overly and erosive surface, tidally-influences fluvial deposits, and isolated, high sinuosity fluvial channels.

Correlation of the Middle Stratigraphic Interval

The middle stratigraphic interval at Bull Canyon (DU-2 and DU-3) correlates landward to DU-2 and DU-3 in Rock House Cove (Gooley, 2010) and basinward to the middle facies association (FA-2) in Kelly Grade (Gallin, 2010). Throughout the correlated area, this interval includes the portion of the section that is characterized by the finest-grained sediment, absence (or reduced abundance) of tidal indicators, and reduced lateral extent of channel belts.

Coal is almost completely absent in Rock House Cove, but the middle interval in Bull Canyon (basinward) contains coastal plain coal mire deposits and in Kelly Grade (further basinward) contains lagoonal and estuarine coastal plain mires related to Christianson and Rees coal zones (Peterson, 1969b; Vaninetti, 1979; Gallin, 2010; Gooley, 2010). This interval of abundant coal formation on the coastal plain and the furthest landward deposition of estuarine and lagoonal facies is interpreted to represent accelerating rates of base level rise (DU-2) and maintained high rates of base level rise (DU-3). This interpretation is fitting with the interpretations of Gallin (2010) and Gooley (2010).

Correlation of the Upper Stratigraphic Interval

The upper stratigraphic interval consists of a coarsening upward succession at Bull Canyon and correlates with similar tends in Rock House Cove (DU-4 through DU-6; Gooley, 2010) and in Kelly Grade (FA-3; Gallen, 2010). Additional trends common throughout the upper stratigraphic interval include increasing channel belt size and channel belt complexity. This interval is interpreted as developing due to high sediment supply relative to accommodation, which fits observations made by Gallin (2010) and Gooley (2010).

Relationship Between Fluvial Architecture and Shoreline Successions

The interpreted correlation of fluvial through marginal marine strata along the western edge of the Kaiparowits Plateau is shown in Figure 38 (A-A" in Figure 1). This correlation is based on large-scale trends present in the stratigraphic architecture at four locations subject to detailed stratigraphic studies, from west to east: Rock House Cove (Gooley, 2010), Bull Canyon (this study), Kelly Grade (Gallin, 2010), and Rogers Canyon (Allen, 2009). For each location, a simplified stratigraphic diagram was created to represent characteristic trends of the defined stratigraphic intervals. The use of these locations for a dip-oriented characterization is not ideal in that it does not trace fluvial strata to where they directly communicate with the shoreline. However, interpretations made along this cross-section are valid in that large-scale trends throughout the system should still be related.

The first two shoreface sandstones of the John Henry Member (A and B shorefaces; Figure 38), which are the thickest and extend the furthest landward, correlate to the lower stratigraphic interval identified in the fluvial strata, which has the greatest

degree of tidal influence on any fluvial interval. The most abrupt basinward shift in facies occurs above the B shoreface sandstone, and the overlying shoreface sandstones C, D, and E are thin and represent a period of net transgression. The Christensen and Rees coal zones accumulated behind these shorefaces (Peterson, 1969a, 1969b; Vaninetti, 1979), and correlate with the middle stratigraphic interval in the fluvial section, which contains the highest concentration of coastal plain coal mire facies. The maximum marine flooding surface identified within the E shoreface sandstone by Allen (2009) may roughly correlate to the stratigraphically highest coals in Bull Canyon, located at the base of DU-4. Located above the transgressive shorelines, the F and G shoreface sandstones are aggradational to progradational (Allen, 2009). These shorefaces correlate to the upward coarsening trend in fluvial strata in the upper stratigraphic interval. These interpretations generally match the conclusions of Vaninetti (1979), Gallin (2010), and Gooley (2010).

In summary, the following correlations are made between the fluvial deposits and shorelines (Figure 37 and 38): (1) The most landward, progradational shorelines correlate with a fluvial interval characterized by a vertical decrease in grain size, channel belt size and channel belt amalgamation, and some indication of tidal influence. The greater presence of tidal indicators in this interval likely resulted from being deposited in greater proximity to the coeval shoreline, although shoreline locations indicate this distance increases through this interval (Allen, 2009). (2) Retrogradational (i.e., transgressive) shorelines correlate with a fluvial interval comprised of isolated channel belts and abundant floodplain fines and coal mire facies. (3) Aggradational shorelines correlate with a fluvial interval of vertically increasing channel belt size and amalgamation.

Controls on Fluvial Sequences

In the John Henry Member, hinterland tectonics and the associated trends in basin subsidence are likely the primary controls on accommodation and sediment supply, and accordingly, are the primary controls on alluvial architecture. Alluvial stratigraphy can be influenced by a number of factors, including allogenic controls (hinterland tectonics and basin subsidence, sea-level change, climate, and sediment supply) and autogenic controls (avulsion and progradation) (Paola et al., 1992; DeCelles and Giles, 1996; Miall, 2000). While certain factors will have a greater influence on sedimentation, alluvial architecture represents the net result from the dynamic interaction of all the controlling factors. The following is a discussion of the factors that may have influenced the alluvial architecture, including: tectonics, eustacy, climate, sediment supply, and autogenic processes.

Tectonic activity in the Sevier orogenic belt was likely the dominant factor controlling alluvial architecture in the Kaiparowits basin, insomuch as it strongly influenced basin subsidence (i.e., accommodation) and sedimentation (Goldstrand, 1994; Little, 1995, 1997). During the middle of the Cretaceous, flexural loading of the lithosphere caused by continued development of the orogenic belt, accumulation synorogenic sediments, and dynamic subsidence caused the development of the foreland basin (Fillmore, 1991; Pang and Nummedal, 1995; Liu et al., 2011). The Upper Cretaceous sediments of the Kaiparowits Plateau were deposited into this basin about 150 km east of the leading edge of the thrust belt (DeCelles, 2004).

In a stratigraphic study of the Kaiparowits basin, Little (1997) proposed that accommodation in proximal portions of the basin to be solely controlled by tectonic processes (Figure 4b). Accommodation in distal portions of the basin, while still

dominantly controlled by tectonics, might have been influenced by eustatic changes (Little 1997). In this model, periods of tectonic activity cause increased subsidence, narrowing of the basin, and relative base-level rise resulting in coastal transgressions. In contrast, periods of tectonic quiescence resulted in erosion, isostatic rebound (or slowed subsidence), relative base-level fall, and coastal regressions. These observations fit those made in adjacent foreland basins by Kauffman (1984) and Kauffman and Caldwell (1993).

The influence of eustatic sea level change on the depositional patterns of the John Henry Member has been emphasized by a number of studies (Shanley and McCabe, 1991, 1993, 1995; Hettinger et al., 1993; Hettinger, 1995). Backwater length calculations indicate that Rock House Cove and Bull Canyon were located near, or within, the backwater transition zone, which suggests that downstream control (i.e. sea level fluctuations) may have influenced alluvial architecture in these areas. Several fluctuations in eustatic sea level occurred during Coniacian-Santonian time (Haq et al., 1987; Haq et al. 1988; Van Sickel et al., 2004; Miller et al., 2005; Figure 36). Shanley and McCabe (1995) recognized eustatic sea level as the primary control on sequence formation (Figure 4a). This observation was heavily based on the correlation of 3rd order cycles between their local sea-level curve and global sea-level curve of Haq et al. (1988). In addition to the problems inherent in correlating local events to global sea-level curve (Miall, 1992), applying this method to the Straight Cliffs Formation is problematic for a number of reasons: age resolution within the Straight Cliffs Formation is poor, 3rd order eustatic sea level fluctuations are lower than originally predicted by Haq et al. (1988) (Van Sickel et al., 2004; Miller et al, 2005), eustatic sea-level curves do not agree with regional sea level

curves (Figure 36) (Weimer, 1988), and the magnitude of sea level change was probably smaller than the magnitude of induced subsidence (cf., Fillmore, 1991, Pang and Nummedal, 1995; Liu et al., 2011). For these reason, it is unlikely that sea level was the primary control on alluvial architecture in these locations.

One of the key sequence stratigraphic surfaces defined by Shanley and McCabe (1995), the A-sequence boundary (Figure 3) was interpreted as resulting from a drop in eustatic sea level. This surface is not present within the section at Bull Canyon. However, there is a reduction in the abundance of tidal indicators above DU-1, at the approximate location where the proposed sequence boundary should be located. This shift could have resulted from changes in eustatic base level, but more likely represents fluctuations in relative sea level due to tectonic and/or autogenic trends.

The climate along the southwestern edge of the Western Interior Seaway during the Coniacian-Santonian time was characterized by warm temperatures, low to moderate rainfall, and lack of strong seasonality (Kauffman, 1984; Wolfe and Upchurch, 1987); no major shifts in climate have been documented during this time (Roberts and Kirschbaum, 1995). These conditions led to coal development in various locations along the Western Interior Seaway at this time (McCabe and Parrish, 1992). Peat accumulation typically requires a consistent high water table, of the sort that develops in areas where precipitation exceeds evaporation and rainfall is distributed evenly throughout the year (Ziegler et al., 1987). Shifts in the location and abundance of coal development throughout the plateau may have resulted from local climatic changes, either solely or in combination with other factors that affect coal formation (e.g., sediment input) (McCabe and Parrish, 1992). However, other indicators of climate changes, including desiccation

cracks, calcretes and evaporites, are generally not present in the Bull Canyon area and have not been previously documented as extensive features within the John Henry Member.

Time averaged deposition rates for the John Henry Member indicate that the sediment supply was moderately high (Shanley, 1991; Allen, 2009). However, due to changes in the geologic time scale that lengthened the duration of the Coniacian and Santonian (Gradstein et al., 2012), the sedimentation rates were likely overestimated. Gallin (2010) proposed that a shift in the system from axial to longitudinal trunk drainage might have had a significant impact on the sedimentation rate within portions of the basin, even influencing shoreline stacking patterns.

Many of the autogenic processes that are commonly recognized in downstream (delta) environments (such as avulsion, lobe shifting, scouring, and progradation) have equivalents in upstream fluvial fan systems in the continental interior. Variations in externally controlled accommodation and sediment supply coupled with autogenic progradation of a fluvial fan is believed to be an important mechanism in shaping the alluvial architecture with the John Henry Member. This concept is discussed in detail in the following section.

Depositional Model

The depositional model proposed for the John Henry Member employs the concept of a fluvial fan system (or distributive fluvial system; Figure 39; Hartley et al., 2010; Weissmann et al., 2010) that adjusts to tectonically driven changes in accommodation to produce one large-scale depositional cycle (Figure 40 and 41). This

model is a modification of the two-phase model (Heller et al., 1988) and will be discussed in three stages: The first stage (between time 0 to 1 in Figure 40) includes the initiation of active thrusting, increasing subsidence (i.e., accommodation development) adjacent to the thrust belt, and back tilting within the basin. These factors cumulatively decrease the surface gradient within the basin (Flemings and Jordan, 1990; Paola et al., 1992). As a result, transport of coarse sediment is progressively limited the proximal portions of the basin (Paola, 1988; Flemings and Jordan, 1989), and the coarse sediments are deposited in small-scale (alluvial) fans adjacent to the hinterland. This will produce a fining upward trend in more distal potions of the basin. Tidal influence within the fluvial systems may shift landward through a relative sea level rise (i.e., transgression) and/or an increased backwater transition zone. This stage correlates with the upward fining pattern that begins in the lower stratigraphic interval and continues into the middle stratigraphic interval at Bull Canyon. In stage two (between time 1 and 2 in Figure 40), reducing rates of subsidence allows the small (alluvial) fans to grow basinward and develop into larger fluvial fans. Continued growth of the fluvial fans establishes a gradient sufficient to transport coarse material progressively further basinward (Paola, 1988; Flemings and Jordan, 1989), which causes a coarsening upward sequence in distal portions of the foredeep. This stage is represented in the coarsening upward trend from the middle to upper stratigraphic interval. In stage three (between time 2 and 3 in Figure 40), erosion and associated isostatic uplift during a period of tectonic inactivity cause the sediment that was deposited proximal to the thrust belt in alluvial fans to be redistributed as a coarse clastic sheet. This will result in the continuation of the coarsening upward trend that began in stage 2, but is marked by a dramatic increase in maximum grain size caused

by increased stream competency. This stage likely correlates with the appearance of gravel lags in the upper stratigraphic interval of the John Henry Member and continues through the Drip Tank Member.

Slopes calculated for the John Henry Member support the concept of changing depositional gradient in response to tectonic activity. The lower and middle stratigraphic intervals have lower calculated slopes (<0.01°) that reduce vertically and may relate to increasing rates of subsidence, whereas the upper stratigraphic interval has higher calculated slopes that increases vertically (up to ~0.02°) relate to a reduced rate of subsidence (Figures 32b and 34b). These trends are subtle, but may be concurrent with more dramatic trends in the proximal portions of the basin. The vertically increasing slopes and grains size in the upper stratigraphic interval fits the interpretation of a period of decreased subsidence and progradation of a fluvial fan system. The abrupt change in fluvial style at the base of the upper stratigraphic interval may represent the transition from more spatially limited alluvial fans to a larger fluvial fan system (or distributive fluvial systems). The gradient necessary to transport coarser grained material was progressively reestablished as the large fluvial fan continued to grow, which is evidenced by the increasing median and maximum grain size in the upper interval.

Bull Canyon was likely located near the toe of the large fluvial fan, which is supported by calculated paleoslopes (0.003° to 0.02°) that are on the lower end of slopes typical in modern large fluvial fan systems (Hartley et al., 2010). Comparison of paleoslope calculations made at Rock House Cove and Bull Canyon shows that they have the same overall trends (Figures 32b and 33b). These trends include reducing slope into the middle interval followed by a trend of increasing slope towards the top of the section.

On average the calculated paleoslopes at Bull Canyon are slightly lower than Rock House Cove, which is expected from a more basinward location along a graded stream profile.

Paleomorphodynamic calculations indicate that Rock House Cove and Bull Canyon were located within or near the edge of the backwater transition zone during deposition of the John Henry Member (Figure 32d and 33d). There is a reduction in the estimated length of the backwater transition zone during deposition of the upper stratigraphic interval. This change generally fits the interpretation of a prograding fan system that causes an increase in depositional gradient and is supported by the presence of tidal indicators within the lower half of Bull Canyon.

Tidal indicators are most abundant in the lower stratigraphic interval and are primarily absent absent from the middle and upper stratigraphic intervals. If changes in distribution of the tidal signature resulted solely from relative sea level rise due to thrust loading and subsidence, the greatest tidal influence should be coincident with the greatest levels of accommodation development relative to sediment supply (middle stratigraphic interval), which is not the case. Therefore, the reduced presence of tidal indicators above the lower stratigraphic interval is likely due to some other factor influencing relative sea level, a change in sediment routing system, or a eustatic change at the base of the middle interval.

Paleocurrent data from Rock House Cove, Bull Canyon, and Kelly Grade are shown in Figure 42. There is a greater degree of variability in paleocurrent in Rock House Cove than at Bull Canyon or Kelly Grade. This may be representative of the change from avulsions that produce greater changes in stream direction in more proximal parts of a fluvial fan (Rock House Cove) to avulsions with more consistent stream

directions towards the toe of the fan (Bull Canyon and Kelly Grade). Hartley et al. (2010) documented similar spatial variability in the avulsions of modern fluvial fans.

Additionally, there is a transition from consistently eastward paleocurrent directions in Rock House Cove and Bull Canyon to north-northeast in Kelly Grade (Figure 43). Three factors that may have contributed to the deflection of channels to the north include: channels encountering a barrier obstructing direct basinward flow, such as the raised coal mire proposed by McCabe and Shanley (1992); differential subsidence in the basin with increased subsidence to the north, which has been proposed by Bobb (1991) and Hettinger et al. (1993); and the presence of a series of fluvial fans that skirt the hinterland (cf., Hartley et al., 2010), in which case the Kelly Grade channels may not directly related to those at Bull Canyon. These factors are not mutually exclusive, and the change in paleocurrent may have resulted from some combination of these factors.

The true outlet for the fluvial systems (i.e., delta) has not been located, though it likely lies to the north of Left Hand Collet (Figure 43; Allen, 2009; Dooling, in prep). The location of the interface between these systems is an important factor that impacts both marine and nonmarine deposition. The sediment routing system would dramatically differ if the river coalesced into northward flowing trunk streams or they encountered a raised mire that impeded the direct transport of sediment to the shoreline. Additionally, the location of the fluvial output into the shoreline will impact the hydraulic characteristics of the fluvial systems (Van Heijst et al., 2001; Aalto et al., 2003; Jerolmack and Swenson, 2007; Paola et al., 2009).

Figure 36 – A summary of stratigraphic intervals. Graphs and lists of net-to-gross ratios, d50 bedload grain size, average channel belt width, vertical and lateral amalgamation, and bank full depth have been included. A coastal onlap curve from the John Henry Member in Rogers Canyon (Allen, 2009), eustatic sea level curve (Miller et al., 2005), and regional sea level curves from western North America (Weimer, 1988) have been include for comparison with trend in the stratigraphic intervals.

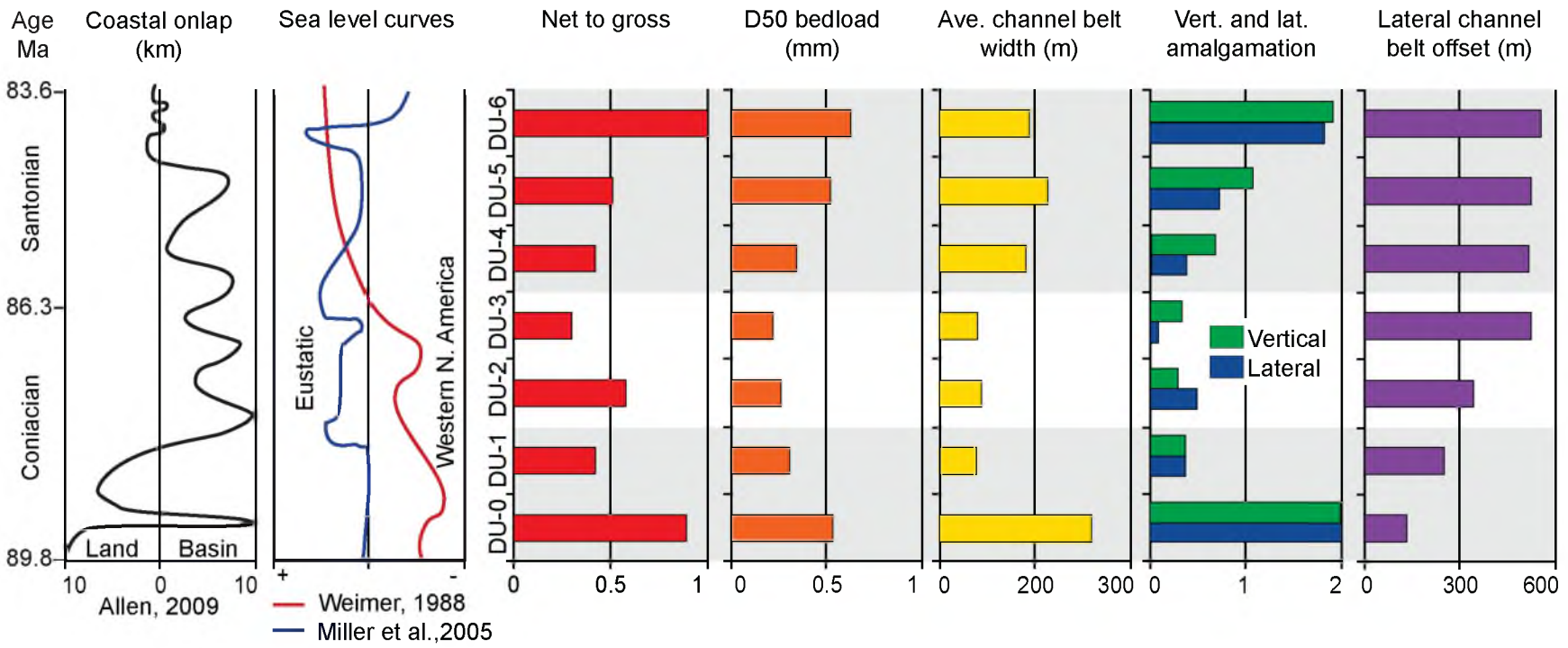

Stratigraphic interval	DU	Ave. thickness (m)	Net to gross	D50 bedload (mm)	Ave. channel belt width (m)	Lat. amalg.	Vert. amalg.	Bankfull depth (m)
Upper	DU-6	11	1.00	0.625	191	1.83	1.92	4.0
	DU-5	43	0.51	0.516	225	0.74	1.09	2.7
	DU-4	71	0.42	0.339	180	0.39	0.70	3.6
Middle	DU-3	46	0.30	0.213	78	0.10	0.35	5.6
	DU-2	17	0.58	0.264	90	0.52	0.31	6.5
Lower	DU-1	14	0.42	0.301	75	0.40	0.40	6.1
	DU-0	13	0.89	0.530	317	2.00	2.00	8.4

Figure 37 – Regional correlation of fluvial strata along the southern edge of the Kaiparowits Plateau (A-A' in Figure 1). The correlation includes logged cores and measured sections from this study, Vaninetti (1979), Gooley (2010), Gallin (2010), Shanley (1991). The locations of three of the detailed outcrop studies (Rock House Cove, Bull Canyon, and Kelly Grade) used in the regional correlation (Figure 37) are highlighted in gray (Gallin, 2010; Gooley, 2010; Allen, 2009). Member name abbreviations include: Tibbet Canyon Member (TCM), Smoky Hollow Member (SHM), John Henry Member (JHM), and Drip Tank Member (DTM).

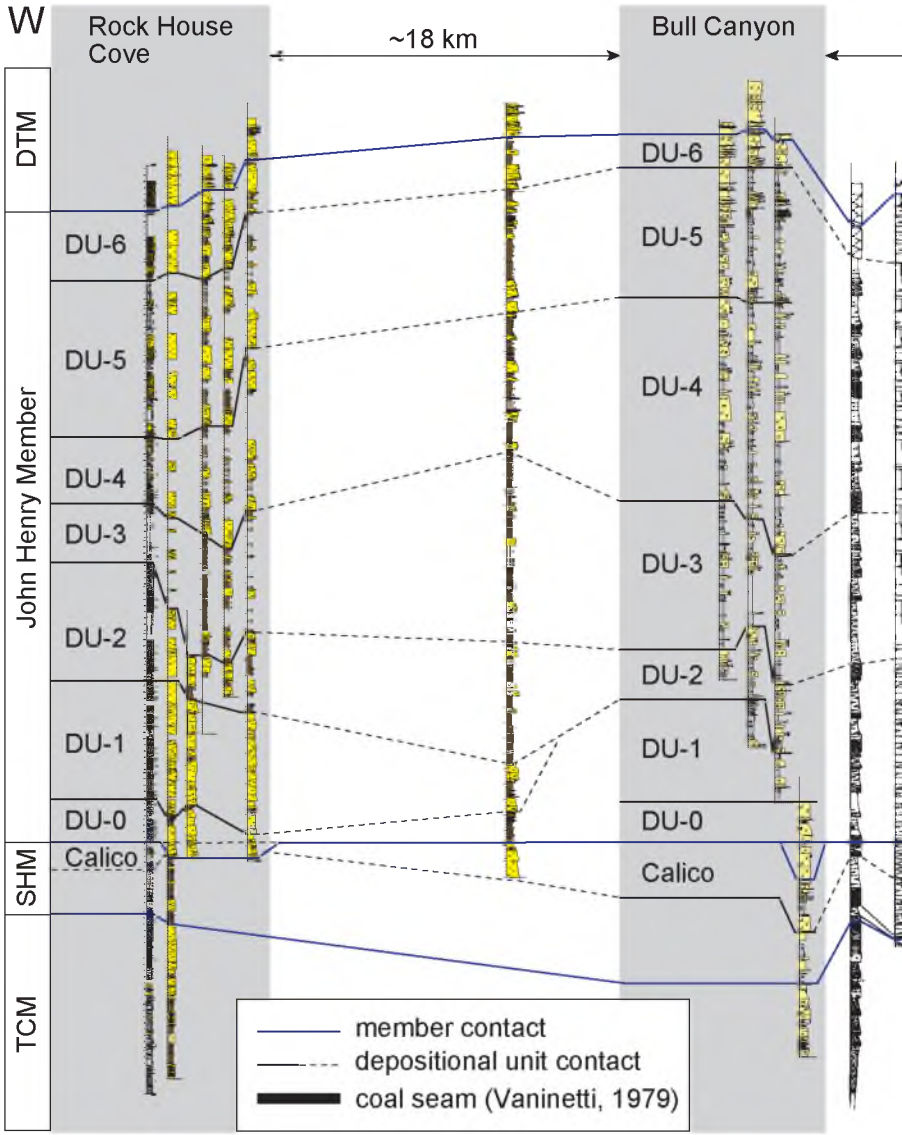
W
Rock House Cove
~18 km
Bull Canyon
DTM
John Henry Member
SHM
TCM
DU-6
DU-5
DU-4
DU-3
DU-2
DU-1
DU-0
Calico
member contact
depositional unit contact
coal seam (Vaninetti, 1979)

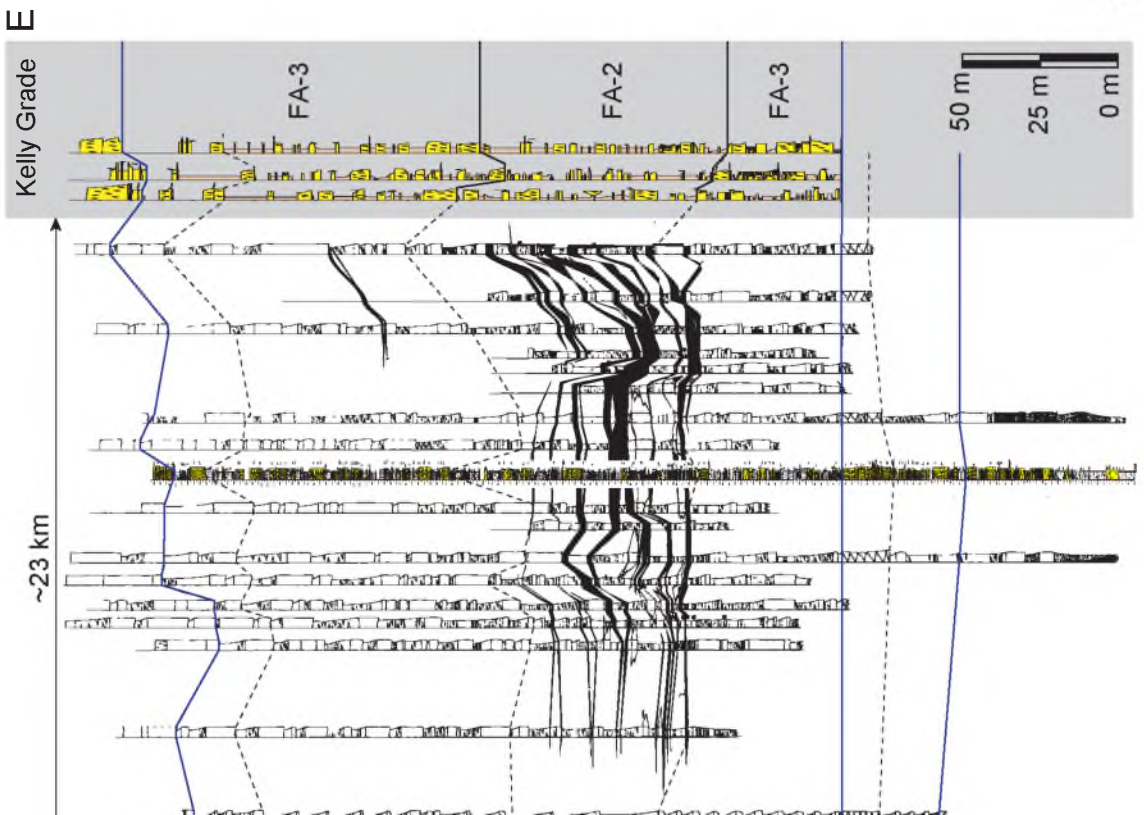
E
Kelly Grade
FA-3
FA-2
FA-3
50 m
25 m
0 m
~23 km

Figure 38 – Regional correlation for fluvial to shoreface strata (A-A" in Figure 1). Simplified stratigraphic diagrams from Rock House Cove (Gooley, 2010), Bull Canyon (this study), Kelly Grade (Gallin, 2010), and Rogers Canyon (Allen, 2009) have been included. Correlations are based on large-scale trends described in the lower, middle and upper stratigraphic intervals (L-SI, M-SI, and U-SI), which were defined in the fluvial strata and related to the shoreface stacking patterns.

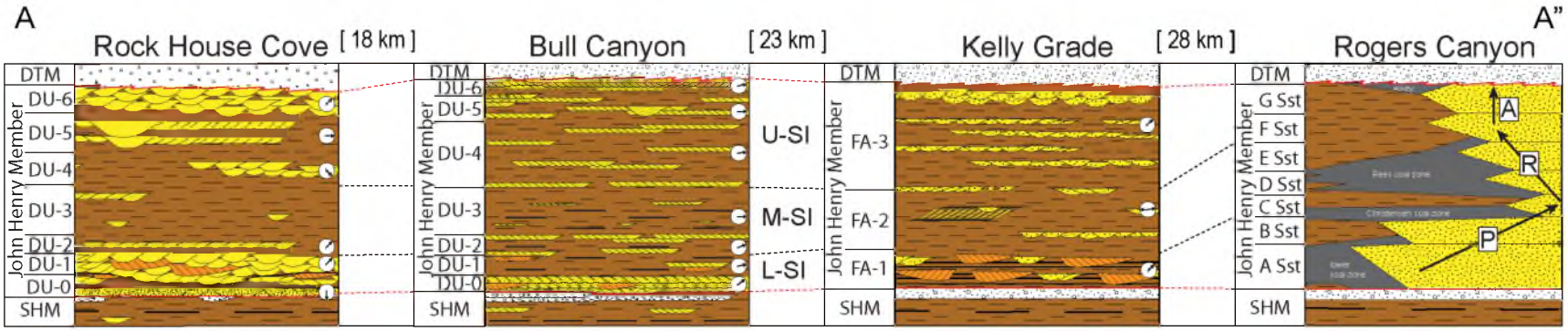
A
A"
Rock House Cove
[18 km]
Bull Canyon
[23 km]
Kelly Grade
[28 km]
Rogers Canyon
DTM
John Henry Member
DU-6
DU-5
DU-4
DU-3
DU-2
DU-1
DU-0
SHM
U-SI
M-SI
L-SI
FA-3
FA-2
FA-1
G Sst
F Sst
E Sst
D Sst
C Sst
B Sst
A Sst
A
R
P
(Gooley, 2010)
(This Study)
(Gallin, 2010)
(Allen, 2009)
Shoreface
Floodplain
Coarse-grained braided river
Coal / coal mire
Member contact
Isolated channels
Channel belts
Vertically amalgamated channel belts
Inclined Heterolithic Strata / Estuarine
Unconformity
Shoreline progradation
Shoreline retrogradation
Shoreline aggradation
Paleocurrent direction

Figure 39 – Large fluvial fans (or distributive fluvial systems). A) Schematic of the planform geometry of large fluvial fans in relation to sediment supply and relative discharge (modified from Hartley et al., 2010). B) A satellite image (from GoogleEarth) and map including three of the large fluvial fans located along western edge of the central Andes and extend into the western Chaco Plain, Bolivia (interpretations modified from Horton and DeCelles, 2001). Numerous smaller fans, some too small to be mapped, are located between the large fans (gray box).

A) Large fluvial fan planform types in relation to gradient and relative discharge.

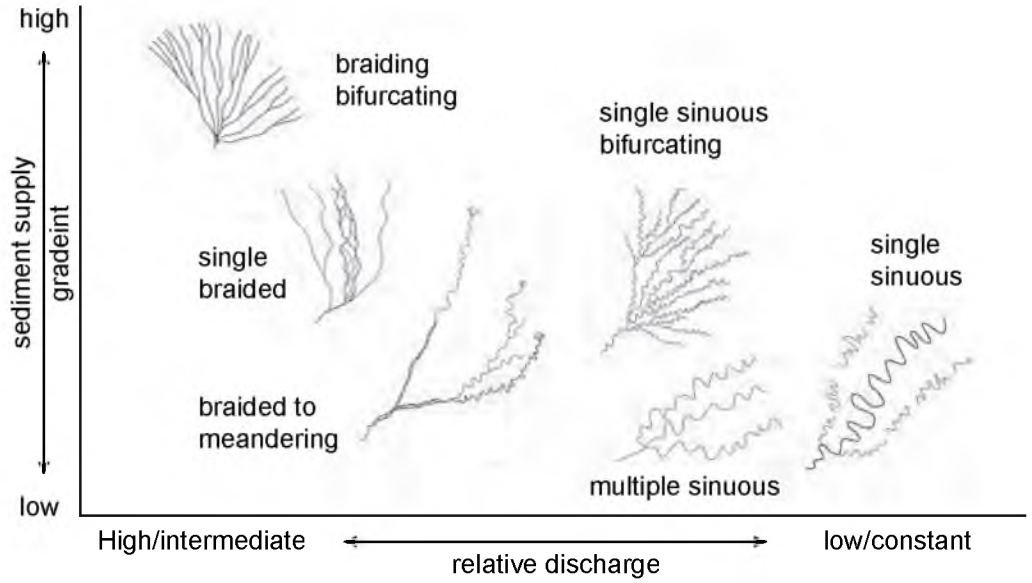

B) Large fluvial fans (or distributive fluvial sustems), western Chaco Plain, Bolivia

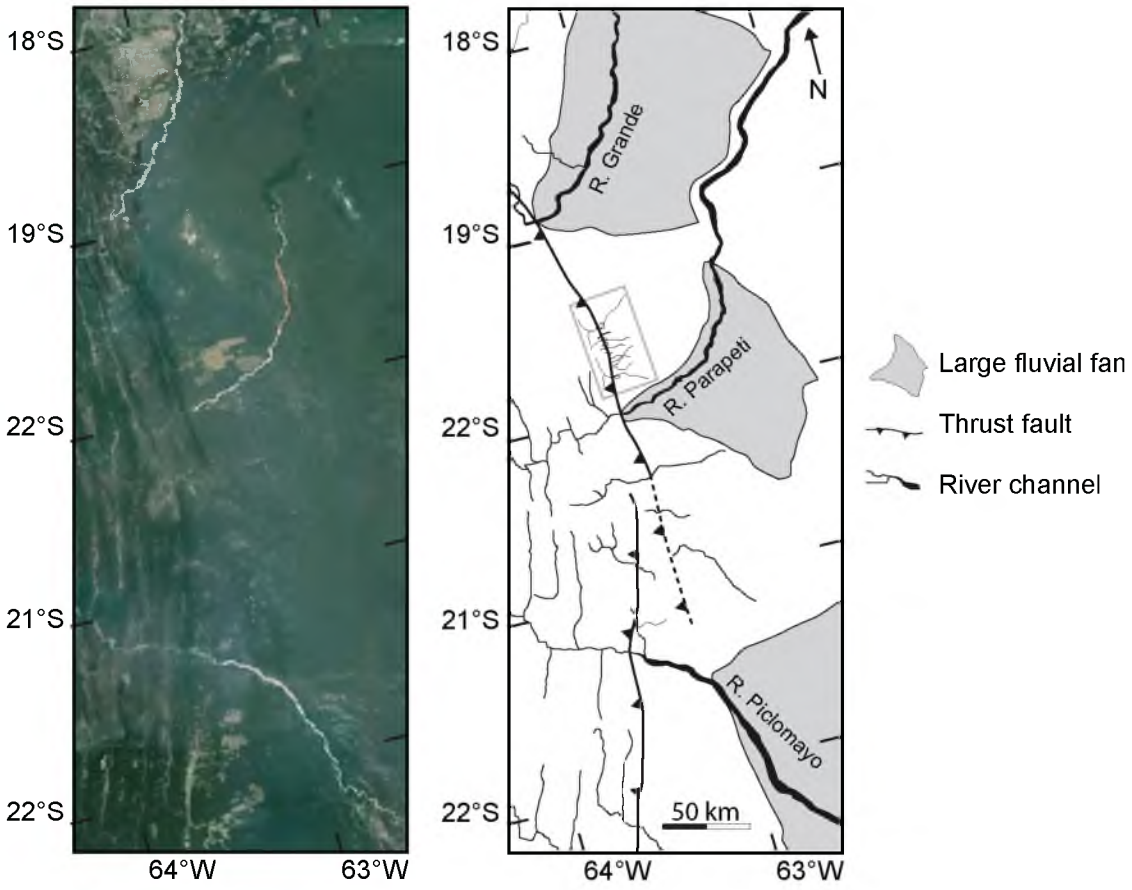

Figure 40 – Generic and unscaled schematic diagrams showing the shape of the foreland basin and resulting sedimentary trends at multiple times during a single pulse of thrusting (modified from Heller et al., 1988 and Paola et al., 1992). The diagrams include: Time 0) The initial topography of a foreland basin before the onset of a pulse of tectonic activity, with the reworked clastic sheet from the last cycle. Dashed lines show the locations at which the current topographic surface will be in the following stages. Time 1) Initial and increasing tectonic activity is accompanied by erosion in the thrust belt, subsidence, and back tilting of the basin. Subsidence and accommodation are concentrated proximal to the thrust belt, which, in conjunction with reduced surface gradients, concentrates deposition in this area. Time 2) Reduced rates of tectonic activity cause reduced rates of accommodation development. As a result, coarse sediment is transported further into the basin as the fluvial system progrades basinward. Time 3) At the end of a tectonic pulse dynamic interaction of erosion and isotactic rebound result in the redistribution of coarse sediment far into the basin. The next tectonic pulse will cause a similar sedimentary cycle to be deposited above this one.

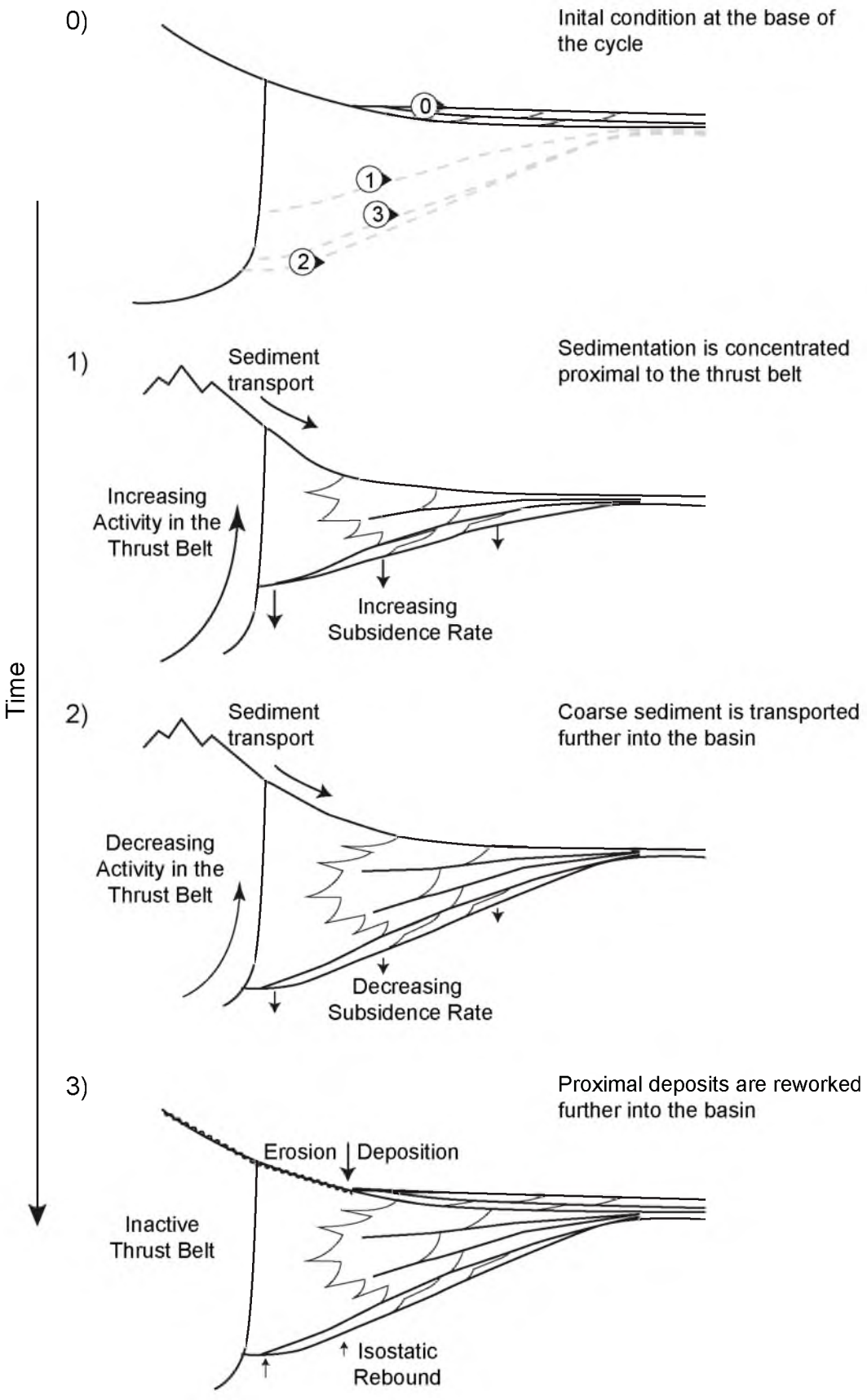
0)
Inital condition at the base of the cycle
0
1
3
2
1)
Sediment transport
Sedimentation is concentrated proximal to the thrust belt
Increasing Activity in the Thrust Belt
Increasing Subsidence Rate
2)
Sediment transport
Coarse sediment is transported further into the basin
Decreasing Activity in the Thrust Belt
Decreasing Subsidence Rate
3)
Proximal deposits are reworked further into the basin
Erosion
Deposition
Inactive Thrust Belt
Isostatic Rebound
Time

Figure 41 – Explanation of tectonically driven depositional cyclicity depicted in Figure 40. Widening and narrowing upward triangles represent the increase and decrease of the various parameters. The approximate relationships between stages in the depositional model and stratigraphic intervals from Bull Canyon are shown on the right.

Depositional model

Bull Canyon

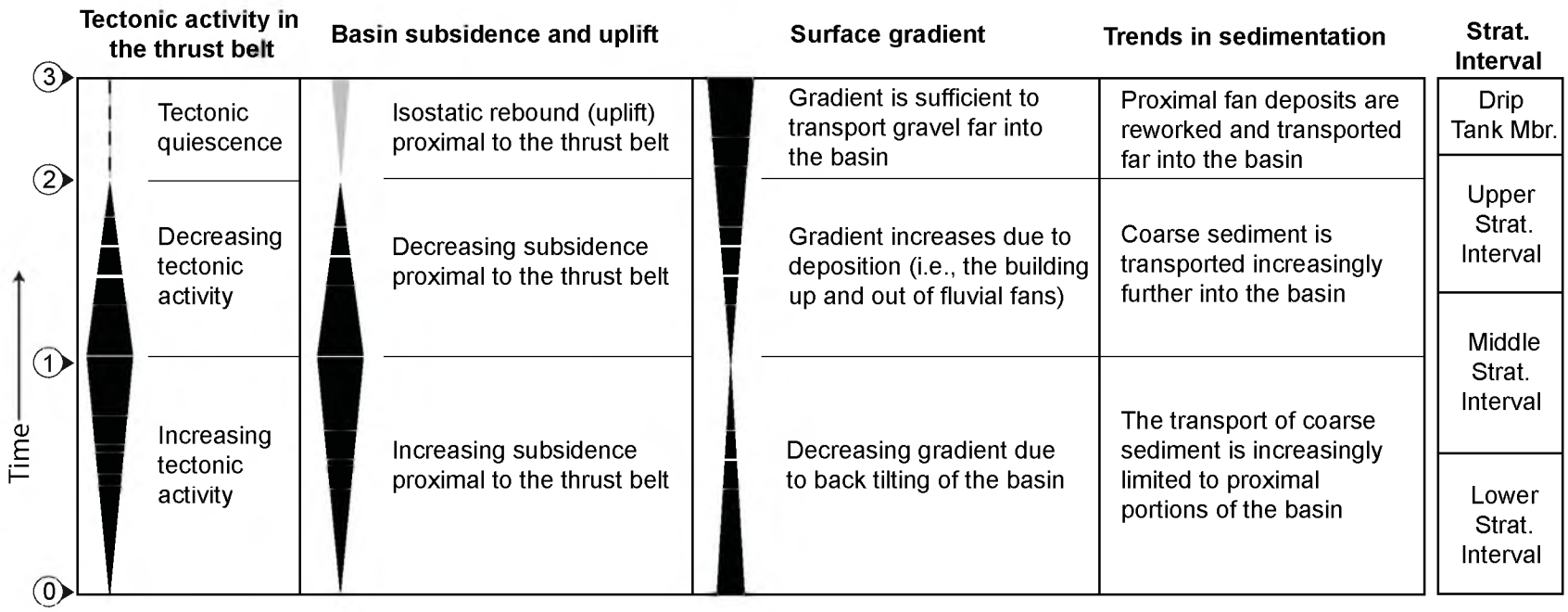

0 Markers indicate the location of the base of the depositional sequence through time in Figure 40.

Figure 42 – Paleocurrent and barform accretion data divided by depositional unit (or facies association) from Rock House Cove (Gooley, 2010), Bull Canyon (this study), and Kelly Grade (Gallin, 2010). Correlations of the three stratigraphic intervals have been included.

Stratigraphic Intervals
Rock House Cove
Gooley (2010)
Bull Canyon
This study
Kelly Grade Area
Gallin (2010)
PC
AC
Upper Stratigraphic Interval
Middle Stratigraphic Interval
Lower Stratigraphic Interval
DU-6
DU-5
DU-4
DU-3
DU-2
DU-1
DU-0
N = 205
N = 8
N = 332
N = 12
N = 249
N = 111
N = 237
N = 12
N = 437
N = 74
N = 41
N = 91
N = 63
N = 174
N = 140
N = 420
N = 58
N = 94
N = 91
N = 183
N = 87
N = 109
N = 133
N = 117
N = 1346
N = 92
N = 600
N = 24
N = 270
N = 35
49°
47°
84°
65°
127°
126°
22°
107°
66°
21°
75°
26°
89°
66°
90°
51°
71°
51°
91°
71°
88°
58°
53°
37°
40°
5°
14°
112°
21°
113°
DA
LA
N/A
FA-3
FA-2
FA-1

Figure 43 – Map of the Kaiparowits Plateau showing sediment transport directions and net coal thickness within the John Henry Member (modified from Hettinger, 2000). Arrows to the west of the paleo-shoreline indicate the mean direction of sediment transport by rivers (Gooley, 2010; Gallin, 2010). Arrows to the east of the paleo-shoreline indicate the approximate direction of longshore drift (Allen, 2009; Dooling, in prep). The dotted arrow indicates the possible location of a delta in the northern portion of the plateau.

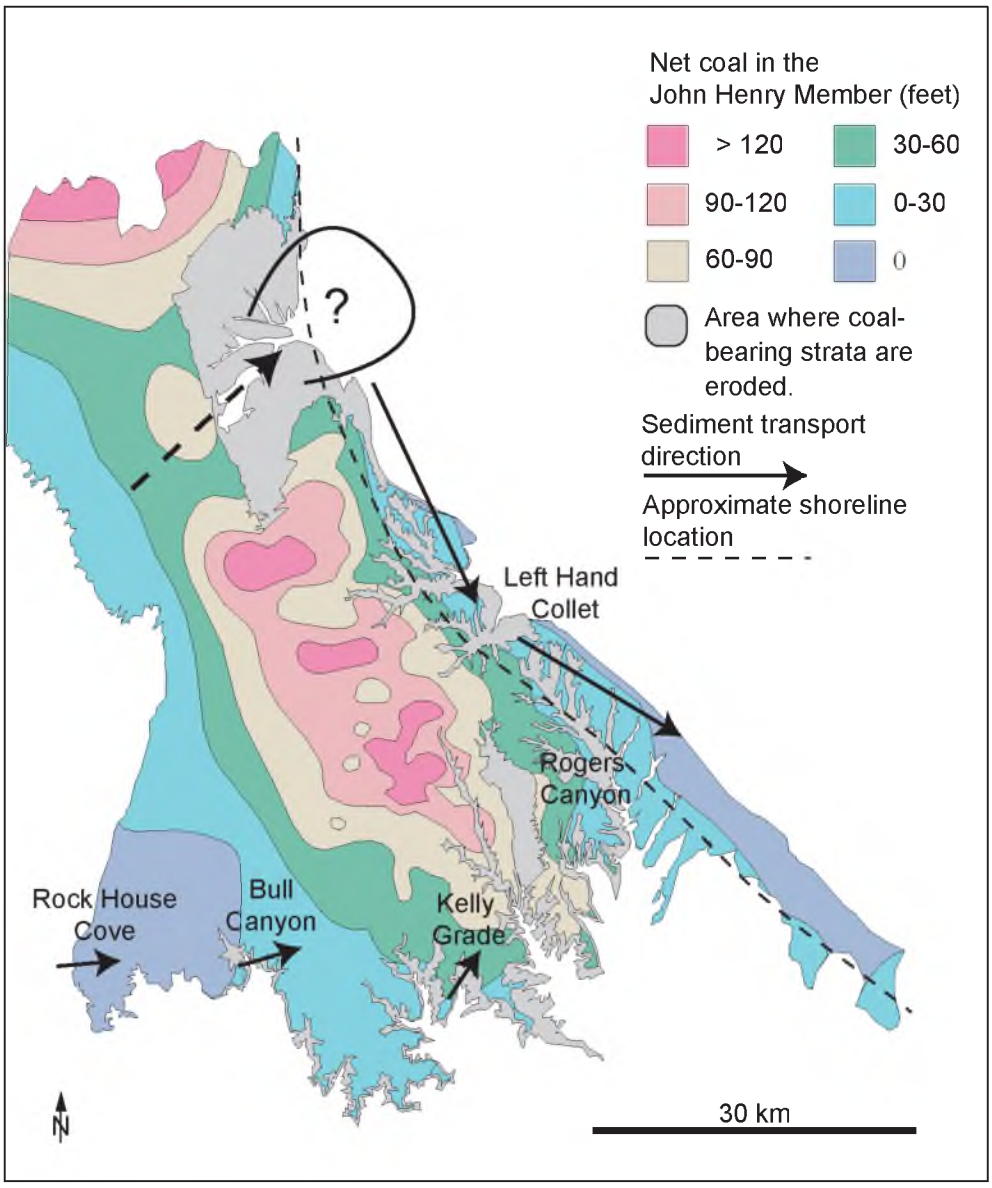
Net coal in the
John Henry Member (feet)
> 120
90-120
60-90
30-60
0-30
0
Area where coal-bearing strata are eroded.
Sediment transport direction
Approximate shoreline location
?
Left Hand Collet
Rogers Canyon
Rock House Cove
Bull Canyon
Kelly Grade
N
30 km

CONCLUSIONS

The fluvial strata of the John Henry Member at Bull Canyon were divided into seven depositional units, which are part of larger depositional trends that can be correlated regionally through proximal fluvial, paralic, and marginal marine strata. The depositional units include: DU-0, which overlies an unconformity at the top of the Smoky Hollow Member, consists of thick, laterally extensive (ave. 316 m wide), and highly amalgamated fluvial channel belts. DU-1 consists of laterally isolated (ave. 75 m wide), tidally influenced fluvial channel belts with limited amalgamation. DU-2 consists of moderately extensive (ave. 92 m wide), meandering fluvial channel belts with moderate amalgamation. DU-3 consists of laterally isolated (ave. 74 m wide) meandering or anastomosing channel belts with limited amalgamation in thick floodplain and coal mire deposits. DU-4 consists of laterally extensive (ave. 180 m wide), meandering channel belts with moderate amalgamation. DU-5 consists of laterally extensive (ave. 225 m wide) meandering channel belts with areas of high amalgamation and channels that were more competent than those of DU-4. DU-6 consists of laterally extensive (ave. 191 m wide), fully amalgamated channel belts with characteristics that transition vertically from meandering fluvial facies into braided fluvial facies. The overlying Drip Tank Member consists of fully amalgamated, braided fluvial channel belts.

Paleomorphodynamic calculations from the lower half of the section (DU-1 through DU-3) show low, decreasing paleoslopes ($<0.01°$) and predict a relatively large

backwater transition zone (>100 km). However, some of the backwater calculations may be overestimated if the sediment was deposited within the backwater transition zone, as propose in this study. Calculations for the upper half of the section (DU-3 through DU-6) show relatively high and vertically increasing paleoslopes (up to 0.02°) and predict a greatly reduced backwater transition zone (generally <75 km).

Large-scale trends in alluvial architecture (i.e., grain size and channel belt characteristics) were used to define three stratigraphic intervals, which are related to changes in the ratio of accommodation to sediment supply: The lower stratigraphic interval (which includes DU-0 and DU-1) exhibits vertical trends of decreasing channel belt thickness and width, and increase in tidal influence and preservation of floodplain and coal mire facies. This interval relates to a period of increasing rate of accommodation relative to sediment supply. The middle stratigraphic interval (which includes DU-2 and DU-3) records an overarching trend of laterally restricted channel belts in thick accumulations of floodplain and coal mire facies. This interval relates to the highest rates of accommodation relative to sediment supply. The upper stratigraphic interval (which includes DU-4, DU-5, DU6, and the base of the Drip Tank Member) exhibits vertical trends of increased channel belt width and amalgamation, reduced amounts of preserved floodplain and coal mire facies, and the transition from meandering to braided fluvial facies. This interval relates to decreasing and low rates of accommodation relative to sediment supply.

The depositional model proposed for the John Henry Member links stratigraphic trends to tectonically driven changes in accommodation and sedimentation. The variations in accommodation and sedimentation alter the fluvial system and produce

large-scale depositional trends. The depositional model includes three stages: In the first stage, increasing tectonic activity in the hinterland produces an upward fining trend in the basin foredeep. This first stage correlates to the lower and middle stratigraphic intervals. In the second stage, reducing rates of tectonic loading produce a coarsening upward sequence. The second stage correlates to the upper depositional interval. In the third stage, erosion and subsidence related to tectonic quiescence result in the deposition of a coarse clastic sheet. The third stage correlates to the dramatic grain size increase that begins near the top of the upper stratigraphic interval of the John Henry Member and continues into the Drip Tank Member.

APPENDIX A

MEASURED STRATIGRAPHIC SECTIONS

The stratigraphic sections measured in Bull Canyon of the Kaiparowits Plateau are included in Appendix A. A symbols legend precedes the measured sections, which included: BC SXN 1, BC SXN 2, BC SXN 3, BC SXN 4.1, and BC SXN 4.2 (Figure A.1). The locations of the measured stratigraphic sections are shown on the map in Figure 6 and are marked in the interpreted photomosaics in Appendix B.

Figure A.1 – Measured stratigraphic sections from Bull Canyon: BC SXN 1, BC SXN 2, BC SXN 3, BC SXN 4.1, and BC SXN 4.2.

Stratigraphic Sections Legend

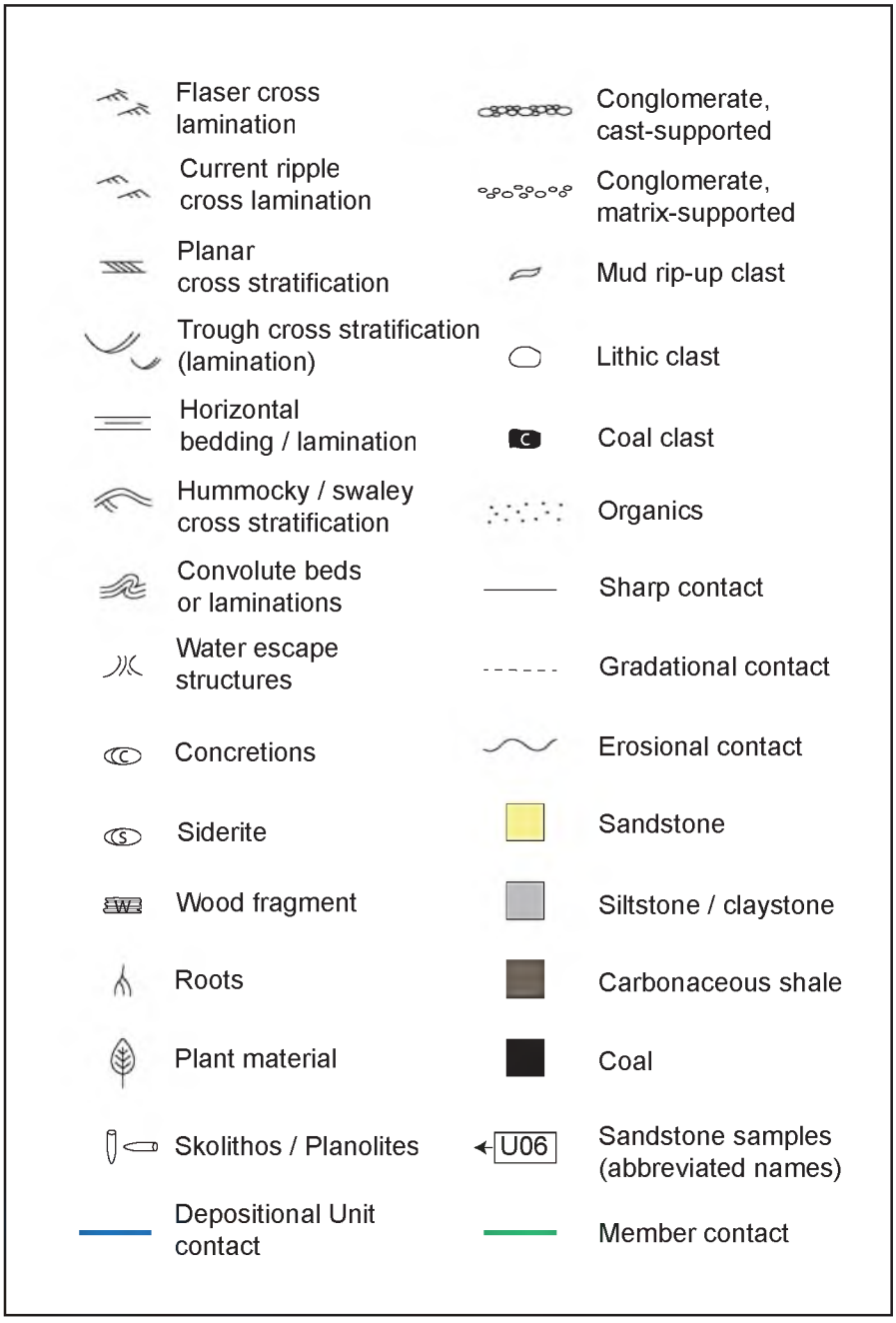

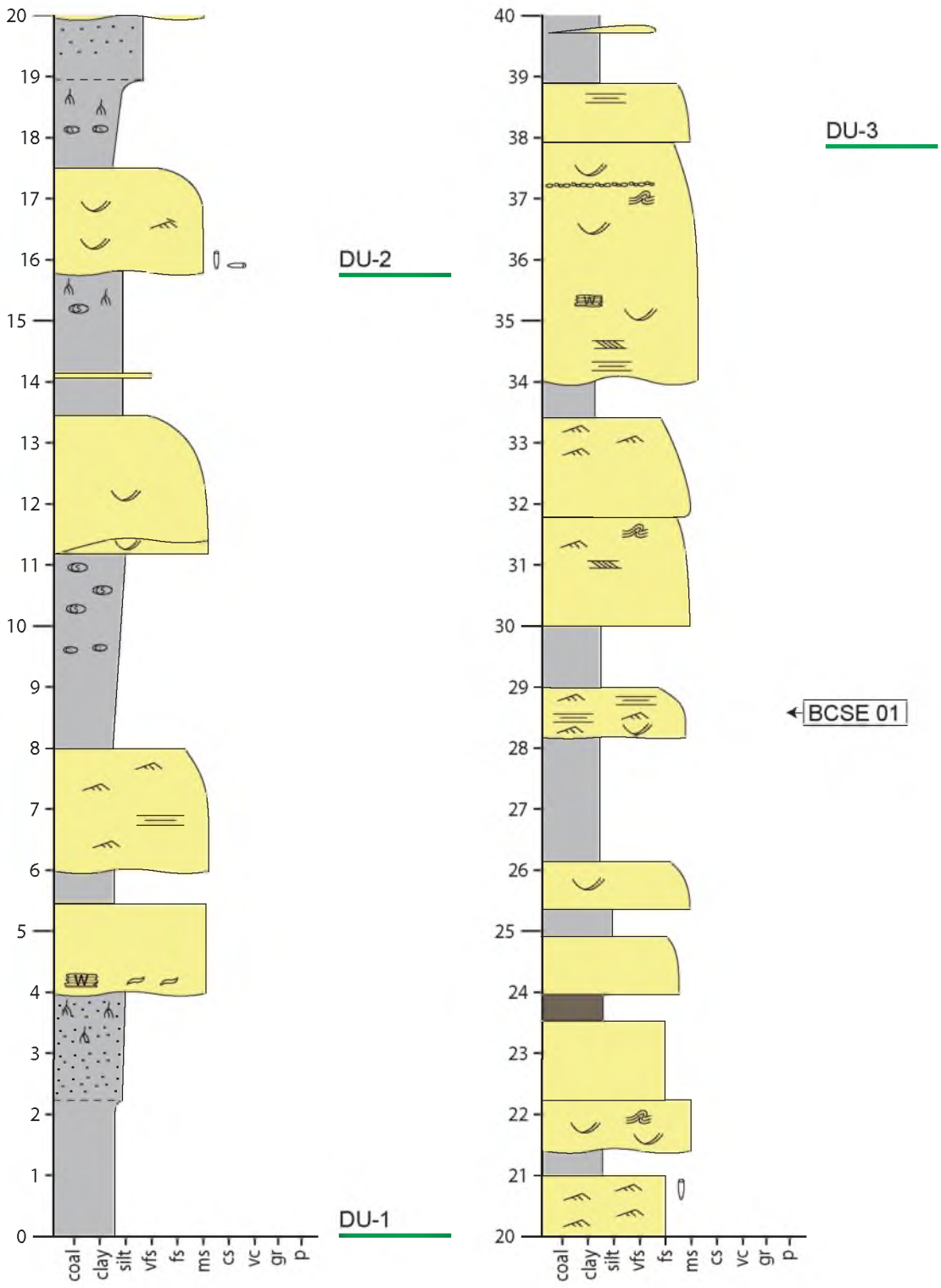

Figure A.1 continued

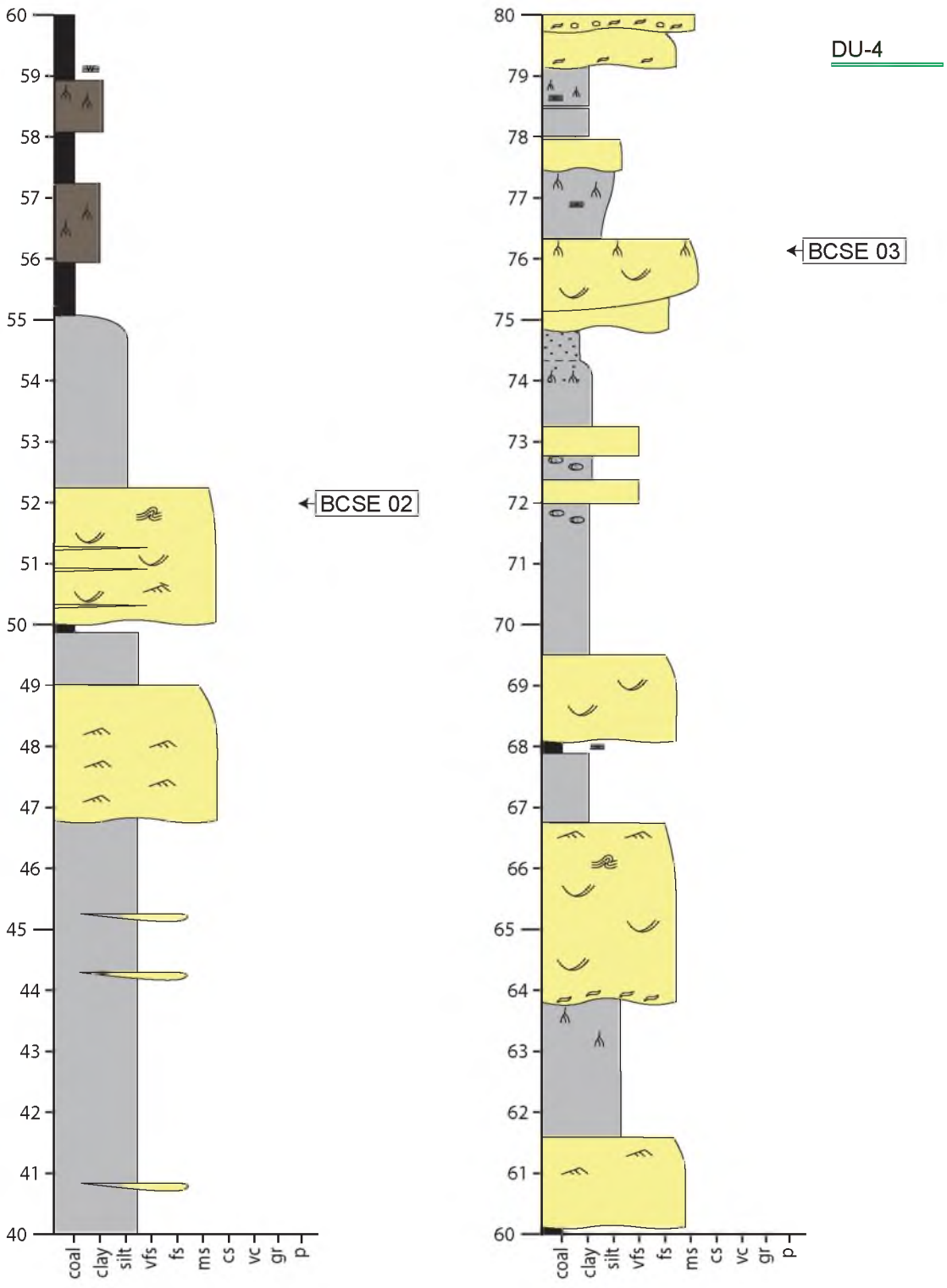

Figure A.1 continued

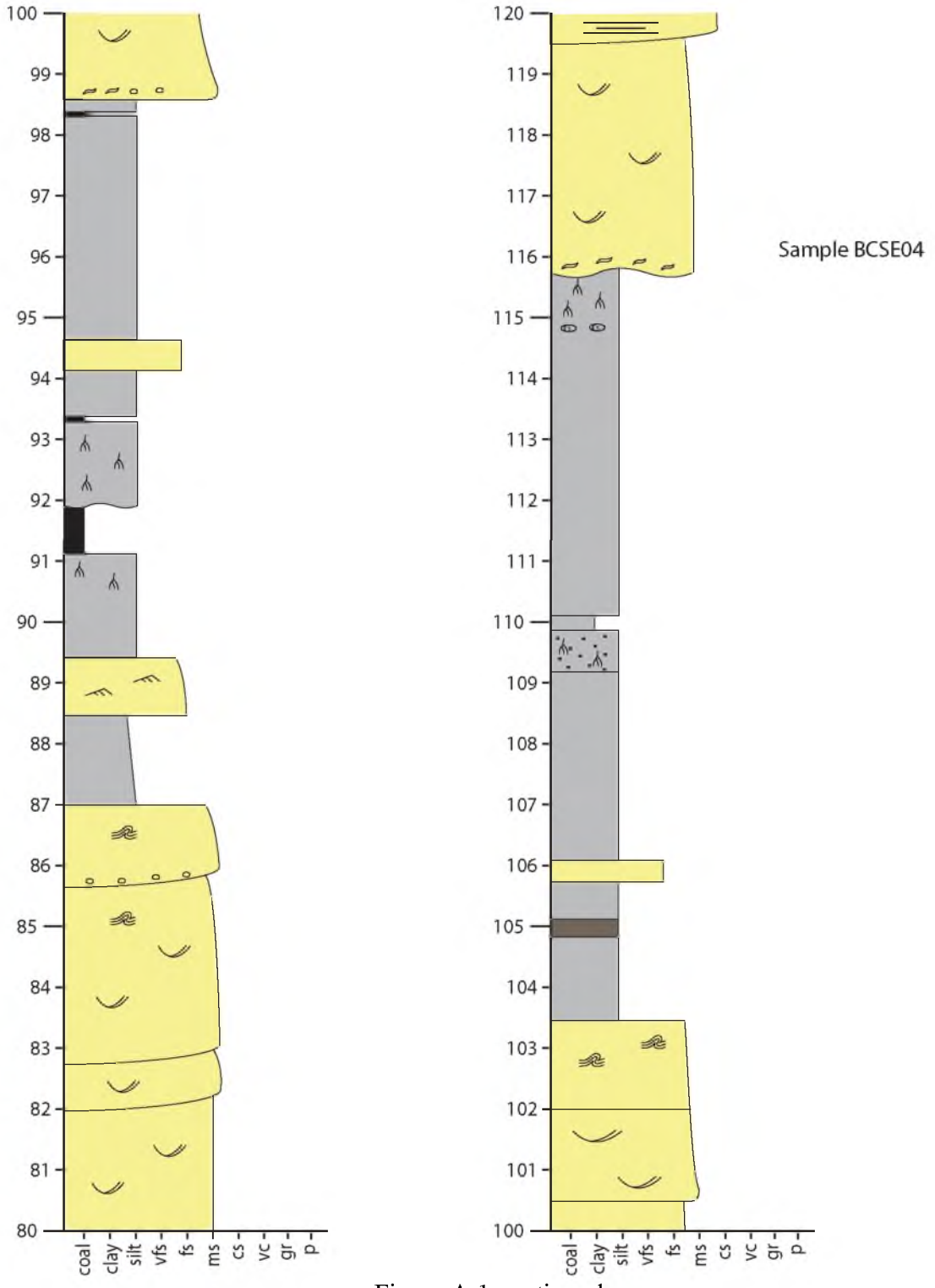

Figure A.1 continued

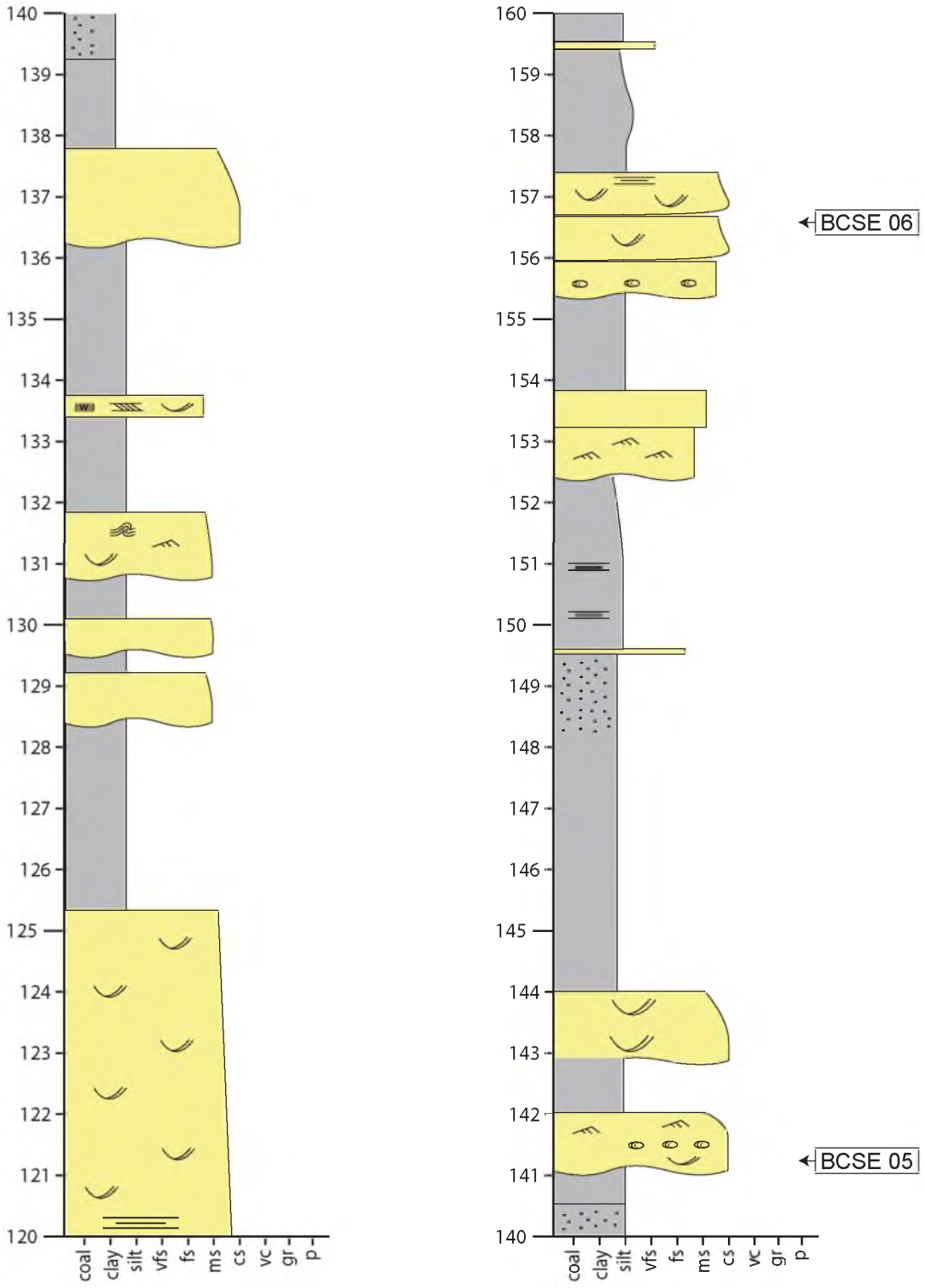

Figure A.1 continued

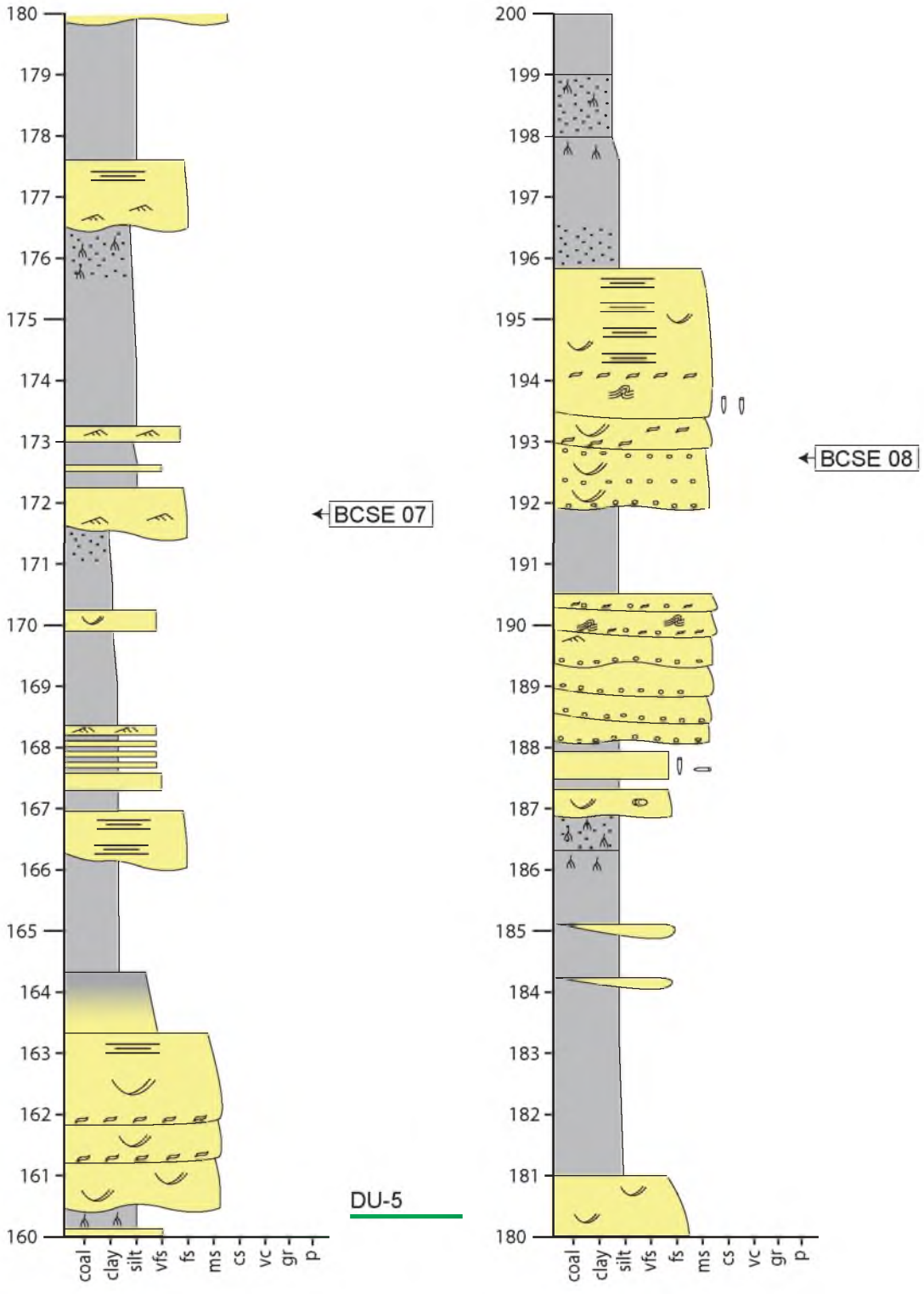

Figure A.1 continued

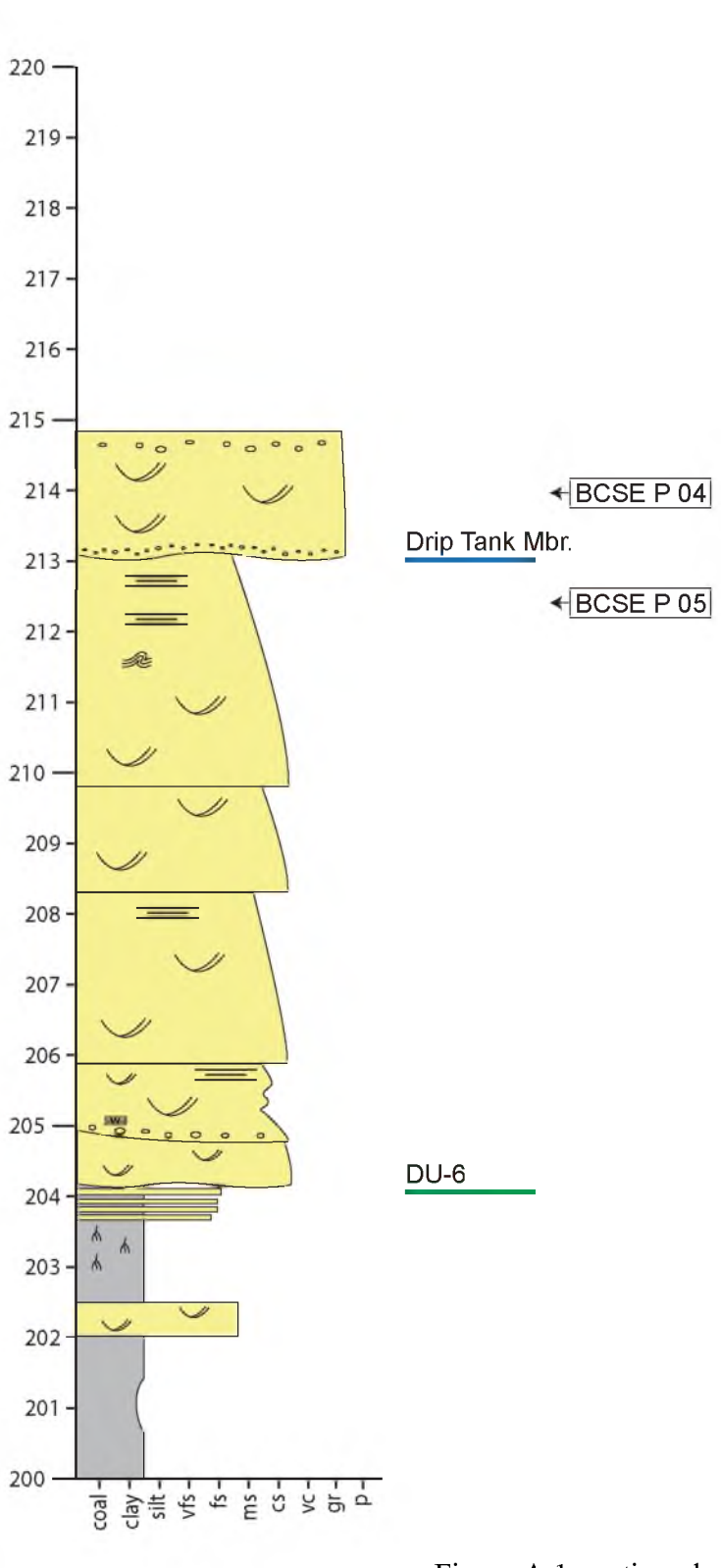

Figure A.1 continued

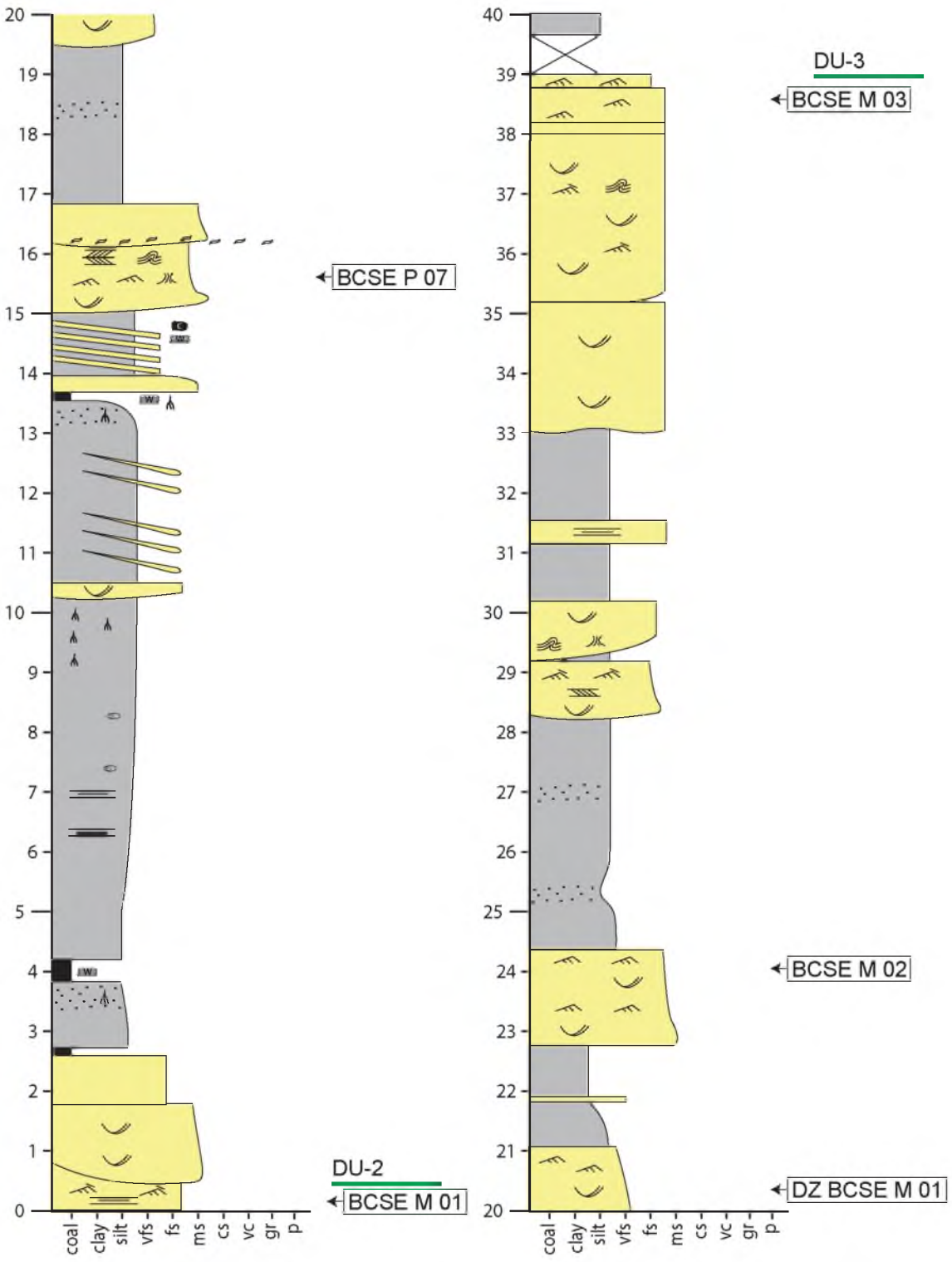

Figure A.1 continued

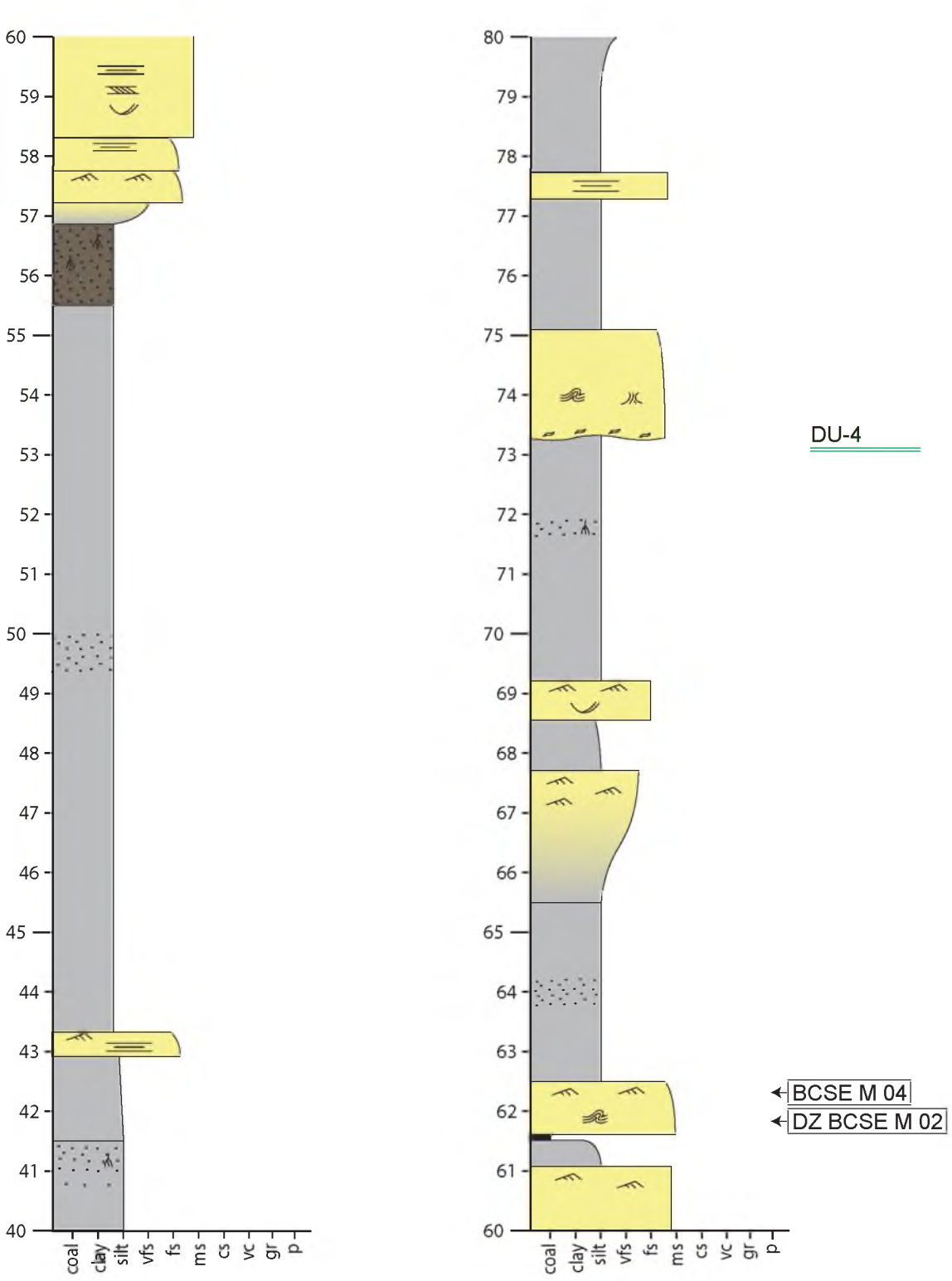

Figure A.1 continued

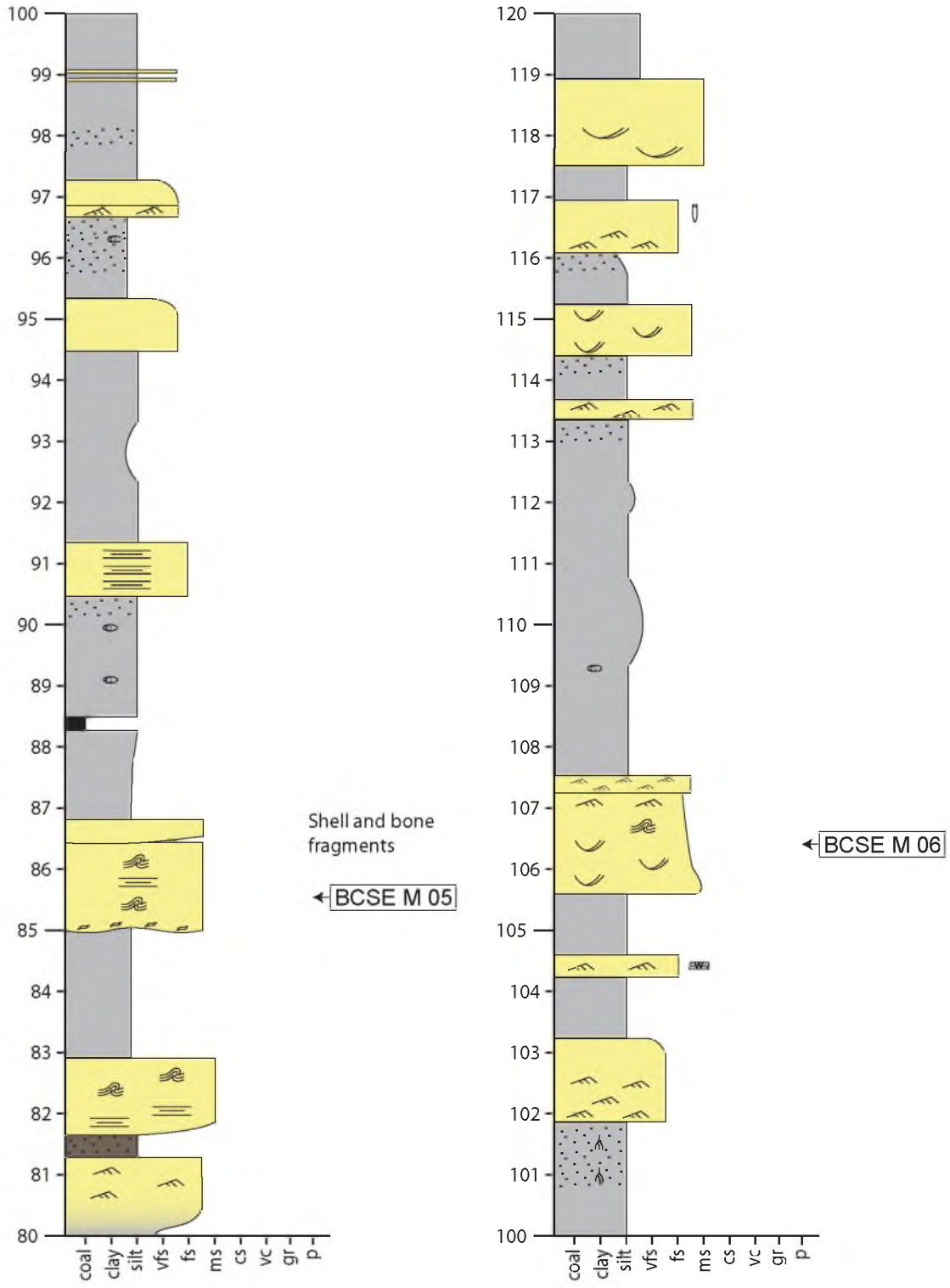

Figure A.1 continued

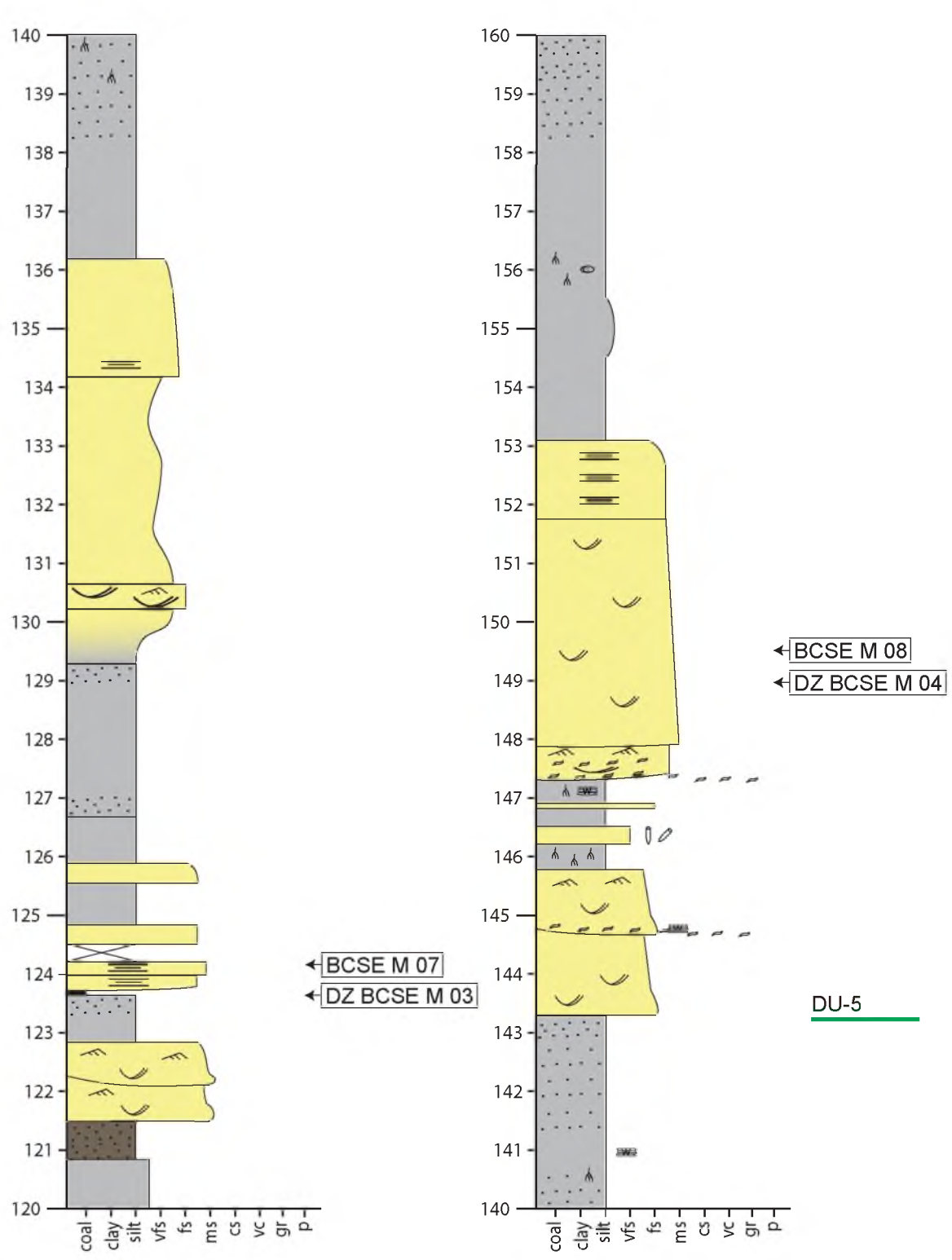

Figure A.1 continued

BC SXN 2 (160-200 m)

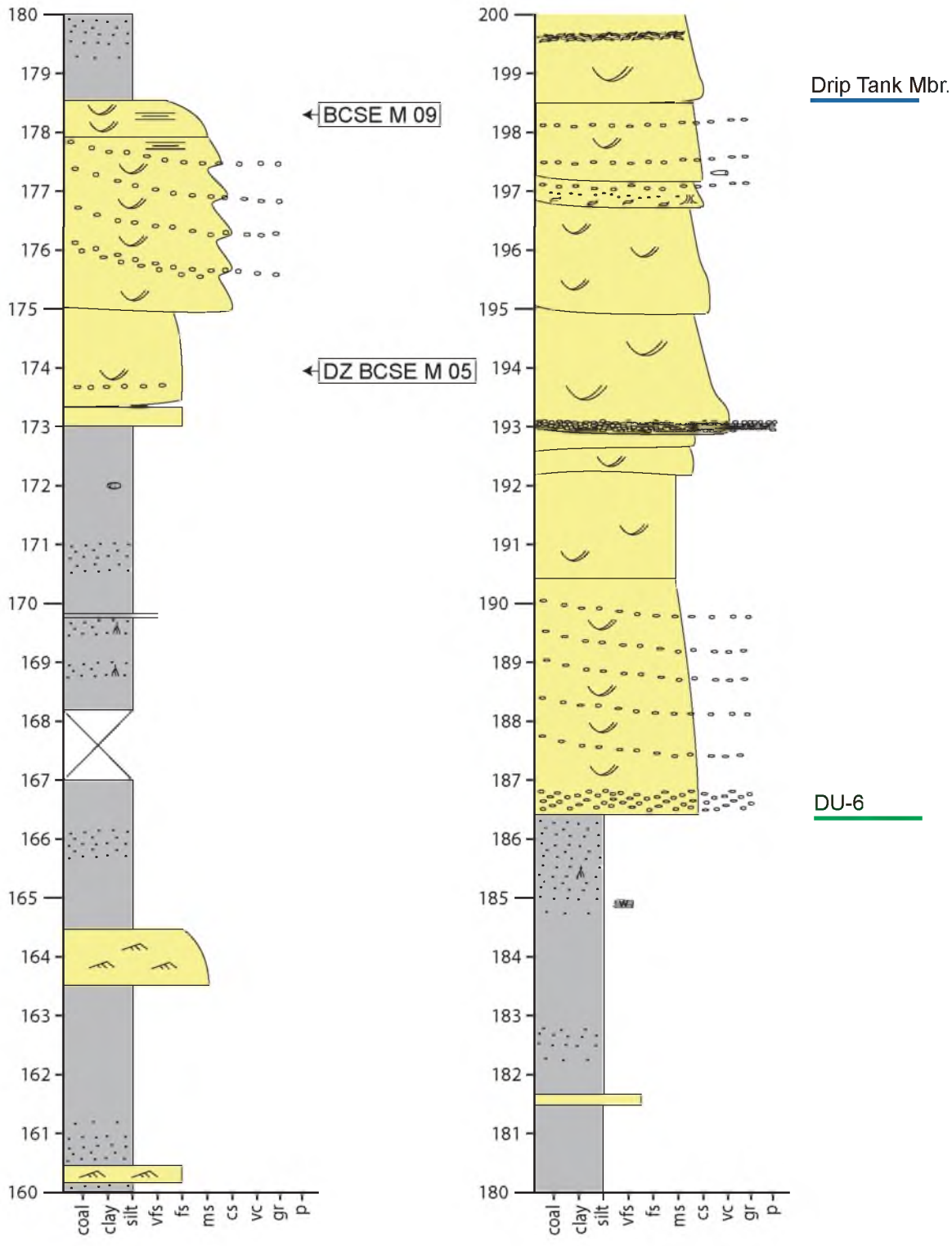

Figure A.1 continued

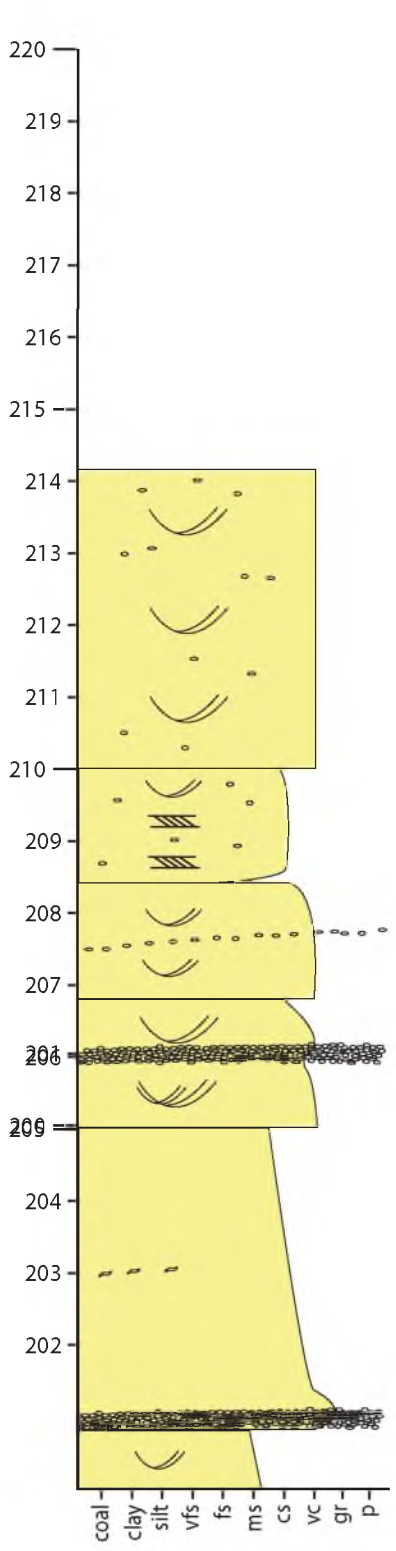

Figure A.1 continued

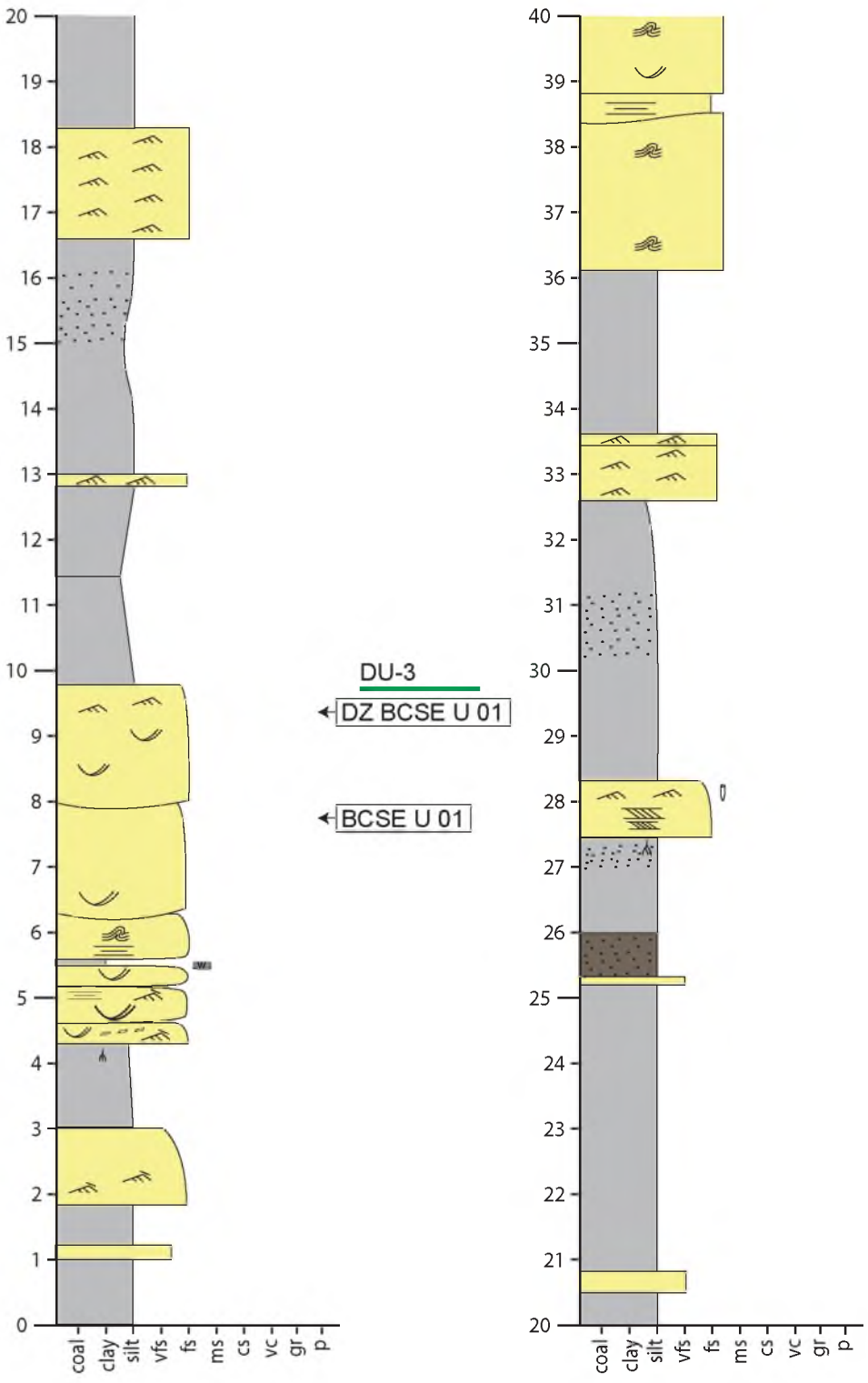

Figure A.1 continued

BC SXN 3 (40-80 m)

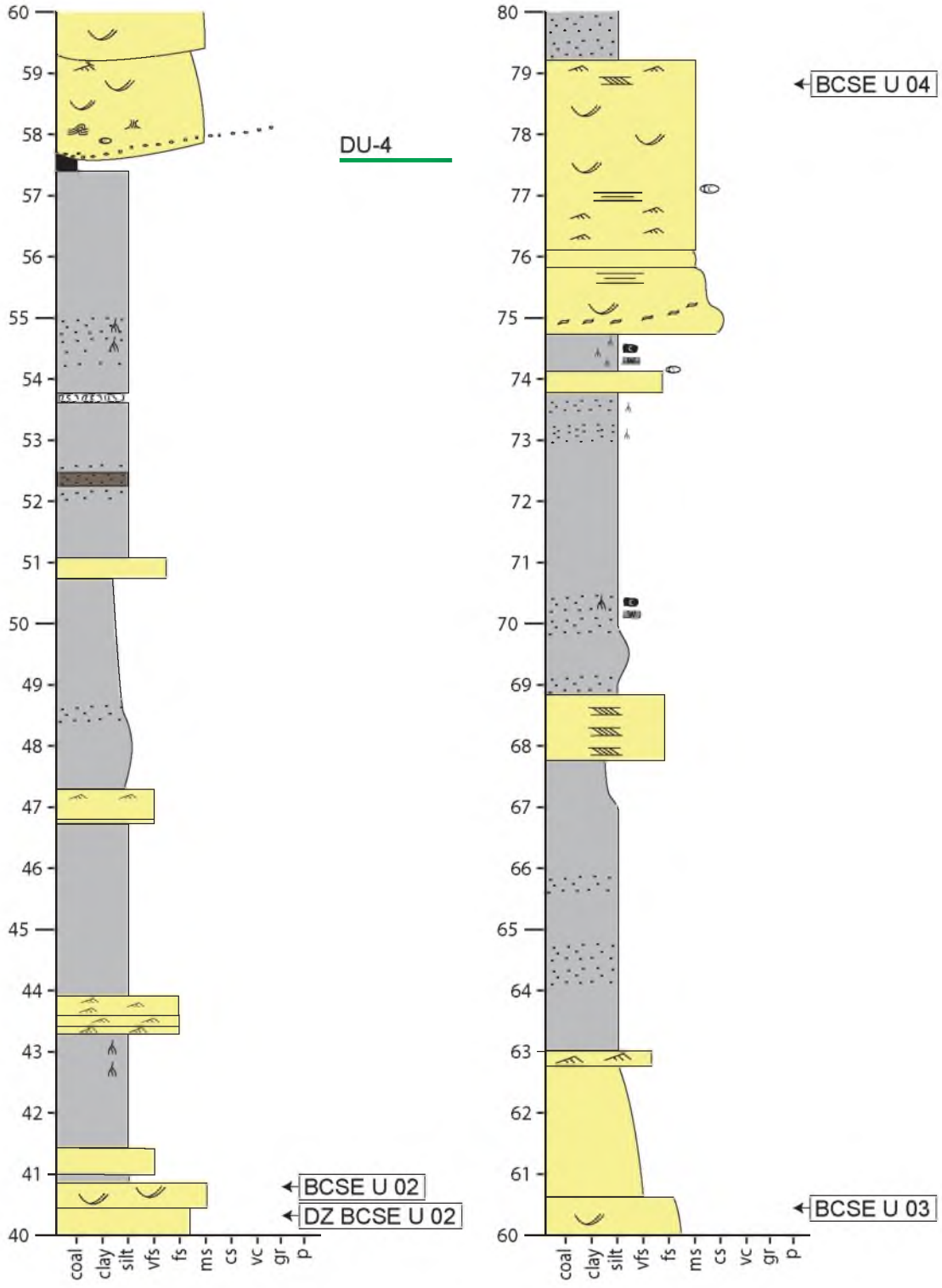

Figure A.1 continued

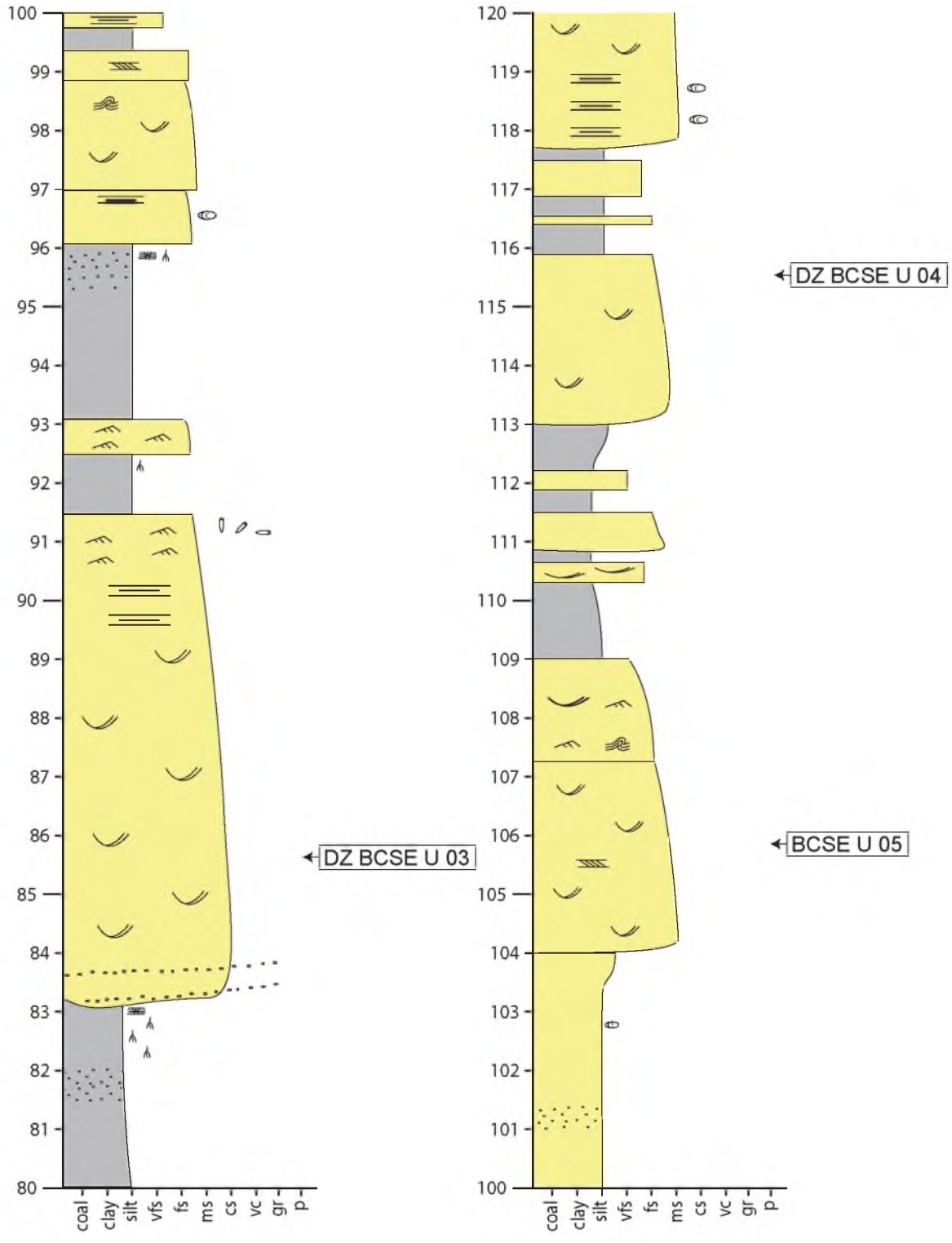

Figure A.1 continued

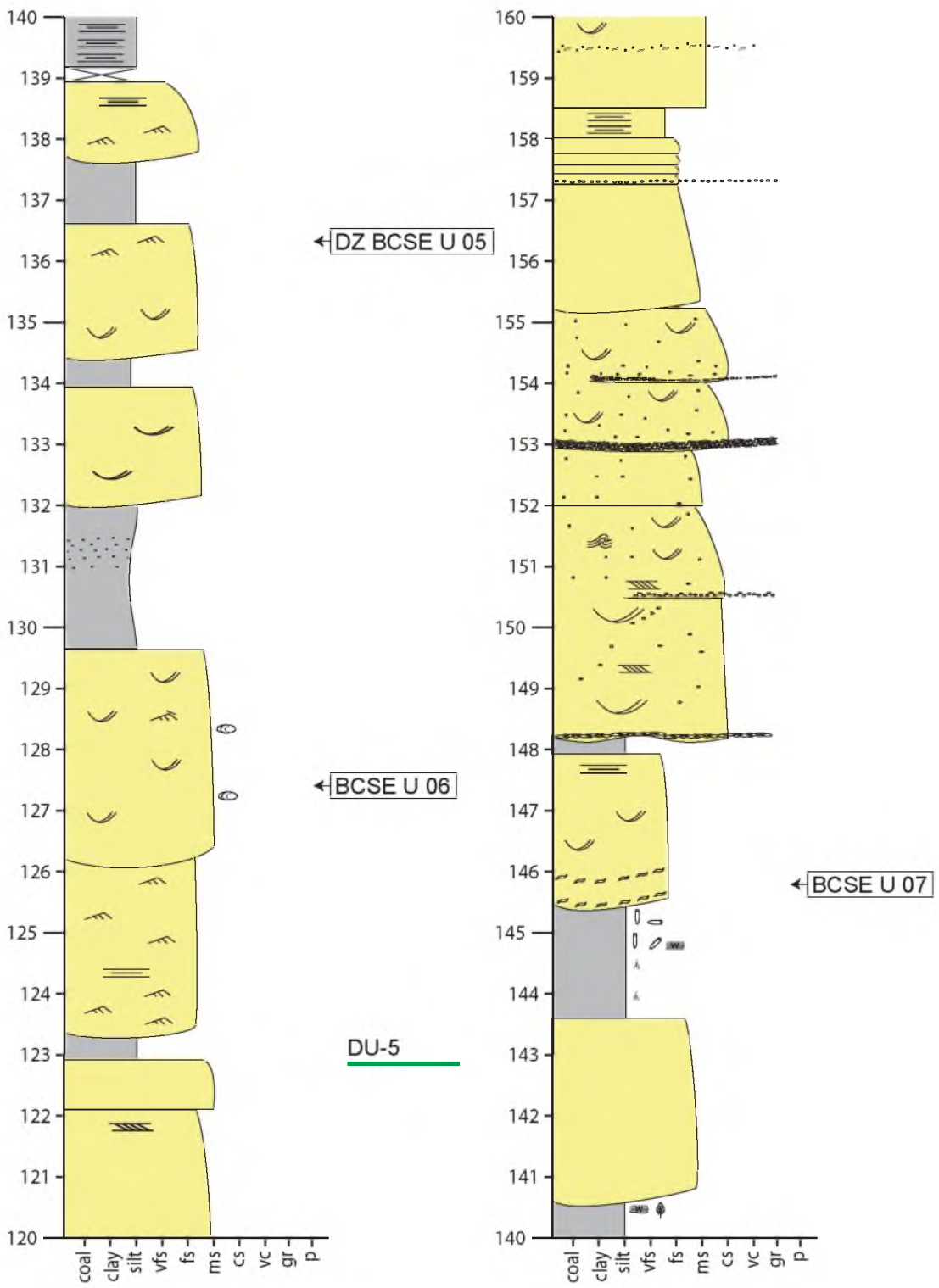

Figure A.1 continued

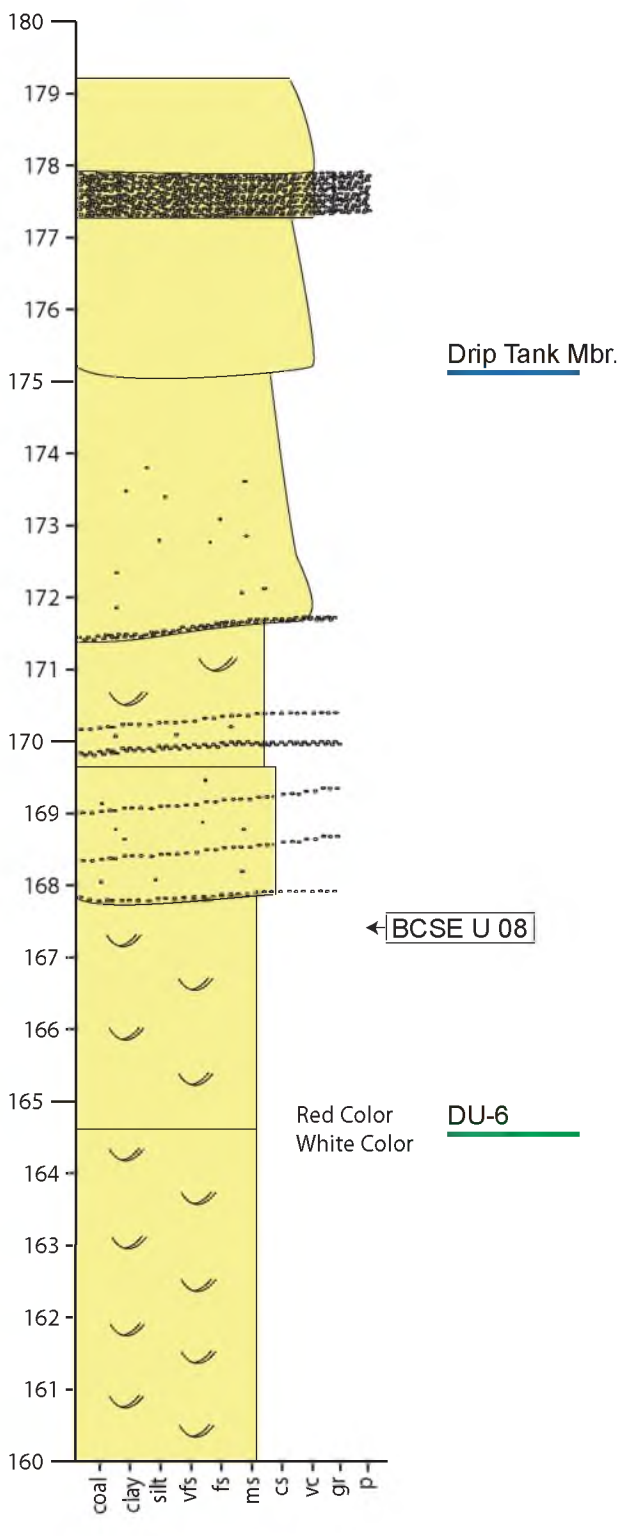

Figure A.1 continued

BC SXN 4.1 (0-40 m)

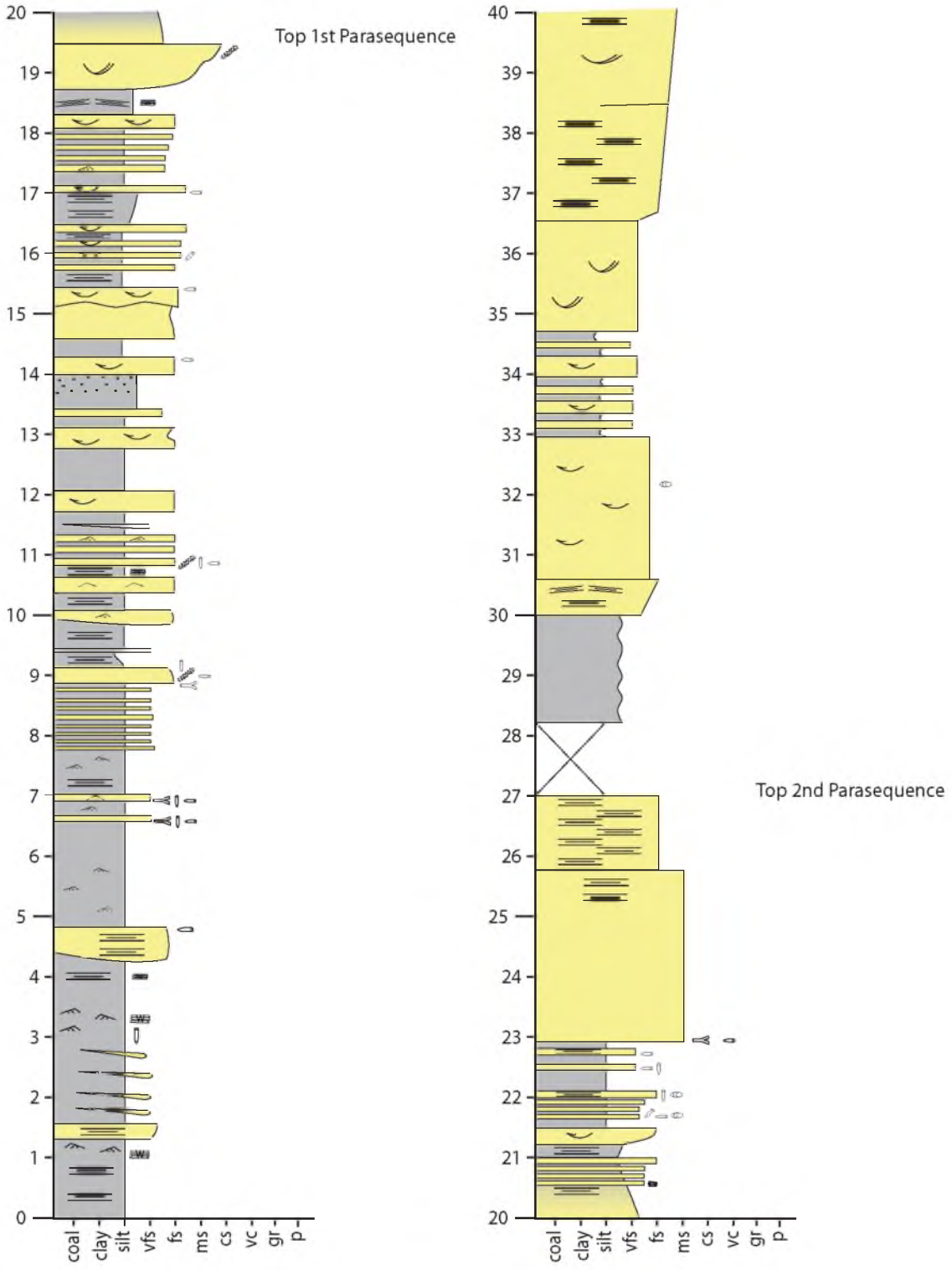

Figure A.1 continued

BC SXN 4.1 (40-41 m)

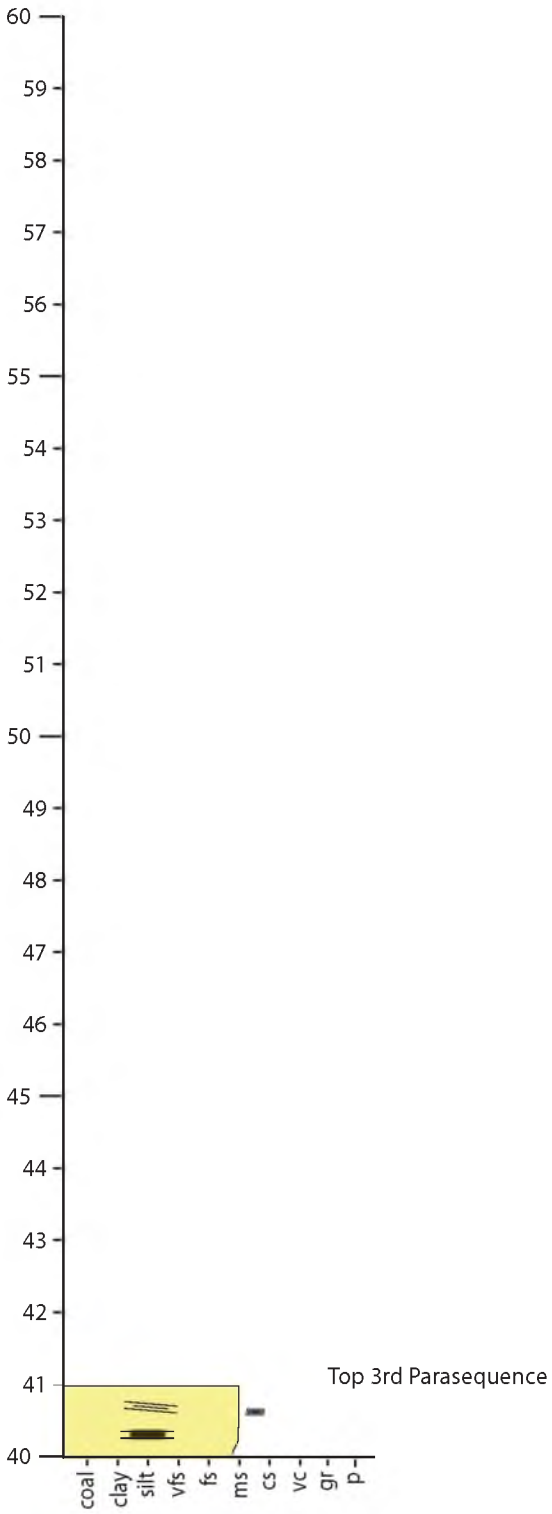

Figure A.1 continued

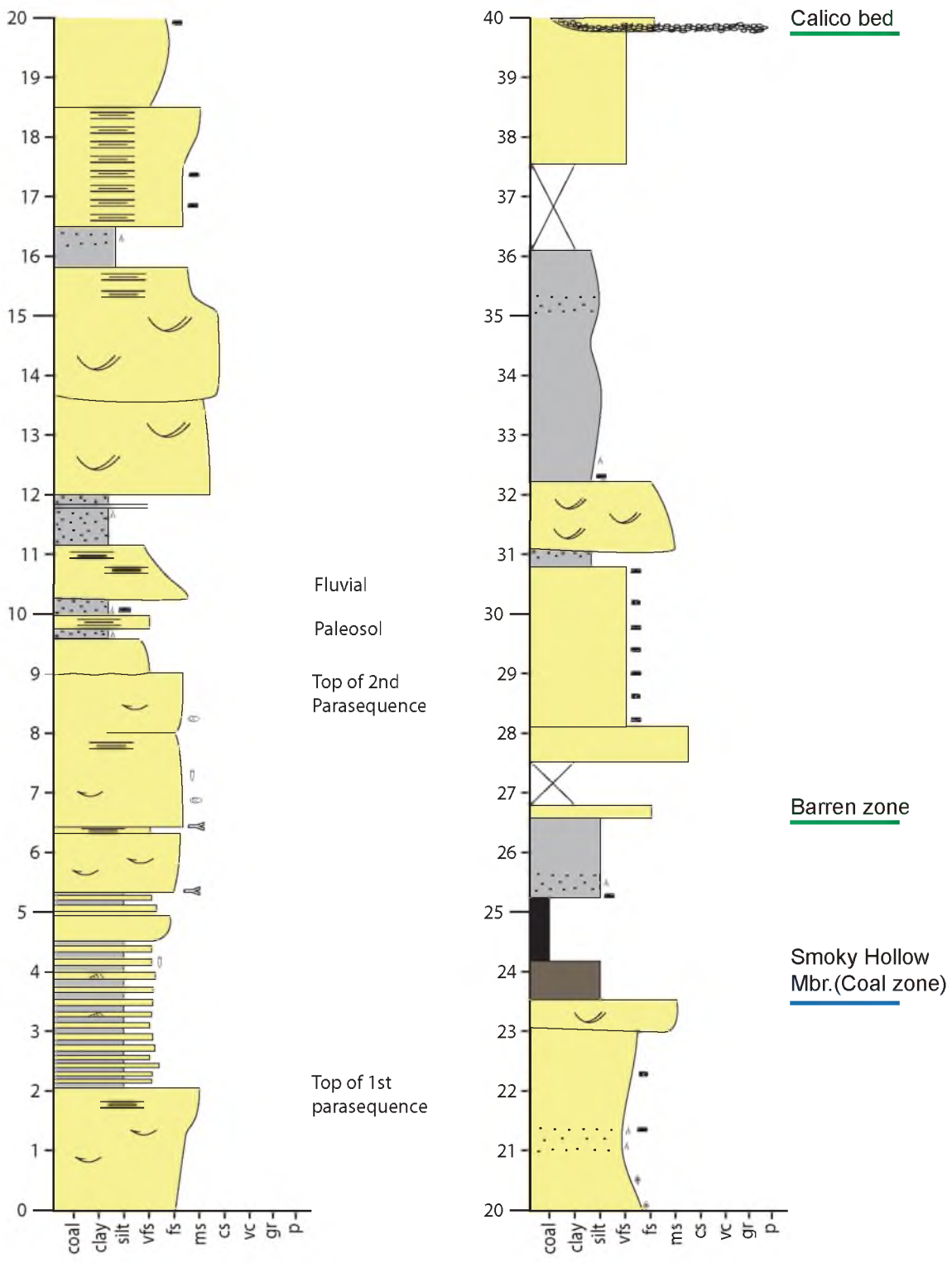

Figure A.1 continued

BC SXN 4.2 (40-80 m)

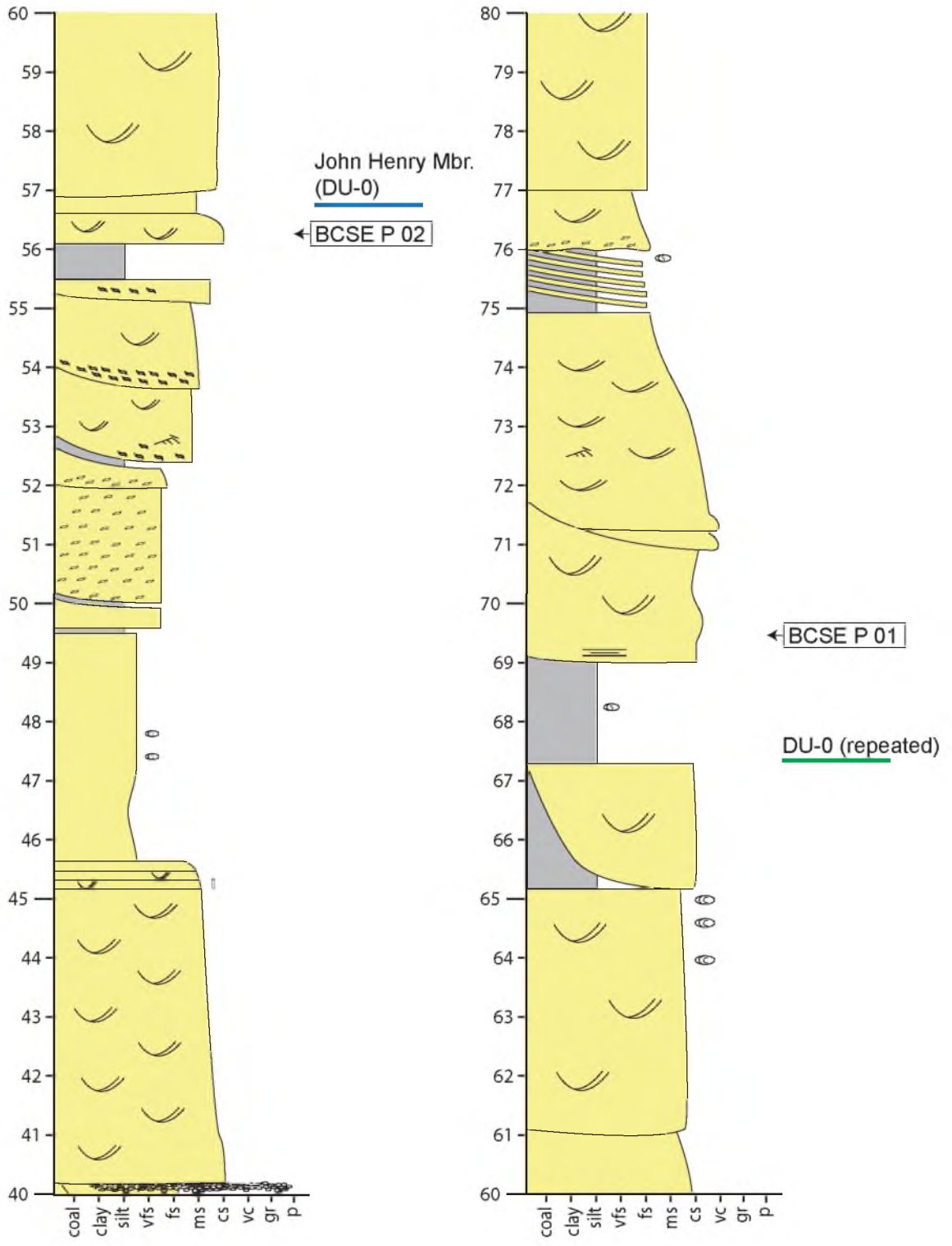

Figure A.1 continued

BC SXN 4.2 (80-82 m)

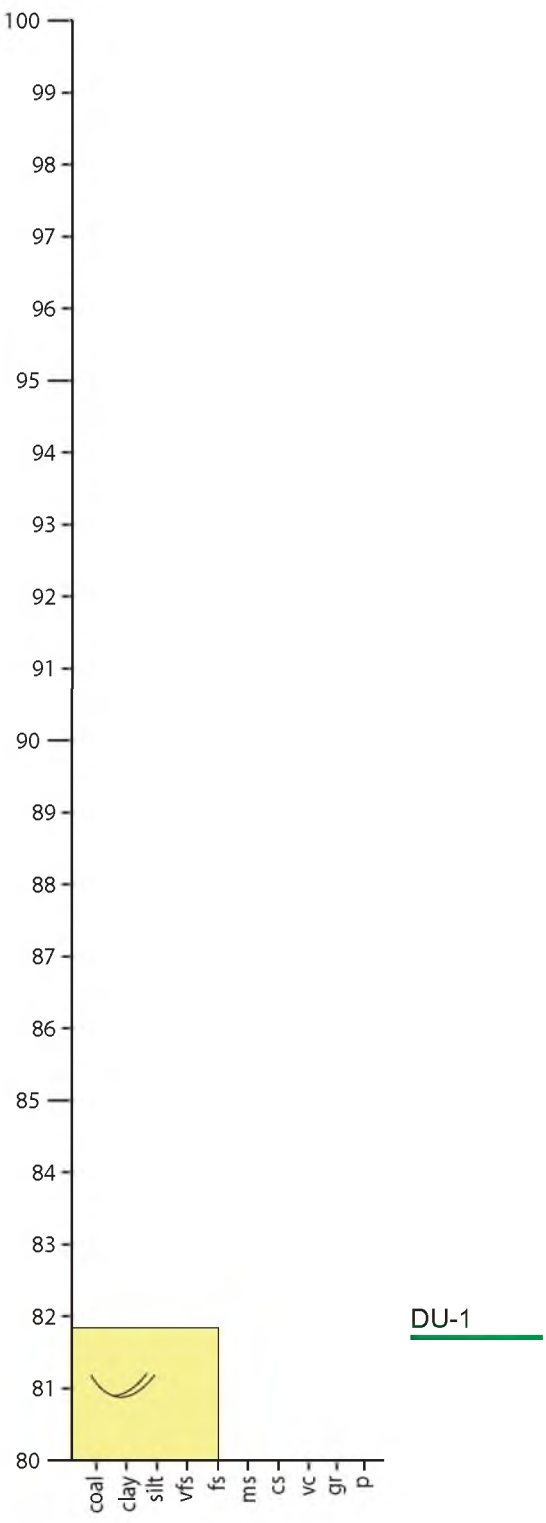

Figure A.1 continued

APPENDIX B

INTERPRETED PHOTOMOSAICS

A symbols legend (Figure B.1) is included for the interpreted photomosaics from Bull Canyon: Lower East Bull Canyon, Upper East Bull Canyon, and West Bull Canyon (Figures B.2, B.3, and B.4). The locations of these photographs are shown on Figure 6.

Figure B.1 – Legend for the symbols and labels used in the interpreted photomosaics (Figures B.2, B.3, and B.4).

Legend for Interpreted Photomosaics

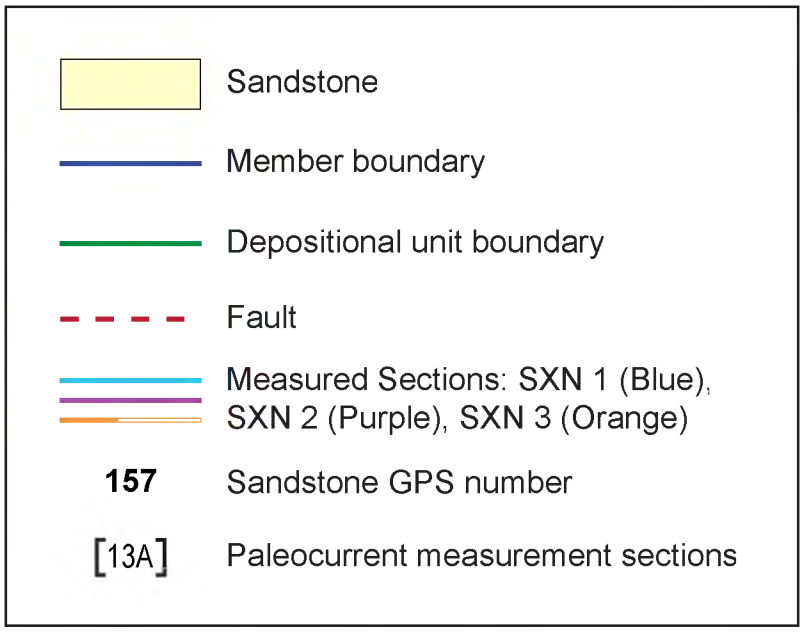

Figure B.2 – Interpreted photomosaic of the outcrops in the lower portion Bull Canyon. Figure B.1 is a legend for the symbols and labels.

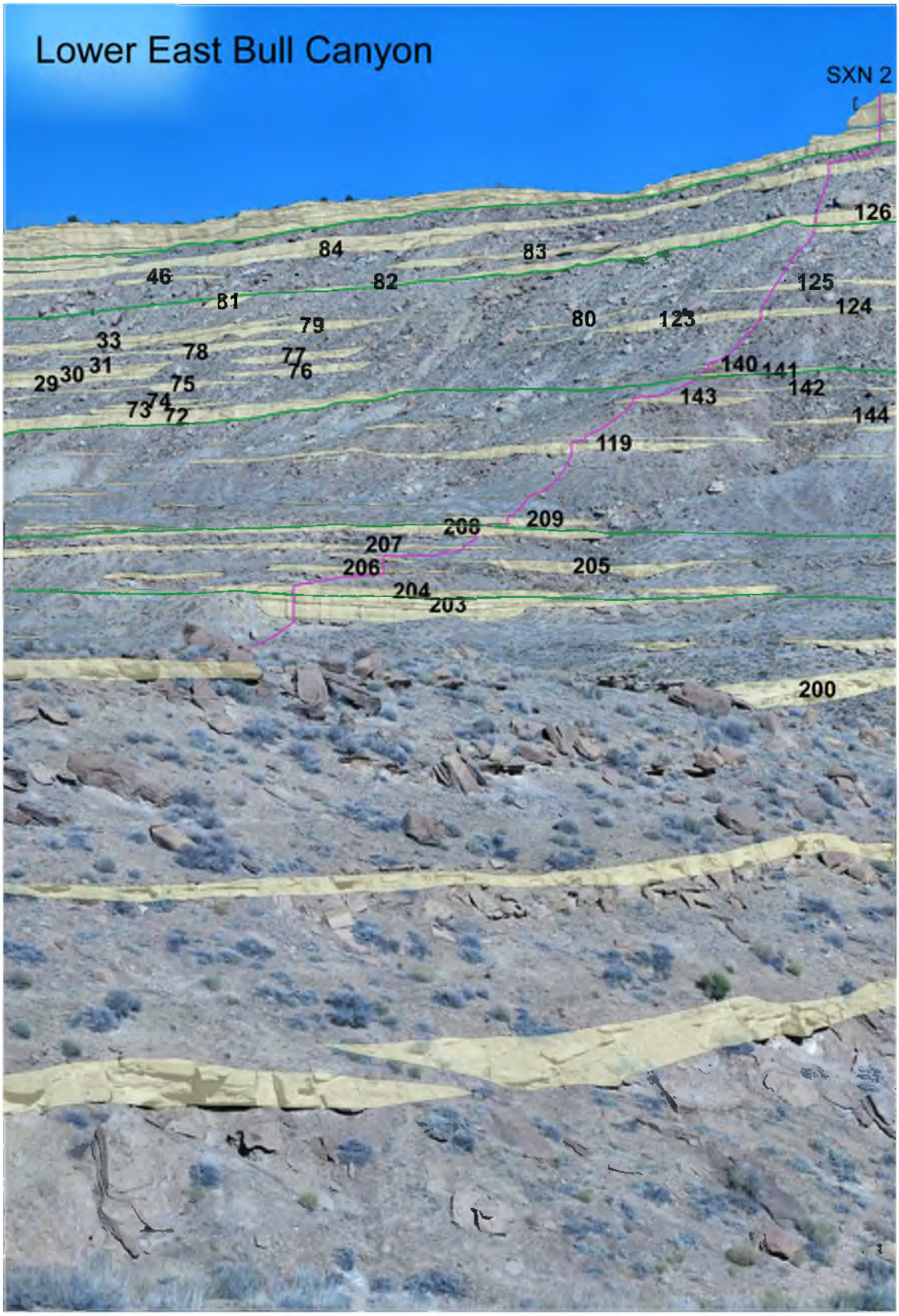
Lower East Bull Canyon
SXN 2
126
84
83
46
82
125
81
124
80
123
79
33
78
77
140
141
31
76
142
29
30
75
143
74
144
73
72
119
209
208
207
206
205
204
203
200

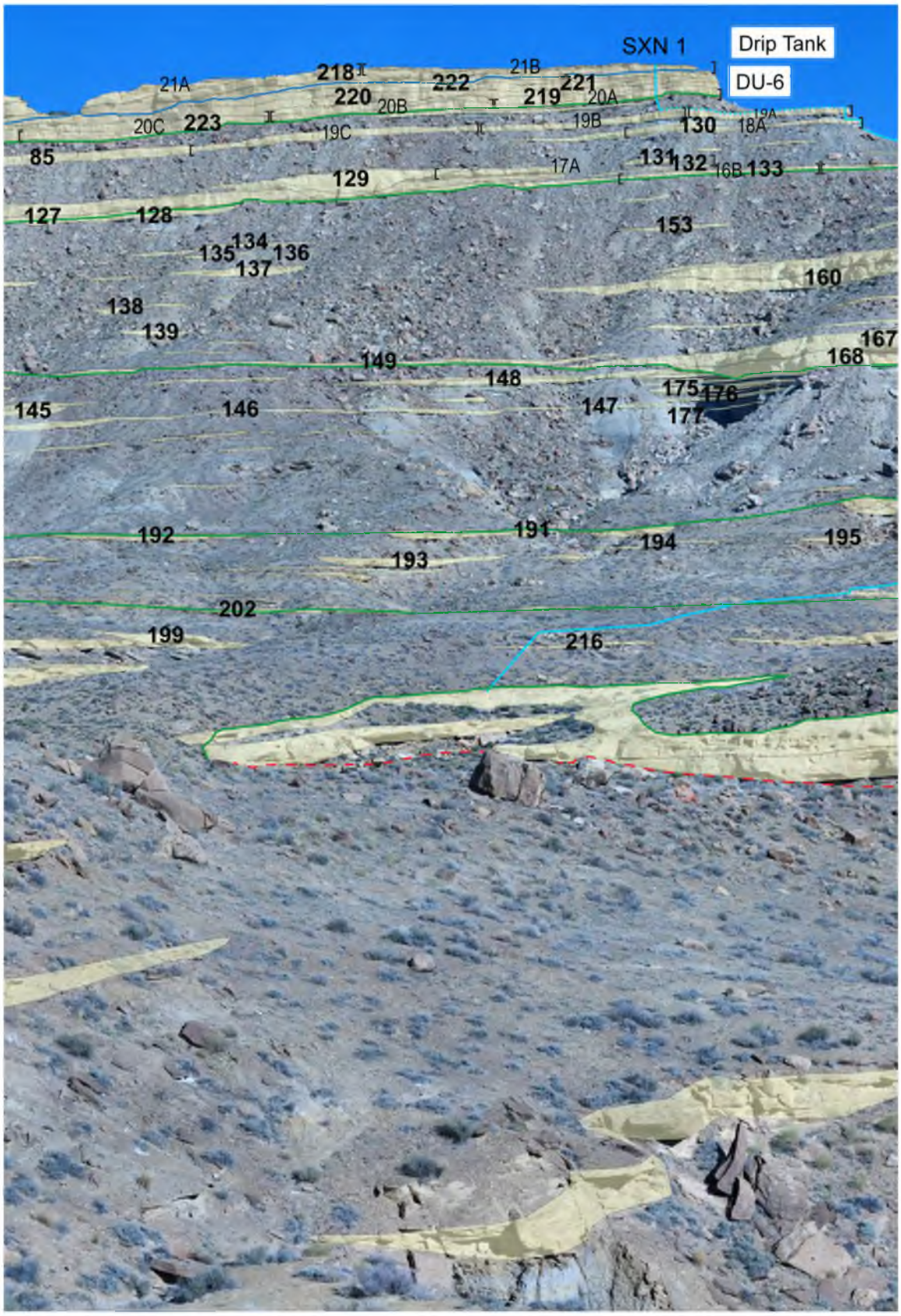

Figure B.2 continued

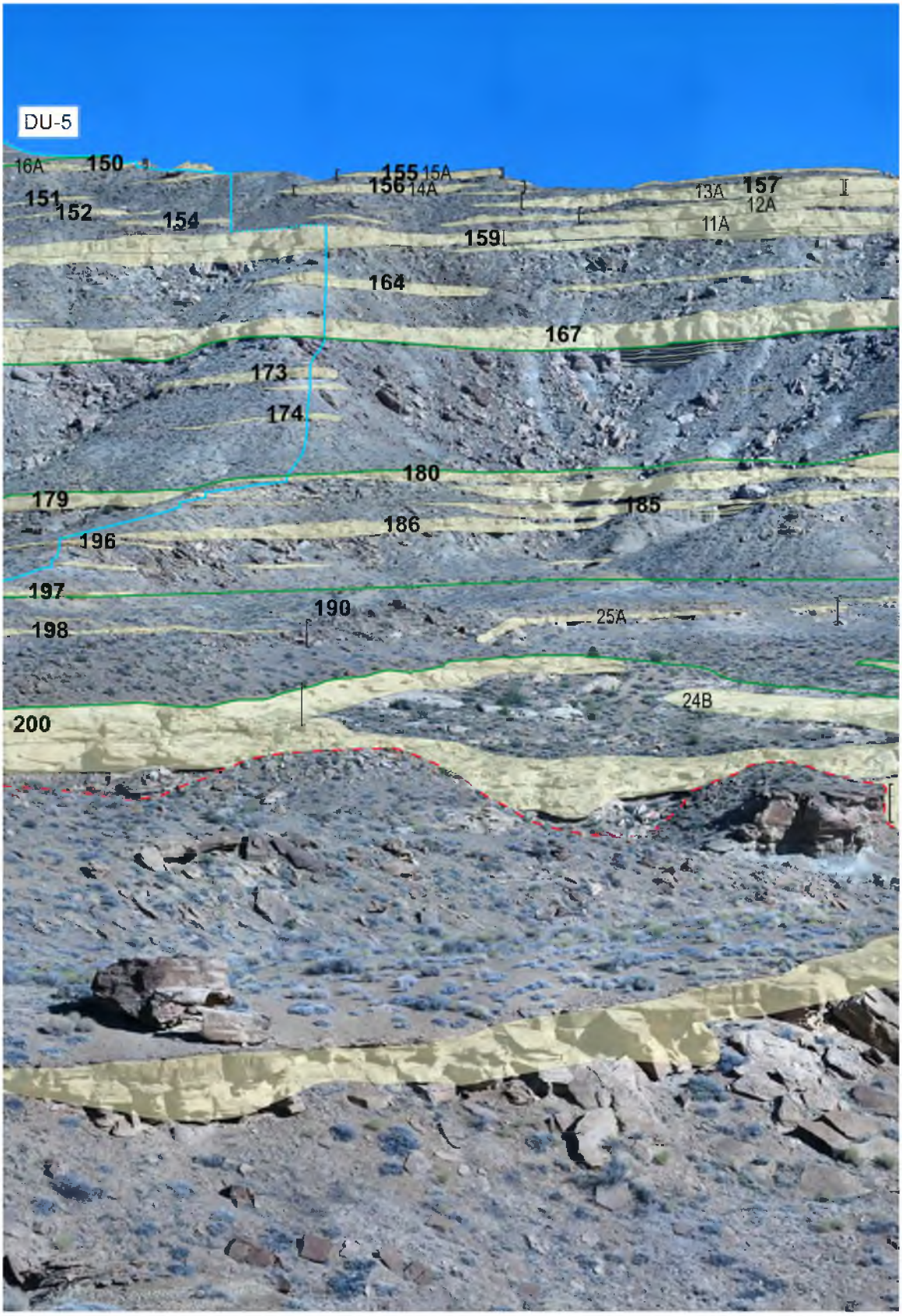

Figure B.2 continued

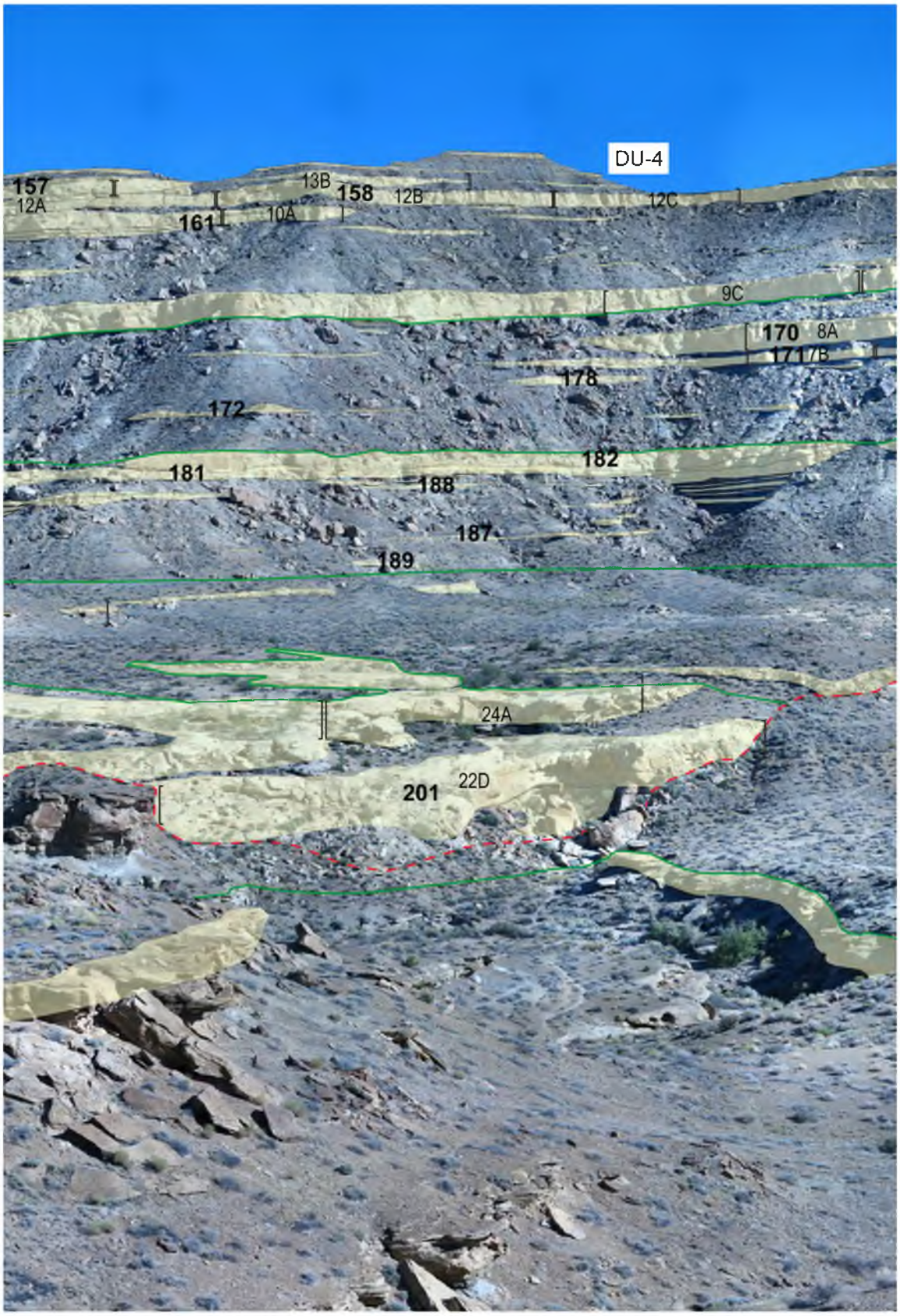

Figure B.2 continued

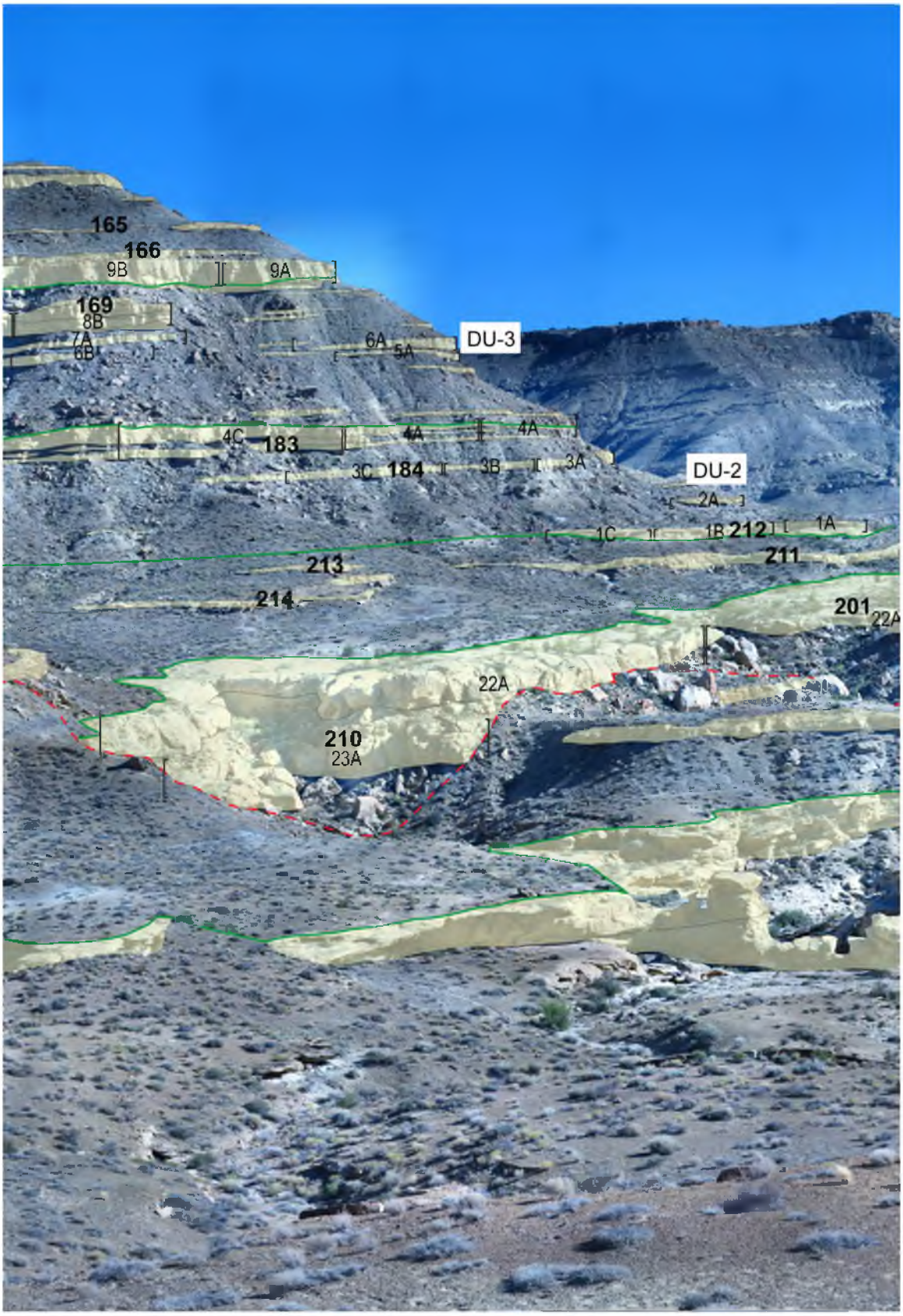

Figure B.2 continued

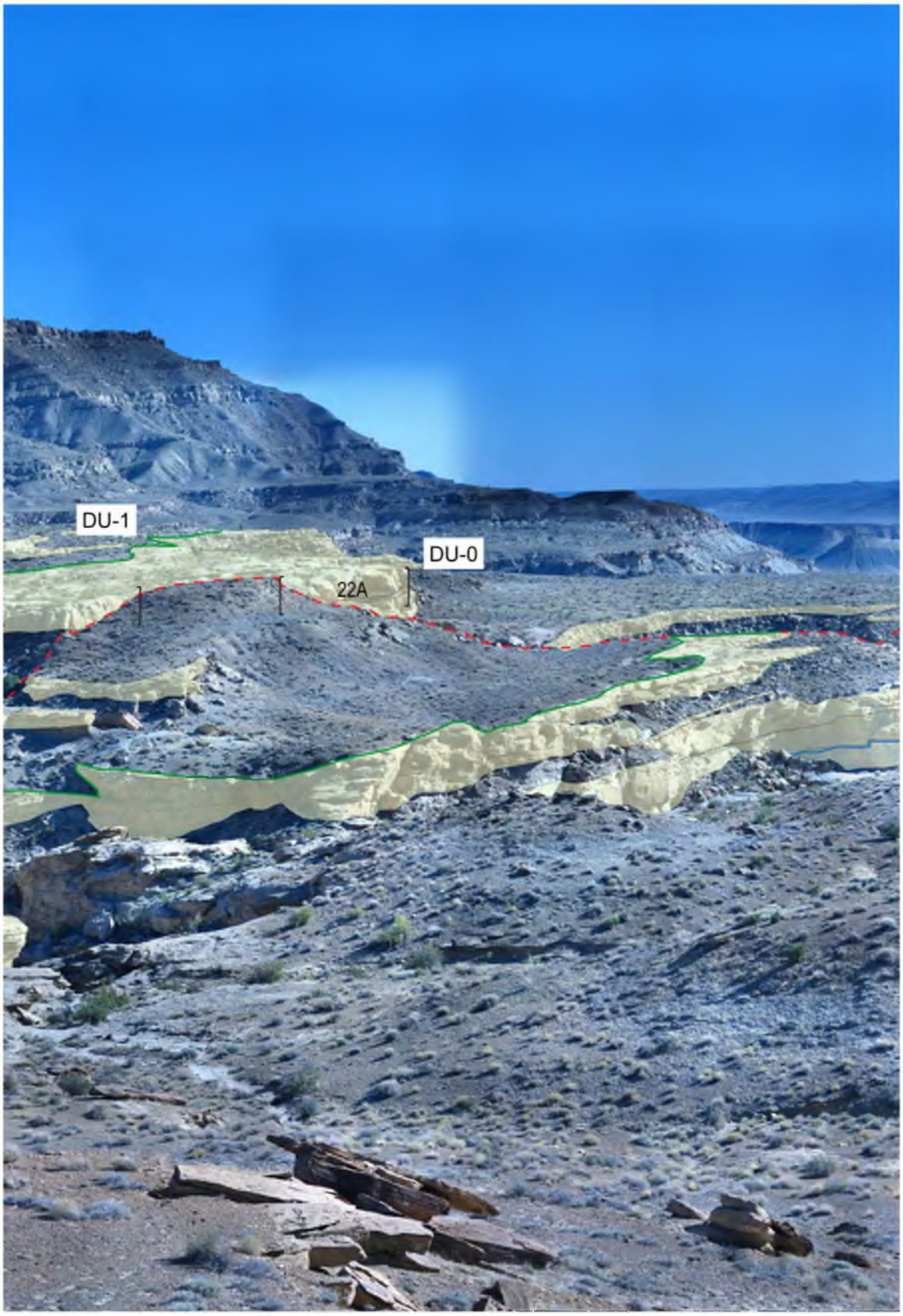

Figure B.2 continued

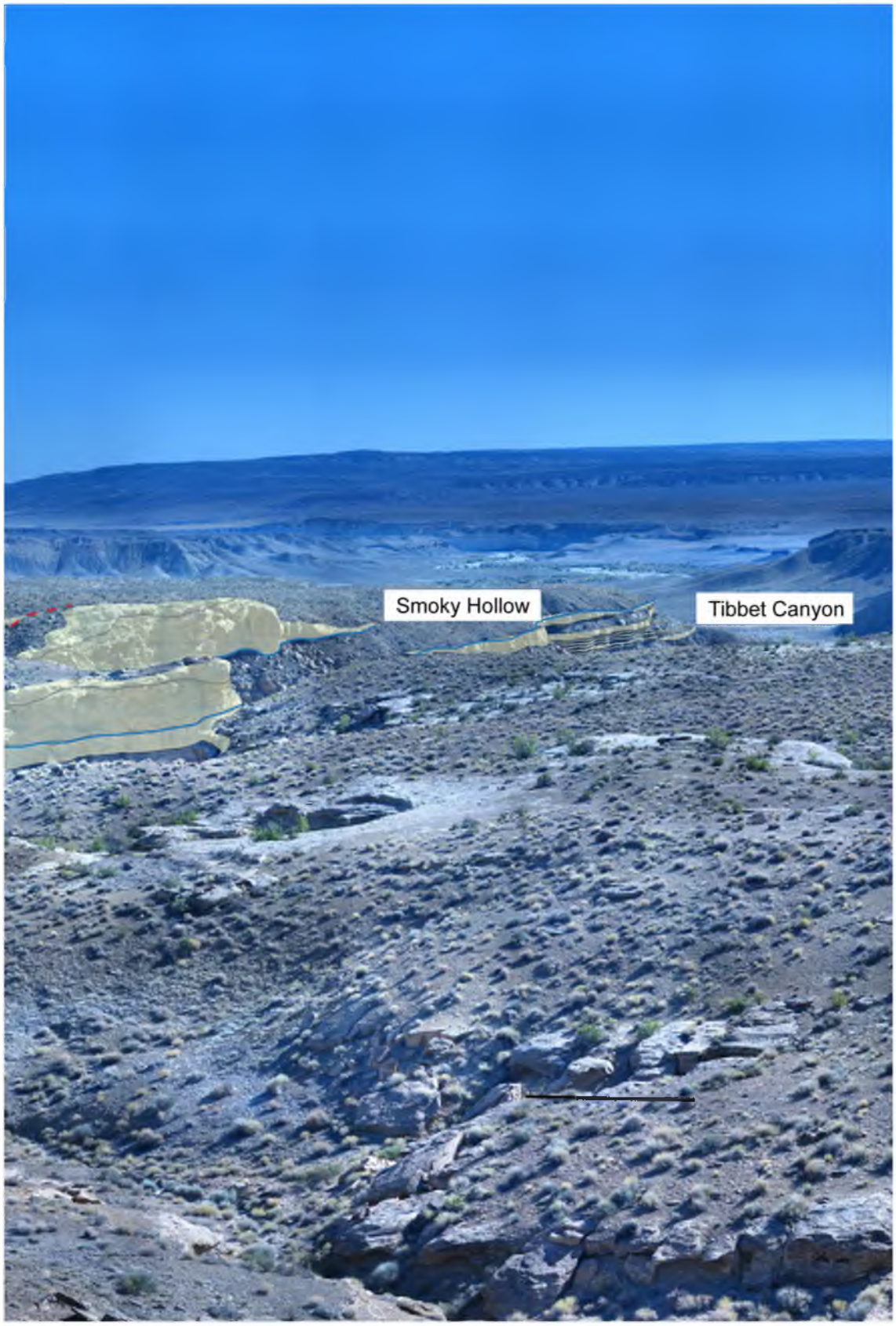

Figure B.2 continued

Figure B.3 – Interpreted photomosaic of the outcrop in the east side of upper Bull Canyon. Figure B.1 is a legend for the symbols and labels.

Upper East Bull Canyon
23
22
17

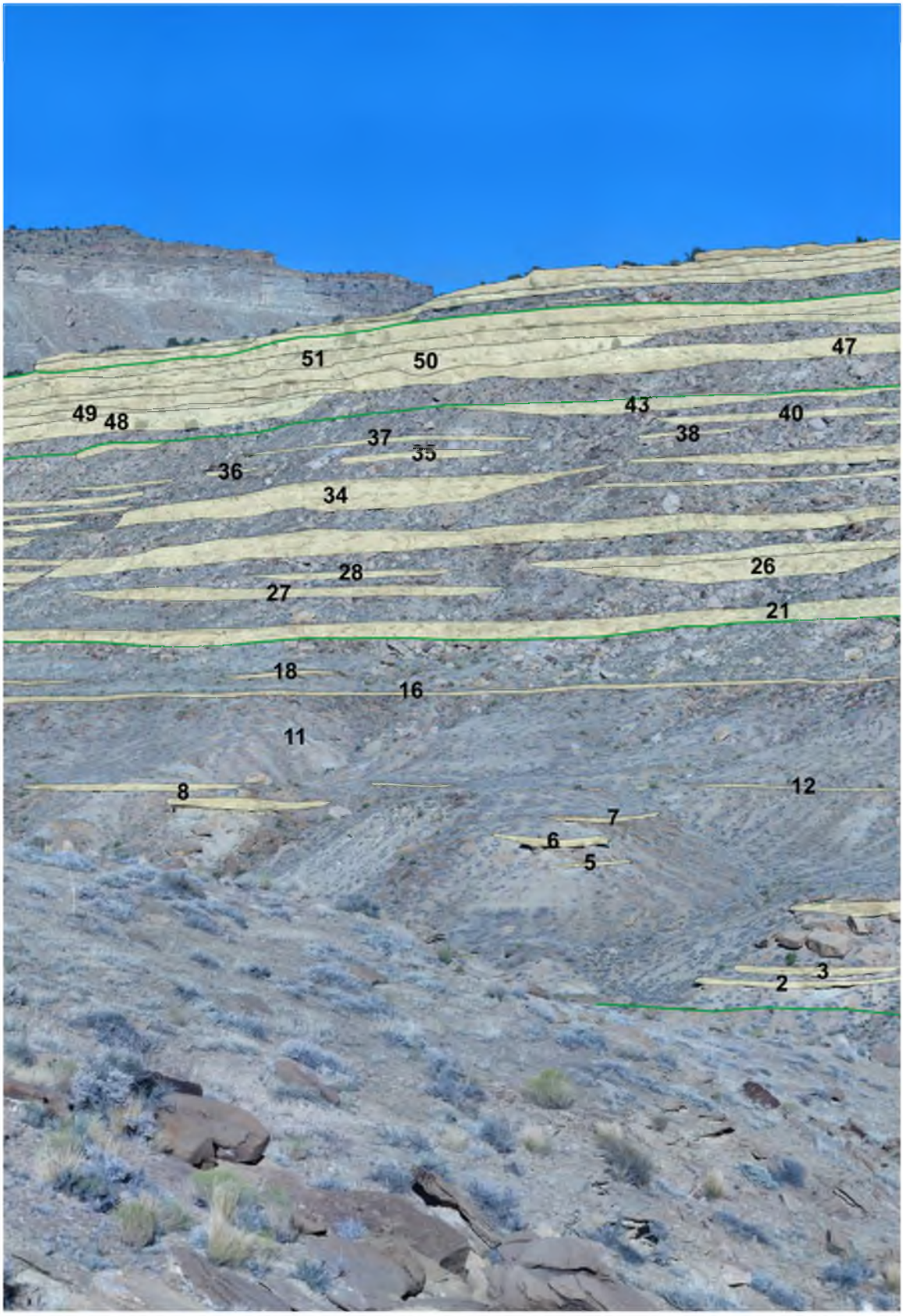

Figure B.3 continued

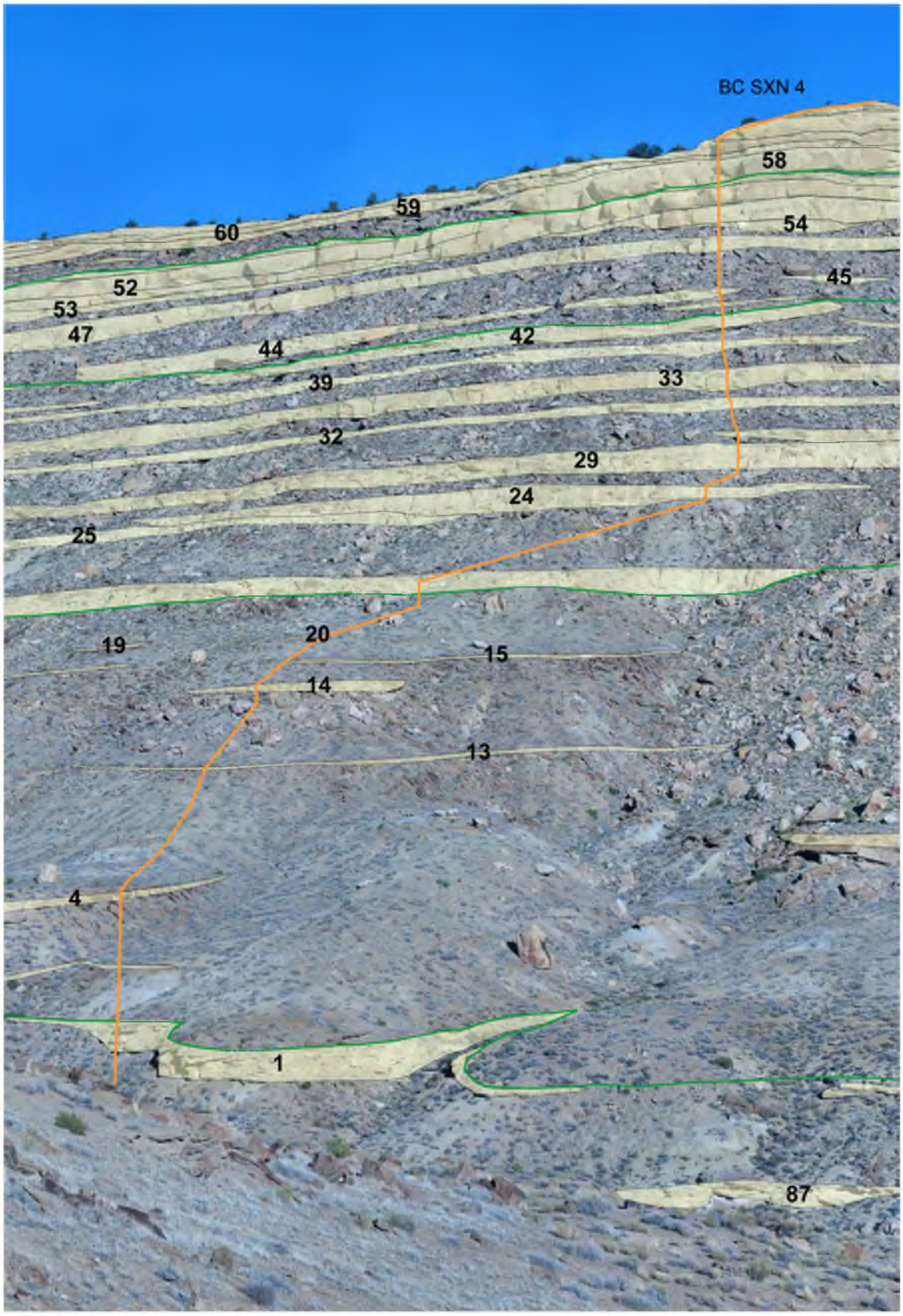

Figure B.3 continued

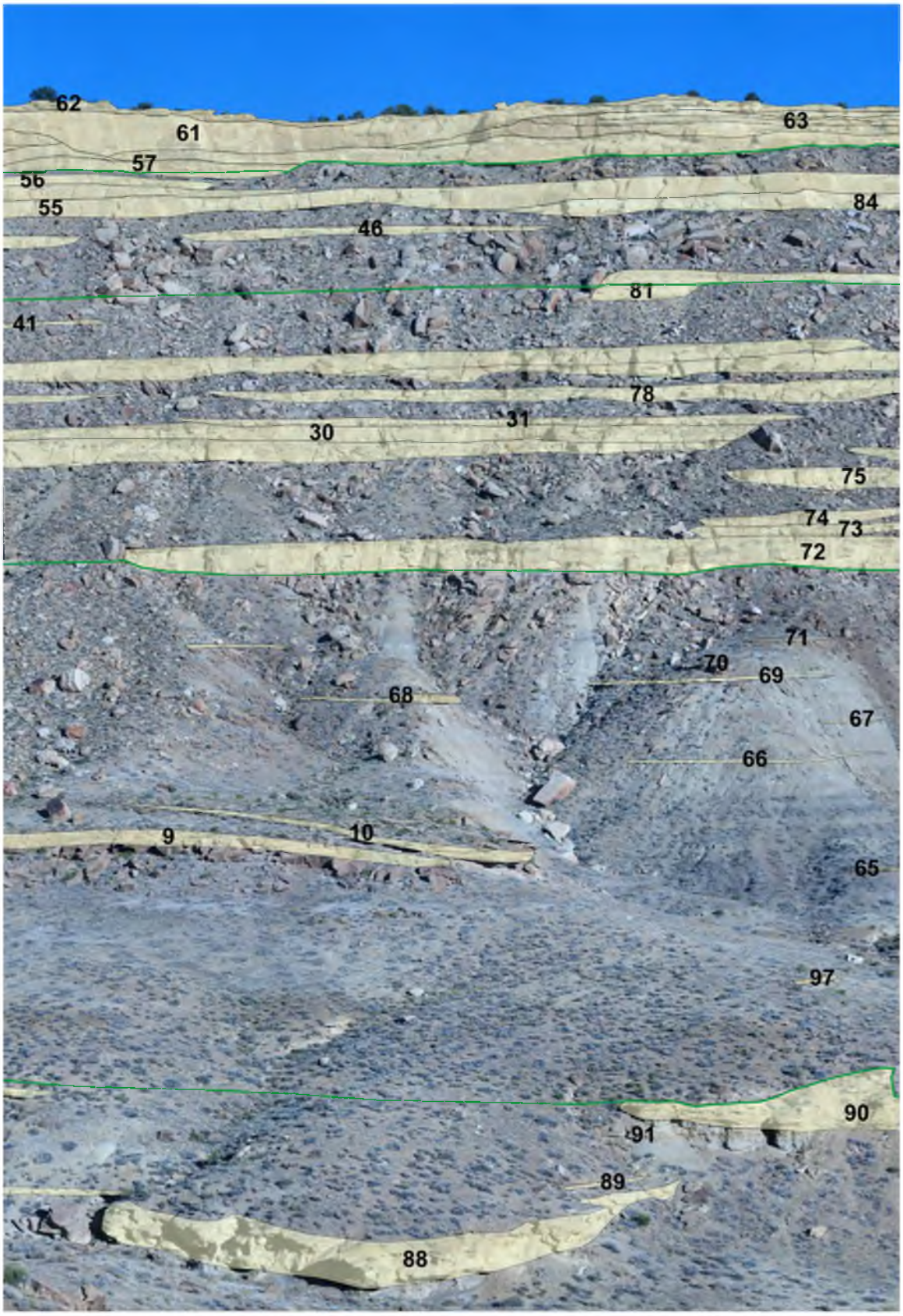

Figure B.3 continued

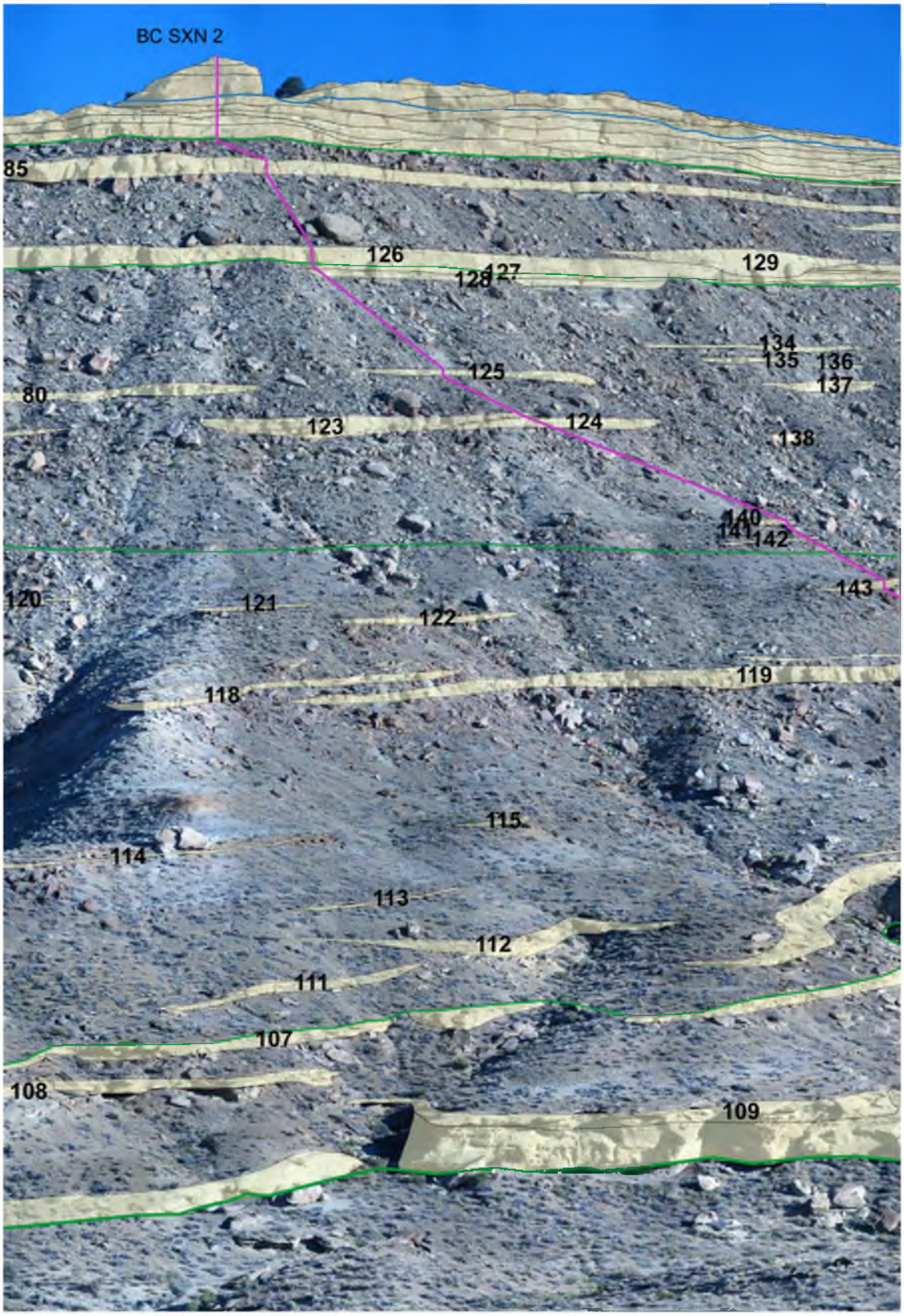

Figure B.3 continued

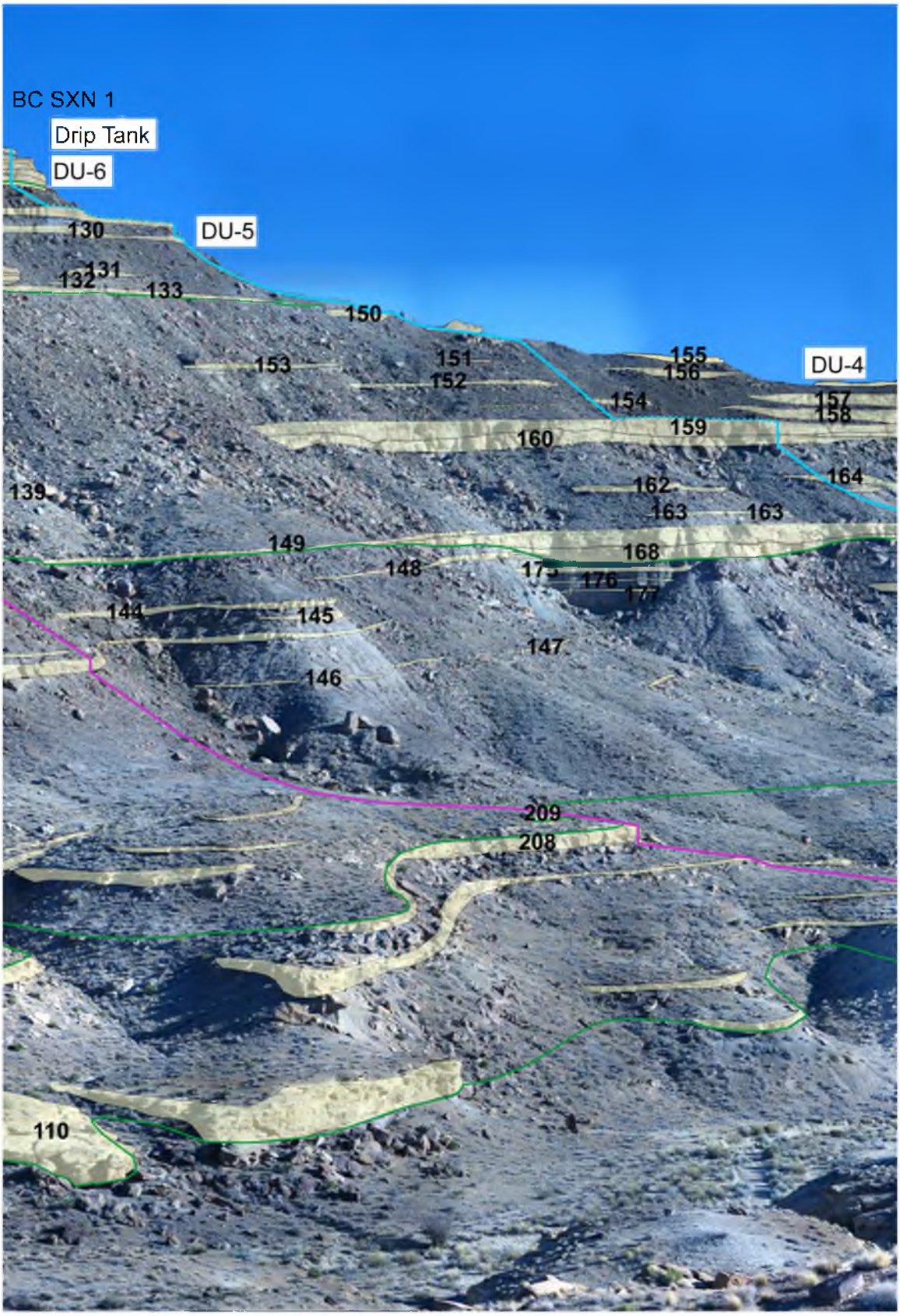

Figure B.3 continued

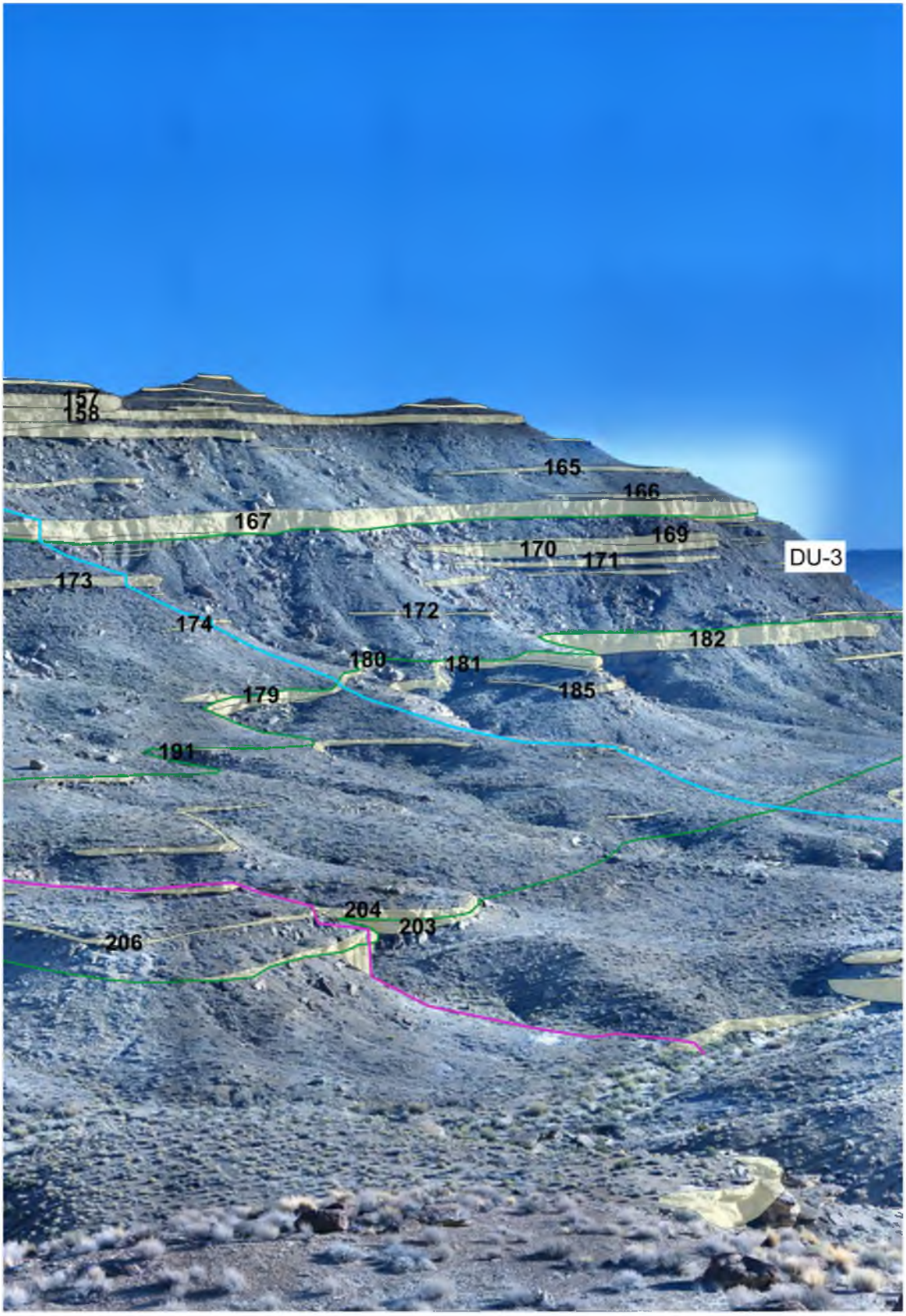

Figure B.3 continued

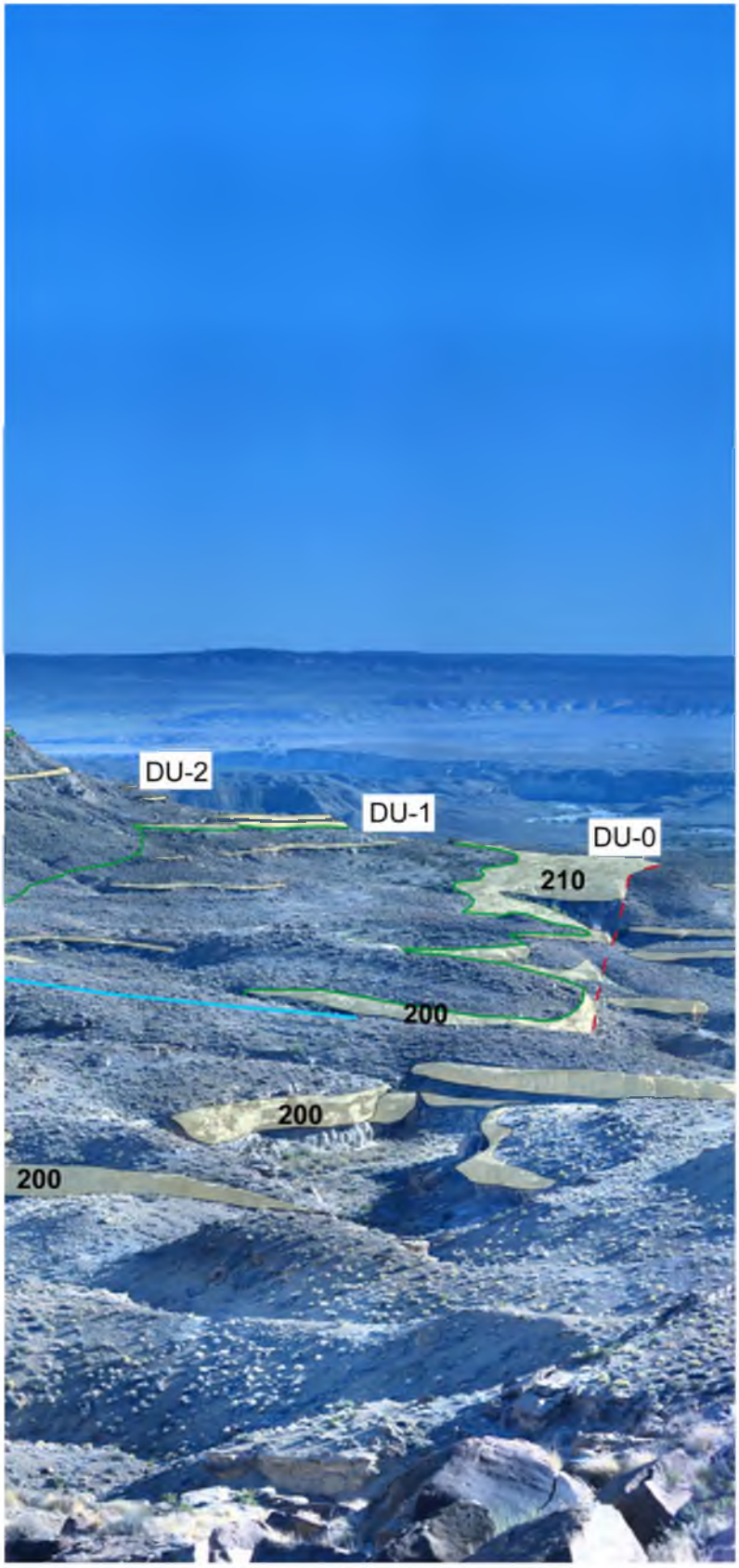

Figure B.3 continued

Figure B.4 – Interpreted photomosaic of the outcrop in west Bull Canyon. Figure B.1 is a legend for the symbols and labels

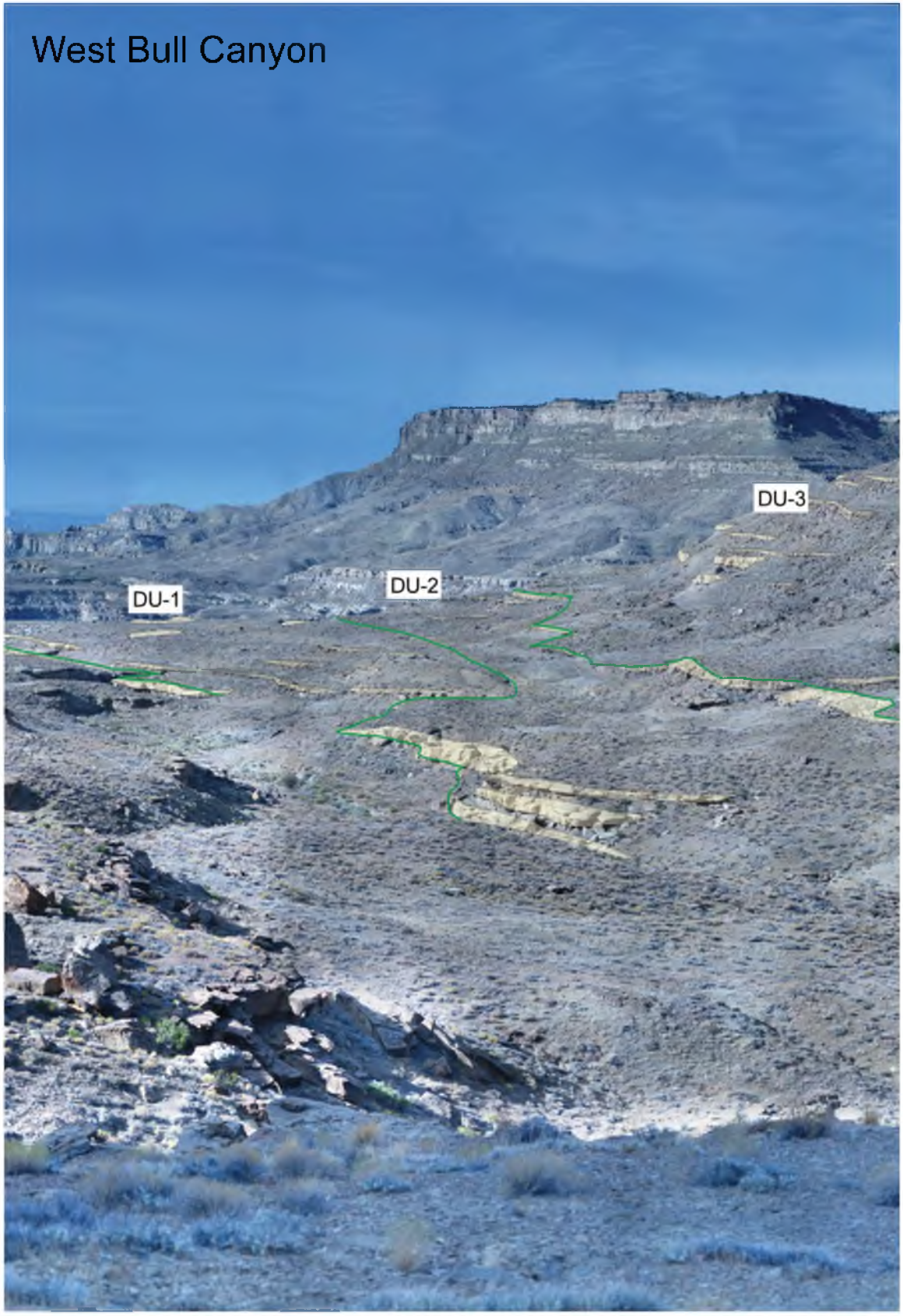
West Bull Canyon
DU-3
DU-2
DU-1

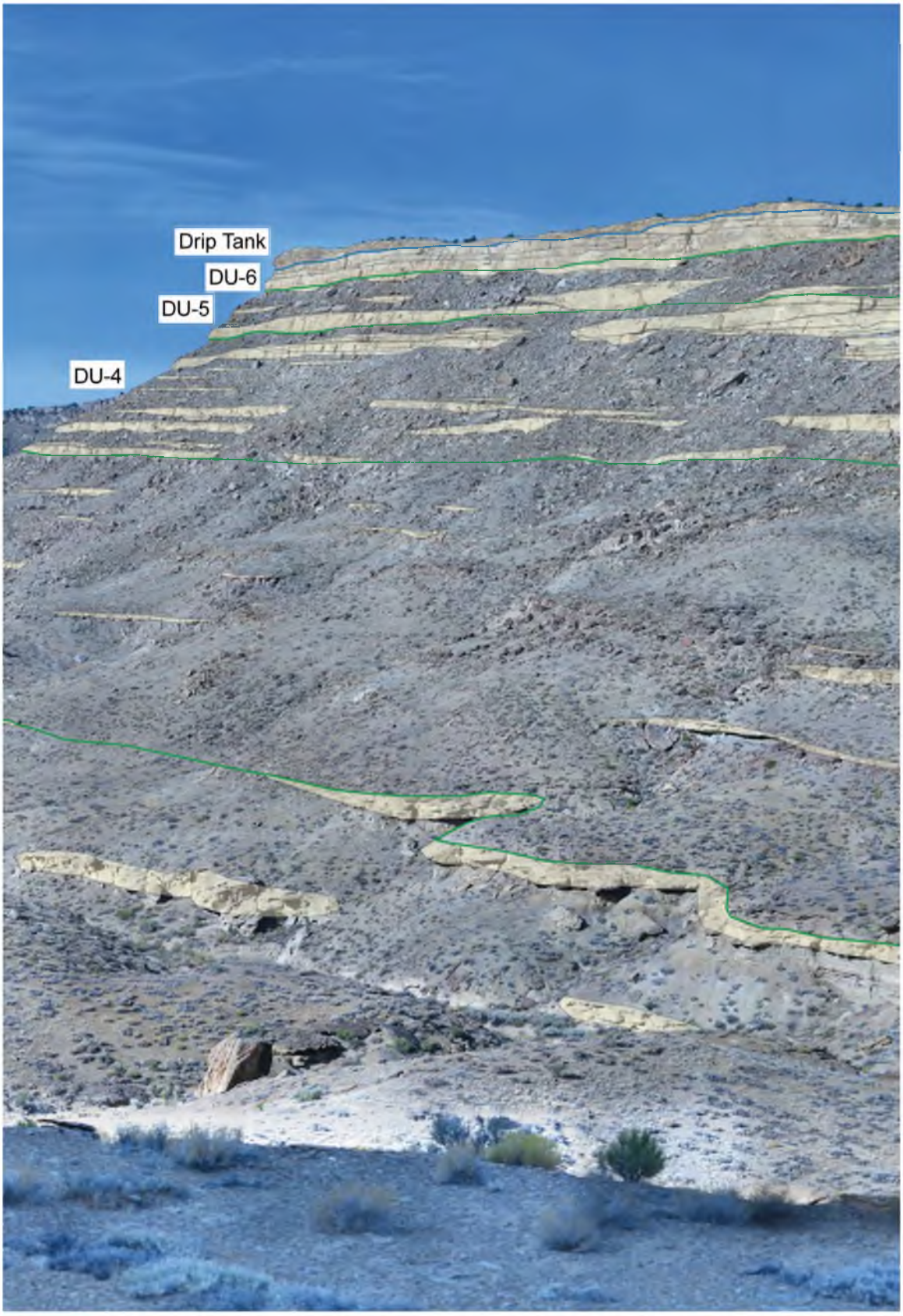

Figure B.4 continued

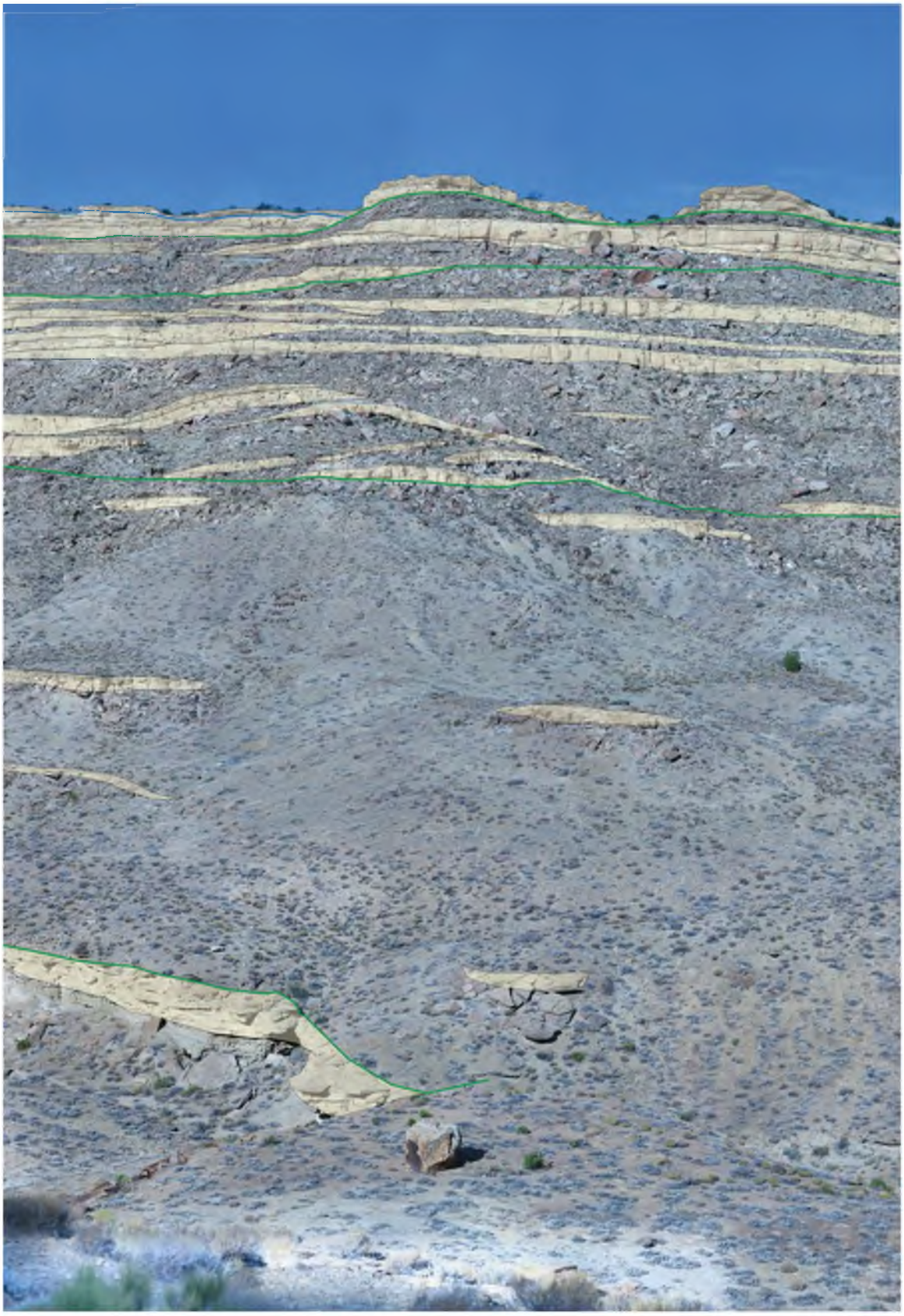

Figure B.4 continued

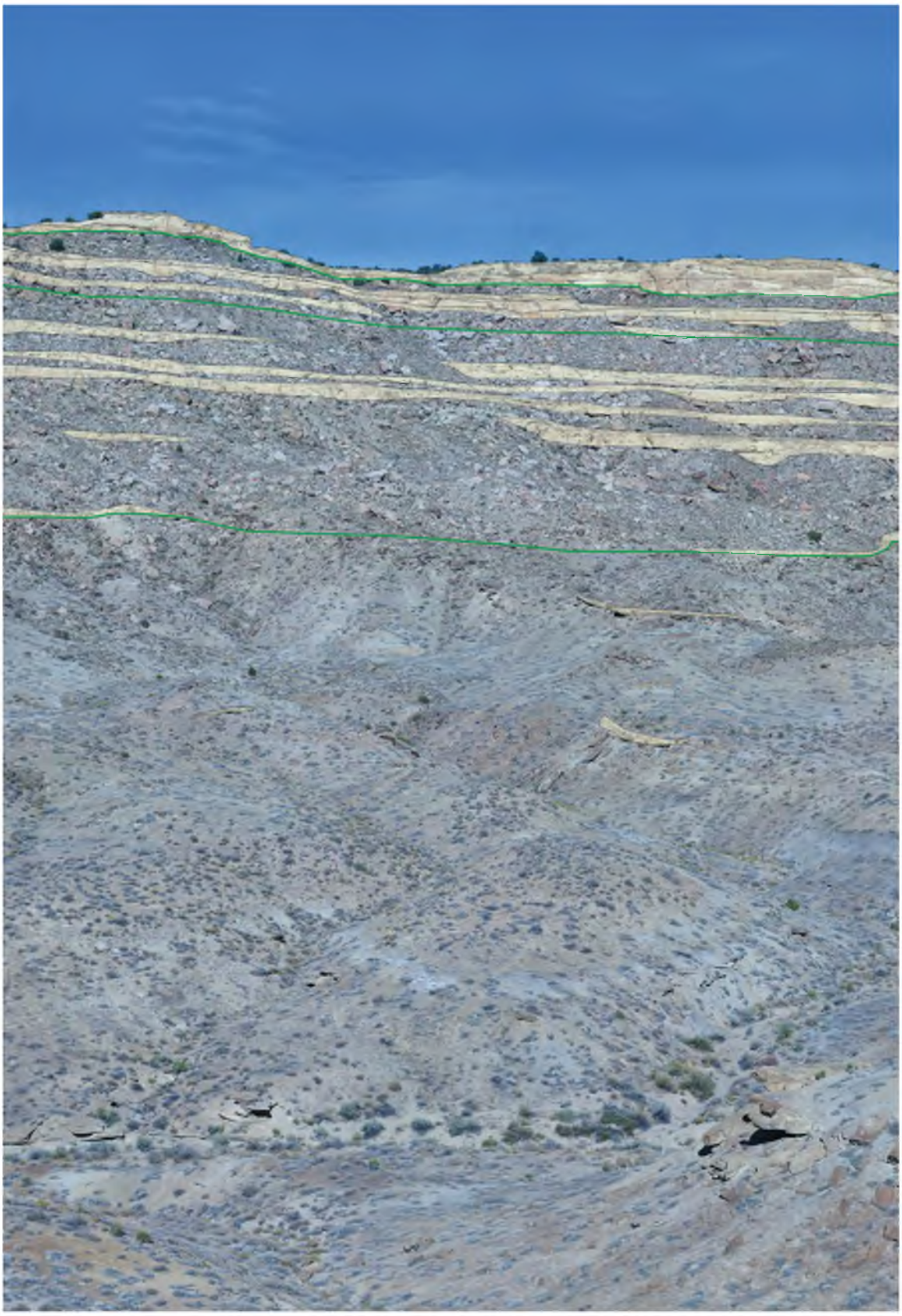

Figure B.4 continued

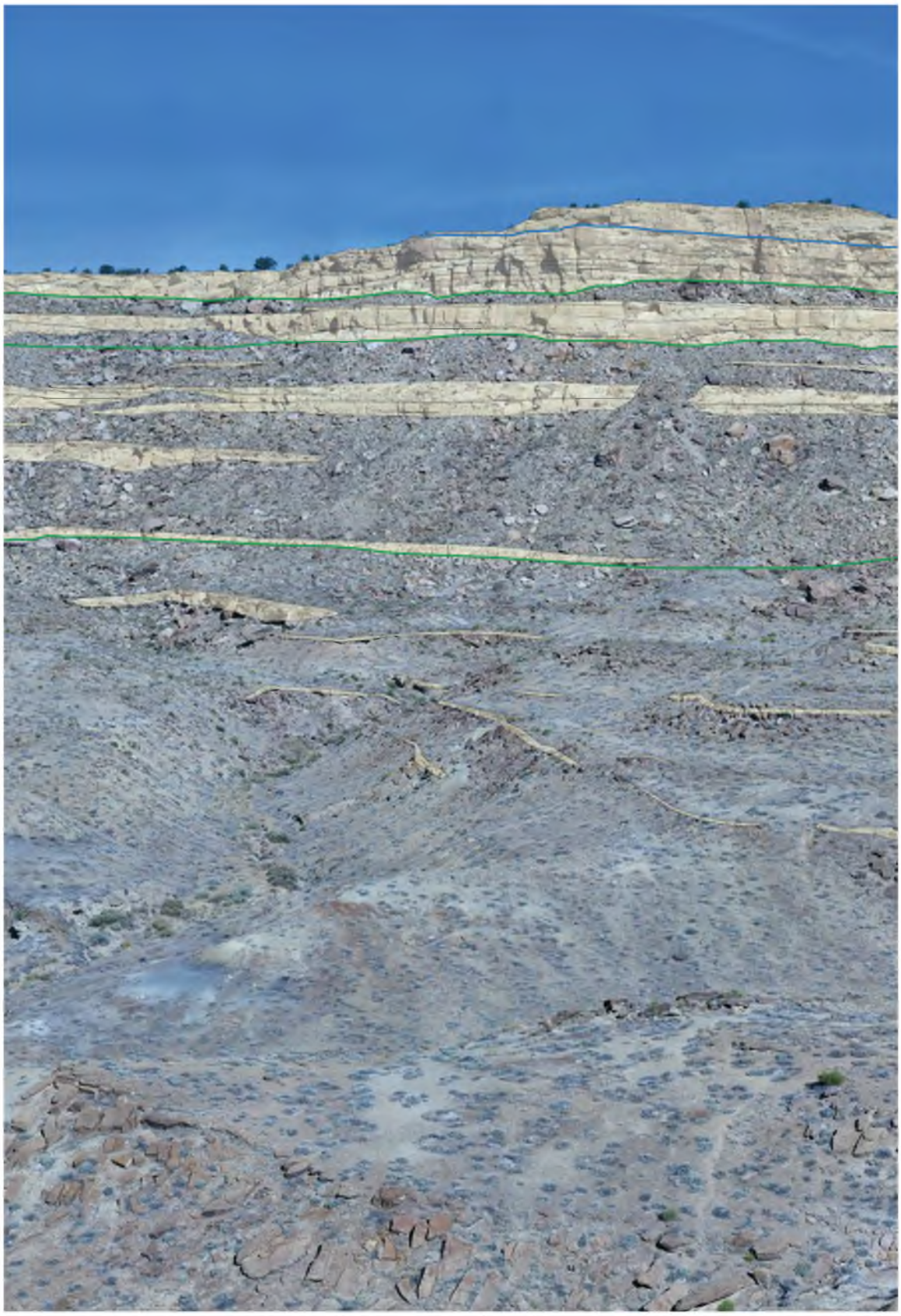

Figure B.4 continued

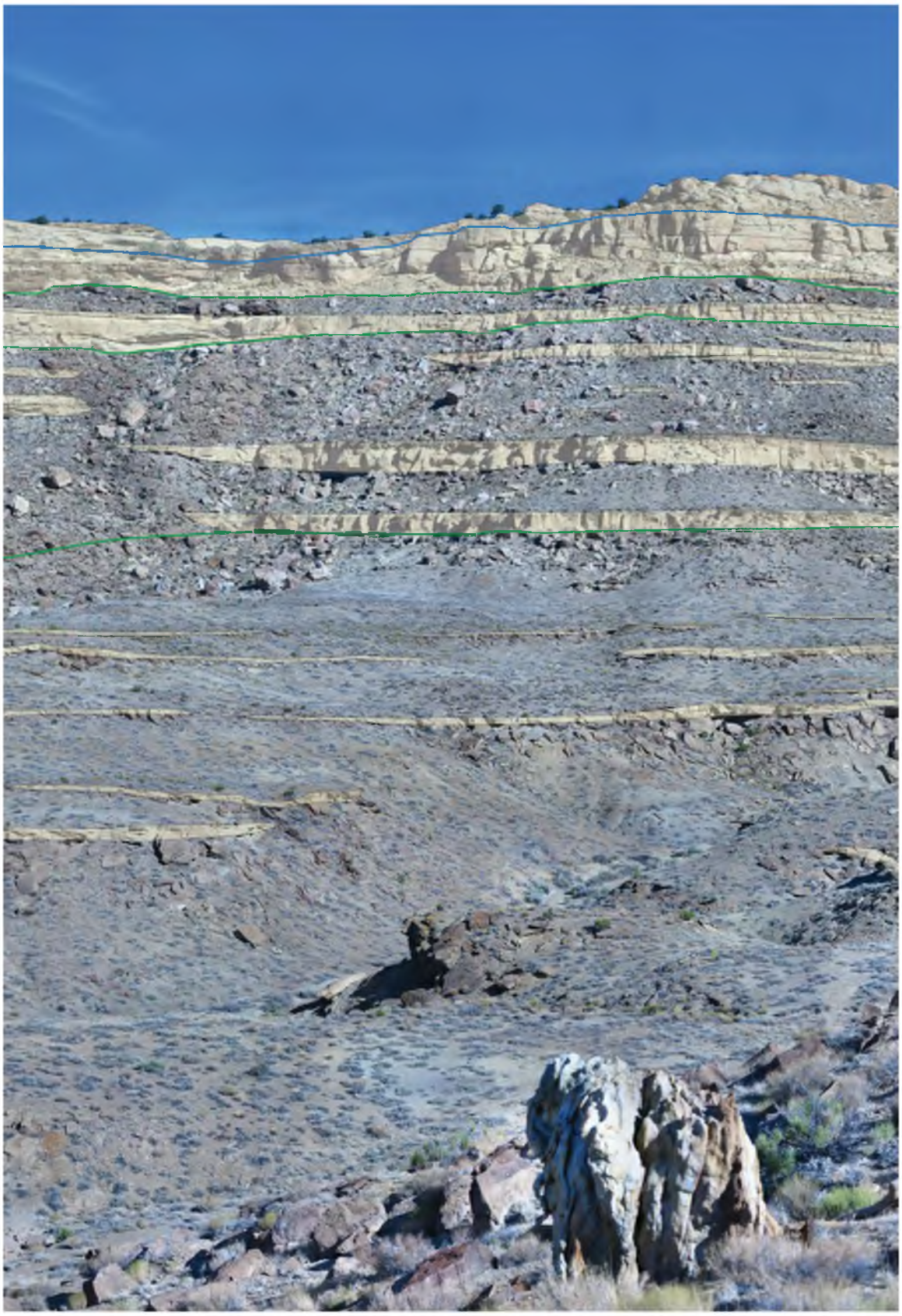

Figure B.4 continued

Figure B.4 continued

APPENDIX C

PALEOCURRENT AND ACCRETION DATA

The paleocurrent and accretion measurements acquired in Bull Canyon are included in Table C.1. Measurements were taken on sedimentary structures in channel deposits ranging from the base of the John Henry Member to Drip Tank Member. The measurements are grouped by depositional unit and then by section (Sec.), which are marked on the interpreted photomosaic of lower east Bull Canyon (Figure B.1). The structure abbreviations include: TCS = trough cross stratification, PCS = planar (tabular) cross stratification, RCL = ripple cross lamination, SCS = sigmoidal, AC = accretion set. The dip, dip direction (Dir.), and cross set height (H) of each structure are listed.

Table C.1

Paleocurrent and Accretion Data

DU	Sec.	Dip	Dir.	Str.	H
DTM	21A	6	69	AC	-
DTM	21A	7	110	AC	-
DTM	21A	7	229	AC	-
DTM	21A	11	86	AC	-
DTM	21A	8	331	AC	-
DTM	21A	3	18	AC	-
DTM	21A	5	12	AC	-
DTM	21A	3	350	AC	-
DTM	21A	7	10	AC	-
DTM	21A	4	330	AC	-
DTM	21A	10	55	AC	-
DTM	21A	8	346	AC	-
DTM	21A	4	112	AC	-
DTM	21A	15	140	AC	-
DTM	21A	6	101	AC	-
DTM	21A	16	10	AC	-
DTM	21A	12	156	AC	-
DTM	21A	10	80	AC	-
DTM	21A	15	32	AC	-
DTM	21A	22	54	AC	-
DTM	21A	20	70	AC	-
DTM	21A	20	73	AC	-
DTM	21A	25	80	AC	-
DTM	21A	20	351	AC	-
DTM	21A	18	353	AC	-
DTM	21A	19	73	AC	-
DTM	21A	19	355	AC	-
DTM	21A	9	18	AC	-
DTM	21A	14	32	AC	-
DTM	21A	20	36	AC	-
DTM	21A	9	342	AC	-
DTM	21A	24	150	AC	-
DTM	21A	28	10	AC	-
DTM	21A	25	45	AC	-
DTM	21B	25	67	AC	-
DTM	21B	19	112	AC	-
DTM	21B	14	84	AC	-
DTM	21B	10	190	AC	-
DTM	21B	11	114	AC	-
DTM	21B	12	12	AC	-
DTM	21B	28	70	AC	-
DTM	21B	12	73	AC	-
DTM	21B	18	25	AC	-
DTM	21B	-	22	RCL	-
DTM	21A	-	95	TCS	2
DTM	21A	-	127	TCS	3
DTM	21A	-	146	TCS	10
DTM	21A	-	165	TCS	10
DTM	21A	-	118	TCS	15
DTM	21A	-	119	TCS	32
DTM	21A	-	140	TCS	9
DTM	21A	-	215	TCS	-
DTM	21A	-	160	TCS	-
DTM	21A	-	78	TCS	-
DTM	21A	-	76	TCS	-
DTM	21B	-	159	TCS	2
DTM	21B	-	137	TCS	3
DTM	21B	-	198	TCS	5
DTM	21B	-	90	TCS	10
DTM	21B	-	64	TCS	-
DTM	21B	-	195	TCS	-
DTM	21B	-	55	TCS	-
DTM	21B	-	44	TCS	-
DTM	21B	-	64	TCS	-
DTM	21B	-	31	TCS	29
DTM	21B	-	64	TCS	-

Table C.1 continued

DU	Sec.	Dip	Dir.	Str.	H	DU	Sec.	Dip	Dir.	Str.	H	DU	Sec.	Dip	Dir.	Str.	H
DTM	21B	-	70	TCS	-	6	20A	9	25	AC	-	6	20B	20	138	AC	-
DTM	21B	-	65	TCS	-	6	20A	24	0	AC	-	6	20B	17	73	AC	-
6	20A	1	24	AC	-	6	20A	20	303	AC	-	6	20B	20	266	AC	-
6	20A	10	16	AC	-	6	20A	14	50	AC	-	6	20B	28	65	AC	-
6	20A	9	210	AC	-	6	20A	9	63	AC	-	6	20B	8	55	AC	-
6	20A	13	72	AC	-	6	20A	14	72	AC	-	6	20B	18	29	AC	-
6	20A	5	16	AC	-	6	20A	18	132	AC	-	6	20B	18	52	AC	-
6	20A	11	56	AC	-	6	20A	8	56	AC	-	6	20B	32	44	AC	-
6	20A	20	15	AC	-	6	20A	26	42	AC	-	6	20C	20	10	AC	-
6	20A	10	13	AC	-	6	20B	5	205	AC	-	6	20C	9	311	AC	-
6	20A	11	8	AC	-	6	20B	14	43	AC	-	6	20C	16	18	AC	-
6	20A	9	331	AC	-	6	20B	1	26	AC	-	6	20C	18	4	AC	-
6	20A	18	200	AC	-	6	20B	7	37	AC	-	6	20C	11	296	AC	-
6	20A	6	300	AC	-	6	20B	1	331	AC	-	6	20C	4	20	AC	-
6	20A	7	61	AC	-	6	20B	2	358	AC	-	6	20C	5	222	AC	-
6	20A	7	352	AC	-	6	20B	6	29	AC	-	6	20C	6	346	AC	-
6	20A	10	67	AC	-	6	20B	17	218	AC	-	6	20C	13	344	AC	-
6	20A	18	105	AC	-	6	20B	6	357	AC	-	6	20C	5	8	AC	-
6	20A	12	50	AC	-	6	20B	12	15	AC	-	6	20C	2	20	AC	-
6	20A	17	28	AC	-	6	20B	10	3	AC	-	6	20C	1	4	AC	-
6	20A	23	28	AC	-	6	20B	19	83	AC	-	6	20C	9	2	AC	-
6	20A	13	290	AC	-	6	20B	15	49	AC	-	6	20C	14	23	AC	-
6	20A	18	2	AC	-	6	20B	14	55	AC	-	6	20C	6	126	AC	-
6	20A	18	50	AC	-	6	20B	12	33	AC	-	6	20C	3	16	AC	-

Table C.1 continued

DU	Sec.	Dip	Dir.	Str.	H	DU	Sec.	Dip	Dir.	Str.	H	DU	Sec.	Dip	Dir.	Str.	H
6	20C	7	22	AC	-	6	20A	3	84	TCS	4	6	20B	-	109	TCS	16
6	20C	8	55	AC	-	6	20A	-	265	TCS	5	6	20B	-	71	TCS	48
6	20C	19	36	AC	-	6	20A	-	114	TCS	1	6	20B	-	103	TCS	7
6	20C	11	32	AC	-	6	20A	-	88	TCS	18	6	20B	-	292	TCS	41
6	20C	15	352	AC	-	6	20A	-	95	TCS	11	6	20B	-	40	TCS	30
6	20C	18	349	AC	-	6	20A	-	80	TCS	14	6	20C	-	83	TCS	20
6	20C	26	36	AC	-	6	20A	-	73	TCS	14	6	20C	-	64	TCS	10
6	20C	15	43	AC	-	6	20A	-	36	TCS	25	6	20C	-	37	TCS	23
6	20C	9	35	AC	-	6	20A	-	29	TCS	30	6	20C	-	43	TCS	14
6	20C	21	31	AC	-	6	20A	-	68	TCS	29	6	20C	-	63	TCS	54
6	20C	18	33	AC	-	6	20A	-	105	TCS	9	6	20C	-	96	TCS	33
6	20C	9	76	AC	-	6	20A	-	94	TCS	14	6	20C	-	52	TCS	41
6	20C	22	25	AC	-	6	20A	-	90	TCS	15	6	20C	-	40	TCS	18
6	20C	27	55	AC	-	6	20A	-	105	TCS	12	6	20C	-	4	TCS	16
6	20C	11	31	AC	-	6	20B	-	115	TCS	5	5	16A	9	7	AC	-
6	20C	10	350	AC	-	6	20B	-	80	TCS	5	5	16A	14	12	AC	-
6	20C	12	28	AC	-	6	20B	-	80	TCS	2	5	16A	12	217	AC	-
6	20C	24	226	AC	-	6	20B	-	83	TCS	1	5	16A	4	334	AC	-
6	20C	12	54	AC	-	6	20B	-	70	TCS	5	5	16A	25	124	AC	-
6	20C	24	46	AC	-	6	20B	-	60	TCS	12	5	16A	16	207	AC	-
6	20C	26	320	AC	-	6	20B	-	63	TCS	10	5	16A	9	215	AC	-
6	20A	-	111	TCS	10	6	20B	-	82	TCS	28	5	16A	4	89	AC	-
6	20A	-	105	TCS	2	6	20B	-	79	TCS	28	5	16A	10	134	AC	-
6	20A	-	104	TCS	7	6	20B	-	50	TCS	12	5	16A	19	128	AC	-

Table C.1 continued

DU	Sec.	Dip	Dir.	Str.	H	DU	Sec.	Dip	Dir.	Str.	H	DU	Sec.	Dip	Dir.	Str.	H
5	16A	19	332	AC	-	5	16B	16	200	AC	-	5	16B	20	134	AC	-
5	16A	14	224	AC	-	5	16B	3	240	AC	-	5	17A	14	164	AC	-
5	16A	18	12	AC	-	5	16B	8	194	AC	-	5	17A	25	207	AC	-
5	16A	10	31	AC	-	5	16B	9	207	AC	-	5	17A	13	130	AC	-
5	16A	20	16	AC	-	5	16B	23	195	AC	-	5	17A	12	24	AC	-
5	16A	6	7	AC	-	5	16B	19	248	AC	-	5	17A	14	81	AC	-
5	16A	12	342	AC	-	5	16B	19	150	AC	-	5	17A	1	149	AC	-
5	16A	7	50	AC	-	5	16B	14	155	AC	-	5	17A	20	349	AC	-
5	16A	21	42	AC	-	5	16B	13	152	AC	-	5	17A	10	347	AC	-
5	16A	15	15	AC	-	5	16B	16	122	AC	-	5	17A	9	348	AC	-
5	16A	19	26	AC	-	5	16B	10	146	AC	-	5	17A	6	130	AC	-
5	16A	26	71	AC	-	5	16B	24	120	AC	-	5	17A	11	355	AC	-
5	16A	12	44	AC	-	5	16B	14	124	AC	-	5	17A	22	106	AC	-
5	16A	15	22	AC	-	5	16B	20	164	AC	-	5	17A	27	65	AC	-
5	16A	18	65	AC	-	5	16B	18	130	AC	-	5	17A	9	106	AC	-
5	16A	14	83	AC	-	5	16B	21	142	AC	-	5	17A	16	59	AC	-
5	16A	18	94	AC	-	5	16B	22	105	AC	-	5	18A	6	334	AC	-
5	16A	20	100	AC	-	5	16B	18	161	AC	-	5	18A	11	34	AC	-
5	16A	11	44	AC	-	5	16B	18	145	AC	-	5	18A	12	190	AC	-
5	16A	14	109	AC	-	5	16B	10	175	AC	-	5	18A	14	27	AC	-
5	16A	16	98	AC	-	5	16B	16	251	AC	-	5	18A	11	35	AC	-
5	16B	13	230	AC	-	5	16B	20	231	AC	-	5	18A	13	36	AC	-
5	16B	9	32	AC	-	5	16B	21	147	AC	-	5	18A	5	73	AC	-
5	16B	20	194	AC	-	5	16B	22	138	AC	-	5	18A	4	273	AC	-

Table C.1 continued

DU	Sec.	Dip	Dir.	Str.	H
5	18A	12	43	AC	-
5	18A	8	97	AC	-
5	18A	9	100	AC	-
5	18A	4	336	AC	-
5	18A	18	46	AC	-
5	18A	20	123	AC	-
5	18A	17	56	AC	-
5	19A	5	24	AC	-
5	19A	19	37	AC	-
5	19A	10	24	AC	-
5	19A	7	17	AC	-
5	19A	10	289	AC	-
5	19A	14	174	AC	-
5	19A	6	18	AC	-
5	19A	18	76	AC	-
5	19A	9	100	AC	-
5	19A	12	190	AC	-
5	19A	21	180	AC	-
5	19A	14	126	AC	-
5	19A	13	130	AC	-
5	19A	14	42	AC	-
5	19A	8	75	AC	-
5	19A	4	55	AC	-
5	19A	10	40	AC	-
5	19A	7	54	AC	-
5	19B	6	61	AC	-
5	19B	6	356	AC	-
5	19B	7	2	AC	-
5	19B	22	185	AC	-
5	19B	12	333	AC	-
5	19B	11	2	AC	-
5	19B	6	9	AC	-
5	19B	28	44	AC	-
5	19B	6	14	AC	-
5	19B	17	33	AC	-
5	19B	29	20	AC	-
5	19B	5	77	AC	-
5	19B	9	190	AC	-
5	19B	5	128	AC	-
5	19B	12	136	AC	-
5	19B	22	76	AC	-
5	19B	10	113	AC	-
5	19B	63	15	AC	-
5	19B	23	48	AC	-
5	19B	20	90	AC	-
5	19B	13	90	AC	-
5	19B	27	68	AC	-
5	19B	14	96	AC	-
5	19B	26	72	AC	-
5	19B	30	75	AC	-
5	19B	13	75	AC	-
5	19C	1	175	AC	-
5	19C	19	358	AC	-
5	19C	7	11	AC	-
5	19C	10	214	AC	-
5	19C	11	11	AC	-
5	19C	13	180	AC	-
5	19C	9	291	AC	-
5	19C	12	344	AC	-
5	19C	6	336	AC	-
5	19C	10	24	AC	-
5	19C	15	128	AC	-
5	19C	15	15	AC	-
5	19C	16	357	AC	-
5	19C	14	47	AC	-
5	19C	15	38	AC	-
5	19C	18	75	AC	-
5	19C	14	42	AC	-
5	19C	30	0	AC	-
5	19C	20	338	AC	-
5	19C	25	6	AC	-
5	19C	6	22	AC	-

Table C.1 continued

DU	Sec.	Dip	Dir.	Str.	H	DU	Sec.	Dip	Dir.	Str.	H	DU	Sec.	Dip	Dir.	Str.	H
5	19C	22	22	AC	-	5	16A	-	88	TCS	2	5	19A	-	111	TCS	1
5	19C	7	12	AC	-	5	16A	-	77	TCS	3	5	19A	-	120	TCS	7
5	19C	21	13	AC	-	5	16A	-	115	TCS	16	5	19A	-	114	TCS	2
5	19C	23	50	AC	-	5	16A	-	88	TCS	37	5	19A	-	121	TCS	1
5	19C	17	105	AC	-	5	16A	-	70	TCS	34	5	19A	-	310	TCS	3
5	19C	20	305	AC	-	5	16A	-	78	TCS	35	5	19A	-	40	TCS	8
5	19C	28	35	AC	-	5	16A	-	78	TCS	12	5	19A	-	180	TCS	30
5	19C	12	56	AC	-	5	16A	-	87	TCS	15	5	19A	-	148	TCS	11
5	19C	23	28	AC	-	5	16B	-	136	TCS	9	5	19A	-	144	TCS	6
5	19C	22	24	AC	-	5	16B	-	100	TCS	13	5	19A	-	110	TCS	14
5	19C	22	55	AC	-	5	16B	-	120	TCS	5	5	19A	-	115	TCS	5
5	19C	25	356	AC	-	5	16B	-	82	TCS	8	5	19B	-	87	TCS	7
5	19C	23	345	AC	-	5	16B	-	120	TCS	11	5	19B	4	100	TCS	4
5	EX4	9	213	AC	-	5	16B	-	116	TCS	8	5	19B	-	255	TCS	4
5	EX4	10	203	AC	-	5	17A	-	65	TCS	15	5	19B	-	89	TCS	1
5	EX4	13	190	AC	-	5	17A	-	74	TCS	10	5	19B	-	120	TCS	1
5	EX4	12	224	AC	-	5	17A	-	85	TCS	42	5	19B	-	106	TCS	17
5	EX4	12	95	AC	-	5	17A	-	105	TCS	8	5	19B	-	65	TCS	19
5	EX4	13	83	AC	-	5	17A	-	83	TCS	14	5	19B	-	74	TCS	18
5	EX4	17	84	AC	-	5	18A	-	306	TCS	5	5	19B	-	69	TCS	12
5	16A	4	82	PCS	8	5	18A	-	73	TCS	18	5	19B	-	82	TCS	30
5	16A	-	62	RCL	2	5	18A	-	88	TCS	5	5	19B	-	77	TCS	22
5	17A	23	107	TA	9	5	18A	-	47	TCS	7	5	19C	-	89	TCS	2
5	16A	-	53	TCS	4	5	19A	5	118	TCS	8	5	19C	-	20	TCS	1

Table C.1 continued

DU	Sec.	Dip	Dir.	Str.	H
5	19C	-	109	TCS	4
5	19C	-	49	TCS	5
5	19C	-	117	TCS	13
5	19C	-	42	TCS	3
5	19C	-	50	TCS	5
5	19C	-	100	TCS	6
5	19C	-	77	TCS	29
5	19C	-	73	TCS	7
5	19C	-	74	TCS	8
5	19C	-	71	TCS	47
5	19C	-	70	TCS	14
4	9A	22	43	AC	-
4	9A	12	39	AC	-
4	9A	7	29	AC	-
4	9A	12	51	AC	-
4	9A	14	32	AC	-
4	9A	15	75	AC	-
4	9A	10	48	AC	-
4	9A	20	146	AC	-
4	9A	20	16	AC	-
4	9A	26	31	AC	-
4	9A	8	79	AC	-
4	9A	14	82	AC	-
4	9A	20	9	AC	-
4	9B	10	110	AC	-
4	9B	10	342	AC	-
4	9B	12	0	AC	-
4	9B	9	359	AC	-
4	9B	6	2	AC	-
4	9B	2	45	AC	-
4	9B	4	12	AC	-
4	9B	13	185	AC	-
4	9B	17	62	AC	-
4	9B	5	55	AC	-
4	9B	10	12	AC	-
4	9B	17	71	AC	-
4	9B	16	355	AC	-
4	9B	6	202	AC	-
4	9B	14	30	AC	-
4	9B	7	21	AC	-
4	9B	20	242	AC	-
4	9B	18	8	AC	-
4	9B	29	82	AC	-
4	9B	11	62	AC	-
4	9B	35	290	AC	-
4	9B	5	82	AC	-
4	9B	18	280	AC	-
4	9B	11	25	AC	-
4	9B	14	80	AC	-
4	9B	28	94	AC	-
4	9B	22	86	AC	-
4	9B	22	95	AC	-
4	9B	25	174	AC	-
4	9B	28	40	AC	-
4	9B	23	105	AC	-
4	9B	18	52	AC	-
4	9B	11	105	AC	-
4	9B	10	170	AC	-
4	9B	25	116	AC	-
4	9B	24	52	AC	-
4	9C	16	12	AC	-
4	9C	7	25	AC	-
4	9C	5	31	AC	-
4	9C	13	42	AC	-
4	9C	16	14	AC	-
4	9C	11	65	AC	-
4	9C	11	102	AC	-
4	9C	19	234	AC	-
4	9C	14	214	AC	-
4	9C	0	26	AC	-
4	9C	14	18	AC	-
4	9C	13	47	AC	-

Table C.1 continued

DU	Sec.	Dip	Dir.	Str.	H
4	9C	14	38	AC	-
4	9C	5	20	AC	-
4	9C	9	12	AC	-
4	9C	15	0	AC	-
4	9C	5	180	AC	-
4	9C	15	26	AC	-
4	9C	9	4	AC	-
4	9C	21	186	AC	-
4	9C	7	95	AC	-
4	9C	17	186	AC	-
4	9C	18	36	AC	-
4	9C	18	85	AC	-
4	9C	30	55	AC	-
4	9C	8	65	AC	-
4	9C	32	36	AC	-
4	9C	22	78	AC	-
4	9C	14	84	AC	-
4	9C	20	79	AC	-
4	9C	17	59	AC	-
4	9C	14	182	AC	-
4	9C	20	75	AC	-
4	9C	17	65	AC	-
4	9C	9	32	AC	-
4	9C	10	325	AC	-
4	9C	22	50	AC	-
4	9C	18	45	AC	-
4	9C	7	60	AC	-
4	9C	20	61	AC	-
4	10A	9	31	AC	-
4	10A	22	20	AC	-
4	10A	20	86	AC	-
4	10A		90	AC	-
4	10A	5	15	AC	-
4	10A	16	149	AC	-
4	10A	9	75	AC	-
4	10A	21	102	AC	-
4	10A	21	239	AC	-
4	10A	9	55	AC	-
4	10A	3	204	AC	-
4	10A	19	41	AC	-
4	10A	6	0	AC	-
4	10A	10	18	AC	-
4	10A	7	102	AC	-
4	10A	10	209	AC	-
4	10A	24	218	AC	-
4	10A	20	52	AC	-
4	10A	20	190	AC	-
4	10A	18	67	AC	-
4	10A	18	62	AC	-
4	10A	8	225	AC	-
4	10A	18	128	AC	-
4	10A	14	153	AC	-
4	10A	23	31	AC	-
4	10A	8	56	AC	-
4	10A	6	114	AC	-
4	10A	14	145	AC	-
4	10A	12	107	AC	-
4	10A	23	110	AC	-
4	10A	14	89	AC	-
4	11A	15	350	AC	-
4	11A	12	224	AC	-
4	11A	22	215	AC	-
4	11A	3	15	AC	-
4	11A	3	225	AC	-
4	11A	7	13	AC	-
4	11A	16	194	AC	-
4	11A	5	355	AC	-
4	11A	5	36	AC	-
4	11A	6	204	AC	-
4	11A	5	306	AC	-
4	11A	11	11	AC	-
4	11A	12	226	AC	-

Table C.1 continued

DU	Sec.	Dip	Dir.	Str.	H	DU	Sec.	Dip	Dir.	Str.	H	DU	Sec.	Dip	Dir.	Str.	H
4	11A	14	9	AC	-	4	11A	8	92	AC	-	4	12A	14	338	AC	-
4	11A	18	143	AC	-	4	11A	18	64	AC	-	4	12A	15	7	AC	-
4	11A	14	19	AC	-	4	11A	14	82	AC	-	4	12A	6	337	AC	-
4	11A	13	171	AC	-	4	11A	13	65	AC	-	4	12A	8	9	AC	-
4	11A	24	144	AC	-	4	11A	16	64	AC	-	4	12A	17	189	AC	-
4	11A	24	180	AC	-	4	11A	14	148	AC	-	4	12A	11	345	AC	-
4	11A	12	41	AC	-	4	11A	18	49	AC	-	4	12A	1	350	AC	-
4	11A	20	182	AC	-	4	11A	16	30	AC	-	4	12A	1	347	AC	-
4	11A	16	75	AC	-	4	12A	3	312	AC	-	4	12A	20	40	AC	-
4	11A	16	26	AC	-	4	12A	14	17	AC	-	4	12A	14	46	AC	-
4	11A	18	26	AC	-	4	12A	14	107	AC	-	4	12A	16	49	AC	-
4	11A	22	80	AC	-	4	12A	13	206	AC	-	4	12A	20	53	AC	-
4	11A	12	55	AC	-	4	12A	7	20	AC	-	4	12A	10	45	AC	-
4	11A	7	128	AC	-	4	12A	8	339	AC	-	4	12A	10	80	AC	-
4	11A	17	32	AC	-	4	12A	10	343	AC	-	4	12A	4	105	AC	-
4	11A	8	157	AC	-	4	12A	5	90	AC	-	4	12A	1	124	AC	-
4	11A	18	165	AC	-	4	12A	4	70	AC	-	4	12A	1	61	AC	-
4	11A	24	29	AC	-	4	12A	11	21	AC	-	4	12A	11	64	AC	-
4	11A	18	18	AC	-	4	12A	8	24	AC	-	4	12A	20	86	AC	-
4	11A	33	18	AC	-	4	12A	3	10	AC	-	4	12A	12	54	AC	-
4	11A	9	180	AC	-	4	12A	7	5	AC	-	4	12A	16	94	AC	-
4	11A	11	1	AC	-	4	12A	4	45	AC	-	4	12A	13	86	AC	-
4	11A	9	185	AC	-	4	12A	14	346	AC	-	4	12A	10	58	AC	-
4	11A	25	210	AC	-	4	12A	13	12	AC	-	4	12A	23	36	AC	-

Table C.1 continued

DU	Sec.	Dip	Dir.	Str.	H
4	12A	17	22	AC	-
4	12A	14	100	AC	-
4	12A	19	66	AC	-
4	12A	12	20	AC	-
4	12A	20	23	AC	-
4	12A	4	65	AC	-
4	12A	14	28	AC	-
4	12A	6	52	AC	-
4	12A	20	67	AC	-
4	12A	10	110	AC	-
4	12A	18	60	AC	-
4	12A	16	67	AC	-
4	12A	14	49	AC	-
4	12A	28	2	AC	-
4	12A	19	64	AC	-
4	12A	16	83	AC	-
4	12B	5	9	AC	-
4	12B	17	14	AC	-
4	12B	27	5	AC	-
4	12B	20	24	AC	-
4	12B	11	108	AC	-
4	12B	6	43	AC	-
4	12B	7	17	AC	-
4	12B	6	316	AC	-

DU	Sec.	Dip	Dir.	Str.	H
4	12B	20	6	AC	-
4	12B	10	19	AC	-
4	12B	13	32	AC	-
4	12B	10	355	AC	-
4	12B	11	89	AC	-
4	12B	10	342	AC	-
4	12B	11	80	AC	-
4	12B	2	325	AC	-
4	12B	2	22	AC	-
4	12B	11	14	AC	-
4	12B	11	120	AC	-
4	12B	10	351	AC	-
4	12B	3	25	AC	-
4	12B	18	70	AC	-
4	12B	16	138	AC	-
4	12B	20	70	AC	-
4	12B	22	53	AC	-
4	12B	13	42	AC	-
4	12B	12	62	AC	-
4	12B	16	48	AC	-
4	12B	16	313	AC	-
4	12B	22	15	AC	-
4	12B	10	311	AC	-
4	12B	18	24	AC	-

DU	Sec.	Dip	Dir.	Str.	H
4	12B	11	325	AC	-
4	12B	12	84	AC	-
4	12B	7	12	AC	-
4	12C	9	351	AC	-
4	12C	8	102	AC	-
4	12C	6	359	AC	-
4	12C	23	112	AC	-
4	12C	12	326	AC	-
4	12C	2	349	AC	-
4	12C	14	34	AC	-
4	12C	7	151	AC	-
4	12C	6	321	AC	-
4	12C	5	330	AC	-
4	12C	6	26	AC	-
4	12C	10	221	AC	-
4	12C	22	35	AC	-
4	12C	18	42	AC	-
4	12C	22	68	AC	-
4	12C	16	52	AC	-
4	12C	23	49	AC	-
4	12C	10	100	AC	-
4	12C	20	351	AC	-
4	12C	8	78	AC	-
4	12C	3	186	AC	-

Table C.1 continued

DU	Sec.	Dip	Dir.	Str.	H	DU	Sec.	Dip	Dir.	Str.	H	DU	Sec.	Dip	Dir.	Str.	H
4	12C	16	38	AC	-	4	13A	19	70	AC	-	4	13B	8	56	AC	-
4	13A	15	191	AC	-	4	13A	23	77	AC	-	4	13B	24	99	AC	-
4	13A	13	59	AC	-	4	13A	14	63	AC	-	4	13B	19	105	AC	-
4	13A	14	45	AC	-	4	13A	4	109	AC	-	4	13B	16	124	AC	-
4	13A	16	354	AC	-	4	13A	20	103	AC	-	4	13B	3	125	AC	-
4	13A	18	339	AC	-	4	13A	16	70	AC	-	4	13B	18	145	AC	-
4	13A	10	41	AC	-	4	13A	18	96	AC	-	4	13B	14	70	AC	-
4	13A	11	31	AC	-	4	13A	19	61	AC	-	4	13B	27	137	AC	-
4	13A	7	342	AC	-	4	13A	17	95	AC	-	4	13B	10	156	AC	-
4	13A	11	26	AC	-	4	13A	15	73	AC	-	4	13B	24	103	AC	-
4	13A	11	60	AC	-	4	13B	1	111	AC	-	4	13B	20	83	AC	-
4	13A	11	77	AC	-	4	13B	14	7	AC	-	4	13B	18	74	AC	-
4	13A	11	31	AC	-	4	13B	3	40	AC	-	4	13B	20	43	AC	-
4	13A	9	56	AC	-	4	13B	12	13	AC	-	4	13B	18	106	AC	-
4	13A	6	22	AC	-	4	13B	2	194	AC	-	4	13B	27	25	AC	-
4	13A	8	89	AC	-	4	13B	11	27	AC	-	4	13B	16	101	AC	-
4	13A	9	87	AC	-	4	13B	10	39	AC	-	4	13B	11	95	AC	-
4	13A	1	16	AC	-	4	13B	11	11	AC	-	4	13B	19	64	AC	-
4	13A	6	63	AC	-	4	13B	19	228	AC	-	4	13B	24	66	AC	-
4	13A	9	113	AC	-	4	13B	3	309	AC	-	4	13B	16	34	AC	-
4	13A	20	101	AC	-	4	13B	10	357	AC	-	4	13B	18	53	AC	-
4	13A	21	78	AC	-	4	13B	13	167	AC	-	4	13B	10	80	AC	-
4	13A	25	50	AC	-	4	13B	4	334	AC	-	4	13B	22	68	AC	-
4	13A	16	80	AC	-	4	13B	14	21	AC	-	4	13B	8	109	AC	-

Table C.1 continued

DU	Sec.	Dip	Dir.	Str.	H
4	14A	3	16	AC	-
4	14A	16	185	AC	-
4	14A	4	319	AC	-
4	14A	10	31	AC	-
4	14A	12	175	AC	-
4	14A	9	218	AC	-
4	14A	1	38	AC	-
4	14A	7	10	AC	-
4	14A	1	124	AC	-
4	14A	4	33	AC	-
4	14A	7	92	AC	-
4	14A	7	37	AC	-
4	14A	22	10	AC	-
4	14A	10	352	AC	-
4	14A	18	67	AC	-
4	14A	23	25	AC	-
4	14A	18	72	AC	-
4	14A	7	35	AC	-
4	14A	14	110	AC	-
4	14A	18	127	AC	-
4	14A	26	56	AC	-
4	14A	7	85	AC	-
4	14A	7	109	AC	-
4	14A	18	42	AC	-
4	14A	54	8	AC	-
4	14A	20	15	AC	-
4	15A	1	88	AC	-
4	15A	9	359	AC	-
4	15A	13	215	AC	-
4	15A	5	346	AC	-
4	15A	12	52	AC	-
4	15A	4	111	AC	-
4	15A	12	71	AC	-
4	15A	15	90	AC	-
4	15A	14	359	AC	-
4	15A	6	16	AC	-
4	15A	9	11	AC	-
4	15A	15	1	AC	-
4	15A	17	35	AC	-
4	15A	6	356	AC	-
4	15A	17	96	AC	-
4	15A	27	107	AC	-
4	15A	9	15	AC	-
4	15A	12	19	AC	-
4	15A	21	84	AC	-
4	15A	14	19	AC	-
4	15A	25	39	AC	-
4	15A	24	275	AC	-
4	15A	5	161	AC	-
4	15A	28	45	AC	-
4	15A	17	18	AC	-
4	15A	16	5	AC	-
4	15A	7	352	AC	-
4	15A	16	155	AC	-
4	15A	18	325	AC	-
4	15A	7	354	AC	-
4	15A	20	7	AC	-
4	15A	22	324	AC	-
4	15A	22	354	AC	-
4	15A	20	25	AC	-
4	15A	26	9	AC	-
4	15A	18	344	AC	-
4	15A	9	9	AC	-
4	15A	23	9	AC	-
4	15A	37	74	AC	-
4	15A	20	7	AC	-
4	EX3	14	83	AC	-
4	EX3	3	14	AC	-
4	EX3	20	140	AC	-
4	EX3	10	111	AC	-
4	EX3	9	18	AC	-
4	EX3	9	24	AC	-

Table C.1 continued

DU	Sec.	Dip	Dir.	Str.	H	DU	Sec.	Dip	Dir.	Str.	H	DU	Sec.	Dip	Dir.	Str.	H
4	9A	18	26	TCS	14	4	9C	-	133	TCS	3	4	11A	14	42	TCS	10
4	11A	8	48	PCS	15	4	9C	-	118	TCS	2	4	11A	12	85	TCS	16
4	12A	6	95	PCS	10	4	9C	-	151	TCS	14	4	11A	-	88	TCS	11
4	12A	9	110	PCS	5	4	9C	5	135	TCS	29	4	11A	-	108	TCS	7
4	15A	3	25	PCS	5	4	9C	-	101	TCS	31	4	11A	8	150	TCS	11
4	9A	14	153	TCS	14	4	9C	-	160	TCS	8	4	11A	-	315	TCS	28
4	9C	-	35	TCS	2	4	9C	-	145	TCS	13	4	11A	-	295	TCS	12
4	9A	12	64	TCS	51	4	9C	25	73	TCS	25	4	11A	-	112	TCS	14
4	9A	10	61	TCS	65	4	9C	-	120	TCS	20	4	11A	-	156	TCS	12
4	9A	-	39	TCS	9	4	9C	-	145	TCS	12	4	11A	-	150	TCS	7
4	9A	14	80	TCS	18	4	9C	18	109	TCS	16	4	11A	-	24	TCS	14
4	9A	12	104	TCS	17	4	9C	8	70	TCS	20	4	11A	-	80	TCS	29
4	9B	11	302	TCS	-	4	9C	8	103	TCS	24	4	11A	-	113	TCS	7
4	9B	1	89	TCS	3	4	9C	14	78	TCS	14	4	11A	-	112	TCS	38
4	9B	6	72	TCS	1	4	9C	6	93	TCS	25	4	11A	-	99	TCS	13
4	9B	9	111	TCS	2	4	9C	8	62	TCS	45	4	11A	-	113	TCS	12
4	9B	4	300	TCS	3	4	10A	2	84	TCS	2	4	11A	-	56	TCS	12
4	9B	6	133	TCS	21	4	10A	-	77	TCS	2	4	11A	12	50	TCS	7
4	9B	21	102	TCS	33	4	10A	9	13	TCS	20	4	11A	11	65	TCS	14
4	9B	8	121	TCS	28	4	10A	-	305	TCS	44	4	11A	-	98	TCS	9
4	9B	-	107	TCS	16	4	10A	-	95	TCS	6	4	11A	-	100	TCS	12
4	9B	-	100	TCS	26	4	10A	12	106	TCS	24	4	12A	7	71	TCS	10
4	9B	-	75	TCS	20	4	10A	-	104	TCS	16	4	12A	11	84	TCS	4
4	9C	12	41	TCS	1	4	11A	-	66	TCS	11	4	12A	11	83	TCS	-

Table C.1 continued

DU	Sec.	Dip	Dir.	Str.	H	DU	Sec.	Dip	Dir.	Str.	H	DU	Sec.	Dip	Dir.	Str.	H
4	12A	-	68	TCS	10	4	13A	-	73	TCS	3	4	13B	-	63	TCS	21
4	12A	9	71	TCS	15	4	13A	-	121	TCS	10	4	13B	-	64	TCS	13
4	12A	6	131	TCS	13	4	13A	3	134	TCS	4	4	13B	8	75	TCS	17
4	12A	-	90	TCS	10	4	13A	-	310	TCS	9	4	14A	-	251	TCS	5
4	12A	-	68	TCS	9	4	13A	-	91	TCS	66	4	14A	-	114	TCS	-
4	12A	-	112	TCS	8	4	13A	-	90	TCS	48	4	14A	-	118	TCS	4
4	12A	11	150	TCS	36	4	13A	-	128	TCS	43	4	14A	-	74	TCS	15
4	12A	-	83	TCS	17	4	13A	7	110	TCS	32	4	14A	-	102	TCS	34
4	12A	-	77	TCS	14	4	13A	-	105	TCS	9	4	14A	-	90	TCS	12
4	12A	-	90	TCS	8	4	13A	-	122	TCS	20	4	14A	-	82	TCS	7
4	12A	-	90	TCS	13	4	13A	-	100	TCS	13	4	14A	-	118	TCS	12
4	12B	3	87	TCS	30	4	13A	-	150	TCS	13	4	14A	-	97	TCS	16
4	12B	-	322	TCS	23	4	13B	12	112	TCS	6	4	14A	-	98	TCS	8
4	12B	-	95	TCS	13	4	13B	-	39	TCS	2	4	14A	-	85	TCS	20
4	12C	3	54	TCS	3	4	13B	-	71	TCS	30	4	15A	-	142	TCS	5
4	12C	-	66	TCS	5	4	13B	-	112	TCS	6	4	15A	-	100	TCS	1
4	12C	-	310	TCS	5	4	13B	-	113	TCS	8	4	15A	-	95	TCS	3
4	12C	-	62	TCS	15	4	13B	-	115	TCS	33	4	15A	-	62	TCS	19
4	12C	-	95	TCS	27	4	13B	-	106	TCS	32	4	15A	-	82	TCS	20
4	12C	-	30	TCS	17	4	13B	-	118	TCS	12	4	15A	-	82	TCS	10
4	12C	-	63	TCS	16	4	13B	-	109	TCS	9	3	5A	30	49	AC	-
4	12C	-	110	TCS	4	4	13B	-	69	TCS	7	3	5A	20	29	AC	-
4	13A	-	114	TCS	3	4	13B	-	76	TCS	5	3	5A	18	4	AC	-
4	13A	-	67	TCS	5	4	13B	-	74	TCS	14	3	5A	3	11	AC	-

Table C.1 continued

DU	Sec.	Dip	Dir.	Str.	H
3	7B	17	215	AC	-
3	7B	14	340	AC	-
3	7B	14	62	AC	-
3	7B	12	88	AC	-
3	7B	20	54	AC	-
3	7B	4	158	AC	-
3	7B	8	170	AC	-
3	7B	9	107	AC	-
3	7B	6	115	AC	-
3	7B	23	94	AC	-
3	7B	10	0	AC	-
3	7B	18	60	AC	-
3	7B	14	62	AC	-
3	7B	22	36	AC	-
3	7B	16	186	AC	-
3	7B	21	50	AC	-
3	7B	26	152	AC	-
3	7B	8	153	AC	-
3	7B	25	83	AC	-
3	7B	19	90	AC	-
3	7B	18	101	AC	-
3	7B	19	69	AC	-
3	7B	12	138	AC	-
3	7B	21	53	AC	-
3	7B	7	56	AC	-
3	7B	20	151	AC	-
3	7B	23	40	AC	-
3	7B	13	90	AC	-
3	7B	21	37	AC	-
3	7B	18	37	AC	-
3	7B	18	20	AC	-
3	7B	30	97	AC	-
3	7B	12	29	AC	-
3	8A	26	353	AC	-
3	8A	15	350	AC	-
3	8A	14	171	AC	-
3	8A	16	150	AC	-
3	8A	13	169	AC	-
3	8A	12	356	AC	-
3	8A	17	40	AC	-
3	8A	10	13	AC	-
3	8A	11	15	AC	-
3	8A	24	46	AC	-
3	8A	15	183	AC	-
3	8A	9	50	AC	-
3	8A	12	27	AC	-
3	8A	15	75	AC	-
3	8A	12	55	AC	-
3	8A	9	30	AC	-
3	8A	10	30	AC	-
3	8A	10	95	AC	-
3	8A	20	90	AC	-
3	8A	24	180	AC	-
3	8A	18	95	AC	-
3	8A	10	155	AC	-
3	8A	17	31	AC	-
3	8A	4	80	AC	-
3	8A	2	54	AC	-
3	8A	9	140	AC	-
3	8A	4	329	AC	-
3	8A	16	185	AC	-
3	8A	20	65	AC	-
3	8A	14	156	AC	-
3	8A	8	36	AC	-
3	8A	16	143	AC	-
3	8A	16	30	AC	-
3	8A	23	74	AC	-
3	8A	22	45	AC	-
3	8A	10	111	AC	-
3	8A	13	84	AC	-
3	8A	8	61	AC	-
3	8A	18	64	AC	-

Table C.1 continued

DU	Sec.	Dip	Dir.	Str.	H	DU	Sec.	Dip	Dir.	Str.	H	DU	Sec.	Dip	Dir.	Str.	H
3	8B	11	56	AC	-	3	8B	20	45	AC	-	3	5A	7	54	TCS	28
3	8B	7	35	AC	-	3	8C	26	173	AC	-	3	5A	8	53	TCS	30
3	8B	12	75	AC	-	3	8C	6	63	AC	-	3	5A	7	54	TCS	15
3	8B	10	29	AC	-	3	8C	2	352	AC	-	3	6A	11	233	TCS	7
3	8B	16	155	AC	-	3	8C	12	178	AC	-	3	6A	3	263	TCS	10
3	8B	9	91	AC	-	3	8C	23	45	AC	-	3	6A	9	38	TCS	65
3	8B	9	303	AC	-	3	8C	18	2	AC	-	3	6A	15	43	TCS	62
3	8B	21	272	AC	-	3	8C	16	28	AC	-	3	6A	16	9	TCS	26
3	8B	17	177	AC	-	3	8C	10	137	AC	-	3	6A	17	18	TCS	29
3	8B	2	203	AC	-	3	8C	21	3	AC	-	3	6A	6	56	TCS	140
3	8B	2	34	AC	-	3	8C	12	23	AC	-	3	6A	9	80	TCS	21
3	8B	20	58	AC	-	3	5A	3	90	PCS	5	3	6A	8	99	TCS	32
3	8B	12	142	AC	-	3	5A	11	44	PCS	30	3	6A	4	98	TCS	21
3	8B	13	35	AC	-	3	5A	10	84	PCS	17	3	6A	12	115	TCS	7
3	8B	17	60	AC	-	3	5A	13	105	PCS	20	3	6A	-	94	TCS	40
3	8B	18	49	AC	-	3	6A	5	101	PCS	22	3	6A	7	104	TCS	17
3	8B	14	57	AC	-	3	5A	4	330	RCL	80	3	7A	6	150	TCS	2
3	8B	18	102	AC	-	3	6A	7	77	RCL	18	3	7A	6	340	TCS	2
3	8B	14	72	AC	-	3	6A	9	89	RCL	80	3	7A	7	88	TCS	13
3	8B	24	40	AC	-	3	8A	-	70	RCL	2	3	7A	13	95	TCS	16
3	8B	15	126	AC	-	3	8A	18	74	RCL	3	3	7A	7	107	TCS	18
3	8B	5	73	AC	-	3	5A	8	70	TCS	12	3	7B	18	300	TCS	30
3	8B	13	125	AC	-	3	5A	7	89	TCS	21	3	7B	2	75	TCS	3
3	8B	9	18	AC	-	3	5A	8	108	TCS	23	3	7B	3	174	TCS	16

Table C.1 continued

DU	Sec.	Dip	Dir.	Str.	H	DU	Sec.	Dip	Dir.	Str.	H	DU	Sec.	Dip	Dir.	Str.	H
3	7B	60	128	TCS	30	3	8A	6	125	TCS	13	2	3A	23	33	AC	12
3	7B	10	140	TCS	26	3	8B	3	90	TCS	5	2	3A	19	4	AC	17
3	7B	3	120	TCS	21	3	8B	9	332	TCS	16	2	3A	12	55	AC	10
3	7B	7	112	TCS	11	3	8B	17	98	TCS	19	2	3A	26	0	AC	21
3	7B	6	168	TCS	23	3	8B	5	115	TCS	19	2	3A	7	35	AC	7
3	7B	8	124	TCS	18	3	8B	-	103	TCS	28	2	3A	17	57	AC	18
3	7B	8	136	TCS	26	3	8B	7	76	TCS	13	2	3A	7	185	AC	18
3	7B	11	113	TCS	36	3	8B	-	95	TCS	21	2	3A	4	23	AC	32
3	7B	6	120	TCS	26	3	8C	5	122	TCS	4	2	3A	12	82	AC	8
3	7B	9	100	TCS	30	3	8C	-	80	TCS	28	2	3A	20	75	AC	15
3	7B	6	99	TCS	16	3	8C	6	74	TCS	30	2	3B	24	32	AC	40
3	7B	22	103	TCS	23	3	8C	3	58	TCS	7	2	3B	12	77	AC	6
3	7B	7	98	TCS	17	3	8C	-	52	TCS	17	2	3B	19	75	AC	26
3	7B	-	90	TCS	9	2	2A	5	100	AC	15	2	3B	2	69	AC	3
3	7B	-	56	TCS	26	2	2A	10	94	AC	16	2	3B	19	73	AC	10
3	7B	-	44	TCS	37	2	2A	3	120	AC	14	2	3B	17	359	AC	20
3	8A	4	115	TCS	37	2	2A	17	35	AC	46	2	3B	17	80	AC	115
3	8A	10	295	TCS	33	2	2A	18	98	AC	26	2	3B	20	16	AC	16
3	8A	12	115	TCS	42	2	2A	15	31	AC	37	2	3C	20	40	AC	25
3	8A	7	106	TCS	46	2	2A	9	78	AC	32	2	3C	7	20	AC	20
3	8A	5	125	TCS	10	2	2A	17	190	AC	60	2	3C	20	62	AC	29
3	8A	6	132	TCS	16	2	2A	14	131	AC	60	2	3C	25	60	AC	6
3	8A	4	116	TCS	18	2	2A	16	139	AC	40	2	3C	12	45	AC	15
3	8A	14	116	TCS	40	2	2A	10	156	AC	7	2	3C	13	32	AC	30

Table C.1 continued

DU	Sec.	Dip	Dir.	Str.	H	DU	Sec.	Dip	Dir.	Str.	H	DU	Sec.	Dip	Dir.	Str.	H
2	3C	7	50	AC	45	2	4B	22	125	AC	37	2	EX1	20	224	AC	26
2	4A	17	30	AC	65	2	4B	20	69	AC	90	2	EX1	10	340	AC	17
2	4A	22	30	AC	28	2	4B	30	78	AC	19	2	EX1	10	12	AC	22
2	4A	20	45	AC	48	2	4B	14	63	AC	32	2	EX1	18	25	AC	105
2	4A	26	33	AC	5	2	4B	12	12	AC	20	2	EX1	17	16	AC	30
2	4A	14	22	AC	33	2	4B	9	35	AC	20	2	EX1	13	44	AC	170
2	4A	14	134	AC	34	2	4B	13	39	AC	18	2	EX1	19	33	AC	60
2	4A	20	358	AC	17	2	4B	12	25	AC	15	2	EX1	8	226	AC	185
2	4A	10	45	AC	75	2	4B	7	18	AC	10	2	EX1	9	14	AC	71
2	4A	15	359	AC	12	2	4B	9	350	AC	15	2	EX1	4	290	AC	53
2	4A	19	83	AC	28	2	4B	8	328	AC	32	2	3C	12	120	AC	7
2	4A	16	24	AC	18	2	4C	20	90	AC	60	2	3A	14	125	PCS	20
2	4A	14	36	AC	9	2	4C	17	49	AC	13	2	3B	5	90	PCS	35
2	4A	22	105	AC	24	2	4C	21	72	AC	48	2	4B	18	102	PCS	36
2	4A	14	32	AC	14	2	4C	18	40	AC	42	2	4C	6	144	PCS	41
2	4A	11	169	AC	30	2	4C	26	94	AC	26	2	3B	10	50	RCL	20
2	4A	11	338	AC	40	2	4C	28	44	AC	41	2	4A	13	5	RCL	15
2	4A	23	23	AC	40	2	4C	6	80	AC	15	2	4B	6	100	RCL	50
2	4A	27	12	AC	45	2	4C	10	345	AC	40	2	4B	-	37	RCL	10
2	4A	19	77	AC	30	2	4C	8	65	AC	45	2	2A	4	55	TCS	15
2	4A	34	123	AC	15	2	4C	10	350	AC	20	2	2A	8	50	TCS	16
2	4A	13	132	AC	15	2	EX1	6	33	AC	80	2	2A	3	45	TCS	28
2	4A	19	152	AC	10	2	EX1	9	12	AC	35	2	2A	12	82	TCS	34
2	4A	22	130	AC	60	2	EX1	18	18	AC	32	2	2A	4	67	TCS	32

Table C.1 continued

DU	Sec.	Dip	Dir.	Str.	H	DU	Sec.	Dip	Dir.	Str.	H	DU	Sec.	Dip	Dir.	Str.	H
2	2A	15	88	TCS	1	2	4A	-	66	TCS	42	1	1A	24	36	AC	-
2	2A	-	72	TCS	2	2	4A	12	60	TCS	21	1	1A	20	5	AC	-
2	2A	-	103	TCS	2	2	4A	10	54	TCS	18	1	1A	21	68	AC	-
2	3A	22	52	TCS	19	2	4A	7	65	TCS	10	1	1A	21	317	AC	-
2	3A	8	81	TCS	15	2	4A	6	82	TCS	60	1	1A	22	342	AC	-
2	3A	10	80	TCS	7	2	4B	13	67	TCS	70	1	1A	18	337	AC	-
2	3A	12	44	TCS	12	2	4B	10	83	TCS	25	1	1A	11	349	AC	-
2	3A	5	64	TCS	25	2	4B	9	97	TCS	90	1	1A	14	8	AC	-
2	3A	4	76	TCS	7	2	4B	-	85	TCS	45	1	1A	21	65	AC	-
2	3B	14	105	TCS	19	2	4B	5	74	TCS	30	1	1A	10	66	AC	-
2	3B	16	40	TCS	18	2	4B	-	90	TCS	5	1	1A	10	82	AC	-
2	3B	9	75	TCS	35	2	4B	29	340	TCS	60	1	1A	18	51	AC	-
2	3B	20	63	TCS	42	2	4C	10	84	TCS	42	1	1A	21	329	AC	-
2	3B	11	75	TCS	13	2	4C	10	114	TCS	17	1	1A	26	5	AC	-
2	3B	10	82	TCS	17	2	4C	8	140	TCS	22	1	1A	30	53	AC	-
2	3B	7	33	TCS	-	2	4C	12	133	TCS	31	1	1A	18	145	AC	-
2	3B	20	355	TCS	20	2	4C	12	134	TCS	28	1	1A	14	92	AC	-
2	3C	10	22	TCS	19	2	4C	14	80	TCS	19	1	1A	29	120	AC	-
2	3C	-	94	TCS	-	2	4C	-	61	TCS	30	1	1A	34	106	AC	-
2	4A	17	36	TCS	45	1	1A	19	64	AC	-	1	1A	8	100	AC	-
2	4A	10	50	TCS	22	1	1A	22	150	AC	-	1	1A	10	128	AC	-
2	4A	7	42	TCS	24	1	1A	30	314	AC	-	1	1A	12	79	AC	-
2	4A	12	55	TCS	34	1	1A	12	51	AC	-	1	1A	10	335	AC	-
2	4A	2	220	TCS	29	1	1A	20	32	AC	-	1	1A	13	14	AC	-

Table C.1 continued

DU	Sec.	Dip	Dir.	Str.	H
1	1A	9	105	AC	-
1	1A	9	11	AC	-
1	1A	6	355	AC	-
1	1A	14	149	AC	-
1	1A	20	32	AC	-
1	1A	22	25	AC	-
1	1B	12	42	AC	-
1	1B	18	321	AC	-
1	1B	20	2	AC	-
1	1B	27	0	AC	-
1	1B	16	53	AC	-
1	1B	18	74	AC	-
1	1B	10	9	AC	-
1	1B	8	287	AC	-
1	1B	17	70	AC	-
1	1B	11	82	AC	-
1	1B	20	20	AC	-
1	1B	7	110	AC	-
1	1B	12	2	AC	-
1	1B	22	84	AC	-
1	1B	21	64	AC	-
1	1B	3	29	AC	-
1	1B	18	27	AC	-
1	1B	18	162	AC	-

DU	Sec.	Dip	Dir.	Str.	H
1	1B	8	75	AC	-
1	1B	19	4	AC	-
1	1B	20	148	AC	-
1	1B	8	72	AC	-
1	1B	20	120	AC	-
1	1B	12	69	AC	-
1	1C	247	85	AC	-
1	1C	11	110	AC	-
1	1C	14	75	AC	-
1	1C	12	100	AC	-
1	1C	24	105	AC	-
1	1C	27	126	AC	-
1	25A	20	50	AC	-
1	25A	10	80	AC	-
1	25A	15	122	AC	-
1	25A	14	78	AC	-
1	25A	9	60	AC	-
1	25A	11	31	AC	-
1	25A	6	98	AC	-
1	25A	24	110	AC	-
1	26A	23	154	AC	-
1	26A	16	156	AC	-
1	26A	21	189	AC	-
1	26A	13	83	AC	-

DU	Sec.	Dip	Dir.	Str.	H
1	27A	13	355	AC	-
1	27A	6	357	AC	-
1	27A	8	327	AC	-
1	27A	13	82	AC	-
1	27A	3	85	AC	-
1	27A	11	106	AC	-
1	27A	11	351	AC	-
1	27A	5	354	AC	-
1	27A	12	104	AC	-
1	27A	12	125	IHS	-
1	27A	9	39	IHS	-
1	27A	12	160	IHS	19
1	27A	13	102	IHS	-
1	27A	12	127	IHS	-
1	27A	9	94	IHS	-
1	27A	7	82	IHS	70
1	27A	7	70	IHS	60
1	27A	6	25	IHS	40
1	27A	12	43	IHS	45
1	27A	10	50	IHS	24
1	27A	7	65	IHS	80
1	27A	12	52	IHS	60
1	27A	8	64	IHS	120
1	27A	14	72	IHS	130

Table C.1 continued

DU	Sec.	Dip	Dir.	Str.	H
1	27A	20	72	IHS	80
1	27A	12	328	IHS	3
1	27A	8	53	IHS	7
1	25A	19	90	PCS	8
1	1A	7	115	PCS	32
1	1B	3	105	PCS	14
1	25A	14	80	PCS	11
1	26A	10	154	PCS	100
1	27A	18	93	PCS	28
1	1A	-	69	RCL	21
1	1B	10	338	RCL	38
1	25A	14	94	RCL	19
1	27A	-	72	RCL	1.5
1	27A	14	100	RCL	24
1	27A	7	65	RCL	18
1	27A	9	85	RCL	3
1	27A	16	124	RCL	60
1	27A	19	79	RCL	30
1	27A	16	146	RCL	20
1	27A	19	89	RCL	23
1	27A	14	99	RCL	5
1	27A	1	54	RCL	25
1	27A	9	320	SCS	32
1	27A	12	244	SCS	52
1	27A	7	310	SCS	50
1	27A	10	320	SCS	47
1	25A	27	123	PCS	25
1	1A	18	148	TCS	32
1	1A	11	62	TCS	24
1	1A	6	73	TCS	70
1	1A	15	72	TCS	29
1	1A	21	57	TCS	41
1	1A	-	45	TCS	32
1	1A	19	78	TCS	32
1	1A	13	69	TCS	44
1	1A	10	1	TCS	34
1	1A	4	26	TCS	19
1	1A	6	28	TCS	35
1	1A	-	51	TCS	54
1	1A	10	9	TCS	79
1	1A	12	150	TCS	20
1	1A	5	0	TCS	70
1	1A	11	329	TCS	-
1	1B	14	35	TCS	13
1	1B	9	38	TCS	18
1	1B	9	25	TCS	50
1	1B	10	82	TCS	31
1	1B	12	105	TCS	34
1	1B	8	37	TCS	26
1	1B	2	147	TCS	3
1	1B	4	55	TCS	3
1	1B	8	83	TCS	10
1	1B	15	110	TCS	10
1	1B	15	145	TCS	-
1	1B	10	107	TCS	2
1	1B	18	161	TCS	10
1	1B	9	63	TCS	4
1	1B	23	59	TCS	5
1	1B	25	110	TCS	7
1	1B	6	73	TCS	2
1	1B	19	77	TCS	1
1	1C	17	78	TCS	38
1	1C	16	69	TCS	33
1	1C	7	79	TCS	7
1	1C	10	65	TCS	11
1	1C	6	52	TCS	18
1	1C	18	118	TCS	21
1	1C	15	149	TCS	7
1	1C	20	172	TCS	10
1	1C	20	154	TCS	6
1	1C	28	154	TCS	5
1	1C	18	161	TCS	15

Table C.1 continued

DU	Sec.	Dip	Dir.	Str.	H	DU	Sec.	Dip	Dir.	Str.	H	DU	Sec.	Dip	Dir.	Str.	H
1	1C	23	144	TCS	5	0	22A	9	44	AC	-	0	22B	17	28	AC	-
1	1C	7	128	TCS	-	0	22A	22	348	AC	-	0	22B	16	8	AC	-
1	25A	15	100	TCS	27	0	22A	18	64	AC	-	0	22B	15	274	AC	-
1	25A	10	110	TCS	23	0	22A	11	34	AC	-	0	22B	6	23	AC	-
1	25A	12	126	TCS	18	0	22A	9	5	AC	-	0	22B	13	80	AC	-
1	25A	9	100	TCS	24	0	22A	4	81	AC	-	0	22B	14	65	AC	-
1	25A	20	97	TCS	32	0	22A	9	23	AC	-	0	22B	11	66	AC	-
1	25A	-	95	TCS	13	0	22A	15	10	AC	-	0	22B	6	350	AC	-
1	25A	-	99	TCS	30	0	22A	14	25	AC	-	0	22B	12	323	AC	-
1	25A	-	113	TCS	21	0	22A	23	38	AC	-	0	22B	8	341	AC	-
1	25A	-	84	TCS	18	0	22A	3	213	AC	-	0	22B	12	316	AC	-
1	25A	18	84	TCS	41	0	22A	5	1	AC	-	0	22B	16	0	AC	-
1	25A	-	68	TCS	60	0	22A	10	36	AC	-	0	22C	-	54	AC	-
1	25A	-	83	TCS	80	0	22A	14	255	AC	-	0	22C	-	52	AC	-
1	26A	-	95	TCS	24	0	22A	11	356	AC	-	0	22C	12	25	AC	-
1	26A	-	105	TCS	31	0	22A	7	321	AC	-	0	22C	14	20	AC	-
1	26A	-	102	TCS	35	0	22A	11	340	AC	-	0	22C	18	42	AC	-
1	26A	-	87	TCS	28	0	22A	10	12	AC	-	0	22C	6	61	AC	-
1	26A	-	56	TCS	50	0	22A	9	349	AC	-	0	22C	8	120	AC	-
1	26A	-	143	TCS	2	0	22B	-	66	AC	-	0	22C	5	32	AC	-
1	27A	-	64	TCS	11	0	22B	29	352	AC	-	0	22C	10	30	AC	-
1	27A	7	27	TCS	25	0	22B	7	33	AC	-	0	22C	7	353	AC	-
0	22A	13	58	AC	-	0	22B	10	339	AC	-	0	22C	1	32	AC	-
0	22A	10	59	AC	-	0	22B	18	37	AC	-	0	22C	21	341	AC	-

Table C.1 continued

DU	Sec.	Dip	Dir.	Str.	H
0	22C	17	36	AC	-
0	22C	3	108	AC	-
0	22C	11	54	AC	-
0	22C	21	294	AC	-
0	22C	16	15	AC	-
0	22C	12	18	AC	-
0	22C	17	62	AC	-
0	22C	5	10	AC	-
0	22C	7	84	AC	-
0	22C	16	32	AC	-
0	22C	5	0	AC	-
0	22C	20	323	AC	-
0	22C	7	237	AC	-
0	22C	12	70	AC	-
0	22C	9	85	AC	-
0	22C	24	156	AC	-
0	22C	20	152	AC	-
0	22C	7	34	AC	-
0	22D	22	4	AC	-
0	22D	14	50	AC	-
0	22D	12	13	AC	-
0	22D	15	22	AC	-
0	22D	11	12	AC	-
0	22D	9	63	AC	-

DU	Sec.	Dip	Dir.	Str.	H
0	22D	13	3	AC	-
0	22D	8	50	AC	-
0	22D	11	70	AC	-
0	22D	10	78	AC	-
0	22D	7	25	AC	-
0	22D	4	349	AC	-
0	22D	12	30	AC	-
0	22D	12	25	AC	-
0	23A	9	85	AC	-
0	23A	7	346	AC	-
0	23A	28	116	AC	-
0	23A	20	104	AC	-
0	24A	4	129	AC	-
0	24A	14	87	AC	-
0	24A	27	85	AC	-
0	24A	18	62	AC	-
0	24A	18	123	AC	-
0	24A	25	97	AC	-
0	24A	20	132	AC	-
0	24A	18	104	AC	-
0	24B	11	22	AC	-
0	24B	10	298	AC	-
0	24B	15	334	AC	-
0	24B	10	6	AC	-

DU	Sec.	Dip	Dir.	Str.	H
0	24B	14	95	AC	-
0	24B	19	126	AC	-
0	24B	14	16	AC	-
0	24B	24	75	AC	-
0	24B	10	11	AC	-
0	28A	-	33	AC	-
0	28A	17	83	AC	-
0	28A	20	64	AC	-
0	28A	18	71	AC	-
0	28A	14	72	AC	-
0	28A	19	22	AC	-
0	28A	10	20	AC	-
0	28A	17	80	AC	-
0	28A	10	31	AC	-
0	28A	9	20	AC	-
0	28A	13	20	AC	-
0	22A	12	50	AC	-
0	22A	14	56	AC	-
0	28A	-	85	AC	-
0	24A	20	106	PCS	170
0	24A	9	94	PCS	160
0	24A	19	83	PCS	100
0	24A	14	134	PCS	80
0	24A	25	113	PCS	200

Table C.1 continued

DU	Sec.	Dip	Dir.	Str.	H	DU	Sec.	Dip	Dir.	Str.	H	DU	Sec.	Dip	Dir.	Str.	H
0	24A	17	110	PCS	290	0	22A	-	72	TCS	27	0	22C	27	10	TCS	18
0	24B	15	46	PCS	80	0	22A	14	48	TCS	7	0	22C	-	67	TCS	13
0	24B	14	73	PCS	200	0	22A	16	7	TCS	22	0	22C	18	69	TCS	15
0	24B	24	65	PCS	50	0	22A	-	23	TCS	-	0	22C	20	45	TCS	17
0	24B	21	115	PCS	50	0	22A	19	8	TCS	8	0	22C	-	335	TCS	-
0	24B	14	90	PCS	44	0	22A	-	76	TCS	4	0	22C	-	346	TCS	15
0	24B	20	344	PCS	130	0	22A	-	115	TCS	-	0	22C	-	342	TCS	-
0	24B	14	340	PCS	110	0	22B	-	336	TCS	26	0	22C	22	30	TCS	21
0	24B	14	82	PCS	50	0	22B	13	356	TCS	35	0	22C	-	64	TCS	23
0	28A	21	80	PCS	100	0	22B	-	348	TCS	30	0	22C	22	40	TCS	26
0	28A	28	25	PCS	50	0	22B	-	43	TCS	-	0	22C	24	18	TCS	14
0	28A	13	26	PCS	75	0	22B	-	4	TCS	-	0	22C	14	27	TCS	28
0	22A	16	50	IHS	62	0	22B	23	342	TCS	28	0	22C	-	47	TCS	18
0	22A	12	89	IHS	24	0	22B	16	32	TCS	6	0	22C	5	44	TCS	28
0	22A	22	62	PCS	7	0	22B	-	13	TCS	-	0	22C	-	52	TCS	7
0	22A	12	85	PCS	42	0	22B	-	43	TCS	-	0	22C	-	40	TCS	3
0	24A	9	115	PCS	15	0	22B	-	153	TCS	14	0	22C	-	51	TCS	3
0	24A	-	74	PCS	45	0	22B	17	23	TCS	22	0	22C	-	0	TCS	2
0	22A	-	30	TCS	14	0	22B	-	53	TCS	-	0	22C	-	138	TCS	4
0	22A	-	77	TCS	-	0	22B	20	44	TCS	19	0	22C	-	138	TCS	-
0	22A	-	97	TCS	-	0	22B	14	83	TCS	12	0	22D	30	40	TCS	16
0	22A	9	73	TCS	31	0	22B	-	69	TCS	-	0	22D	-	320	TCS	19
0	22A	17	54	TCS	18	0	22B	-	75	TCS	-	0	22D	-	252	TCS	37
0	22A	-	37	TCS	53	0	22C	-	17	TCS	11	0	22D	20	315	TCS	34

Table C.1 continued

DU	Sec.	Dip	Dir.	Str.	H
0	22D	-	90	TCS	14
0	22D	7	15	TCS	23
0	22D	30	358	TCS	19
0	22D	9	90	TCS	12
0	22D	-	93	TCS	27
0	22D	-	80	TCS	19
0	22D	10	125	TCS	11
0	22D	-	112	TCS	49
0	22D	-	333	TCS	30
0	22D	-	325	TCS	-
0	22D	-	109	TCS	7
0	22D	-	87	TCS	10
0	22D	-	109	TCS	20
0	23A	-	96	TCS	20
0	23A	18	20	TCS	14
0	23A	20	14	TCS	21
0	23A	13	41	TCS	19
0	23A	9	48	TCS	17
0	23A	10	57	TCS	13
0	23A	10	32	TCS	19
0	23A	21	45	TCS	13
0	23A	24	354	TCS	53
0	23A	22	33	TCS	11
0	23A	5	20	TCS	12
0	23A	12	103	TCS	34
0	23A	-	104	TCS	43
0	24A	17	12	TCS	47
0	24A	24	36	TCS	51
0	24B	26	49	TCS	32
0	24B	-	34	TCS	-
0	24B	-	30	TCS	-
0	24B	15	80	TCS	20
0	28A	-	81	TCS	-
0	28A	-	60	TCS	-
0	28A	-	243	TCS	-
0	28A	-	75	TCS	-
0	28A	-	62	TCS	-
0	28A	-	51	TCS	-
0	28A	-	47	TCS	18
0	28A	-	68	TCS	32
0	28A	-	95	TCS	21
0	28A	-	73	TCS	25
0	28A	-	99	TCS	34
0	28A	-	22	TCS	19
0	28A	-	23	TCS	22
0	28A	-	103	TCS	43
0	28A	-	61	TCS	-
0	28A	-	34	TCS	12
0	28A	-	79	TCS	18
0	28A	-	71	TCS	15
0	28A	-	96	TCS	30
0	28A	-	40	TCS	11
0	28A	-	54	TCS	10
0	28A	-	85	TCS	20
0	28A	24	64	TCS	25
0	28A	-	25	TCS	10

APPENDIX D

PALEOMORPHODYNAMIC SPREADSHEET

An excel file containing the paleomorphodynamic workflow is included in a supplemental digital file. The file includes completed workflows for the depositional units at Rock House Cove and Bull Canyon.

Paleomorphodynamics Workflow (Hajek and Wolinsky, 2012)

Mean dune height (h_m) (Bridge and Tye, 2000; Leclair and Bridge, 2001)

1. Measured barform rollover
2. Calculated from mean x-set thickness (s_m)

(To use this method: s_d/s_m = .88 +/- .3; s_d = standard deviation of x-set thickness)

Formulas:

```
a = 4-8 (min-max)
B = sm/1.8
hm = aB (min-max)
hm = 2.22B^1.32
hm = 2.9 +/- .7 * sm
```

(Mean dune height is approximately 6x to 10x mean dune height)

Bankfull Depth (H) = 11.6(h_m)^0.84 (Bridge and Tye, 2000; Leclair and Bridge, 2001)

Relative Roughness = (d50/H) (Hajek and Wolinsky, 2012)

d50 = bed load, median grain size

Slope (S) = Rt*(d50/H) (Paola and Mohrig, 1996)

R = Submerged specific gravity quarts, 1.65

t* = Shields stress for sand bed, 1.0

Drag (Cd) = (d50/H)^(1/6) (Hajek and Wolinsky, 2012)

Depth Avg. Velocity (U) = sqrt(t/Cd) (Hajek and Wolinsky, 2012)

t = kinematic shear stress (= stress / fluid density; $(m/s)^2$)

Froude number (Fr) = U/sqrt(g*H) (Parker, E-book)

g = gravitational acceleration, 9.8 m/s

Fr^2

Fr^2 = ~1 far up stream

Fr^2 = ~0 far downstream

Fr^2 << 0 in transition zone, where flow "feels" the influence of upstream flow and downstream base level

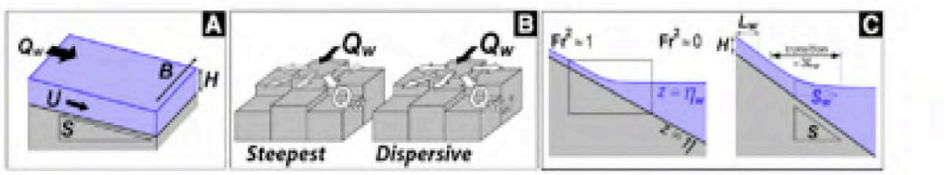

Fig. 1. Hydrodynamics concepts. Schematic diagrams illustrating key hydrodynamics concepts and variables. A) Normal flow. B) Cellular flow routing approaches. C) Backwater and low-Froude flows. In steep upland rivers the water surface typically parallels the bed, but in gently-sloping lowland rivers the water surface commonly diverges from the surface topography (left). In the backwater transition zone the influence of base level is felt upstream (right).

(Hajek and Wolinsky, 2012)

Backwater length (L_w) = H/S (Bridge and Mackey, 1993)

Upstream “normal flow” depth and slope

Channel belt width (cbw) (Bridge and Mackey, 1993 cited in Bridge and Tye, 2000)

$cbw = 59.9(dm)^{1.8}$

$cbw = 192(dm)^{1.37}$

dm = mean flow depth

	Data		mean dune height (h_{mean}) - in m			bankfull depth (H)			bankfull depth min, med, max (H)			Relative Roughness (d50 / H)			Paleoslope (S)			Drag (Cd)			U = depth ave vel (m/s)			Fr (Froude Number)			Fr^2			Backwater Length			Calculations - channel belt width in METERS		
						* uses H =11.6(hm)^0.84									Slope = R1*(d/H) (Hajek and Wolinsky,						t=Cd(U^2)			Hajek and Wolinsky, 2012; eq 8b			Hajek and Wolinsky, 2012; Figure 1			Lw=H/S (m)			Bridge and Mackey (1993) cited in Bridge and Tye (2000)		
															1* =constant (??), 1.0 (sand) vs 0.4 (grav			Cd approx = (d/H)^(1/6)			U = sqrt(t/Cd)			Fr = U/(sqrt (g*H))									here dm is actually Hm (mean bankflow depth)		
DU - 6	Area	East Bull Canyo	*Sd/Sm*	***0.77***		meters			H min (6xhn	H med (8xhn	H max (10xh	minimum	median	max	minimum	median	max	minimum	median	max	minimum	median	max	minimum	median	max	minimum	median	max	minimum	median	max	minimum	median	max
	Depositional unit	6.00	*a = 4-8 (min-max)*	*4.00*	*6.00*	*8.00*			2.97	3.96	4.94	2.11E-04	1.58E-04	1.26E-04	3.48E-04	2.61E-04	2.09E-04	0.24	0.23	0.22	1.42	1.46	1.51	0.264	0.234	0.217	0.070	0.055	0.047	8534.60	15172.63	23707.23	cbw = 59.9(c	424	712	1,064
	Mean xset height (r	0.17	*B = Sm/1.8*	*0.09*					H minimum	H median	H max																					cbw = 192 (d	852	1,263	1,715
	n	41.00	h_m = aB (min-max)	0.38	0.57	0.76	5.13	7.22	9.19																									
	St Dev	0.13	h_m = 2.22B^1.32	0.10			1.66			5.09	6.42	7.34																						
			hm = 2.9 +/- .7 * Si	0.38	0.49	0.58	5.09	6.42	7.34																									
DU - 5	Area	East Bull Canyo	*Sd/Sm*	***0.85***																														
	Depositional unit	5.00	*a = 4-8 (min-max)*	*4.00*	*6.00*	*8.00*																												
	Mean xset height (r	0.12	*B = Sm/1.8*	*0.07*																														
	n	60.00	h_m = aB (min-max)	0.26	0.40	0.53	3.78	5.32	6.77																									
	St Dev	0.10	h_m = 2.22B^1.32	0.06			1.11																											
			hm = 2.9 +/- .7 * Si	0.26	0.34	0.40	3.75	4.73	5.41																									
DU - 4	Area	East Bull Canyo	*Sd/Sm*	***0.78***																														
	Depositional unit	4.00	*a = 4-8 (min-max)*	*4.00*	*6.00*	*8.00*																												
	Mean xset height (r	0.15	*B = Sm/1.8*	*0.09*																														
	n	133.00	h_m = aB (min-max)	0.34	0.52	0.69	4.73	6.64	8.46																									
	St Dev	0.12	h_m = 2.22B^1.32	0.09			1.49																											
			hm = 2.9 +/- .7 * Si	0.34	0.45	0.53	4.69	5.91	6.75																									
DU - 3	Area	East Bull Canyo	*Sd/Sm*	***0.81***																														
	Depositional unit	3.00	*a = 4-8 (min-max)*	*4.00*	*6.00*	*8.00*																												
	Mean xset height (r	0.24	*B = Sm/1.8*	*0.13*																														
	n	64.00	h_m = aB (min-max)	0.54	0.80	1.07	6.87	9.65	12.29																									
	St Dev	0.19	h_m = 2.22B^1.32	0.16			2.44																											
			hm = 2.9 +/- .7 * Si	0.53	0.70	0.82	6.81	8.59	9.82																									
DU - 2	Area	East Bull Canyo	*Sd/Sm*	***0.73***																														
	Depositional unit	2.00	*a = 4-8 (min-max)*	*4.00*	*6.00*	*8.00*																												
	Mean xset height (r	0.28	*B = Sm/1.8*	*0.16*																														
	n	49.00	h_m = aB (min-max)	0.62	0.94	1.25	7.80	10.97	13.96																									
	St Dev	0.21	h_m = 2.22B^1.32	0.19			2.89																											
			hm = 2.9 +/- .7 * Si	0.62	0.81	0.95	7.74	9.76	11.15																									
DU - 1	Area	East Bull Canyo	*Sd/Sm*	***72.08***																														
	Depositional unit	1.00	*a = 4-8 (min-max)*	*4.00*	*6.00*	*8.00*																												
	Mean xset height (r	0.26	*B = Sm/1.8*	*0.15*																														
	n	71.00	h_m = aB (min-max)	0.59	0.88	1.17	7.40	10.41	13.25																									
	St Dev	19.00	h_m = 2.22B^1.32	0.18			2.69																											
			hm = 2.9 +/- .7 * Si	0.58	0.76	0.90	7.34	9.26	10.58																									
DU - 0	Area	East Bull Canyo	*Sd/Sm*	***1.24***																														
	Depositional unit	0.00	*a = 4-8 (min-max)*	*4.00*	*6.00*	*8.00*																												
	Mean xset height (r	0.36	*B = Sm/1.8*	*0.20*																														
	n	132.00	h_m = aB (min-max)	0.80	1.20	1.60	9.62	13.52	17.22																									
	St Dev	0.45	h_m = 2.22B^1.32	0.27			3.81																											
			hm = 2.9 +/- .7 * Si	0.79	1.04	1.22	9.54	12.03	13.75																									

Bankfull Depth (H)

DU	Value	Min Error	Max Error	Min H	Med H	Max H
0	8.352	2.088	2.088	6.26	8.35	10.44
1	6.11552	1.52888	1.52888	4.59	6.12	7.64
2	6.50992	1.62748	1.62748	4.88	6.51	8.14
3	5.59352	1.39838	1.39838	4.20	5.59	6.99
4	3.5844	0.8961	0.8961	2.69	3.58	4.48
5	2.7492	0.6873	0.6873	2.06	2.75	3.44
6	3.9556	0.9889	0.9889	2.97	3.96	4.94

(H based on 6x, 8x, and 10x dune height)
(Dune height is 2.9x avg bar height)

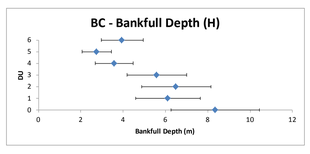

Relative Roughness (d50/H)

DU	Value	Min Erro	Max Error	Value with min, med, and max H: Min H	Med H	Max H
0	6.34579E-05	1.26916E-05	2.11526E-05	8.46E-05	6.35E-05	5.08E-05
1	4.9219E-05	9.84381E-06	1.64063E-05	6.56E-05	4.92E-05	3.94E-05
2	4.04767E-05	8.09534E-06	1.34922E-05	5.40E-05	4.05E-05	3.24E-05
3	3.79904E-05	7.59808E-06	1.26635E-05	5.07E-05	3.80E-05	3.04E-05
4	9.4437E-05	1.88874E-05	3.1479E-05	1.26E-04	9.44E-05	7.55E-05
5	0.000187691	3.75382E-05	6.25637E-05	2.50E-04	1.88E-04	1.50E-04
6	0.000158004	3.16008E-05	5.26679E-05	2.11E-04	1.58E-04	1.26E-04

(d50 estimated from measured sections)

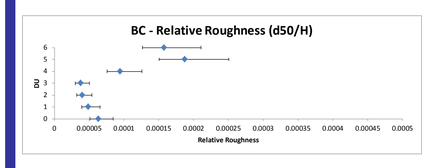

Paleoslope (S)

DU	Value	Min Error	Max Error	Value with min, med, and max H: Min H	Med H	Max H
0	0.000104705	2.09E-05	3.49E-05	1.40E-04	1.05E-04	8.38E-05
1	8.12114E-05	1.62E-05	2.71E-05	1.08E-04	8.12E-05	6.50E-05
2	6.67865E-05	1.34E-05	2.23E-05	8.90E-05	6.68E-05	5.34E-05
3	6.26841E-05	1.25E-05	2.09E-05	8.36E-05	6.27E-05	5.01E-05
4	0.000155821	3.12E-05	5.19E-05	2.08E-04	1.56E-04	1.25E-04
5	0.000309069	6.19E-05	1.03E-04	4.13E-04	3.10E-04	2.48E-04
6	0.000260706	5.21E-05	8.69E-05	3.48E-04	2.61E-04	2.09E-04

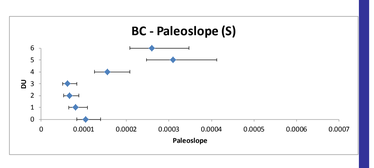

Paleoslope (Degrees)

DU	Value	Min Error	Max Error
0	0.005999181	0.0012	0.002
1	0.004653071	0.000931	0.001551
2	0.003826587	0.000765	0.001276
3	0.003591537	0.000718	0.001197
4	0.008927889	0.001786	0.002976
5	0.017743935	0.003549	0.005915
6	0.014937373	0.002987	0.004979

Fr^2

DU	Value	Min Error	Max Error	Value with min, med, and max H: Min	Med	max
0	0.02935	4.05E-03	8.02E-03	0.03737	0.02935	0.02529
1	0.03805	5.26E-03	1.04E-02	0.04845	0.03805	0.03279
2	0.03612	4.99E-03	9.87E-03	0.04599	0.03612	0.03113
3	0.04099	5.66E-03	1.12E-02	0.05	0.04	0.04
4	0.05939	8.21E-03	1.62E-02	0.07562	0.05939	0.05118
5	0.07408	1.02E-02	2.02E-02	0.09433	0.07408	0.06385
6	0.05471	7.56E-03	1.50E-02	0.06966	0.05471	0.04715

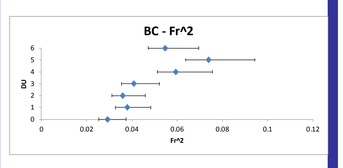

Backwater Length (Lw) in m

DU	Value	Min Error	Max Error	Value with min, med, and max H: Min H	Med H	Max H
0	79766.6	3.49E+04	4.49E+04	######	######	######
1	75303.7	3.29E+04	4.24E+04	######	######	######
2	97473.5	4.26E+04	5.48E+04	######	######	######
3	89233.4	3.90E+04	5.02E+04	######	######	######
4	23003.3	1.01E+04	1.29E+04	######	######	35942.67
5	8877.26	3.88E+03	4.99E+03	4993.46	8877.26	13870.72
6	15172.6	6.64E+03	8.53E+03	8534.60	######	23707.23

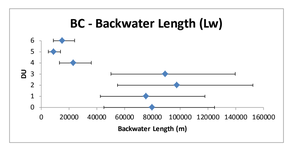

Backwater Length (Lw) in Km

DU	Value	Min Error	Max Error
0	79.7666	34.8979	44.8687
1	75.3037	32.9454	42.3583
2	97.4735	42.6447	54.8289
3	89.2334	39.0396	50.1938
4	23.0033	10.0639	12.9394
5	8.87726	3.8838	4.99346
6	15.1726	6.63802	8.5346

Channe Belt Width (conservative)

DU	Value	Min Error	Max Error	Value with min, med, and max H: Min H	Med H	Max H
0	2733.1	1.10E+03	1.35E+03	1628.40	2733.06	4084.02
1	1559.6	6.30E+02	7.71E+02	929.22	1559.58	2330.48
2	1745.3	7.05E+02	8.63E+02	1039.86	1745.27	2607.96
3	1328.2	5.37E+02	6.57E+02	791.35	1328.19	1984.72
4	596.18	2.41E+02	2.95E+02	355.21	596.18	890.87
5	369.83	1.49E+02	1.83E+02	220.35	369.83	552.63
6	711.88	2.88E+02	3.52E+02	424.15	711.88	1063.77

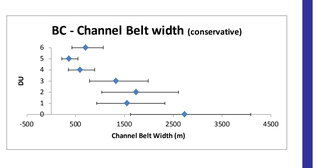

	Data		mean dune height ($h_{ss\ or\ dh}$) - in m			bankfull depth (H)			bankfull depth min, med, max (H)			Hm revised - best guesses			Relative Roughness (d50/H)			Paleoslope (S)			Drag (Cd)			U = depth ave vel (m/s)			Fr (Froude Number)			Fr^2			Backwater Length			Calculations - channel belt width in METERS		
DU - 6	Area	South Rock House Cove	Sd/Sm		0.51	* uses H =11.6(hm)^0.84			H min (6xhm) H med (8xhm H max (10xhm			Hm min	Hm med	Hm max	gr size C (in m) 0.00071000			S = Rt*(d/H) (Hajek and Wolinsky, 20			Cd approx = (d/H)^(1/6)			U = sqrt(tiCd)			Hajek and Wolinsky, 2012; eq 8			Hajek and Wolinsky, 2012; Figure 1			Lw =H/S (m)			Bridge and Mackey (1993) cited in Bridge and Tye (2000)		
	Depositional unit		a = 4-8 (min-max)	4.00	6.00 8.00	meters			2.74 3.61 4.23			2.06	3.61	4.95	minimum median max			5.68E-04 3.25E-04 2.37E-04			0.26 0.24 0.23			1.35 1.42 1.46			Fr = U/(sqrt (g*H))			minimum median max			minimum median max			here dm is actually Hm (mean bankflow depth)		
	Mean xset height (m)		B = Sm/1.8	0.12					H minimum H median H max																												
	n	185.00	h_{ss} = aB (min-max)	0.46	0.69 0.92	6.05	8.51	10.83	2.06 7.57 10.83																												
	St Dev	0.11	h_{ss} = 2.22B^1.32	0.13		2.06			H minimum H median H max																												
			hm = 2.9 +/- .7 * Sm	0.46	0.60 0.70	6.00	7.57	8.65	2.06 7.57 10.83																												
									4.95 <based on jared's est																												
DU - 5	Area	South Rock House Cove	Sd/Sm		0.69										gr size Mu 0.000425																						
	Depositional unit	5.00	a = 4-8 (min-max)	4.00	6.00 8.00				H min (6xhm) H med (8xhm H max (10xhm			Hm min	Hm med	Hm max	minimum median max			minimum median max			minimum median max			minimum median max			minimum median max			minimum median max			minimum median max					
	Mean xset height (m)	0.21	B = Sm/1.8	0.12					H minimum H median H max																												
	n	307.00	h_{ss} = aB (min-max)	0.46	0.69 0.92	6.05	8.51	10.83	2.74 3.61 4.23																												
	St Dev	0.14	h_{ss} = 2.22B^1.32	0.13		2.06			H minimum H median H max																												
			hm = 2.9 +/- .7 * Sm	0.46	0.60 0.71	6.00	7.57	8.65	2.06 7.57 10.83																												
									4.95 <based on jared's est																												
DU - 4	Area	South Rock House Cove	Sd/Sm		0.74										gr size M 0.00035																						
	Depositional unit	4.00	a = 4-8 (min-max)	4.00	6.00 8.00				H min (6xhm) H med (8xhm H max (10xhm			Hm min	Hm med	Hm max	minimum median max			minimum median max			minimum median max			minimum median max			minimum median max			minimum median max			minimum median max					
	Mean xset height (m)	0.26	B = Sm/1.8	0.14					H minimum H median H max																												
	n	178.00	h_{ss} = aB (min-max)	0.57	0.86 1.15	7.27	10.22	13.01	3.41 4.49 5.26																												
	St Dev	0.19	h_{ss} = 2.22B^1.32	0.17		2.63			H minimum H median H max																												
			hm = 2.9 +/- .7 * Sm	0.57	0.75 0.88	7.21	9.09	10.39	2.63 9.09 13.01																												
									6.15 <based on jared's est																												
DU-3	Area	south RHC							based on story thicknesses, no cross setc						gr size MI 0.0003																						
	Depositional unit	DU-3							H min (story thic Hmed H max			Hm min	Hm med	Hm max	minimum median max			minimum median max			minimum median max			minimum median max			minimum median max			minimum median max			minimum median max					
									2 2.4 4			2.00	2.40	4.00	0.00015 0.000125 0.000075			2.48E-04 2.06E-04 1.24E-04			0.23 0.22 0.21			1.45 1.47 1.54			0.328 0.304 0.245			0.107 0.092 0.060			8080.81 11636.36 32323.23			cbw = 59.9(dm)^1.8	209	290 726
																																			cbw = 192 (dm)^1.37	496	637 1,283
DU - 2	Area	South Rock House Cove	Sd/Sm		0.51										gr size M 0.00035																						
	Depositional unit	2.00	a = 4-8 (min-max)	4.00	6.00 8.00				H min (6xhm) H med (8xhm H max (10xhm			Hm min	Hm med	Hm max	minimum median max			minimum median max			minimum median max			minimum median max			minimum median max			minimum median max			minimum median max					
	Mean xset height (m)	0.24	B = Sm/1.8	0.13					H minimum H median H max																												
	n	112.00	h_{ss} = aB (min-max)	0.53	0.80 1.06	6.81	9.58	12.20	3.15 4.16 4.87																												
	St Dev	0.12	h_{ss} = 2.22B^1.32	0.15		2.41			H minimum H median H max																												
			hm = 2.9 +/- .7 * Sm	0.53	0.69 0.83	6.76	8.52	9.74	2.41 8.52 12.20																												
									5.75 <based on jared's est																												
DU - 1	Area	South Rock House Cove	Sd/Sm		0.71										gr size MU 0.000425																						
	Depositional unit	1.00	a = 4-8 (min-max)	4.00	6.00 8.00				H min (6xhm) H med (8xhm H max (10xhm			Hm min	Hm med	Hm max	minimum median max			minimum median max			minimum median max			minimum median max			minimum median max			minimum median max			minimum median max					
	Mean xset height (m)	0.29	B = Sm/1.8	0.16					H minimum H median H max																												
	n	223.00	h_{ss} = aB (min-max)	0.65	0.97 1.30	8.06	11.33	14.43	3.85 5.08 5.95																												
	St Dev	0.21	h_{ss} = 2.22B^1.32	0.20		3.01			H minimum H median H max																												
			hm = 2.9 +/- .7 * Sm	0.64	0.85 0.99	7.99	10.08	11.52	3.01 10.08 14.43																												
									7.05 <based on jared's est																												
DU - Base	Area	South Rock House Cove	Sd/Sm		1.02										gr size = C 0.00071000																						
	Depositional unit	Base	a = 4-8 (min-max)	4.00	6.00 8.00				H min (6xhm) H med (8xhm H max (10xhm			Hm min	Hm med	Hm max	minimum median max			minimum median max			minimum median max			minimum median max			minimum median max			minimum median max			minimum median max					
	Mean xset height (m)	0.20	B = Sm/1.8	0.11					H minimum H median H max																												
	n	201.00	h_{ss} = aB (min-max)	0.44	0.66 0.88	5.80	8.16	10.39	2.60 3.43 4.03																												
	St Dev	0.20	h_{ss} = 2.22B^1.32	0.12		1.95			H minimum H median H max																												
			hm = 2.9 +/- .7 * Sm	0.43	0.57 0.67	5.75	7.26	8.30	1.95 7.26 10.39																												
									4.75 <based on jared's est																												

Notes: yellow boxes highlight best guess based on jared's table 1.4

Bankfull Depth (H)

DU	Value	Min Error	Max Error	Min H	Med H	Max H
0	3.433254	1.479733	1.32	1.95	3.43	4.75
1	5.07643	2.06238	1.97357	3.01	5.08	7.05
2	4.156425	1.74172	1.593575	2.41	4.16	5.75
3	2.4	0.4	1.6	2.00	2.40	4.00
4	4.488809	1.859084	1.661191	2.63	4.49	6.15
5	3.608091	1.543963	1.341909	2.06	3.61	4.95
6	3.607914	1.543898	1.342086	2.06	3.61	4.95

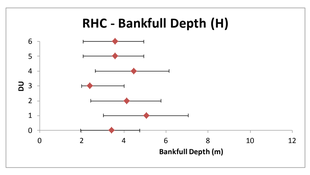

Relative Roughness (d50/H)

DU	Value	Min Erro	Max Error	Value with min, med, and max H		
				Min H	Med H	Max H
0	0.000206801	5.73272E-05	0.000156645	3.63E-04	2.07E-04	1.49E-04
1	8.37202E-05	2.34366E-05	5.7286E-05	1.41E-04	8.37E-05	6.03E-05
2	8.4207E-05	2.33374E-05	6.07383E-05	1.45E-04	8.42E-05	6.09E-05
3	0.000125	0.00005	0.000025	0.00015	0.000125	0.000075
4	7.79717E-05	2.10611E-05	5.51221E-05	1.33E-04	7.80E-05	5.69E-05
5	0.000117791	3.19322E-05	8.81073E-05	2.06E-04	1.18E-04	8.59E-05
6	0.00019679	5.33553E-05	0.0001472	3.44E-04	1.97E-04	1.43E-04

(d50 estimated from measured sections)

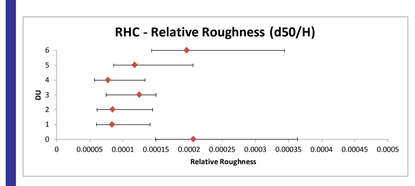

Paleoslope (S)

DU	Value	Min Error	Max Error	Value with min, med, and max H		
				Min H	Med H	Max H
0	0.000341	9.46E-05	2.58E-04	6.00E-04	3.41E-04	2.47E-04
1	0.000138	3.87E-05	9.45E-05	2.33E-04	1.38E-04	9.95E-05
2	0.000139	3.85E-05	1.00E-04	2.39E-04	1.39E-04	1.00E-04
3	0.000206	8.25E-05	4.12E-05	2.48E-04	2.06E-04	1.24E-04
4	0.000129	3.48E-05	9.10E-05	2.20E-04	1.29E-04	9.39E-05
5	0.000194	5.27E-05	1.45E-04	3.40E-04	1.94E-04	1.42E-04
6	0.000325	8.80E-05	2.43E-04	5.68E-04	3.25E-04	2.37E-04

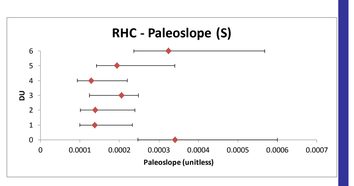

Paleoslope (Degrees)

DU	Value	Min Error	Max Error
0	0.019551	0.0054196	0.014809
1	0.007915	0.0022156	0.0054157
2	0.007961	0.0022063	0.0057421
3	0.011817	0.0047269	0.0023635
4	0.007371	0.0019911	0.0052111
5	0.011136	0.0030188	0.0083295
6	0.018604	0.0050441	0.013916

Fr^2

DU	Value	Min Error	Max Error	Value with min, med, and max H		
				Min	Med	max
0	0.059289	1.41E-02	3.56E-02	0.094852	0.059289	0.04524
1	0.04662	1.12E-02	2.54E-02	0.071986	0.04662	0.03546
2	0.056884	1.35E-02	3.26E-02	0.089442	0.056884	0.0434
3	0.092238	3.20E-02	1.51E-02	0.107373	0.092238	0.06026
4	0.053352	1.23E-02	3.00E-02	0.083305	0.053352	0.04104
5	0.061964	1.44E-02	3.67E-02	0.098687	0.061964	0.04761
6	0.056887	1.32E-02	3.37E-02	0.090601	0.056887	0.04371

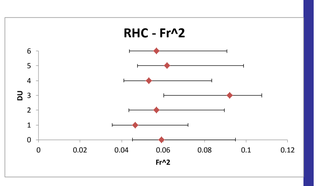

Backwater Length (Lw) in m

DU	Value	Min Error	Max Error	Value with min, med, and max H		
				Min H	Med H	Max H
0	10061.7	6.80E+03	9.20E+03	3257.57	10061.66	19259.50
1	36748.9	2.38E+04	3.41E+04	12954.72	36748.87	70877.01
2	29914.9	1.98E+04	2.73E+04	10096.62	29914.92	57251.08
3	11636.4	3.56E+03	2.07E+04	8080.81	11636.36	32323.23
4	34890.7	2.29E+04	3.06E+04	11974.81	34890.75	65493.51
5	18564.5	1.25E+04	1.64E+04	6075.76	18564.45	34941.18
6	11111.4	7.47E+03	9.80E+03	3636.50	11111.43	20915.49

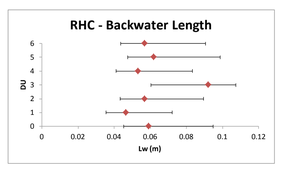

Backwater length (Lw) in km

DU	Value	Min Error	Max Error	Min H	Med H	Max H
0	10.0617	6.80E+00	9.20E+00	3.26	10.06	19.26
1	36.7489	2.38E+01	3.41E+01	12.95	36.75	70.88
2	29.9149	1.98E+01	2.73E+01	10.10	29.91	57.25
3	11.6364	3.56E+00	2.07E+01	8.08	11.64	32.32
4	34.8907	2.29E+01	3.06E+01	11.97	34.89	65.49
5	18.5645	1.25E+01	1.64E+01	6.08	18.56	34.94
6	11.1114	7.47E+00	9.80E+00	3.64	11.11	20.92

Channel Belt Widths (conservative)

DU	Value	Min Error	Max Error	Value with min, med, and max H		
				Min H	Med H	Max H
0	551.69	3.52E+02	4.38E+02	199.94	551.69	989.64
1	1115.40	6.79E+02	8.99E+02	436.41	1115.40	2014.50
2	778.26	4.85E+02	6.18E+02	292.81	778.26	1395.82
3	289.61	8.10E+01	4.37E+02	208.58	289.61	726.33
4	893.85	5.52E+02	6.82E+02	341.40	893.85	1575.44
5	603.29	3.83E+02	4.63E+02	220.78	603.29	1065.90
6	603.24	3.82E+02	4.63E+02	220.75	603.24	1065.90

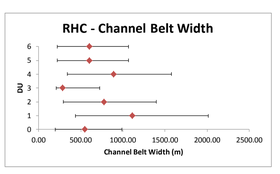

South Rock Hosse Cove
(cloudy, 2018)

DU	son	dip	dip dir.	sense	sed struc	cross-set (cm)
6	A	23	5	N	TCS	20
6	A	23	110	ESE	TCS	10
6	A	20	247	WSW	TCS	30
6	A	20	84	E	TCS	30
6	A	18	57	NE	TCS	20
6	A	19	54	NE	TCS	20
6	A	24	118	SE	TCS	30
6	A	24	46	NE	TCS	5
6	A	19	297	SW	TCS	15
6	A	24	92	E	TCS	30
6	B	10	28	NE	TCS	10
6	B	14	340	NE	TCS	30
6	B	14	67	E	TCS	25
6	B	26	235	W	TCS	25
6	B	19	311	NW	TCS	20
6	B	16	0	N	TCS	20
6	C	11	37	NE	TCS	20
6	C	15	296	WSW	TCS	20
6	C	7	99	E	TCS	30
6	D	18	90	NE	TCS	30
6	D	18	50	NW	TCS	30
6	D	23	337	NW	PCS	30
6	E	24	78	ENE	TCS	30
6	E	12	124	SE	TCS	30
6	E	19	68	SE	TCS	10
6	E	19	68	E	TCS	10
6	E	12	94	E	TCS	30
6	E	21	46	NE	TCS	15
6	E	20	53	NE	TCS	10
6	E	24	41	NW	TCS	30
6	F	25	21	NE	TCS	15
6	F	22	72	NE	TCS	15
6	F	22	45	NE	TCS	20
6	G	18	112	ESE	TCS	20
6	G	15	45	NE	TCS	30
6	G	24	74	ENE	TCS	30
6	G	17	77	ENE	TCS	30
6	G	12	56	NE	TCS	30
6	G	20	59	ENE	TCS	20
6	G	9	300	WNW	TCS	30
6	G	3	225	SW	TCS	20
6	H	9	275	W	TCS	10
6	H	15	73	ENE	TCS	10
6	H	22	49	NE	TCS	20
6	H	12	8	N	TCS	20
6	H	12	158	SSW	TCS	10
6	H	10	65	NE	TCS	15
6	H	10	62	NE	TCS	15
6	I	24	176	E	TCS	5
6	I	18	330	WNW	TCS	30
6	I	21	312	NW	PCS	30
6	I	14	36	NE	TCS	30
6	I	4	231	WNW	TCS	10
6	J	19	345	NNW	TCS	15
6	J	14	61	ENE	TCS	30
6	J	5	354	N	TCS	20
6	V	26	0	N	TCS	20
6	V	14	69	ENE	TCS	30
6	V	24	339	NW	PCS	20
6	V	24	0	N	PCS	30
6	W	15	100	E	PCS	30
6	W	12	21	NNE	PCS	10
6	W	17	67	ENE	PCS	30
6	W	14	67	ENE	PCS	30
6	W	21	25	NNE	PCS	30
6	W	9	330	NW	TCS	10
6	W	35	340	NNW	TCS	10
6	W	15	112	ESE	TCS	30
6	W	15	90	E	TCS	40
6	W	39	7	N	TCS	40
6	X	5	278	NE	TCS	30
6	X	17	40	NE	TCS	30
6	X	27	0	N	TCS	30
6	X	15	87	SE	TCS	40
6	X	8	58	NE	TCS	30
6	X	33	62	ENE	TCS	30
6	X	22	122	SE	TCS	30
6	X	15	90	E	PCS	40
6	X	32	100	E	PCS	30
6	X	17	90	E	PCS	30
6	Y	17	90	E	PCS	30
6	Y	16	126	SE	PCS	30
6	Y	33	116	SE	PCS	30
6	Y	24	82	E	PCS	20
6	Y	18	76	E	TCS	20
6	Y	28	20	NNE	PCS	10
6	Y	8	79	E	TCS	20
6	Z	31	68	ENE	TCS	30
6	Z	26	20	NE	TCS	30
6	Z	38	66	ENE	TCS	30
6	Z	21	14	NNE	TCS	30
6	Z	22	130	SE	PCS	40
6	Z	31	353	N	TCS	10
6	X	13	117	SE	PCS	20
6	X	11	80	N	TCS	30
6	X	16	97	E	TCS	30
6	X	9	62	E	PCS	30
6	X	23	45	NE	TCS	10
6	X	25	56	NNE	TCS	10
6	Y	25	75	E	TCS	30
6	Y	30	31	NE	TCS	30
6	Y	33	116	SE	TCS	40
6	Y	24	82	E	TCS	30
6	Z	17	345	NNW	TCS	20
6	Z	10	312	NW	PCS	20
6	Z	13	345	WNW	TCS	20
6	Z	7	164	S	TCS	20
6	Z	25	342	NE	TCS	20
6	Z	24	90	NE	TCS	30
6	Z	24	90	NE	TCS	10
6	Z	26	336	NNW	PCS	30

DU	son	dip	dip dir.	sense	sed struc	cross-set (cm)
1	A	28	29	NNE	TCS	50
1	A	23	96	N	TCS	10
1	A	25	247	WSW	TCS	10
1	A	19	107	ESE	TCS	10
1	A	20	87	ESE	TCS	15
1	A	10	60	E	TCS	5
1	A	9	60	ENE	TCS	5
1	A	9	225	SW	TCS	40
1	A	23	334	NW	TCS	5
1	A	15	42	SW	TCS	1
1	A	23	109	ESE	TCS	10
1	A	19	334	NW	TCS	20
1	A	7	201	SSW	TCS	20
1	A	21	213	ESE	TCS	15
1	A	9	39	NE	TCS	40
1	A	18	39	NE	TCS	5
1	A	20	60	ENE	TCS	30
1	A	24	353	WNW	TCS	25
1	A	25	116	E	TCS	40
1	A	23	128	SE	TCS	30
1	A	10	225	SW	TCS	20
1	A	23	137	SE	TCS	30
1	A	22	155	ESE	TCS	30
1	A	22	131	SE	TCS	30
1	A	21	121	ESE	TCS	30
1	A	21	169	E	TCS	10
1	A	22	94	E	TCS	30
1	A	23	140	SE	TCS	30
1	A	20	121	SE	TCS	30
1	A	11	124	SSE	TCS	20
1	A	19	46	NE	TCS	30
1	A	15	70	SE	TCS	20
1	B	17	118	ESE	TCS	40
1	B	14	92	ENE	TCS	30
1	B	11	128	SE	TCS	30
1	B	13	84	NE	TCS	20
1	B	15	70	NE	TCS	30
1	B	8	320	NW	TCS	40
1	B	9	111	E	TCS	30
1	B	17	149	SE	TCS	30
1	B	26	126	SE	TCS	30
1	B	30	24	NNE	TCS	30
1	B	27	78	NE	TCS	30
1	C	29	28	NE	TCS	20
1	C	14	48	E	TCS	25
1	C	19	75	ENE	TCS	30
1	C	10	91	ENE	TCS	10
1	C	18	85	SE	TCS	30
1	C	24	146	SE	TCS	30
1	C	31	133	SE	TCS	30
1	C	24	134	SE	TCS	20
1	C	28	369	N	TCS	20
1	C	16	105	E	TCS	30
1	C	28	102	E	TCS	30
1	C	22	47	ENE	TCS	30
1	D	10	47	SE	TCS	30
1	D	23	106	ENE	TCS	30
1	D	16	280	NNW	TCS	15
1	D	12	67	NNE	TCS	20
1	D	21	39	ENE	TCS	30
1	D	23	0	N	TCS	20
1	D	18	182	ESE	TCS	40
1	D	24	154	SSE	TCS	30
1	D	24	137	SE	TCS	30
1	D	20	141	SE	TCS	30
1	D	17	138	SSE	TCS	30
1	D	13	131	SE	TCS	30
1	D	15	154	SSE	TCS	30
1	D	18	158	ESE	TCS	30
1	E	6	139	SE	TCS	30
1	E	23	134	SE	TCS	30
1	E	30	114	ESE	TCS	30
1	E	19	125	SE	TCS	30
1	E	19	156	SSE	TCS	15
1	E	27	125	SE	TCS	30
1	E	30	97	ENE	TCS	30
1	E	31	138	SE	TCS	30
1	E	16	249	WSW	TCS	20
1	E	6	277	S	TCS	30
1	E	7	264	SW	TCS	30
1	E	20	117	ESE	TCS	30
1	E	12	54	E	TCS	30
1	E	15	42	NE	PCS	30
1	E	22	111	ESE	TCS	30
1	E	17	68	ENE	TCS	30
1	E	19	113	ESE	TCS	30
1	E	20	165	E	TCS	30
1	E	15	101	E	TCS	30
1	E	22	154	ESE	TCS	30
1	E	22	121	SE	TCS	30
1	E	22	154	ESE	PCS	30
1	E	23	71	E	TCS	30
1	E	24	96	E	TCS	30
1	E	23	142	SE	TCS	30
1	E	14	96	E	TCS	30
1	E	17	70	ENE	TCS	30
1	E	23	149	SSE	TCS	15
1	E	14	145	SE	TCS	30
1	E	20	146	SE	TCS	30

DU	son	dip	dip dir.	sense	sed struc	cross-set (cm)
2	A	8	33	NNE	TCS	10
2	A	14	26	NE	TCS	10
2	A	10	204	SSW	TCS	10
2	A	14	183	SSE	TCS	5
2	A	18	149	ESE	TCS	15
2	A	15	49	NE	TCS	10
2	A	19	159	ESE	TCS	10
2	A	12	121	E	TCS	30
2	A	30	111	ESE	TCS	30
2	A	21	117	ESE	TCS	30
2	A	15	94	E	TCS	30
2	A	16	59	SE	TCS	20
2	A	27	72	E	TCS	30
2	A	27	66	E	TCS	20
2	A	27	123	E	TCS	30
2	A	27	84	E	TCS	30
2	A	15	74	E	PCS	30
2	A	29	57	SE	TCS	30
2	A	27	91	E	TCS	30
2	A	25	107	E	TCS	30
2	A	25	71	ENE	TCS	30
2	A	25	182	SSW	TCS	30
2	A	25	341	WSW

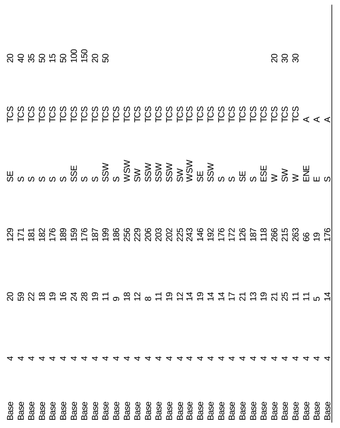

| | | |

North Rock House Cove Paleocurrent Measurements
(Gooley, 2010)

DU	sxn	dip	dip dir.	sense	sed struct	cross-set (cm)	DU	sxn	dip	dip dir.	sense	sed struct	cross-set (cm)	DU	sxn	dip	dip dir.	sense	sed struct	cross-set (cm)
6	A	14	10	N	TCS	20	5	B	15	342	NNW	TCS	30	5	G	18	32	NNE	TCS	20
6	A	26	357	N	TCS	20	5	C	25	12	NNE	TCS	5	5	G	17	70	ENE	TCS	20
6	A	23	12	NNE	TCS	30	5	C	18	32	NNE	TCS	2	5	G	22	24	NNE	TCS	20
6	A	15	31	NNE	TCS	20	5	C	25	320	NW	TCS	5	5	G	32	65	ENE	TCS	20
6	A	18	11	N	TCS	20	5	C	18	3	N	TCS	5	5	G	15	57	ENE	TCS	10
6	A	22	104	ESE	TCS	30	5	C	24	55	NE	TCS	20	5	G	14	69	ENE	TCS	5
6	B	33	347	NNW	TCS	15	5	D	26	39	NE	TCS	40	5	G	15	29	NNE	TCS	5
6	B	14	11	N	TCS	15	5	D	28	32	NNE	TCS	30	5	G	31	66	ENE	TCS	5
6	B	18	34	NE	TCS	10	5	D	14	20	NNE	TCS	15	5	G	21	69	ENE	TCS	5
6	B	17	16	NNE	TCS	20	5	D	33	28	NNE	TCS	20	5	G	15	60	ENE	TCS	5
6	B	11	81	E	TCS	15	5	D	23	220	SW	TCS	5	5	G	27	23	NNE	TCS	10
6	C	11	81	E	TCS	15	5	D	25	54	NE	TCS	15	5	G	10	71	ENE	TCS	15
6	C	24	109	ESE	TCS		5	D	27	53	NE	TCS	10	5	G	24	18	NNE	TCS	10
5	A	22	91	E	TCS	40	5	D	14	34	NE	TCS	10	5	G	23	63	ENE	TCS	10
5	A	18	71	ENE	TCS	40	5	E	25	60	ENE	TCS	30	5	G	16	73	ENE	TCS	15
5	A	22	22	NNE	TCS	30	5	E	21	108	ESE	TCS	30	5	G	11	29	NNE	TCS	10
5	A	19	15	NNE	TCS	20	5	E	22	43	NE	TCS	15	5	G	18	74	ENE	TCS	20
5	A	17	2	N	TCS	15	5	E	13	77	ENE	TCS	5	5	J	17	23	NNE	TCS	40
5	A	21	51	NE	TCS	20	5	E	12	111	ESE	TCS	5	5	J	17	80	E	TCS	40
5	A	27	12	NNE	A		5	E	15	106	ESE	TCS	15	5	J	13	82	E	TCS	50
5	A	22	21	NNE	A		5	E	24	73	ENE	TCS	30	5	J	12	46	NE	TCS	30
5	B	20	37	NE	TCS	30	5	E	28	36	NE	TCS	10	5	J	24	38	NE	TCS	30
5	B	28	27	NNE	TCS	30	5	G	27	60	ENE	TCS	15	5	K	9	55	NE	TCS	
5	B	25	337	NNW	A		5	G	13	78	ENE	TCS	5	5	K	22	43	NE	TCS	20
5	B	16	338	NNW	A		5	G	14	37	NE	TCS	5	5	K	33	350	N	TCS	50
5	B	22	335	NNW	TCS		5	G	19	54	NE	TCS	30	5	K	23	347	NNW	TCS	50

Table D.4 continued

DU	sxn	dip	dip dir.	sense	sed struct	cross-set (cm)	DU	sxn	dip	dip dir.	sense	sed struct	cross-set (cm)	DU	sxn	dip	dip dir.	sense	sed struct	cross-set (cm)
5	K	29	95	E	TCS	50	2	A	15	184	S	TCS	10	2	D	22	32	NNE	TCS	10
5	K	14	7	N	TCS	30	2	A	7	50	NE	TCS	15	2	D	32	64	ENE	TCS	5
5	K	20	14	NNE	TCS	30	2	A	21	108	ESE	A		2	D	32	42	NE	TCS	20
5	L	34	95	E	TCS	30	2	A	21	55	NE	TCS	15	2	D	26	70	ENE	TCS	5
5	L	34	352	N	TCS	30	2	B	19	57	ENE	TCS	20	2	D	34	12	NNE	TCS	20
5	L	18	19	NNE	TCS	30	2	B	20	5	N	TCS	5	2	E	33	61	ENE	TCS	20
5	L	24	44	NE	TCS	20	2	B	30	54	NE	TCS	30	2	E	21	65	ENE	TCS	20
5	M	20	73	ENE	TCS	25	2	B	13	65	ENE	TCS	15	2	E	24	24	NNE	TCS	5
5	M	12	29	NNE	TCS	15	2	B	19	73	ENE	TCS	30	2	E	25	355	N	TCS	10
5	M	23	44	NE	TCS	30	2	B	16	54	NE	TCS	15	2	E	21	48	NE	TCS	5
5	M	10	62	ENE	TCS	50	2	B	25	35	NE	TCS	15	2	E	22	76	ENE	TCS	10
4	A	12	10	N	TCS	30	2	B	16	64	ENE	TCS	15	2	E	38	24	NNE	TCS	20
4	A	23	332	NNW	TCS	30	2	B	18	72	ENE	TCS	15	2	F	11	55	NE	TCS	30
4	A	10	19	NNE	TCS	40	2	C	14	78	ENE	TCS	20	2	F	22	74	ENE	TCS	25
4	A	15	346	NNW	TCS	40	2	C	20	8	N	TCS	10	2	F	8	130	SE	TCS	25
4	B	27	44	NE	TCS	30	2	C	19	19	NNE	TCS	20	2	F	24	71	ENE	TCS	10
4	B	20	82	E	TCS	30	2	C	9	108	ESE	TCS	40	2	F	14	86	E	TCS	10
4	B	8	50	NE	TCS	20	2	C	18	42	NE	TCS	20	2	F	25	97	E	TCS	20
4	B	14	8	N	TCS	20	2	C	18	66	ENE	TCS	20	2	F	16	31	NNE	TCS	20
4	B	25	357	N	TCS	20	2	D	20	76	ENE	TCS	15	2	G	21	359	N	TCS	40
4	B	19	351	N	TCS		2	D	19	43	NE	TCS	10	2	G	20	76	ENE	TCS	15

2	A	40	41	NE	TCS	10	2	D	18	19	NNE	TCS	10	2	G	29	121	ESE	TCS	5
2	A	26	49	NE	TCS	10	2	D	27	62	ENE	TCS	5	2	G	22	69	ENE	TCS	10
2	A	23	39	NE	TCS	10	2	D	11	87	E	TCS	10	2	G	30	35	NE	TCS	20
2	A	26	53	NE	TCS	30	2	D	4	105	ESE	TCS	5	2	G	34	36	NE	TCS	20
2	A	25	64	ENE	TCS	20	2	D	34	11	N	TCS	5	2	G	18	88	E	TCS	5
2	A	3	49	NE	TCS	10	2	D	21	28	NNE	TCS	5	2	G	13	21	NNE	TCS	15
2	A	10	50	NE	TCS	5	2	D	26	24	NNE	TCS	10	2	G	27	64	ENE	TCS	15

Table D.4 continued

DU	sxn	dip	dip dir.	sense	sed struct	cross-set (cm)	DU	sxn	dip	dip dir.	sense	sed struct	cross-set (cm)	DU	sxn	dip	dip dir.	sense	sed struct	cross-set (cm)
2	G	34	34	NE	TCS	10	Base		6	130	SE	A		Base		26	32	NNE	TCS	20
1	U	14	131	SE	TCS	20	Base		10	24	NNE	TCS	20	Base		27	90	E	TCS	60
1	U	13	115	ESE	TCS	10	Base		16	41	NE	TCS	15	Base		15	134	SE	TCS	60
1	U	16	93	E	TCS	10	Base		15	39	NE	TCS	15	Base		22	50	NE	TCS	30
1	U	11	144	SE	TCS	5	Base		8	58	ENE	TCS	50							
1	U	12	107	ESE	TCS	10	Base		21	13	NNE	TCS	50							
1	U	14	132	SE	A		Base		13	42	NE	TCS	50							
1	U	19	196	SSW	TCS		Base		28	56	NE	TCS	20							
1	U	20	120	ESE	TCS		Base		25	12	NNE	TCS	20							
1	U	7	123	ESE	A		Base		27	108	ESE	TCS	20							
1	U	15	98	E	TCS		Base		22	24	NNE	TCS	20							
1	L	22	263	W	TCS	50	Base		15	105	ESE	TCS	20							
1	L	21	21	NNE	TCS	10	Base		25	62	ENE	TCS	30							
1	L	14	231	SW	TCS	15	Base		12	8	N	A								
1	L	6	149	SSE	TCS	30	Base		24	23	NNE	A								
1	L	14	159	SSE	TCS	30	Base		22	35	NE	TCS	5							
1	L	10	204	SSW	TCS	30	Base		21	218	SW	TCS	20							
1	L	19	89	E	TCS	15	Base		22	124	SE	TCS	20							
1	L	11	66	ENE	TCS	15	Base		11	55	NE	TCS	15							
1	L	24	97	E	TCS	15	Base		20	49	NE	TCS	15							
1	L	22	78	ENE	TCS	25	Base		16	222	SW	TCS	20							
1	L	17	115	ESE	TCS	10	Base		20	151	SSE	TCS	30							
1	L	23	77	ENE	TCS	10	Base		26	104	ESE	TCS	30							
1	L	14	82	E	TCS	10	Base		19	2	N	TCS	30							
Base		22	68	ENE	TCS	30	Base		23	96	E	TCS	30							
Base		12	15	NNE	TCS	20	Base		20	146	SE	TCS	15							
Base		9	47	NE	TCS	15	Base		11	142	SE	TCS	15							
Base		13	28	NNE	TCS	15	Base		17	48	NE	TCS	10							

APPENDIX E

SANDSTONE SAMPLES LIST

A list of the sandstone samples collected for this study is included in Table E.1. The date of collection, GPS location, and stratigraphic interval of the collection location are all recorded. Stratigraphic intervals include: Calico bed (Calico) of the Smoky Hollow Member (SHM), DU-0 through DU-6 of the John Henry Member, and the Drip Tank Member (DTM). For samples that were collected along the measured stratigraphic sections, the section name (SXN) and elevation (EL.) along the section from which the sample was collected are also documented. Sample names that begin with a DZ were collected for future detrital zircon analysis.

Table E.1

Sandstone Samples List

Sample #	Date	GPS location	Strat. Interval	SXN	El.
BCSE-001	5/13/11	N37°12.963, W111°42.685	DU-2	SXN1	28.9 m
BCSE-002	5/13/11	N37°12.963, W111°42.685	DU-3	SXN1	53
BCSE-003	5/14/11	N37°12.963, W111°42.685	DU-3	SXN1	79.5
BCSE-004	5/14/11	N37°12.963, W111°42.685	DU-4	SXN1	116.5
BCSE-005	5/14/11	N37°12.963, W111°42.685	DU-4	SXN1	142
BCSE-006	5/15/11	N37°12.963, W111°42.685	DU-4	SXN1	156.2
BCSE-007	5/15/11	N37°12.963, W111°42.685	DU-5	SXN1	171.6
BCSE-008	5/16/11	N37°12.963, W111°42.685	DU-5	SXN1	193.2
BCSE-M-001	9/9/11	N37°13.121, W111°42.664	DU-0	SXN2	1.2
BCSE-M-002	9/9/11	N37°13.121, W111°42.664	DU-2	SXN2	24.5
BCSE-M-003	9/9/11	N37°13.121, W111°42.664	DU-2	SXN2	38.7
BCSE-M-004	9/9/11	N37°13.121, W111°42.664	DU-3	SXN2	62.8
BCSE-M-005	9/9/11	N37°13.121, W111°42.664	DU-4	SXN2	86
BCSE-M-006	9/9/11	N37°13.121, W111°42.664	DU-4	SXN2	107.5
BCSE-M-007	9/9/11	N37°13.121, W111°42.664	DU-4	SXN2	124
BCSE-M-008	9/10/11	N37°13.121, W111°42.664	DU-5	SXN2	149.5
BCSE-M-009	9/10/11	N37°13.121, W111°42.664	DU-5	SXN2	178
DZ-BCSE-M-001	9/9/11	N37°13.121, W111°42.664	DU-2	SXN2	20.7
DZ-BCSE-M-002	9/9/11	N37°13.121, W111°42.664	DU-3	SXN2	62.8
DZ-BCSE-M-003	9/10/11	N37°13.121, W111°42.664	DU-4	SXN2	124
DZ-BCSE-M-004	9/10/11	N37°13.121, W111°42.664	DU-5	SXN2	149.5
DZ-BCSE-M-005	9/10/11	N37°13.121, W111°42.664	DU-5	SXN2	173.3
BCSE-U-001	9/12/11	N37°13.411, W111°42.533	DU-2	SXN3	8.1
BCSE-U-002	9/12/11	N37°13.411, W111°42.533	DU-3	SXN3	40.5
BCSE-U-003	9/12/11	N37°13.411, W111°42.533	DU-4	SXN3	60.2
BCSE-U-004	9/12/11	N37°13.411, W111°42.533	DU-4	SXN3	79
BCSE-U-005	9/13/11	N37°13.411, W111°42.533	DU-4	SXN3	105
BCSE-U-006	9/13/11	N37°13.411, W111°42.533	DU-5	SXN3	127.2
BCSE-U-007	9/13/11	N37°13.411, W111°42.533	DU-5	SXN3	147
BCSE-U-008	9/13/11	N37°13.411, W111°42.533	DU-6	SXN3	167.8
DZ-BCSE-U-001	9/12/11	N37°13.411, W111°42.533	DU-2	SXN3	9.7
DZ-BCSE-U-002	9/12/11	N37°13.411, W111°42.533	DU-3	SXN3	40.5
DZ-BCSE-U-003	9/13/11	N37°13.411, W111°42.533	DU-4	SXN3	83.2
DZ-BCSE-U-004	9/13/11	N37°13.411, W111°42.533	DU-4	SXN3	115.8
DZ-BCSE-U-005	9/13/11	N37°13.411, W111°42.533	DU-5	SXN3	136.2

Table E.1 Continued

Sample #	Date	GPS location	Strat. Interval	SXN	El.
BC-P-01	5/11/12	N 37°12.687, W111°42.774	DU-0	NA	NA
BC-P-02	5/11/12	N 37°12.687, W111°42.774	SHM (Calico)	NA	NA
BC-P-03	5/11/12	N 37°12.687, W111°42.774	Calico & JHM	NA	NA
BC-P-04	5/14/12	N 37°13.016, W111°42.303	DTM	NA	NA
BC-P-05	5/14/12	N 37°12.997, W111°42.318	DU-6	NA	NA
BC-P-06	5/14/12	N 37°12.524, W111°42.627	SHM (Calico)	NA	NA
BC-P-07	6/7/12	N 37°13.128, W111°42.632	DU-1	NA	NA

APPENDIX F

PETROGRAPHIC DATA

The petrographic data in Figure F.1 are from thin section analysis of the sandstone samples collected in Bull Canyon (Table E.1). The elevation (El.) represents the approximate elevation relative to the base of the John Henry Member. The depositional unit column includes: Smoky Hollow Member (SHM), DU-0 through DU-6 of the John Henry Member, and Drip Tank Member (DTM). The grain sizes of samples are listed: lower fine sandstone (fL), upper fine sandstone (fU), lower medium sandstone (mL), and upper medium sandstone (mU). Point count data abbreviations include: Qm = monocrystalline quartz, Qp = polycrystalline quartz, Cht = chert, P = plagioclase feldspar, K = potassium feldspar, Other = total count of grains other than quartz and feldspar, M/C = matrix and cement, Pore = pore space, Lc = calcite lithic, Ls = sedimentary lithic, Lv = volcanic lithic, Qt = total quartz (Qm, Qp, Cht), Qpt = total polycrystalline quartz (Qp, Cht), F = total feldspars (P, K), Lu = undifferentiated lithics (Lc, Ls, Lm, Lv), Lt = total lithics (Lu, Cht).

Table F.1

Petrographic Data From Bull Canyon Sandstone Samples

El.	Sample	DU	Size	Qm	Qp	Cht	P	K	Other	M/C	Pore	Lc	Ls	Lm	Lv	Qt	Qpt	F	Lu	Lt
229	BC-P-04	DTM	fU-mU	299	11	31	0	69	96	90	40	51	45	0	0	341	42	69	96	138
223	BC-P-05	DU-6	mU	233	20	33	0	151	73	81	20	2	70	1	0	286	53	151	73	126
220	BCSE-U-008	DU-6	mU-cL	326	41	30	0	99	62	97	60	6	55	1	0	397	71	99	62	133
207	BCSE-008	DU-5	mL	340	32	28	0	65	56	27	74	0	53	3	0	400	60	65	56	116
198	BCSE-U-007	DU-5	mL-mU	259	27	25	0	106	88	88	36	49	39	0	0	311	52	106	88	140
186	BCSE-007	DU-5	fU	292	22	34	0	93	92	58	56	68	24	0	0	348	56	93	92	148
178	BCSE-U-006	DU-5	fU	287	14	21	0	85	95	66	68	66	29	0	0	322	35	85	95	130
170	BCSE-006	DU-4	mL	322	22	45	1	80	53	47	76	5	46	4	0	389	67	81	55	122
157	BCSE-U-005	DU-4	mL	263	23	20	0	75	126	68	69	94	32	0	0	306	43	75	126	169
156	BCSE-005	DU-4	mL	263	17	56	0	108	74	103	39	1	66	7	0	336	73	108	74	147
139	BCSE-M-006	DU-4	fU-mL	276	21	45	1	79	57	58	56	14	42	1	0	342	66	80	57	123
130	BCSE-004	DU-4	fU-mL	247	6	26	0	68	173	51	52	147	26	0	0	279	32	68	173	205
114	BCSE-U-004	DU-4	mL	248	33	25	1	91	102	79	75	56	43	3	0	306	58	92	102	160
96	BCSE-U-003	DU-4	fU-mL	264	32	42	2	55	115	100	45	66	41	8	0	338	74	57	115	189
90	BCSE-003	DU-3	mL-mU	232	10	34	0	69	159	138	17	122	38	0	0	276	44	69	160	204
66	BCSE-002	DU-3	mL	217	27	28	2	51	177	54	42	131	30	16	0	272	55	53	177	232
42	BCSE-001	DU-2	fL-fU	356	13	9	0	34	88	80	46	68	19	1	0	378	22	34	88	110
28	BC-P-07	DU-1	fU-mL	256	38	38	1	80	89	75	57	64	23	4	0	332	76	81	91	167
14	BCSE-M-001	DU-0	fU-mL	338	10	21	0	88	56	96	56	31	24	1	0	369	31	88	56	87
1	BC-P-01	DU-0	mL	305	29	8	1	112	56	75	65	20	36	1	0	342	37	113	57	94
0	BC-P-06	SHM	mU	492	8	0	0	0	0	71	70	0	0	0	0	500	8	0	0	8
-2	BC-P-02	SHM	mU	498	1	0	0	0	1	15	52	0	1	0	0	499	1	0	1	2

APPENDIX G

GPS POINT DATA AND MEASUREMENTS

GPS point data

The GPS point data collected for the sandstone bodies and paths of the measured sections are contained in Tables G.1 and G.2. The locations (easting and northing) of points were recorded using the NAD83 coordinate system and UTM zone 12N. Elevation was recorded in meters above mean sea level (MSL). In Table G.1, the SS Body column contains the assigned sandstone body number, which are marked on the photomosics in Appendix B, and the locations of the points around the edge of the sandstone body were documented: top (T), base (B), left (L), and right (R). In Table G.2, the points taken along the paths of each measured sections (SXN) are numbered (PT. No.) in order from base to top.

Channel belt measurements

Table G.3 contains information collected from the 136 channel belts. The column headings included: assigned stratigraphic order (Order), depositional unit (DU), sandstone body number (SS Body), lateral (L) and vertical (V) amalgamation index numbers (Amalg), channel belt width (width), channel belt thickness (thickness), width to thickness ratio (W/T). Channel belt width and thickness categories include: measurements from GPS points (M), corrected or true width

(True), moving average with a range of five (MA), and average for each depositional unit (DU Ave).

Projected channel belt centers

Table G.4 contains the relative locations (in meters) of channel body centers projected onto planes oriented parallel to the outcrop (Parallel) and perpendicular the average paleocurrent (Perpendicular). The same projections were used after the points had been rotated to remove a slight structural dip (Parallel Rotated and Perpendicular Rotated).

Table G.1

Sandstone Body GPS Points

Easting	Northing	MSL	SS body	
437140.30	4119929.07	1446.21	1	L
437118.81	4119895.10	1449.54	1	T
437129.74	4119883.27	1448.27	1	T
437115.00	4119893.51	1445.65	1	B
437127.67	4119881.85	1443.71	1	B
437101.76	4119818.72	1449.40	1	R
437151.19	4119965.74	1448.48	2	L
437148.25	4119947.66	1448.64	2	T
437149.74	4119947.28	1447.30	2	B
437151.71	4119938.76	1449.59	2	R
437150.96	4119961.34	1449.83	3	L
437150.77	4119946.57	1450.45	3	T
437151.06	4119945.95	1448.56	3	B
437146.94	4119911.31	1453.23	3	R
437209.05	4119981.70	1454.23	4	L
437170.21	4119942.65	1457.36	4	T
437186.58	4119934.37	1457.61	4	T
437169.35	4119943.65	1456.07	4	B
437183.70	4119933.10	1456.47	4	B
437198.90	4119926.84	1457.89	4	R
437188.08	4120016.36	1457.11	5	L
437191.46	4120009.63	1457.07	5	T
437191.26	4120008.39	1457.14	5	B
437201.24	4120003.14	1457.47	5	R
437197.25	4120025.80	1460.87	6	L
437192.68	4120012.91	1460.02	6	T
437192.10	4120013.41	1458.47	6	B
437200.59	4120006.61	1460.66	6	R
437209.14	4120037.49	1462.30	7	L
437201.81	4120019.51	1464.29	7	T
437201.91	4120016.38	1462.01	7	B
437226.98	4120013.90	1461.84	7	R
437251.26	4120174.46	1458.93	8	L
437231.97	4120101.68	1459.94	8	T
437251.03	4120152.77	1460.17	8	T
437229.22	4120104.13	1459.92	8	B
437251.13	4120151.27	1458.21	8	B
437247.67	4120083.54	1460.77	8	R
437244.35	4119869.63	1461.22	9	L
437215.56	4119847.74	1463.02	9	T
437205.26	4119811.28	1464.54	9	T
437191.27	4119777.10	1462.06	9	T
437216.64	4119847.51	1461.04	9	B
437202.73	4119808.63	1460.51	9	B
437187.45	4119775.70	1461.70	9	B
437190.84	4119787.26	1463.62	9	R
437224.56	4119815.10	1467.38	10	L
437210.62	4119800.18	1467.46	10	T
437206.66	4119782.70	1467.08	10	T
437203.32	4119767.75	1465.03	10	T
437207.17	4119797.43	1465.76	10	B

Easting	Northing	MSL	SS body	
437207.17	4119797.43	1465.76	10	B
437194.71	4119780.70	1464.08	10	B
437197.23	4119767.31	1461.29	10	B
437190.76	4119764.13	1463.05	10	R
437311.94	4120154.11	1466.47	11	L
437323.14	4120151.56	1466.34	11	T
437323.24	4120148.58	1465.26	11	B
437333.87	4120134.83	1466.32	11	R
437254.92	4120091.44	1462.89	12	L
437249.14	4119986.58	1466.26	12	T
437253.74	4120016.38	1463.14	12	B
437247.36	4119987.25	1465.46	12	B
437249.41	4119977.01	1465.55	12	R
437256.45	4119977.59	1468.93	13	L
437259.30	4119916.80	1469.23	13	T
437276.37	4119896.31	1470.67	13	T
437289.30	4119879.19	1471.36	13	T
437257.44	4120014.99	1463.87	13	T
437259.67	4119916.14	1468.50	13	B
437273.24	4119898.24	1470.69	13	B
437285.49	4119875.19	1469.10	13	B
437283.15	4119865.12	1471.90	13	R
437288.16	4119998.58	1477.43	14	L
437273.18	4119947.09	1480.74	14	T
437282.62	4119928.43	1481.51	14	T
437271.49	4119947.95	1479.89	14	B
437280.87	4119927.52	1479.10	14	B
437281.45	4119923.91	1482.72	14	R
437287.17	4119953.61	1484.86	15	L
437314.78	4119898.51	1485.07	15	T
437306.47	4119912.07	1485.83	15	T
437312.94	4119897.72	1483.36	15	B
437303.22	4119909.65	1483.30	15	B
437323.84	4119882.18	1485.61	15	R
437287.03	4120262.73	1473.68	16	L
437304.78	4120242.00	1472.33	16	T
437333.32	4120171.02	1474.91	16	T
437332.23	4120065.58	1476.31	16	T
437294.48	4119986.28	1483.57	16	T
437303.85	4120238.90	1471.17	16	B
437327.50	4120168.31	1472.69	16	B
437328.95	4120068.13	1478.31	16	B
437291.95	4119984.62	1482.66	16	B
437317.75	4120009.29	1481.88	16	R
437338.42	4120355.92	1472.97	17	L
437328.39	4120245.93	1475.97	17	T
437323.95	4120244.42	1477.19	17	B
437338.79	4120227.98	1475.26	17	R
437345.83	4120200.63	1477.34	18	L
437352.36	4120180.27	1479.56	18	T
437350.33	4120176.66	1477.25	18	B

Table G.1 continued

Easting	Northing	MSL	SS	body
437363.89	4120171.27	1477.34	18	R
437332.28	4120006.56	1485.62	19	L
437306.49	4119980.50	1487.20	19	T
437305.67	4119980.00	1485.38	19	B
437306.41	4119975.77	1487.70	19	R
437302.04	4119957.73	1488.46	20	L
437299.95	4119948.43	1489.37	20	T
437299.12	4119947.91	1488.50	20	B
437299.80	4119944.25	1488.86	20	R
437446.65	4120498.50	1482.58	21	L
437380.98	4120267.86	1486.23	21	T
437411.97	4120135.71	1490.26	21	T
437354.66	4119979.35	1498.42	21	T
437360.81	4119890.13	1499.95	21	T
437378.60	4120263.32	1482.25	21	B
437409.55	4120130.76	1486.63	21	B
437349.92	4119977.79	1495.37	21	B
437358.19	4119889.15	1494.42	21	B
437354.95	4119861.41	1500.14	21	R
437441.52	4120604.45	1478.23	22	L
437447.25	4120491.87	1481.80	22	T
437371.27	4120324.44	1480.98	22	R
437457.30	4120598.34	1481.03	23	L
437440.67	4120500.87	1481.37	23	R
437399.51	4119979.09	1515.17	24	L
437393.40	4119961.96	1513.46	24	T
437382.09	4119923.44	1516.69	24	T
437383.70	4119900.52	1516.20	24	T
437388.99	4119876.42	1516.07	24	T
437391.69	4119967.82	1512.53	24	B
437378.38	4119924.95	1513.60	24	B
437380.76	4119900.44	1513.22	24	B
437387.83	4119877.00	1515.06	24	B
437391.91	4119857.90	1516.98	24	R
437449.93	4120174.15	1502.34	25	L
437450.91	4120107.59	1505.19	25	T
437429.42	4120048.71	1507.79	25	T
437390.33	4119970.61	1511.53	25	T
437439.75	4120102.78	1502.32	25	B
437411.55	4120041.62	1505.80	25	B
437391.29	4119971.07	1510.58	25	B
437378.54	4119927.94	1510.35	25	R
437436.85	4120157.53	1501.22	26	L
437442.06	4120123.75	1501.57	26	T
437437.11	4120099.47	1504.52	26	T
437438.29	4120124.01	1497.79	26	B
437434.62	4120096.31	1499.64	26	B
437425.51	4120069.36	1500.29	26	R
437430.39	4120318.63	1497.21	27	L
437426.59	4120222.58	1495.41	27	T
437417.98	4120258.69	1497.15	27	T
437420.79	4120217.20	1492.63	27	B
437416.13	4120254.94	1494.42	27	B
437431.40	4120190.70	1499.20	27	R
437423.70	4120260.72	1499.06	28	L
437427.83	4120216.60	1501.87	28	T
437424.36	4120211.64	1499.10	28	B
437431.53	4120200.61	1500.33	28	R
437476.08	4120331.27	1510.78	29	L
437393.91	4119733.48	1525.53	29	T
437405.43	4119819.47	1524.71	29	T
437395.19	4119893.54	1524.61	29	T
437403.18	4119967.79	1523.48	29	T
437462.71	4120103.61	1515.33	29	T
437462.86	4120182.73	1513.83	29	T
437392.30	4119732.50	1521.74	29	B
437403.98	4119818.21	1520.79	29	B
437392.96	4119894.78	1520.58	29	B
437396.37	4119964.48	1516.81	29	B
437460.11	4120118.31	1511.89	29	B
437457.54	4120181.80	1508.39	29	B
437381.71	4119703.24	1526.22	29	R
437397.77	4119887.38	1527.62	30	L
437404.23	4119875.24	1526.71	30	T
437408.65	4119800.89	1527.48	30	T
437403.02	4119746.79	1527.33	30	T
437395.07	4119723.56	1527.41	30	T
437401.83	4119876.52	1525.58	30	B
437407.99	4119799.83	1525.49	30	B
437402.28	4119746.74	1524.49	30	B
437391.37	4119722.57	1524.35	30	B
437384.48	4119702.28	1528.17	30	R
437405.28	4119805.23	1530.07	31	L
437410.44	4119801.14	1529.61	31	T
437407.57	4119761.00	1530.72	31	T
437407.42	4119801.54	1528.41	31	B
437405.96	4119759.92	1527.72	31	B
437387.02	4119693.77	1529.02	31	R
437472.02	4120196.24	1519.80	32	L
437417.29	4119878.23	1534.81	32	T
437412.78	4119926.49	1535.97	32	T
437455.80	4120030.80	1529.19	32	T
437482.75	4120095.84	1524.77	32	T
437417.11	4119876.15	1532.71	32	B
437409.97	4119918.88	1529.38	32	B
437457.77	4120027.93	1524.60	32	B
437477.45	4120096.92	1523.32	32	B
437415.13	4119852.85	1534.71	32	R
437493.35	4120169.51	1531.82	33	L
437495.38	4120108.40	1532.34	33	T
437477.76	4120045.69	1536.14	33	T
437428.18	4119946.20	1538.23	33	T
437431.92	4119840.11	1543.31	33	T
437417.00	4119731.59	1545.74	33	T
437410.85	4119690.33	1546.88	33	T
437491.64	4120109.06	1529.57	33	B

Table G.1 continued

Easting	Northing	MSL	SS body	
437467.35	4120038.52	1530.37	33	B
437425.82	4119945.18	1533.76	33	B
436876.81	4119710.16	1478.33	33	B
437417.63	4119728.79	1540.99	33	B
436876.79	4119710.15	1478.38	33	B
437404.64	4119670.35	1546.42	33	R
437507.65	4120356.32	1521.24	34	L
437480.48	4120230.80	1527.10	34	T
437475.14	4120231.66	1517.15	34	B
437490.84	4120178.52	1529.17	34	R
437495.15	4120266.16	1533.93	35	L
437493.81	4120249.89	1534.21	35	T
437487.52	4120248.16	1532.42	35	B
437505.47	4120190.51	1534.99	35	R
437501.49	4120313.16	1529.71	36	L
437490.68	4120282.69	1531.41	36	R
437520.72	4120322.81	1538.37	37	L
437501.47	4120258.63	1540.85	37	T
437500.06	4120251.63	1536.05	37	B
437503.19	4120202.23	1535.34	37	R
437502.95	4120195.62	1535.97	38	L
437505.54	4120155.11	1538.97	38	T
437502.43	4120151.26	1535.88	38	B
437499.99	4120169.05	1532.47	38	R
437509.25	4120106.05	1538.51	39	L
437481.89	4120060.67	1535.82	39	T
437412.61	4119900.78	1536.09	39	T
437479.26	4120052.15	1529.21	39	B
437410.81	4119898.07	1531.88	39	B
437433.29	4119870.99	1550.06	39	R
437515.08	4120171.39	1543.98	40	L
437434.71	4119903.19	1549.77	40	T
437437.91	4119945.84	1548.73	40	T
437469.15	4119997.55	1544.09	40	T
437431.81	4119897.83	1545.09	40	B
437434.24	4119935.18	1543.65	40	B
437457.50	4119994.40	1541.77	40	B
437501.93	4120052.16	1545.15	40	R
437438.91	4119869.93	1552.72	41	L
437446.24	4119860.43	1552.78	41	T
437445.02	4119861.18	1552.67	41	B
437444.49	4119826.42	1555.57	41	R
437494.30	4120020.68	1548.64	42	L
437492.82	4120021.13	1548.40	42	T
437442.50	4119928.27	1550.65	42	T
437449.10	4119881.72	1556.97	42	T
437487.60	4120018.49	1546.66	42	B
437443.01	4119921.73	1549.32	42	B
437445.18	4119884.87	1555.56	42	B
437434.68	4119880.76	1553.17	42	R
437521.95	4120241.28	1548.70	43	L
437517.86	4120167.28	1549.86	43	T
437516.92	4120219.15	1545.48	43	T
437517.33	4120166.87	1545.70	43	B
437517.59	4120221.51	1545.66	43	B
437533.28	4120125.32	1551.91	43	R
437529.14	4120087.31	1553.72	44	L
437518.55	4120076.09	1554.56	44	T
437499.68	4120016.54	1557.33	44	T
437464.07	4119960.57	1560.03	44	T
437452.81	4119914.11	1560.86	44	T
437515.41	4120072.82	1547.66	44	B
437486.21	4120015.22	1553.47	44	B
437462.63	4119959.96	1556.43	44	B
437448.97	4119913.90	1558.19	44	B
437446.83	4119877.19	1561.87	44	R
437447.85	4119873.05	1563.08	45	L
437462.57	4119875.77	1563.94	45	T
437457.85	4119877.74	1563.35	45	B
437458.39	4119849.55	1563.55	45	R
437468.29	4119797.17	1576.27	46	L
437481.46	4119788.52	1577.15	46	T
437477.06	4119774.14	1577.27	46	T
437477.48	4119790.12	1575.47	46	B
437475.10	4119770.76	1572.58	46	B
437461.53	4119726.06	1577.06	46	R
437643.44	4120564.42	1560.93	47	L
437548.15	4120139.20	1566.29	47	T
437515.32	4120007.61	1572.35	47	T
437495.92	4119965.11	1576.08	47	T
437477.91	4119921.65	1575.88	47	T
437474.33	4119864.51	1574.99	47	T
437546.85	4120133.40	1558.86	47	B
437510.85	4120004.21	1567.94	47	B
437495.09	4119962.28	1567.45	47	B
437469.25	4119920.93	1571.21	47	B
437475.61	4119864.85	1572.99	47	B
437471.65	4119828.06	1575.11	47	R
437627.88	4120533.15	1556.22	48	L
437532.58	4120258.24	1560.66	48	T
437533.30	4120192.12	1561.07	48	T
437531.26	4120257.13	1557.50	48	B
437530.31	4120191.67	1557.94	48	B
437544.21	4120304.94	1553.01	48	R
437631.71	4120526.73	1561.98	49	L
437630.34	4120453.82	1562.52	49	R
437635.57	4120489.29	1568.44	50	L
437543.50	4120214.15	1569.09	50	T
437536.18	4120259.22	1567.01	50	T
437540.62	4120213.73	1564.43	50	B
437533.59	4120257.07	1560.61	50	B
437548.44	4120182.13	1568.34	50	R
437643.36	4120513.22	1573.98	51	L
437549.31	4120202.16	1573.29	51	T
437542.51	4120248.98	1572.82	51	T
437546.65	4120194.83	1568.10	51	B

Table G.1 continued

Easting	Northing	MSL	SS body	
437538.40	4120243.76	1567.62	51	B
437555.36	4120171.48	1571.97	51	R
437643.57	4120494.06	1575.54	52	L
437489.01	4119851.24	1587.05	52	T
437483.59	4119921.21	1587.20	52	T
437528.87	4120012.59	1584.69	52	T
437560.43	4120110.96	1577.19	52	T
437542.98	4120222.87	1578.68	52	T
437546.36	4120273.69	1576.57	52	T
437488.18	4119847.69	1584.51	52	B
437484.65	4119920.40	1582.74	52	B
437527.04	4120015.89	1579.51	52	B
437554.80	4120115.63	1572.65	52	B
437543.17	4120226.77	1574.48	52	B
437544.12	4120273.83	1573.31	52	B
437484.10	4119797.40	1587.78	52	R
437559.09	4120124.11	1571.02	53	L
437555.63	4120116.13	1572.86	53	T
437542.89	4120053.65	1574.61	53	T
437552.08	4120118.79	1569.90	53	B
437538.91	4120048.67	1572.53	53	B
437539.07	4120022.08	1572.88	53	R
437469.24	4119877.40	1578.36	54	L
437474.88	4119890.51	1578.60	54	T
437478.24	4119878.99	1578.62	54	T
437471.26	4119889.44	1576.90	54	B
437475.19	4119877.02	1574.76	54	B
437473.95	4119854.45	1579.48	54	R
437499.09	4119941.47	1578.17	55	L
437491.58	4119783.24	1587.78	55	T
437490.11	4119832.52	1586.58	55	T
437476.53	4119896.77	1582.53	55	T
437489.57	4119783.01	1581.82	55	B
437484.26	4119830.23	1581.08	55	B
437475.78	4119897.66	1579.09	55	B
437469.60	4119732.95	1586.33	55	R
437477.38	4119880.31	1589.82	56	L
437487.87	4119844.29	1591.17	56	T
437484.29	4119871.57	1591.71	56	T
437488.16	4119841.00	1587.72	56	B
437484.27	4119869.31	1589.35	56	B
437481.60	4119808.23	1590.21	56	R
437478.00	4119847.50	1591.47	57	L
437503.13	4119809.16	1594.96	57	T
437489.44	4119844.62	1593.66	57	T
437501.41	4119809.97	1592.35	57	B
437489.29	4119843.46	1590.24	57	B
437491.66	4119770.84	1594.31	57	R
437519.24	4119954.41	1590.01	58	L
437485.91	4119859.55	1599.34	58	T
437479.68	4119898.87	1596.75	58	T
437501.27	4119949.68	1594.06	58	T
437486.52	4119859.70	1596.05	58	B
437478.92	4119897.50	1591.96	58	B
437502.01	4119943.72	1584.21	58	B
437484.68	4119811.88	1595.28	58	R
437558.11	4120228.18	1583.91	59	L
437481.61	4119901.85	1598.41	59	T
437575.27	4120147.97	1588.46	59	T
437554.33	4120252.61	1586.59	59	T
437484.02	4119901.39	1597.63	59	B
437570.59	4120150.14	1586.66	59	B
437554.62	4120252.83	1583.61	59	B
437478.91	4119836.86	1598.53	59	R
437580.24	4120117.38	1592.38	60	L
437482.40	4119898.59	1599.47	60	T
437485.34	4119871.87	1602.01	60	T
437484.48	4119899.23	1598.73	60	B
437486.22	4119870.98	1598.72	60	B
437478.84	4119825.29	1599.32	60	R
437482.54	4119881.20	1602.70	61	L
437481.22	4119891.36	1605.69	61	T
437488.97	4119858.12	1606.58	61	T
437492.84	4119842.05	1605.47	61	T
437507.90	4119798.65	1604.64	61	T
437487.89	4119723.75	1607.28	61	T
437479.01	4119889.55	1598.31	61	B
437487.65	4119858.92	1601.78	61	B
437493.09	4119844.36	1596.46	61	B
437506.96	4119797.38	1599.82	61	B
437488.30	4119724.88	1605.13	61	B
437461.32	4119659.12	1607.76	61	R
437476.29	4119863.43	1606.29	62	L
437491.12	4119856.32	1608.00	62	T
437505.90	4119815.25	1607.09	62	T
437488.45	4119856.86	1605.26	62	B
437500.31	4119818.80	1606.11	62	B
437489.56	4119743.93	1606.87	62	R
437487.91	4119743.70	1599.65	63	L
437492.14	4119732.56	1604.79	63	T
437481.59	4119652.76	1605.34	63	T
437472.24	4119615.61	1607.67	63	T
437490.99	4119734.63	1600.11	63	B
437480.49	4119654.99	1601.75	63	B
437473.05	4119612.27	1601.33	63	B
437447.33	4119539.84	1602.02	63	R
437166.97	4119675.58	1453.36	64	L
437183.81	4119668.57	1454.46	64	T
437184.55	4119667.40	1453.29	64	B
437163.66	4119646.25	1454.39	64	R
437219.75	4119693.95	1456.02	65	L
437238.87	4119710.13	1456.16	65	T
437236.83	4119709.49	1455.63	65	B
437222.56	4119676.98	1455.32	65	R
437272.00	4119723.66	1468.98	66	L
437280.79	4119732.72	1469.86	66	T

Table G.1 continued

Easting	Northing	MSL	SS body	
437422.08	4119695.86	1563.21	82	L
437443.76	4119694.05	1564.15	82	T
437437.38	4119639.07	1564.83	82	T
437427.00	4119577.72	1565.95	82	T
437436.30	4119694.25	1560.04	82	B
437432.91	4119639.61	1561.14	82	B
437423.37	4119580.62	1560.30	82	B
437358.46	4119453.85	1566.84	82	R
437416.67	4119604.91	1571.30	83	L
437440.33	4119617.62	1571.93	83	T
437431.13	4119547.77	1575.04	83	T
437439.00	4119619.85	1569.61	83	B
437426.33	4119546.02	1569.20	83	B
437384.36	4119481.50	1575.68	83	R
437456.43	4119711.49	1581.29	84	L
437474.01	4119733.88	1582.68	84	T
437461.63	4119686.40	1583.76	84	T
437460.64	4119638.24	1584.29	84	T
437472.80	4119732.81	1578.22	84	B
437462.07	4119688.45	1581.70	84	B
437459.67	4119639.36	1578.83	84	B
437403.81	4119502.88	1585.86	84	R
437464.78	4119737.37	1582.18	85	L
437483.15	4119754.29	1587.66	85	L
437478.90	4119740.31	1587.83	85	T
437473.52	4119718.16	1587.79	85	T
437463.91	4119687.29	1588.21	85	T
437463.54	4119661.61	1587.35	85	T
437462.51	4119643.12	1588.57	85	T
437456.23	4119596.18	1588.76	85	T
437453.79	4119567.11	1589.52	85	T
437453.03	4119540.32	1588.54	85	T
437450.69	4119523.46	1590.14	85	T
437442.30	4119508.57	1590.67	85	T
437432.74	4119477.40	1594.39	85	T
437420.34	4119457.64	1595.91	85	T
437401.48	4119433.29	1595.80	85	T
437395.39	4119401.97	1596.67	85	T
437397.81	4119370.21	1599.26	85	T
437399.26	4119334.41	1598.75	85	T
437400.29	4119297.86	1601.81	85	T
437399.58	4119267.97	1601.50	85	T
437408.69	4119224.04	1605.33	85	T
437412.84	4119188.42	1604.84	85	T
437410.03	4119157.47	1606.82	85	T
437401.87	4119140.61	1609.35	85	T
437410.75	4119120.70	1607.08	85	T
437401.28	4119144.98	1607.50	85	T
437399.01	4119294.21	1600.95	85	T
437411.98	4119445.21	1596.65	85	T
437454.60	4119594.36	1589.74	85	T
437464.36	4119676.98	1588.46	85	T
437482.83	4119746.88	1586.47	85	T

Easting	Northing	MSL	SS body	
437403.22	4119093.14	1603.82	85	B
437405.69	4119140.41	1605.57	85	B
437410.46	4119162.67	1603.49	85	B
437408.61	4119197.80	1601.90	85	B
437407.54	4119224.98	1602.54	85	B
437396.63	4119252.96	1599.16	85	B
437401.36	4119296.87	1599.71	85	B
437394.85	4119331.95	1593.73	85	B
437394.62	4119361.80	1593.98	85	B
437392.15	4119405.02	1592.57	85	B
437400.44	4119431.41	1590.43	85	B
437413.03	4119448.28	1587.87	85	B
437421.97	4119461.26	1590.42	85	B
437436.29	4119491.61	1588.53	85	B
437440.98	4119512.18	1586.93	85	B
437449.14	4119529.30	1585.20	85	B
437445.77	4119539.05	1585.19	85	B
437451.87	4119569.55	1585.87	85	B
437451.78	4119590.68	1583.94	85	B
437454.50	4119616.21	1583.58	85	B
437458.65	4119638.34	1583.76	85	B
437464.17	4119663.56	1584.30	85	B
437467.14	4119703.62	1583.45	85	B
437473.11	4119730.60	1582.41	85	B
437476.72	4119742.27	1582.03	85	B
437477.22	4119752.82	1581.15	85	B
437482.16	4119767.02	1581.10	85	B
437484.30	4119773.62	1582.66	85	B
437487.32	4119769.64	1585.29	85	B
437484.35	4119760.77	1583.60	85	B
437482.11	4119759.51	1585.37	85	B
437402.44	4119145.73	1606.15	85	B
437395.74	4119293.85	1596.94	85	B
437409.96	4119445.05	1589.83	85	B
437454.35	4119592.33	1583.35	85	B
437464.19	4119678.00	1584.18	85	B
437477.61	4119747.63	1581.24	85	B
437337.61	4119260.75	1601.80	85	R
437408.35	4119089.33	1609.20	85	R
437420.25	4119565.30	1589.97	86	L
437381.92	4119440.03	1593.55	86	R
437134.91	4119921.10	1447.96	87	L
437130.01	4119911.25	1448.30	87	T
437117.09	4119893.59	1448.68	87	T
437129.00	4119881.95	1445.18	87	B
437114.25	4119896.74	1445.54	87	B
437120.56	4119907.98	1444.25	87	B
437128.97	4119918.49	1445.14	87	B
437125.50	4119871.42	1449.78	87	R
437094.10	4119844.10	1442.49	88	L
437087.57	4119816.84	1443.51	88	T
437066.72	4119789.76	1443.91	88	T
437071.39	4119771.32	1444.23	88	T

Table G.1 continued

Easting	Northing	MSL	SS body	
437070.10	4119770.18	1441.26	88	B
437064.80	4119782.13	1440.74	88	B
437075.64	4119805.65	1440.70	88	B
437088.45	4119831.14	1440.21	88	B
437092.40	4119840.50	1440.70	88	B
437087.31	4119759.34	1443.38	88	R
437079.27	4119771.03	1444.85	89	L
437085.91	4119764.72	1444.47	89	T
437087.65	4119761.66	1443.94	89	B
437085.63	4119765.44	1444.50	89	B
437088.05	4119760.21	1444.32	89	R
437095.70	4119763.20	1449.44	90	L
437092.66	4119752.57	1450.14	90	T
437092.00	4119737.77	1450.13	90	T
437080.64	4119770.24	1444.64	90	B
437088.26	4119722.00	1448.93	90	B
437088.42	4119730.19	1447.31	90	B
437089.16	4119740.05	1446.27	90	B
437093.76	4119755.93	1447.96	90	B
437094.27	4119762.83	1448.06	90	B
437088.99	4119720.95	1449.58	90	R
437092.91	4119767.68	1447.30	91	L
437092.33	4119763.10	1447.53	91	T
437092.49	4119760.80	1446.78	91	B
437092.46	4119765.60	1447.40	91	B
437092.94	4119759.28	1447.57	91	R
437087.19	4119721.20	1447.94	92	L
437083.73	4119711.61	1449.19	92	T
437079.14	4119703.09	1448.00	92	B
437082.76	4119711.61	1447.85	92	B
437084.42	4119717.46	1447.57	92	B
437079.01	4119703.10	1449.49	92	R
437081.94	4119719.92	1445.33	93	L
437078.07	4119711.96	1445.63	93	T
437076.01	4119703.95	1445.95	93	T
437075.60	4119697.71	1445.24	93	B
437075.79	4119704.32	1445.26	93	B
437078.33	4119712.35	1444.85	93	B
437075.10	4119697.39	1446.05	93	R
437074.47	4119709.90	1443.69	94	L
437073.17	4119701.00	1443.88	94	T
437072.80	4119692.39	1442.76	94	B
437072.57	4119696.87	1442.89	94	B
437072.43	4119706.11	1442.66	94	B
437073.52	4119709.52	1442.82	94	B
437072.99	4119692.75	1444.18	94	R
437068.22	4119695.14	1439.84	95	L
437055.36	4119641.61	1440.50	95	L
437067.02	4119688.53	1440.66	95	T
437064.24	4119680.47	1440.95	95	T
437057.95	4119627.63	1440.74	95	T
437062.46	4119614.38	1439.98	95	T
437055.53	4119610.32	1441.46	95	T

Easting	Northing	MSL	SS body	
437050.54	4119605.41	1441.83	95	T
437044.06	4119596.99	1442.75	95	T
437038.40	4119591.13	1442.60	95	T
437038.93	4119588.09	1442.55	95	T
437032.44	4119582.43	1443.18	95	T
437024.37	4119574.11	1442.92	95	T
437020.90	4119562.66	1440.09	95	T
437015.05	4119551.31	1441.18	95	T
437012.57	4119539.70	1441.81	95	T
437014.17	4119522.76	1441.87	95	T
437060.34	4119671.44	1437.61	95	B
437065.15	4119685.99	1437.11	95	B
437066.23	4119696.23	1437.45	95	B
437066.23	4119699.93	1437.87	95	B
437013.66	4119508.40	1437.46	95	B
437014.34	4119522.58	1437.23	95	B
437011.90	4119543.60	1438.14	95	B
437021.36	4119577.35	1439.10	95	B
437033.29	4119583.54	1439.24	95	B
437044.82	4119596.48	1438.58	95	B
437058.49	4119611.58	1438.22	95	B
437057.09	4119630.69	1438.32	95	B
437053.38	4119640.29	1438.41	95	B
437054.23	4119644.57	1438.91	95	B
437063.24	4119675.24	1440.96	95	R
437013.27	4119509.72	1442.01	95	R
437012.55	4119571.68	1437.40	95	B
437087.70	4119709.47	1449.72	96	L
437109.49	4119702.50	1447.62	96	T
437125.14	4119695.93	1445.93	96	T
437140.56	4119688.11	1444.37	96	B
437135.84	4119691.25	1445.02	96	B
437127.95	4119694.89	1444.72	96	B
437109.41	4119702.92	1446.82	96	B
437084.69	4119708.01	1449.84	96	B
437143.54	4119687.39	1444.44	96	R
437127.92	4119739.32	1455.78	97	L
437136.37	4119735.24	1455.06	97	T
437134.19	4119734.60	1454.78	97	B
437128.93	4119738.97	1455.20	97	B
437148.57	4119733.57	1454.45	97	R
437196.85	4119685.68	1454.77	98	L
437188.67	4119683.57	1455.38	98	T
437188.35	4119680.87	1454.30	98	B
437189.75	4119685.67	1454.26	98	B
437188.83	4119675.31	1454.75	98	R
437323.37	4119642.11	1488.68	99	L
437312.03	4119634.47	1488.46	99	T
437311.99	4119623.48	1490.03	99	T
437306.62	4119604.09	1491.56	99	T
437308.12	4119590.04	1490.92	99	T
437298.14	4119580.86	1490.74	99	B
437305.98	4119589.86	1490.89	99	B

Table G.1 continued

Easting	Northing	MSL	SS body	
437304.32	4119603.10	1489.98	99	B
437312.18	4119619.54	1490.08	99	B
437306.70	4119627.68	1489.13	99	B
437319.84	4119638.71	1487.85	99	B
437323.62	4119643.70	1487.91	99	B
437299.28	4119581.31	1492.29	99	R
437260.01	4119644.20	1473.69	100	L
437251.93	4119638.82	1473.67	100	T
437253.14	4119634.52	1473.65	100	T
437250.89	4119633.62	1472.37	100	B
437252.17	4119640.14	1473.04	100	B
437261.81	4119627.17	1472.89	100	R
437255.51	4119654.48	1469.71	101	L
437241.37	4119648.02	1470.65	101	T
437224.28	4119643.39	1471.01	101	T
437228.81	4119635.50	1471.50	101	T
437229.78	4119630.81	1470.18	101	B
437225.28	4119633.75	1469.67	101	B
437221.90	4119642.03	1469.80	101	B
437238.13	4119647.32	1470.09	101	B
437251.95	4119624.42	1470.33	101	R
437225.94	4119653.15	1469.77	102	L
437217.33	4119644.73	1469.31	102	T
437217.96	4119642.76	1469.25	102	T
437227.66	4119630.62	1468.94	102	T
437255.34	4119617.40	1467.48	102	T
437248.03	4119605.34	1467.61	102	T
437243.22	4119596.26	1466.32	102	B
437247.01	4119605.62	1465.60	102	B
437228.75	4119631.02	1467.66	102	B
437216.11	4119643.75	1468.70	102	B
437217.20	4119649.71	1468.10	102	B
437242.81	4119591.47	1468.34	102	R
437213.17	4119656.46	1465.29	103	L
437205.55	4119647.60	1465.51	103	T
437207.30	4119636.44	1464.76	103	T
437223.10	4119625.25	1462.76	103	B
437205.45	4119633.23	1462.38	103	B
437203.66	4119643.80	1462.53	103	B
437204.20	4119651.99	1463.15	103	B
437207.62	4119653.79	1464.20	103	B
437226.04	4119624.54	1463.28	103	R
437201.62	4119639.52	1460.31	104	L
437203.43	4119629.53	1460.70	104	T
437208.29	4119620.95	1457.97	104	B
437200.12	4119629.20	1458.54	104	B
437199.82	4119636.45	1459.23	104	B
437206.95	4119623.14	1460.46	104	R
437127.85	4119667.90	1452.44	105	L
437117.11	4119658.77	1454.20	105	T
437115.93	4119638.10	1453.78	105	T
437115.27	4119636.05	1453.33	105	B
437114.29	4119657.63	1453.12	105	B
437117.76	4119630.64	1453.37	105	R
437111.60	4119670.96	1448.62	106	L
437106.05	4119667.76	1449.68	106	T
437106.04	4119668.18	1448.87	106	B
437104.28	4119663.97	1449.40	106	R
437099.09	4119664.99	1447.62	107	L
437091.58	4119654.62	1447.91	107	T
437080.68	4119645.47	1448.61	107	T
437089.48	4119633.58	1448.12	107	T
437086.31	4119628.04	1448.65	107	T
437081.41	4119620.34	1448.88	107	T
437084.04	4119607.74	1449.10	107	T
437086.30	4119595.03	1448.55	107	T
437082.97	4119584.87	1449.13	107	T
437074.39	4119573.38	1449.66	107	T
437061.61	4119561.07	1450.86	107	T
437064.13	4119547.93	1450.55	107	T
437065.05	4119535.89	1450.04	107	T
437068.31	4119525.33	1449.93	107	T
437070.81	4119517.63	1447.72	107	B
437065.02	4119530.39	1448.27	107	B
437062.53	4119551.59	1448.83	107	B
437060.25	4119568.41	1449.11	107	B
437080.11	4119584.65	1447.35	107	B
437086.73	4119600.46	1447.17	107	B
437080.26	4119619.19	1448.22	107	B
437085.17	4119630.22	1446.99	107	B
437080.19	4119646.08	1448.40	107	B
437097.72	4119664.08	1447.04	107	B
437072.39	4119516.06	1449.44	107	R
437094.55	4119670.64	1444.85	108	L
437092.72	4119661.56	1444.88	108	T
437074.38	4119647.15	1446.26	108	T
437079.75	4119637.95	1446.60	108	T
437075.45	4119623.82	1446.85	108	T
437076.17	4119614.26	1446.64	108	T
437075.82	4119608.83	1445.15	108	B
437073.79	4119620.44	1445.79	108	B
437080.36	4119629.23	1445.02	108	B
437079.36	4119636.92	1445.56	108	B
437073.59	4119646.70	1445.40	108	B
437088.69	4119659.40	1444.76	108	B
437093.49	4119664.22	1443.41	108	B
437094.36	4119670.33	1443.87	108	B
437075.37	4119609.49	1446.46	108	R
437072.80	4119607.76	1443.09	109	L
437066.30	4119604.32	1442.94	109	T
437054.74	4119610.36	1443.63	109	T
437049.22	4119602.89	1443.78	109	T
437040.04	4119592.49	1444.82	109	T
437031.97	4119581.88	1445.15	109	T
437031.79	4119570.73	1445.44	109	T
437052.05	4119554.15	1444.66	109	T

Table G.1 continued

Easting	Northing	MSL	SS body	
437051.95	4119552.58	1444.49	109	B
437027.05	4119574.95	1443.89	109	B
437029.91	4119579.90	1443.35	109	B
437039.11	4119588.35	1442.65	109	B
437044.56	4119597.88	1442.46	109	B
437051.50	4119606.85	1441.91	109	B
437055.90	4119609.65	1441.86	109	B
437071.84	4119603.84	1442.03	109	B
437072.69	4119606.46	1442.10	109	B
437054.12	4119548.91	1444.79	109	R
437097.65	4119637.62	1451.11	111	L
437095.36	4119625.05	1451.71	111	T
437095.23	4119611.66	1452.00	111	T
437097.02	4119603.40	1452.72	111	T
437097.39	4119593.05	1452.62	111	T
437095.32	4119587.23	1452.48	111	B
437095.51	4119598.40	1451.70	111	B
437094.63	4119605.95	1450.87	111	B
437092.04	4119617.19	1451.23	111	B
437095.92	4119629.72	1450.93	111	B
437099.64	4119634.47	1450.28	111	B
437094.67	4119584.05	1452.38	111	R
437108.63	4119596.80	1456.23	112	L
437100.21	4119577.19	1455.17	112	T
437102.24	4119552.56	1455.26	112	T
437092.09	4119550.52	1455.37	112	B
437097.43	4119553.02	1453.71	112	B
437094.91	4119565.47	1452.68	112	B
437094.55	4119572.20	1453.50	112	B
437096.44	4119578.43	1454.12	112	B
437105.01	4119592.09	1455.39	112	B
437105.97	4119596.15	1455.46	112	B
437085.90	4119548.81	1456.17	112	R
437115.77	4119592.82	1458.28	113	L
437111.30	4119579.91	1458.58	113	T
437112.89	4119568.58	1459.02	113	T
437115.75	4119561.72	1459.09	113	T
437113.21	4119563.31	1459.29	113	B
437110.92	4119569.23	1458.64	113	B
437111.05	4119579.55	1458.06	113	B
437112.76	4119585.52	1457.71	113	B
437121.53	4119548.49	1458.82	113	R
437143.27	4119613.49	1461.90	114	L
437138.32	4119605.87	1463.48	114	T
437134.54	4119590.31	1463.85	114	T
437134.44	4119575.83	1464.07	114	T
437133.43	4119567.71	1463.44	114	B
437134.44	4119575.85	1464.12	114	B
437133.50	4119589.74	1463.95	114	B
437135.84	4119597.37	1463.51	114	B
437137.51	4119609.40	1462.67	114	B
437143.99	4119615.37	1461.95	114	B
437135.81	4119565.78	1463.80	114	R

Easting	Northing	MSL	SS body	
437142.84	4119538.50	1463.39	115	L
437140.14	4119534.32	1464.49	115	T
437139.21	4119532.95	1464.53	115	T
437136.11	4119530.35	1462.94	115	B
437138.78	4119534.52	1464.04	115	B
437141.13	4119539.56	1463.52	115	B
437135.85	4119529.87	1464.04	115	R
437261.49	4119587.08	1481.17	116	L
437256.25	4119580.65	1481.16	116	T
437253.96	4119576.99	1480.46	116	B
437255.57	4119581.60	1479.77	116	B
437258.06	4119585.90	1479.76	116	B
437253.26	4119575.01	1479.77	116	R
437253.20	4119580.91	1479.02	117	L
437247.37	4119562.30	1478.32	117	T
437247.90	4119553.02	1478.98	117	T
437249.24	4119548.58	1478.28	117	B
437248.13	4119564.23	1478.28	117	B
437250.41	4119573.04	1478.29	117	B
437251.81	4119579.92	1479.00	117	B
437249.26	4119548.60	1479.70	117	R
437193.99	4119559.86	1480.17	118	L
437193.75	4119552.45	1479.57	118	T
437200.42	4119539.15	1480.24	118	T
437201.82	4119533.31	1479.63	118	B
437197.18	4119541.61	1478.97	118	B
437193.54	4119549.78	1478.96	118	B
437193.22	4119558.17	1477.73	118	B
437203.76	4119528.54	1481.59	118	R
437199.24	4119526.59	1479.57	119	L
437197.77	4119516.15	1479.49	119	T
437195.24	4119504.53	1480.15	119	T
437201.34	4119486.68	1480.88	119	T
437199.33	4119468.42	1481.67	119	T
437193.48	4119455.98	1482.41	119	T
437182.06	4119431.91	1483.95	119	T
437172.53	4119411.82	1482.60	119	T
437177.50	4119391.61	1482.82	119	T
437208.45	4119335.97	1485.20	119	T
437176.15	4119313.53	1484.49	119	B
437179.93	4119322.79	1485.30	119	B
437189.21	4119326.37	1484.52	119	B
437201.09	4119329.74	1484.58	119	B
437203.71	4119339.91	1482.75	119	B
437177.20	4119387.33	1480.71	119	B
437171.84	4119415.49	1479.11	119	B
437179.98	4119432.68	1479.77	119	B
437182.24	4119441.19	1478.34	119	B
437196.07	4119461.02	1479.02	119	B
437198.39	4119468.99	1478.99	119	B
437198.78	4119486.63	1479.69	119	B
437193.11	4119497.87	1478.32	119	B
437192.93	4119506.70	1477.69	119	B

Table G.1 continued

Easting	Northing	MSL	SS body	
437194.20	4119518.20	1477.06	119	B
437196.65	4119524.27	1477.73	119	B
437178.57	4119310.30	1487.16	119	R
437280.10	4119540.14	1492.13	120	L
437279.44	4119531.20	1493.77	120	T
437272.96	4119526.52	1493.64	120	B
437277.33	4119531.25	1492.94	120	B
437279.50	4119536.14	1492.18	120	B
437272.25	4119522.64	1493.66	120	R
437239.98	4119520.58	1492.65	121	L
437230.33	4119515.31	1492.41	121	T
437228.22	4119511.66	1493.80	121	T
437223.16	4119504.82	1492.39	121	B
437226.19	4119512.00	1491.66	121	B
437231.33	4119517.15	1492.42	121	B
437231.51	4119519.45	1490.96	121	B
437235.16	4119519.86	1491.05	121	B
437224.13	4119502.58	1493.15	121	R
437216.32	4119504.80	1490.06	122	L
437216.47	4119488.17	1491.06	122	T
437220.83	4119471.37	1491.49	122	T
437219.19	4119468.97	1490.78	122	B
437220.45	4119479.60	1489.21	122	B
437215.28	4119503.04	1489.46	122	B
437215.50	4119505.35	1489.41	122	B
437221.49	4119461.90	1491.69	122	R
437310.23	4119466.41	1529.72	123	L
437303.34	4119454.37	1528.92	123	T
437299.89	4119443.21	1530.08	123	T
437299.71	4119426.53	1531.01	123	T
437294.28	4119411.86	1532.30	123	T
437293.50	4119380.56	1531.39	123	T
437291.74	4119391.27	1530.54	123	B
437291.17	4119408.59	1528.57	123	B
437296.42	4119437.14	1526.53	123	B
437299.58	4119449.58	1526.12	123	B
437305.81	4119461.96	1526.01	123	B
437310.43	4119468.28	1526.94	123	B
437294.47	4119378.61	1531.55	123	R
437289.88	4119404.96	1527.70	124	L
437292.93	4119395.88	1529.42	124	T
437291.88	4119381.61	1531.13	124	T
437297.03	4119365.49	1530.60	124	T
437294.95	4119365.94	1529.45	124	B
437290.78	4119376.60	1528.47	124	B
437289.68	4119388.04	1527.72	124	B
437291.70	4119395.69	1528.35	124	B
437298.82	4119361.54	1531.97	124	R
437317.76	4119423.16	1541.92	125	L
437313.95	4119406.85	1542.65	125	T
437313.17	4119390.15	1542.78	125	T
437313.74	4119379.10	1542.64	125	T
437314.65	4119368.70	1542.51	125	T
437305.70	4119374.55	1538.43	125	B
437309.61	4119388.22	1539.76	125	B
437310.14	4119402.84	1540.71	125	B
437314.08	4119410.23	1540.59	125	B
437314.32	4119417.84	1541.02	125	B
437320.67	4119361.56	1541.61	125	R
437422.00	4119521.89	1568.66	126	L
437407.87	4119491.74	1572.31	126	T
437392.17	4119465.93	1571.67	126	T
437376.59	4119438.17	1573.52	126	T
437362.16	4119405.05	1572.17	126	T
437364.91	4119376.53	1574.07	126	T
437370.61	4119346.72	1576.53	126	T
437369.61	4119307.53	1576.83	126	T
437371.88	4119285.11	1577.01	126	T
437372.73	4119273.75	1577.02	126	T
437374.18	4119259.98	1576.16	126	T
437373.88	4119252.31	1576.87	126	T
437375.55	4119241.05	1578.17	126	T
437376.44	4119233.60	1580.26	126	T
437379.39	4119204.98	1580.96	126	T
437379.62	4119192.29	1579.66	126	B
437375.86	4119220.66	1576.52	126	B
437369.57	4119249.92	1573.06	126	B
437370.53	4119293.71	1573.71	126	B
437368.62	4119321.04	1570.95	126	B
437364.38	4119364.28	1570.89	126	B
437362.45	4119384.42	1569.90	126	B
437363.40	4119404.32	1569.35	126	B
437372.09	4119440.67	1567.65	126	B
437388.62	4119463.30	1565.30	126	B
437403.03	4119488.43	1566.76	126	B
437411.60	4119500.02	1563.20	126	B
437415.18	4119518.94	1564.76	126	B
437383.75	4119184.39	1583.45	126	R
437361.01	4119411.71	1568.29	127	L
437363.47	4119400.75	1569.54	127	T
437359.93	4119382.48	1569.63	127	T
437361.95	4119366.03	1570.29	127	T
437364.43	4119348.67	1570.01	127	T
437365.75	4119335.65	1571.37	127	T
437367.02	4119309.65	1571.71	127	T
437368.11	4119300.12	1572.73	127	T
437367.64	4119294.69	1572.03	127	B
437366.17	4119314.67	1570.01	127	B
437365.51	4119323.62	1570.24	127	B
437366.77	4119341.75	1569.84	127	B
437363.34	4119358.76	1567.92	127	B
437360.89	4119373.22	1569.53	127	B
437361.42	4119391.35	1566.97	127	B
437355.74	4119408.07	1564.84	127	B
437367.66	4119293.19	1572.18	127	R
437352.78	4119411.13	1565.22	128	L

Table G.1 continued

Easting	Northing	MSL	SS body	
437360.44	4119392.04	1567.85	128	T
437358.57	4119374.85	1568.03	128	T
437361.16	4119357.75	1568.78	128	T
437365.31	4119341.50	1569.62	128	T
437365.17	4119328.07	1569.70	128	T
437363.66	4119319.56	1569.22	128	T
437365.32	4119313.99	1571.03	128	T
437363.97	4119297.93	1570.10	128	T
436876.71	4119710.05	1478.09	128	B
437366.30	4119316.03	1567.58	128	B
437362.17	4119339.87	1566.12	128	B
437358.81	4119386.98	1564.88	128	B
437361.58	4119400.84	1566.12	128	B
437353.05	4119413.25	1564.02	128	B
437365.54	4119293.68	1570.66	128	R
437373.01	4119303.47	1580.91	129	L
437372.73	4119272.39	1582.94	129	T
437373.76	4119252.59	1583.96	129	T
437379.74	4119237.25	1586.30	129	T
437376.08	4119224.03	1583.60	129	T
437381.32	4119197.92	1584.36	129	T
437383.29	4119186.80	1583.17	129	B
437381.52	4119204.74	1582.41	129	B
437378.30	4119228.57	1580.92	129	B
437372.72	4119235.59	1579.60	129	B
437372.23	4119239.35	1579.14	129	B
437369.88	4119246.48	1575.75	129	B
437372.60	4119258.38	1576.07	129	B
437372.54	4119270.94	1578.41	129	B
437369.64	4119282.64	1576.91	129	B
437369.84	4119300.24	1577.52	129	B
437383.48	4119184.81	1585.95	129	R
437405.73	4119190.76	1598.89	130	L
437405.03	4119157.19	1605.04	130	T
437407.45	4119110.10	1603.70	130	T
437408.45	4119085.52	1603.21	130	B
437405.88	4119155.71	1599.49	130	B
437409.14	4119085.37	1604.82	130	R
437389.36	4119166.97	1589.16	131	L
437383.06	4119155.23	1589.65	131	T
437380.45	4119154.15	1586.45	131	B
437380.44	4119139.10	1588.14	131	R
437384.37	4119167.44	1582.66	132	L
437380.45	4119150.02	1583.69	132	T
437378.74	4119150.20	1582.01	132	B
437378.50	4119133.87	1583.71	132	R
437377.40	4119239.46	1575.53	133	L
437379.79	4119193.61	1578.89	133	T
437377.78	4119120.28	1582.58	133	T
437379.22	4119197.71	1577.41	133	B
437377.04	4119120.37	1581.08	133	B
437373.75	4119057.03	1583.88	133	R
437344.59	4119322.06	1551.33	134	L
437344.81	4119316.85	1553.92	134	T
437343.86	4119318.07	1552.51	134	B
437342.64	4119221.31	1557.05	134	R
437334.99	4119308.08	1551.26	135	L
437335.78	4119297.91	1552.57	135	T
437336.37	4119296.70	1548.71	135	B
437339.86	4119282.84	1552.94	135	R
437331.94	4119287.45	1549.32	136	L
437339.34	4119277.73	1551.49	136	T
437336.55	4119277.56	1549.83	136	B
437334.91	4119263.46	1552.07	136	R
437327.48	4119308.63	1546.38	137	L
437328.60	4119283.41	1546.24	137	T
437331.97	4119282.37	1544.07	137	B
437327.60	4119260.67	1547.23	137	R
437303.31	4119324.68	1529.85	138	L
437303.37	4119314.83	1531.00	138	T
437298.46	4119315.52	1529.24	138	B
437303.58	4119294.03	1529.56	138	R
437277.49	4119309.49	1523.35	139	L
437278.81	4119298.94	1520.96	139	T
437277.83	4119299.99	1519.69	139	B
437285.29	4119293.53	1521.52	139	R
437235.18	4119397.82	1509.22	140	L
437234.65	4119388.35	1506.71	140	T
437229.87	4119390.64	1507.50	140	B
437233.86	4119386.96	1507.72	140	R
437228.32	4119400.63	1507.50	141	L
437228.44	4119392.63	1506.13	141	T
437226.22	4119393.26	1505.97	141	B
437229.60	4119383.74	1506.06	141	R
437229.16	4119402.13	1505.29	142	L
437226.31	4119393.30	1504.87	142	T
437223.08	4119390.20	1503.45	142	B
437230.69	4119379.43	1504.98	142	R
437201.73	4119409.33	1496.79	143	L
437209.44	4119384.50	1496.90	143	T
436607.24	4119235.76	1453.52	143	B
437224.89	4119371.21	1496.66	143	R
437219.12	4119366.62	1490.75	144	L
437217.74	4119335.41	1492.48	144	T
437192.12	4119316.60	1493.77	144	T
437218.72	4119336.68	1489.26	144	B
437187.65	4119313.90	1490.37	144	B
437192.29	4119289.72	1492.55	144	R
437186.76	4119321.05	1489.36	145	L
437185.23	4119309.56	1490.19	145	T
437183.61	4119307.30	1488.00	145	B
437188.59	4119297.67	1490.27	145	R
437169.22	4119332.58	1478.35	146	L
437170.24	4119284.74	1481.12	146	T
437165.80	4119259.90	1481.81	146	T
437171.27	4119238.52	1483.04	146	T

Table G.1 continued

Easting	Northing	MSL	SS body	
437167.17	4119286.48	1479.00	146	B
437161.82	4119260.71	1480.64	146	B
437193.23	4119201.74	1484.19	147	L
437213.77	4119194.19	1485.31	147	T
437204.92	4119194.79	1482.74	147	B
437199.96	4119197.19	1484.51	147	B
437214.32	4119187.71	1485.30	147	R
437189.80	4119244.67	1491.07	148	L
437206.27	4119208.28	1491.17	148	T
437217.71	4119197.11	1490.89	148	T
437201.45	4119212.69	1490.87	148	B
437216.78	4119198.22	1490.83	148	B
437229.47	4119179.98	1490.56	148	R
437238.29	4119354.71	1499.44	149	L
437240.30	4119322.19	1502.57	149	T
437211.43	4119302.18	1502.29	149	T
437213.64	4119249.33	1505.38	149	T
437240.31	4119195.70	1508.89	149	T
437217.74	4119319.11	1498.65	149	B
437207.22	4119303.87	1501.96	149	B
437210.74	4119249.26	1504.07	149	B
437237.54	4119195.88	1506.42	149	B
437250.48	4119147.39	1510.17	149	R
437370.37	4119054.98	1581.98	150	L
437371.12	4119033.57	1582.93	150	T
437367.11	4119036.02	1579.38	150	B
437369.20	4119018.30	1581.87	150	R
437324.28	4119063.30	1563.70	151	L
437320.02	4119051.08	1564.89	151	T
437318.93	4119050.03	1563.45	151	B
437315.47	4119041.67	1564.58	151	R
437324.98	4119078.94	1555.49	152	L
437316.83	4119066.40	1556.08	152	T
437305.20	4119043.19	1559.14	152	T
437314.87	4119069.46	1553.13	152	B
437301.24	4119041.68	1554.77	152	B
437308.26	4119017.08	1558.00	152	R
437341.67	4119156.95	1556.00	153	L
437340.98	4119136.22	1557.60	153	T
437335.43	4119135.67	1552.94	153	B
437338.73	4119116.99	1560.37	153	R
437287.39	4119028.77	1552.24	154	L
437288.95	4119013.96	1552.99	154	T
437283.64	4119013.08	1551.07	154	B
437286.23	4118993.71	1553.53	154	R
437315.46	4118955.14	1570.08	155	L
437312.47	4118924.47	1570.07	155	T
437309.40	4118930.21	1570.70	155	B
437302.37	4118909.85	1570.93	155	B
437306.65	4118907.85	1573.08	155	R
437312.94	4118977.29	1564.39	156	L
437304.45	4118950.98	1567.32	156	T
437307.62	4118922.21	1566.77	156	T
437302.06	4118951.97	1564.29	156	B
437306.01	4118922.93	1565.17	156	B
437301.36	4118904.45	1568.44	156	R
437288.47	4118923.66	1558.85	157	L
437284.31	4118890.54	1561.73	157	T
437265.67	4118852.30	1561.96	157	T
437243.31	4118822.36	1564.21	157	T
437278.02	4118892.27	1556.76	157	B
437260.34	4118853.83	1557.12	157	B
437242.37	4118821.37	1558.77	157	B
437242.03	4118784.28	1563.02	157	R
437286.20	4118934.56	1555.32	158	L
437281.58	4118912.29	1554.72	158	T
437268.10	4118875.08	1555.34	158	T
437253.81	4118846.95	1558.25	158	T
437238.75	4118798.11	1560.14	158	T
437215.40	4118758.46	1562.17	158	T
437225.56	4118692.08	1563.39	158	T
437210.26	4118610.73	1564.80	158	T
437176.58	4118580.14	1566.29	158	T
437274.36	4118914.36	1549.78	158	B
437264.21	4118877.23	1550.76	158	B
437252.70	4118847.59	1552.72	158	B
437233.82	4118799.87	1552.66	158	B
437208.82	4118763.64	1556.88	158	B
437222.58	4118690.86	1558.84	158	B
437207.19	4118613.87	1559.62	158	B
437169.15	4118577.13	1562.93	158	B
437148.85	4118549.15	1565.62	158	B
437157.42	4118550.71	1572.38	158	R
437304.85	4119180.49	1537.08	159	L
437306.85	4119129.61	1539.25	159	T
437292.55	4119079.73	1544.93	159	T
437273.30	4119048.26	1543.49	159	T
437276.97	4119016.56	1546.41	159	T
437255.30	4118969.66	1547.08	159	T
437275.17	4118918.27	1549.64	159	T
437266.12	4118889.48	1551.53	159	T
437254.90	4118856.92	1552.31	159	T
437232.48	4118812.07	1552.98	159	T
437226.96	4118790.08	1552.70	159	T
437303.96	4119136.27	1537.55	159	B
437290.83	4119077.63	1538.53	159	B
437274.40	4119050.45	1539.89	159	B
437269.79	4119017.61	1539.26	159	B
437247.91	4118970.06	1538.75	159	B
437271.58	4118914.25	1545.48	159	B
437265.84	4118889.63	1546.20	159	B
437257.62	4118862.91	1549.56	159	B
437232.80	4118813.46	1548.93	159	B
437230.23	4118792.67	1551.49	159	B
437218.23	4118773.28	1553.06	159	R
437302.02	4119179.53	1535.39	160	L

Table G.1 continued

Easting	Northing	MSL	SS body	
437303.22	4119137.65	1537.27	160	T
437290.87	4119082.60	1539.48	160	T
437273.90	4119044.32	1538.59	160	T
437271.65	4119010.62	1539.61	160	T
437263.60	4118986.16	1542.26	160	T
437301.88	4119140.30	1534.57	160	B
437290.20	4119081.56	1534.47	160	B
437269.08	4119044.47	1535.63	160	B
437269.50	4119012.63	1536.80	160	B
437259.00	4118983.97	1538.13	160	B
437254.85	4118977.76	1542.90	160	R
437225.71	4118794.24	1548.29	161	L
437220.82	4118774.73	1551.98	161	T
437201.21	4118762.97	1553.60	161	T
437221.05	4118722.16	1554.77	161	T
437215.37	4118682.00	1554.68	161	T
437219.35	4118777.50	1550.27	161	B
437201.75	4118762.56	1548.28	161	B
437216.73	4118725.75	1551.25	161	B
437212.90	4118688.16	1553.94	161	B
437217.32	4118662.52	1557.98	161	R
437252.62	4119083.08	1522.16	162	L
437232.66	4119070.42	1523.88	162	T
437235.27	4119072.06	1522.96	162	B
437240.40	4119049.26	1522.96	162	R
437238.48	4119100.29	1516.90	163	L
437217.44	4119068.68	1515.64	163	T
437216.28	4119072.39	1516.55	163	B
437222.06	4119052.29	1516.53	163	R
437234.52	4118993.45	1529.08	164	L
437222.36	4118974.43	1529.79	164	T
437246.31	4118927.97	1531.92	164	T
437234.74	4118877.57	1530.82	164	T
437212.88	4118851.03	1531.55	164	T
437216.77	4118975.57	1525.62	164	B
437240.81	4118926.52	1525.23	164	B
437234.13	4118877.88	1528.22	164	B
437213.10	4118850.88	1529.04	164	B
437208.90	4118821.83	1534.24	164	R
437160.53	4118631.44	1538.32	165	L
437124.84	4118605.10	1542.24	165	T
437103.73	4118581.05	1544.25	165	T
437125.77	4118608.44	1541.98	165	B
437103.75	4118583.35	1542.61	165	B
437072.28	4118550.68	1542.05	165	R
437114.95	4118638.57	1531.78	166	L
437092.99	4118622.23	1534.41	166	T
437061.94	4118599.95	1532.91	166	T
437090.33	4118623.40	1530.01	166	B
437062.11	4118599.75	1530.21	166	B
437056.96	4118570.90	1533.65	166	R
437249.08	4119135.14	1505.80	167	L
437237.11	4119109.79	1509.70	167	T
437215.16	4119081.86	1511.68	167	T
437215.79	4119034.44	1512.97	167	T
437193.78	4118983.11	1516.11	167	T
437219.73	4118918.16	1515.08	167	T
437185.84	4118839.40	1522.26	167	T
437154.55	4118793.85	1521.22	167	T
437157.05	4118736.93	1523.70	167	T
437146.61	4118665.01	1526.37	167	T
437095.10	4118628.52	1529.92	167	T
437064.56	4118589.26	1531.20	167	T
437043.95	4118554.79	1531.45	167	T
437239.42	4119109.35	1505.40	167	B
437213.04	4119080.15	1507.08	167	B
437217.89	4119036.13	1507.45	167	B
437177.94	4118987.58	1507.93	167	B
437217.47	4118912.51	1507.84	167	B
437185.94	4118837.82	1511.22	167	B
437151.97	4118799.07	1513.38	167	B
437152.33	4118739.46	1514.12	167	B
437144.14	4118671.59	1520.33	167	B
437091.48	4118635.14	1523.78	167	B
437064.43	4118589.41	1522.82	167	B
437046.56	4118555.99	1527.22	167	B
437250.59	4119131.25	1504.83	168	L
437237.66	4119110.63	1505.23	168	T
437207.35	4119070.11	1506.93	168	T
437216.09	4119032.88	1505.14	168	T
437241.43	4119113.28	1503.23	168	B
437208.57	4119069.76	1503.73	168	B
437215.24	4119033.17	1503.93	168	B
437211.05	4119018.07	1504.01	168	R
437135.30	4118678.86	1512.53	169	L
437101.70	4118654.32	1514.90	169	T
437068.55	4118634.09	1515.79	169	T
437096.85	4118653.83	1511.97	169	B
437071.44	4118634.67	1511.91	169	B
437053.19	4118607.70	1514.15	169	B
437051.49	4118607.80	1515.41	169	R
437143.66	4118700.70	1509.24	170	L
437127.46	4118671.46	1511.26	170	T
437105.94	4118657.49	1509.63	170	T
437083.08	4118641.21	1510.74	170	T
437082.77	4118639.48	1508.16	170	T
437063.43	4118627.54	1513.37	170	T
437123.74	4118671.59	1505.72	170	B
437107.41	4118659.82	1506.85	170	B
437059.84	4118625.71	1509.31	170	B
437046.71	4118605.19	1509.95	170	B
437047.15	4118606.88	1511.24	170	R
437136.91	4118744.89	1501.46	171	L
437114.59	4118669.86	1503.96	171	T
437078.47	4118640.72	1503.89	171	T
437054.93	4118614.45	1507.05	171	T

Table G.1 continued

Easting	Northing	MSL	SS body	
437119.01	4118670.93	1501.44	171	B
437078.93	4118642.27	1502.48	171	B
437051.92	4118620.90	1506.58	171	B
437042.96	4118603.57	1507.21	171	R
437156.09	4118876.35	1483.29	172	L
437114.99	4118843.08	1486.01	172	T
437114.97	4118844.53	1483.68	172	B
437109.90	4118776.49	1486.79	172	R
437199.81	4119029.28	1494.11	173	L
437180.92	4119018.84	1496.40	173	T
437147.01	4118989.62	1497.03	173	T
437175.84	4119021.89	1493.84	173	B
437148.53	4118987.78	1495.10	173	B
437199.52	4118949.25	1503.01	173	R
437144.47	4119025.06	1482.76	174	L
437126.02	4118992.55	1484.55	174	T
437188.31	4118925.24	1489.22	174	T
437122.99	4118992.88	1482.37	174	B
437186.59	4118926.14	1487.93	174	B
437188.39	4118898.57	1488.69	174	R
437248.02	4119137.36	1498.83	175	L
437242.55	4119111.91	1498.76	175	T
437245.47	4119117.16	1500.00	175	B
437219.48	4119095.20	1499.64	175	R
437249.76	4119127.95	1495.61	176	L
437246.31	4119114.72	1496.69	176	T
437245.18	4119113.77	1495.49	176	B
437217.92	4119096.74	1497.29	176	R
437247.29	4119123.76	1490.92	177	L
437240.47	4119110.10	1494.04	177	T
437205.48	4119087.45	1496.54	177	T
437238.82	4119111.58	1492.81	177	B
437204.44	4119086.60	1493.22	177	B
437199.51	4119064.55	1493.31	177	R
437132.42	4118757.37	1496.89	178	L
437130.42	4118717.49	1497.22	178	T
437129.11	4118696.70	1499.38	178	T
437129.82	4118718.10	1494.59	178	B
437124.64	4118697.61	1495.24	178	B
437126.10	4118682.72	1498.54	178	R
437096.91	4119077.35	1462.53	179	L
437107.27	4119052.47	1466.60	179	T
437095.69	4119031.13	1466.52	179	T
437105.18	4119052.27	1461.89	179	B
437094.49	4119030.63	1461.88	179	B
437084.16	4119007.97	1469.30	179	R
437080.81	4119005.52	1468.33	180	L
437091.32	4118971.54	1470.01	180	T
437136.99	4118914.57	1470.92	180	T
437085.25	4118974.84	1466.93	180	B
437136.47	4118917.39	1468.76	180	B
437122.38	4118891.83	1475.29	180	R
437135.37	4118935.33	1466.34	181	L
437126.24	4118908.51	1468.63	181	T
437114.73	4118898.21	1471.68	181	T
437092.17	4118863.26	1471.69	181	T
437039.97	4118882.52	1469.96	181	T
437060.69	4118832.81	1469.30	181	T
437083.35	4118785.12	1471.78	181	T
437092.93	4118746.24	1470.35	181	T
437089.74	4118703.26	1471.05	181	T
437059.32	4118692.76	1473.19	181	T
437019.16	4118664.19	1474.34	181	T
437127.45	4118906.52	1464.35	181	B
437110.34	4118898.59	1466.26	181	B
437065.33	4118883.86	1465.62	181	B
437035.55	4118884.87	1466.93	181	B
437057.80	4118833.96	1467.15	181	B
437082.00	4118788.00	1469.45	181	B
437093.98	4118748.68	1470.29	181	B
437091.16	4118701.67	1466.07	181	B
437057.82	4118692.68	1469.45	181	B
437014.83	4118665.94	1471.76	181	B
436998.30	4118635.30	1472.21	181	R
437087.08	4118855.04	1474.83	182	L
437041.46	4118867.12	1472.36	182	T
437058.49	4118830.50	1474.57	182	T
437096.06	4118739.62	1476.57	182	T
437059.20	4118688.88	1475.77	182	T
437013.89	4118652.19	1480.82	182	T
436986.04	4118599.62	1478.03	182	T
437040.67	4118869.12	1469.28	182	B
437059.95	4118833.46	1471.39	182	B
437095.27	4118738.69	1471.71	182	B
437057.60	4118692.71	1474.43	182	B
437015.44	4118654.30	1475.80	182	B
436985.58	4118600.39	1475.41	182	B
436974.93	4118557.70	1480.44	182	R
437002.07	4118622.42	1476.43	183	L
436992.13	4118602.03	1475.50	183	T
436983.98	4118571.77	1476.14	183	T
436985.76	4118605.07	1471.47	183	B
436981.38	4118573.70	1474.72	183	B
436966.66	4118547.57	1477.96	183	R
437000.64	4118660.69	1463.30	184	L
436983.59	4118625.83	1467.32	184	T
436973.21	4118598.73	1467.67	184	T
436959.76	4118555.03	1469.62	184	T
436982.54	4118627.55	1467.30	184	B
436973.94	4118602.59	1466.34	184	B
436954.58	4118553.44	1466.92	184	B
436957.50	4118532.57	1468.63	184	R
437070.04	4118961.83	1461.93	185	L
437098.87	4118910.07	1463.83	185	T
437098.78	4118883.56	1464.07	185	T
437030.22	4118894.15	1464.90	185	T

Table G.1 continued

Easting	Northing	MSL	SS body	
437098.05	4118910.62	1461.75	185	B
437098.84	4118883.51	1460.89	185	B
437027.53	4118893.88	1460.15	185	B
437037.25	4118858.97	1462.51	185	R
436997.35	4119055.26	1455.82	186	L
437066.56	4118986.09	1459.95	186	T
437067.49	4118955.61	1458.23	186	T
437063.98	4118985.45	1454.45	186	B
437066.99	4118954.80	1455.42	186	B
437069.16	4118954.58	1459.20	186	R
437027.75	4118827.92	1453.52	187	L
437046.62	4118792.96	1454.62	187	T
437056.18	4118778.60	1455.74	187	T
437060.77	4118745.67	1454.64	187	T
437041.55	4118795.02	1452.44	187	B
437052.51	4118779.19	1452.38	187	B
437060.78	4118745.64	1453.47	187	B
437062.11	4118726.61	1453.50	187	R
437052.88	4118828.54	1465.09	188	L
437082.13	4118791.01	1467.14	188	T
437081.42	4118793.23	1468.23	188	B
437085.24	4118775.41	1466.31	188	R
436917.38	4118954.37	1444.05	189	L
436975.14	4118881.48	1443.74	189	T
436976.38	4118882.80	1443.73	189	B
436986.66	4118870.39	1444.31	189	R
436938.07	4119022.39	1441.08	190	L
436921.20	4119006.66	1441.23	190	T
436885.80	4119021.11	1443.05	190	T
436919.50	4119011.24	1440.69	190	B
436872.64	4119031.97	1441.79	190	B
436851.75	4119042.55	1443.15	190	R
437071.07	4119182.75	1456.00	191	L
437093.15	4119166.45	1456.98	191	T
437103.42	4119154.34	1457.95	191	T
437128.10	4119133.39	1458.22	191	T
437091.29	4119167.58	1455.24	191	B
437100.20	4119153.10	1456.18	191	B
437124.98	4119133.08	1455.45	191	B
437107.05	4119116.54	1458.98	191	R
437077.86	4119270.17	1454.44	192	L
437067.53	4119258.95	1456.03	192	T
437072.90	4119249.38	1456.88	192	T
437064.53	4119258.77	1456.01	192	B
437067.99	4119246.83	1454.42	192	B
437066.42	4119210.74	1456.03	192	R
437027.37	4119187.80	1451.43	193	L
437038.25	4119178.14	1451.35	193	T
437081.77	4119164.74	1451.97	193	T
437019.31	4119179.93	1449.97	193	B
437080.42	4119162.41	1449.45	193	B
437089.91	4119158.33	1452.80	193	R
437124.05	4119138.88	1453.61	194	L
437113.71	4119127.99	1454.52	194	T
437084.16	4119107.89	1456.14	194	T
437112.73	4119128.19	1452.68	194	B
437079.63	4119106.47	1453.53	194	B
437075.61	4119103.17	1455.21	194	R
437070.11	4119095.09	1456.08	195	L
437066.53	4119083.83	1455.28	195	T
437065.57	4119084.10	1454.36	195	B
437082.21	4119073.97	1455.27	195	R
437005.81	4119072.19	1454.29	196	L
436989.81	4119058.07	1455.01	196	T
436989.80	4119055.65	1453.54	196	B
437034.34	4119028.22	1454.34	196	R
436940.93	4119078.66	1446.42	197	L
436963.78	4119057.11	1445.16	197	T
436939.05	4119070.24	1445.10	197	B
436975.10	4119044.14	1445.54	197	R
436868.19	4119124.90	1439.63	198	L
436894.19	4119095.08	1440.66	198	T
436905.90	4119074.17	1441.07	198	T
436941.80	4119050.21	1440.80	198	T
436891.85	4119095.61	1440.21	198	B
436903.47	4119078.13	1440.61	198	B
436931.40	4119052.30	1439.19	198	B
436962.00	4119029.20	1439.90	198	R
436909.42	4119263.85	1437.12	199	L
436892.48	4119248.29	1438.57	199	T
436897.63	4119226.17	1439.39	199	T
436873.62	4119211.07	1439.61	199	T
436927.76	4119185.02	1438.85	199	T
436933.43	4119161.62	1438.39	199	T
436890.09	4119247.19	1436.28	199	B
436894.54	4119225.76	1438.07	199	B
436872.68	4119212.11	1439.17	199	B
436927.78	4119185.57	1437.14	199	B
436891.86	4119172.65	1439.33	199	B
436884.06	4119165.73	1439.59	199	R
436866.41	4119286.12	1433.71	200	L
436861.42	4119241.10	1434.47	200	T
436895.94	4119190.03	1434.71	200	T
436802.39	4119187.48	1434.27	200	T
436794.17	4119143.79	1434.31	200	T
436855.49	4119107.60	1436.54	200	T
436795.38	4119080.05	1435.26	200	T
436795.58	4119046.04	1436.72	200	T
436807.02	4118901.69	1432.43	200	T
436838.42	4119205.76	1434.03	200	B
436762.66	4119153.48	1425.13	200	B
436790.88	4119138.55	1429.96	200	B
436841.58	4119112.16	1430.92	200	B
436793.95	4119081.28	1428.97	200	B
436790.92	4119046.79	1430.03	200	B
436809.02	4118910.06	1430.73	200	B

Table G.1 continued

Easting	Northing	MSL	SS body	
436796.34	4118894.30	1433.77	200	R
436775.66	4119181.06	1430.89	201	T
436771.51	4119149.53	1429.18	201	T
436795.22	4119088.86	1428.46	201	T
436790.26	4119057.06	1429.84	201	T
436783.75	4118939.37	1428.85	201	T
436782.53	4118909.86	1429.00	201	T
436786.03	4118893.43	1430.58	201	T
436779.84	4118978.68	1427.51	201	T
436792.65	4118929.84	1427.92	201	T
436787.72	4118912.64	1428.63	201	T
436789.10	4118834.53	1427.41	201	T
436815.80	4118795.54	1429.56	201	T
436789.05	4118791.98	1431.60	201	T
436797.70	4118716.53	1432.16	201	T
436769.27	4118661.37	1435.55	201	T
436753.30	4118567.53	1439.74	201	T
436781.05	4118973.91	1427.96	201	T
436790.55	4118933.84	1428.17	201	T
436786.79	4118909.73	1428.20	201	T
436833.98	4119194.55	1426.54	201	B
436803.78	4119189.30	1429.87	201	B
436774.92	4119182.61	1426.65	201	B
436786.36	4119084.34	1420.18	201	B
436783.10	4119061.01	1420.06	201	B
436788.10	4118915.77	1422.72	201	B
436781.51	4118913.13	1424.06	201	B
436773.59	4118975.78	1420.79	201	B
436783.55	4118934.98	1420.95	201	B
436783.82	4118914.76	1422.29	201	B
436787.48	4118835.09	1420.00	201	B
436815.60	4118793.15	1423.37	201	B
436788.54	4118795.55	1424.89	201	B
436794.45	4118717.12	1428.98	201	B
436767.04	4118667.03	1431.38	201	B
436751.28	4118561.87	1432.73	201	B
436774.96	4118973.62	1420.53	201	B
436784.22	4118936.25	1420.94	201	B
436785.21	4118913.79	1422.19	201	B
436937.93	4119229.80	1442.47	202	L
436980.06	4119181.19	1442.90	202	T
436975.18	4119164.72	1441.68	202	T
436997.81	4119146.12	1441.59	202	T
436979.02	4119181.33	1441.63	202	B
436973.08	4119164.48	1441.73	202	B
436990.83	4119147.00	1441.12	202	B
436958.40	4119136.87	1443.98	202	R
436963.25	4119381.63	1441.47	203	L
436972.75	4119355.83	1440.78	203	T
436996.85	4119345.21	1439.45	203	T
437013.62	4119332.46	1440.42	203	T
436972.11	4119357.76	1440.78	203	B
436995.90	4119344.92	1439.46	203	B

Easting	Northing	MSL	SS body	
437036.07	4119333.03	1440.52	203	R
437015.55	4119483.78	1440.25	204	L
437000.58	4119451.80	1441.06	204	T
437021.44	4119437.59	1440.69	204	T
436966.81	4119383.80	1444.75	204	T
436995.26	4119347.63	1443.70	204	T
437014.02	4119335.59	1444.11	204	T
437000.68	4119453.63	1440.23	204	B
437020.76	4119439.04	1441.51	204	B
436964.24	4119382.01	1442.81	204	B
436995.39	4119346.95	1440.88	204	B
437024.70	4119333.61	1440.18	204	B
437042.78	4119325.89	1440.47	204	R
436991.07	4119376.89	1451.49	205	L
436986.98	4119361.28	1450.15	205	T
437029.87	4119350.51	1449.09	205	T
437055.17	4119330.89	1449.70	205	T
437022.04	4119301.41	1449.97	205	T
436988.15	4119360.93	1449.49	205	B
437028.30	4119348.54	1446.82	205	B
437053.50	4119328.92	1445.71	205	B
437011.04	4119300.38	1448.62	205	B
437014.78	4119288.61	1449.31	205	R
437013.13	4119454.14	1444.73	206	L
437012.76	4119448.52	1446.35	206	T
437041.24	4119433.43	1445.22	206	T
436975.66	4119380.90	1448.73	206	T
436985.71	4119358.75	1447.30	206	T
437013.45	4119447.09	1443.97	206	B
437039.95	4119433.79	1443.59	206	B
436972.35	4119381.08	1448.03	206	B
436983.60	4119358.79	1447.32	206	B
437011.25	4119353.92	1446.92	206	R
437079.78	4119647.77	1448.11	207	L
437085.22	4119613.05	1449.33	207	T
437064.37	4119552.17	1450.62	207	T
437038.16	4119502.82	1449.96	207	T
437038.50	4119478.67	1450.93	207	T
437058.64	4119452.99	1450.02	207	T
437067.27	4119426.28	1452.65	207	T
437055.83	4119394.62	1453.47	207	T
437086.64	4119612.80	1446.10	207	B
437062.97	4119555.91	1448.70	207	B
437038.15	4119502.83	1448.23	207	B
437036.31	4119478.45	1450.05	207	B
437052.76	4119455.92	1450.89	207	B
437066.64	4119425.11	1450.05	207	B
436987.03	4119370.26	1452.79	207	B
437052.52	4119369.33	1452.66	207	R
437068.63	4119452.84	1457.08	208	L
437076.05	4119423.24	1457.06	208	T
437068.78	4119400.09	1456.96	208	T
437066.75	4119384.17	1459.40	208	T

Table G.1 continued

Easting	Northing	MSL	SS body	
437072.57	4119426.57	1456.18	208	B
437064.79	4119402.32	1455.23	208	B
437064.24	4119378.99	1454.33	208	B
437080.32	4119370.46	1454.39	208	B
437110.93	4119360.35	1455.32	208	R
437079.01	4119400.90	1460.50	209	L
437080.86	4119385.92	1459.60	209	T
437105.12	4119374.66	1458.05	209	T
437072.31	4119383.22	1457.77	209	B
437100.54	4119376.15	1457.12	209	B
437126.07	4119373.67	1458.21	209	R
436776.83	4118944.91	1418.78	210	L
436790.25	4118918.27	1421.70	210	T
436814.94	4118797.68	1423.04	210	T
436796.10	4118804.74	1422.40	210	T
436782.42	4118791.53	1423.72	210	T
436798.03	4118670.82	1426.08	210	T
436777.47	4118924.66	1415.29	210	B
436803.03	4118805.93	1415.90	210	B
436797.00	4118803.50	1415.51	210	B
436778.93	4118796.98	1416.90	210	B
436915.01	4118648.26	1443.04	211	L
436896.15	4118615.65	1443.09	211	T
436890.57	4118592.14	1445.03	211	T
436864.24	4118575.08	1443.17	211	T
436852.50	4118554.71	1443.26	211	T
436895.06	4118617.30	1441.33	211	B
436884.85	4118594.53	1441.33	211	B
436862.04	4118577.32	1441.35	211	B
436847.85	4118558.02	1440.44	211	B
436853.69	4118504.71	1444.55	211	R
436934.07	4118595.53	1449.06	212	L
436916.67	4118583.82	1450.06	212	T
436915.81	4118534.04	1450.75	212	T
436912.83	4118593.22	1447.96	212	B
436913.03	4118534.71	1448.65	212	B
436902.07	4118518.38	1450.87	212	R
436936.51	4118706.77	1442.91	213	L
436917.53	4118700.40	1445.29	213	T
436909.73	4118689.91	1445.29	213	T
436915.13	4118698.33	1442.89	213	B
436907.23	4118689.18	1442.83	213	B
436923.00	4118669.78	1444.67	213	R
436943.67	4118727.89	1438.92	214	L
436892.89	4118742.76	1438.37	214	T
436877.52	4118734.66	1439.11	214	T
436867.29	4118723.85	1439.09	214	T
436904.76	4118684.64	1442.15	214	T
436890.57	4118747.43	1437.01	214	B
436876.14	4118737.42	1437.73	214	B
436865.43	4118726.24	1438.43	214	B
436902.89	4118684.44	1440.53	214	B
436908.41	4118673.51	1442.12	214	R

Easting	Northing	MSL	SS body	
436839.24	4119034.19	1442.05	215	T
436848.71	4119020.54	1442.48	215	T
436908.35	4118981.62	1442.04	215	T
436914.07	4118962.41	1442.59	215	T
436930.26	4118931.12	1442.19	215	T
436979.31	4118884.29	1443.90	215	T
436838.52	4119034.17	1440.89	215	B
436846.67	4119019.94	1440.91	215	B
436908.57	4118982.59	1440.99	215	B
436914.24	4118963.45	1441.46	215	B
436927.45	4118932.12	1440.45	215	B
436976.66	4118883.22	1441.87	215	B
436986.42	4118871.10	1443.96	215	R
436866.00	4119134.23	1440.35	216	L
436874.57	4119118.36	1439.96	216	T
436878.31	4119110.59	1439.67	216	T
436894.81	4119094.44	1439.53	216	T
436873.18	4119117.33	1438.99	216	B
436877.06	4119111.11	1438.89	216	B
436894.17	4119094.72	1439.56	216	B
436898.80	4119086.06	1439.91	216	R
436875.89	4119127.21	1441.18	217	L
436878.84	4119121.46	1441.48	217	T
436875.89	4119122.26	1441.06	217	B
436885.67	4119114.80	1440.68	217	R
437420.75	4119288.53	1623.57	218	L
437416.69	4119259.52	1623.72	218	T
437421.46	4119214.06	1622.52	218	T
437416.04	4119259.38	1622.15	218	B
437419.84	4119302.43	1609.94	219	L
437425.93	4119200.17	1618.74	219	T
437426.09	4119198.83	1614.50	219	B
437422.80	4119148.97	1616.47	219	R
437420.58	4119414.62	1612.65	220	L
437425.62	4119192.06	1621.11	220	T
437414.76	4119257.76	1620.25	220	T
437417.24	4119361.24	1613.46	220	T
437426.33	4119193.57	1617.10	220	B
437416.30	4119254.01	1613.28	220	B
437417.87	4119362.98	1607.91	220	B
437426.28	4119132.17	1621.05	220	R
437419.78	4119305.24	1615.83	221	L
437418.60	4119276.72	1619.39	221	T
437426.59	4119182.80	1622.50	221	T
437418.17	4119279.43	1618.02	221	B
437426.27	4119182.73	1619.63	221	B
437425.37	4119130.77	1620.91	221	B
437425.61	4119132.09	1623.77	221	R
437420.19	4119219.44	1619.64	222	L
437425.50	4119194.68	1624.11	222	T
437425.80	4119151.99	1624.24	222	T
437424.65	4119195.92	1622.54	222	B
437424.17	4119151.84	1622.47	222	B

Table G.1 continued

Easting	Northing	MSL	SS body	
437427.14	4119133.54	1625.57	222	R
437425.38	4119179.97	1616.64	223	T
437425.98	4119180.08	1613.88	223	B
437414.22	4119299.27	1605.84	223	B
437407.93	4119413.57	1601.43	223	B
437421.61	4119127.91	1615.78	223	R
437418.20	4119297.67	1609.36	223	R
437415.70	4119412.47	1604.27	223	R
437350.66	4119533.52	1523.54	224	L
437344.17	4119518.04	1527.95	224	T

Easting	Northing	MSL	SS body	
437332.87	4119492.17	1526.18	224	T
437338.32	4119508.08	1522.48	224	B
437329.95	4119492.61	1524.13	224	B
437325.44	4119486.06	1525.76	224	R
437399.56	4119623.36	1541.53	225	L
437397.38	4119610.59	1540.61	225	T
437394.63	4119593.17	1541.65	225	T
437399.96	4119608.21	1540.98	225	B
437396.06	4119590.94	1542.83	225	B
437390.85	4119545.78	1543.66	225	R

Table G.2

Measured Stratigraphic Section GPS Points

Easting	Northing	MSL	SXN Pt. No.	
436855.24	4119122.64	1435.40	SXN 1	1
436870.78	4119124.78	1439.58	SXN 1	2
436876.52	4119122.09	1440.63	SXN 1	3
436878.34	4119122.16	1441.76	SXN 1	4
436914.42	4119086.42	1443.18	SXN 1	5
436961.40	4119064.79	1444.06	SXN 1	6
436962.45	4119065.73	1446.05	SXN 1	7
436981.87	4119055.25	1448.58	SXN 1	8
436983.85	4119055.68	1450.30	SXN 1	9
436991.93	4119059.07	1453.81	SXN 1	10
436992.78	4119056.83	1453.87	SXN 1	11
437054.35	4119030.31	1461.16	SXN 1	12
437059.11	4119029.03	1463.47	SXN 1	13
437062.63	4119025.83	1465.02	SXN 1	14
437088.16	4119001.78	1467.51	SXN 1	15
437089.94	4119000.73	1469.20	SXN 1	16
437127.13	4118998.89	1482.99	SXN 1	17
437127.76	4118997.97	1485.42	SXN 1	18
437151.22	4118990.49	1492.02	SXN 1	19
437155.26	4118991.56	1494.23	SXN 1	20
437152.98	4118990.21	1494.01	SXN 1	21
437152.80	4118991.94	1498.25	SXN 1	22
437195.01	4118983.58	1509.02	SXN 1	23
437195.47	4118986.31	1516.57	SXN 1	24
437218.00	4118981.49	1524.75	SXN 1	25
437219.50	4118981.24	1527.95	SXN 1	26
437252.54	4118969.28	1539.78	SXN 1	27
437257.87	4118967.22	1548.15	SXN 1	28
437271.66	4119001.10	1546.37	SXN 1	29
437285.98	4118999.32	1551.16	SXN 1	30
437287.47	4118996.96	1552.62	SXN 1	31
437334.25	4118996.81	1570.61	SXN 1	32
437342.97	4118999.31	1574.65	SXN 1	33
437366.56	4119024.71	1581.36	SXN 1	34
437371.06	4119019.46	1582.36	SXN 1	35
437378.50	4119033.70	1586.25	SXN 1	36
437389.54	4119069.39	1588.23	SXN 1	37
437404.23	4119083.26	1600.57	SXN 1	38
437407.22	4119087.12	1605.20	SXN 1	39
437411.13	4119087.18	1606.10	SXN 1	40
437409.93	4119083.29	1607.21	SXN 1	41
437405.74	4119144.91	1607.01	SXN 1	42
437415.88	4119148.47	1610.76	SXN 1	43
437428.00	4119145.65	1626.02	SXN 1	44
437425.65	4119142.76	1628.20	SXN 1	45
436910.43	4119374.83	1431.04	SXN 2	1
436951.75	4119381.33	1440.57	SXN 2	2
436956.57	4119365.65	1443.14	SXN 2	3
436957.22	4119365.64	1445.02	SXN 2	4
436966.45	4119381.15	1447.43	SXN 2	5
436966.67	4119377.99	1448.34	SXN 2	6
436979.47	4119370.96	1451.16	SXN 2	7
436979.80	4119369.90	1452.32	SXN 2	8
437048.14	4119393.96	1452.67	SXN 2	9
437049.11	4119392.15	1453.16	SXN 2	10
437057.01	4119387.10	1456.49	SXN 2	11
437061.63	4119381.54	1458.72	SXN 2	12
437082.18	4119448.91	1463.42	SXN 2	13
437084.37	4119448.01	1464.52	SXN 2	14
437178.85	4119381.14	1481.65	SXN 2	15
437179.40	4119381.69	1483.99	SXN 2	16
437172.83	4119393.33	1484.61	SXN 2	17
437175.43	4119391.67	1485.40	SXN 2	18
437191.06	4119393.22	1495.68	SXN 2	19
437196.74	4119391.96	1498.24	SXN 2	20
437221.15	4119391.91	1505.58	SXN 2	21
437218.57	4119392.07	1505.47	SXN 2	22
437222.36	4119391.89	1507.29	SXN 2	23
437222.53	4119390.61	1507.35	SXN 2	24
437227.65	4119390.39	1508.38	SXN 2	25
437228.87	4119390.44	1510.10	SXN 2	26
437284.60	4119379.35	1530.01	SXN 2	27
437286.26	4119376.80	1531.25	SXN 2	28
437285.74	4119379.62	1532.86	SXN 2	29
437308.04	4119402.00	1540.75	SXN 2	30
437311.59	4119400.52	1543.13	SXN 2	31
437351.95	4119398.52	1564.44	SXN 2	32
437357.33	4119398.54	1568.19	SXN 2	33
437357.87	4119401.76	1570.02	SXN 2	34
437358.28	4119401.49	1573.18	SXN 2	35
437385.16	4119387.96	1593.31	SXN 2	36
437387.81	4119386.33	1598.24	SXN 2	37
437399.47	4119405.20	1602.65	SXN 2	38
437405.40	4119407.87	1608.92	SXN 2	39
437406.98	4119403.29	1610.81	SXN 2	40
437407.39	4119400.58	1612.29	SXN 2	41
437407.67	4119396.68	1620.67	SXN 2	42
437404.49	4119392.28	1622.83	SXN 2	43
437406.54	4119391.04	1625.72	SXN 2	44
437089.11	4119925.02	1450.22	SXN 3	1
437128.68	4119912.46	1444.70	SXN 3	2
437130.22	4119912.67	1448.77	SXN 3	3
437147.31	4119920.42	1452.00	SXN 3	4
437147.85	4119920.56	1452.74	SXN 3	5
437170.46	4119939.95	1456.41	SXN 3	6
437171.04	4119940.49	1457.83	SXN 3	7
437246.76	4119946.89	1469.57	SXN 3	8
437247.68	4119944.73	1469.53	SXN 3	9
437270.68	4119945.13	1478.61	SXN 3	10
437272.63	4119945.50	1481.46	SXN 3	11
437284.44	4119943.57	1484.80	SXN 3	12
437285.43	4119943.99	1485.38	SXN 3	13

Table G.2 continued

Easting	Northing	MSL	SXN Pt.	No.
437296.64	4119948.67	1488.41	SXN 3	14
437300.40	4119947.58	1489.15	SXN 3	15
437343.03	4119947.60	1496.27	SXN 3	16
437345.91	4119949.94	1498.87	SXN 3	17
437382.48	4119892.03	1513.62	SXN 3	18
437384.18	4119891.75	1516.52	SXN 3	19
437388.48	4119888.93	1519.13	SXN 3	20
437394.07	4119890.05	1524.65	SXN 3	21
437397.69	4119889.42	1527.26	SXN 3	22
437399.53	4119889.13	1528.23	SXN 3	23
437410.27	4119889.50	1531.93	SXN 3	24
437413.84	4119890.40	1536.11	SXN 3	25
437420.71	4119884.79	1538.79	SXN 3	26
437423.18	4119885.88	1543.67	SXN 3	27
437429.59	4119890.88	1546.93	SXN 3	28
437433.77	4119894.83	1549.98	SXN 3	29
437435.66	4119896.06	1551.88	SXN 3	30
437437.94	4119894.23	1554.69	SXN 3	31
437439.92	4119896.24	1556.51	SXN 3	32
437448.94	4119896.57	1563.08	SXN 3	33
437463.03	4119900.39	1571.71	SXN 3	34
437466.22	4119901.65	1576.61	SXN 3	35
437468.37	4119896.39	1578.08	SXN 3	36
437471.95	4119895.09	1579.79	SXN 3	37
437473.98	4119894.01	1583.73	SXN 3	38
437476.76	4119896.17	1590.50	SXN 3	39
437480.22	4119894.90	1596.74	SXN 3	40
437483.46	4119899.61	1598.35	SXN 3	41
437482.82	4119897.99	1600.06	SXN 3	42
437479.79	4119884.01	1604.24	SXN 3	43
437478.24	4119881.66	1608.45	SXN 3	44

Table G.3

Channel Belt Dimensions

Order	DU	SS Body	Amalg L	Amalg V	Width (m) M	Width (m) True	Width (m) MA	Width (m) DU Ave	Thickness (m) M	Thickness (m) MA	Thickness (m) DU Ave	W/T
1	0	210	2	2	634.8	223.0	316.6	316.6	6.8	6.0	6.0	32.7
2	0	201	2	2	71.4	455.9	272.8	316.6	6.2	5.1	6.0	73.3
3	0	200	2	2	756.3	271.0	237.7	316.6	4.8	4.4	6.0	56.0
4	1	211	1	0	131.1	141.4	202.9	75.1	2.5	3.2	1.7	56.0
5	1	199	0	1	72.9	97.2	119.1	75.1	1.4	2.4	1.7	67.4
6	1	216	1	0	282.6	49.3	75.1	75.1	0.9	1.7	1.7	56.3
7	1	213	0	0	77.9	36.5	59.3	75.1	2.4	1.7	1.7	15.1
8	1	203	0	1	319.3	51.1	43.3	75.1	1.4	2.0	1.7	35.7
9	2	212	0	0	72.2	62.6	43.4	92.0	2.1	2.2	2.4	29.8
10	2	95	1	0	94.2	17.2	51.7	92.0	3.3	2.3	2.4	5.3
11	2	109	0	1	108.9	49.6	73.1	92.0	1.7	2.4	2.4	28.7
12	2	88	1	0	70.9	77.9	79.4	92.0	2.8	2.3	2.4	27.8
13	2	204	0	1	352.9	158.2	94.2	92.0	2.1	2.0	2.4	76.3
14	2	206	0	0	210.8	94.2	104.5	92.0	1.6	2.0	2.4	60.0
15	2	205	0	0	23.5	91.2	110.3	92.0	2.1	1.9	2.4	44.1
16	2	208	0	0	714.8	101.2	88.4	92.0	1.5	1.9	2.4	69.5
17	2	187	0	0	118.8	107.0	93.2	92.0	2.2	2.4	2.4	47.8
18	2	193	0	0	34.1	48.2	92.3	92.0	2.0	2.6	2.4	24.7
19	2	186	1	0	118.3	118.6	75.2	92.0	4.2	2.6	2.4	28.5
20	2	185	1	0	21.9	86.6	62.6	92.0	3.3	2.8	2.4	25.9
21	2	94	0	0	134.0	15.7	103.9	92.0	1.1	2.8	2.4	14.1
22	2	87	1	0	121.2	44.0	83.9	92.0	3.7	2.1	2.4	12.0
23	2	207	0	1	104.0	254.4	77.0	92.0	1.7	1.7	2.4	148.0
24	2	93	0	0	25.4	19.1	95.2	92.0	0.8	1.9	2.4	25.1
25	2	108	0	0	60.2	51.6	98.3	92.0	1.1	1.7	2.4	46.2
26	2	184	0	0	36.7	107.2	102.1	92.0	2.0	2.1	2.4	53.2
27	2	183	1	2	152.2	59.3	113.1	92.0	2.7	2.3	2.4	21.8
28	2	182	1	1	44.0	273.3	150.6	92.0	3.8	2.9	2.4	72.6
29	2	191	1	0	250.3	74.4	143.1	92.0	2.1	3.4	2.4	35.5
30	2	181	1	2	120.0	238.9	153.8	92.0	3.8	3.4	2.4	62.2
31	2	179	2	0	247.3	69.9	111.2	92.0	4.7	3.1	2.4	15.0
32	2	180	1	1	30.0	112.7	122.7	92.0	2.6	3.0	2.4	42.9
33	2	192	0	0	225.8	59.9	77.8	92.0	2.5	2.5	2.4	24.4
34	2	107	1	0	107.0	132.1	71.4	92.0	1.4	2.0	2.4	92.8

Table G.3 continued

Order	DU	SS Body	Amalg L	Amalg V	Width (m) M	Width (m) True	Width (m) MA	Width (m) DU Ave	Thickness (m) M	Thickness (m) MA	Thickness (m) DU Ave	W/T
35	2	92	1	0	110.1	14.5	67.2	92.0	1.4	2.3	2.4	10.3
36	2	90	1	0	217.4	37.8	60.5	92.0	2.0	2.1	2.4	18.5
37	2	1	0	0	85.0	91.8	52.4	92.0	4.2	2.2	2.4	21.7
38	3	209	0	1	215.2	26.5	51.6	73.7	1.4	2.0	2.0	19.2
39	3	111	0	1	20.6	53.6	51.5	73.7	1.0	1.8	2.0	52.2
40	3	112	0	1	135.3	48.4	37.4	73.7	1.3	1.2	2.0	37.2
41	3	105	0	0	123.7	37.4	43.2	73.7	1.1	1.1	2.0	33.5
42	3	96	0	0	27.0	21.2	49.1	73.7	1.0	1.5	2.0	21.0
43	3	4	0	0	151.3	55.1	57.6	73.7	1.2	1.6	2.0	45.6
44	3	9	0	0	32.6	83.3	93.5	73.7	2.6	1.9	2.0	31.6
45	3	8	0	0	60.3	91.0	95.8	73.7	2.0	1.9	2.0	46.4
46	3	119	1	0	95.2	216.7	113.4	73.7	2.5	2.1	2.0	85.0
47	3	118	0	0	58.3	32.8	116.9	73.7	1.4	2.0	2.0	23.9
48	3	171	0	0	163.5	143.0	114.8	73.7	2.0	2.1	2.0	72.8
49	3	172	0	0	348.4	100.7	76.1	73.7	2.3	2.0	2.0	43.2
50	3	173	0	0	193.4	80.5	85.0	73.7	2.2	2.4	2.0	35.9
51	3	145	0	1	108.0	23.4	71.4	73.7	2.2	2.3	2.0	10.7
52	3	144	0	1	635.1	77.4	65.8	73.7	3.3	2.4	2.0	23.4
53	3	14	0	0	19.5	75.0	68.8	73.7	1.6	2.6	2.0	46.0
54	3	169	0	1	100.9	72.5	86.7	73.7	2.7	2.6	2.0	27.0
55	3	170	0	1	78.1	95.5	187.5	73.7	3.3	3.3	2.0	29.4
56	4	168	1	2	25.8	113.2	214.0	180.1	2.1	3.5	3.4	52.9
57	4	167	1	2	24.3	581.2	250.9	180.1	6.9	4.0	3.4	83.9
58	4	149	1	0	53.8	207.6	251.2	180.1	2.6	4.2	3.4	81.2
59	4	72	0	1	15.8	256.8	284.6	180.1	5.3	4.9	3.4	48.1
60	4	23	1	1	22.8	97.5	295.8	180.1	-	4.0	3.4	-
61	4	22	1	1	43.6	280.0	268.3	180.1	-	3.6	3.4	-
62	4	21	1	1	80.3	637.3	225.2	180.1	4.1	2.4	3.4	157.4
63	4	73	0	2	13.9	70.0	223.3	180.1	1.5	2.9	3.4	46.6
64	4	74	0	1	19.9	41.3	192.9	180.1	1.8	2.9	3.4	23.1
65	4	26	0	1	13.5	88.2	77.5	180.1	4.3	2.6	3.4	20.4
66	4	27	0	0	43.2	127.9	112.8	180.1	2.8	2.7	3.4	46.3
67	4	28	0	0	76.1	60.1	138.8	180.1	2.8	3.2	3.4	21.7
68	4	25	0	2	35.4	246.3	161.6	180.1	1.9	3.0	3.4	127.0
69	4	164	0	0	48.2	171.7	162.4	180.1	4.0	3.0	3.4	43.0
70	4	160	0	1	48.0	201.9	231.9	180.1	3.5	3.3	3.4	57.3

Table G.3 continued

Order	DU	SS Body	Amalg L	Amalg V	Width (m) M	Width (m) True	Width (m) MA	Width (m) DU Ave	Thickness (m) M	Thickness (m) MA	Thickness (m) DU Ave	W/T
71	4	161	1	0	92.0	132.1	259.5	180.1	2.8	4.0	3.4	46.8
72	4	159	2	2	64.1	407.5	253.0	180.1	4.5	4.2	3.4	91.1
73	4	158	0	2	35.1	384.3	224.4	180.1	5.3	4.2	3.4	72.6
74	4	157	0	1	147.0	139.5	222.3	180.1	5.1	4.0	3.4	27.5
75	4	75	0	0	75.4	58.8	161.9	180.1	3.3	3.8	3.4	17.9
76	4	24	0	1	13.7	121.2	94.5	180.1	2.0	3.2	3.4	60.5
77	4	76	0	0	60.5	105.5	75.5	180.1	3.4	2.6	3.4	30.8
78	4	224	1	2	86.4	47.5	81.3	180.1	2.1	2.6	3.4	23.1
79	4	124	1	0	50.6	44.5	182.7	180.1	2.1	3.1	3.4	21.5
80	4	123	1	0	61.8	87.8	198.6	180.1	3.3	2.8	3.4	26.5
81	4	29	1	1	44.6	628.1	211.4	180.1	4.5	2.9	3.4	138.1
82	4	30	0	2	27.4	185.1	219.1	180.1	2.3	3.1	3.4	82.2
83	4	31	0	1	80.5	111.5	216.2	180.1	2.1	3.0	3.4	53.2
84	4	77	0	0	98.3	82.9	102.9	180.1	3.4	2.5	3.4	24.3
85	4	80	0	0	81.5	73.5	97.9	180.1	2.6	2.8	3.4	28.3
86	4	125	0	0	275.0	61.7	144.3	180.1	2.0	3.1	3.4	30.6
87	4	78	0	0	18.7	159.8	143.3	180.1	3.9	2.7	3.4	40.7
88	4	32	0	0	169.8	343.7	165.8	180.1	3.7	2.9	3.4	93.3
89	4	225	0	0	74.5	77.6	253.3	180.1	1.2	3.4	3.4	66.3
90	4	79	1	0	115.6	186.1	256.9	180.1	3.5	3.6	3.4	52.5
91	4	33	2	0	109.9	499.3	235.3	180.1	4.4	3.7	3.4	112.5
92	4	34	1	0	259.2	178.0	234.9	180.1	5.0	3.8	3.4	35.6
93	4	39	0	0	616.5	235.3	221.5	180.1	4.2	3.9	3.4	55.9
94	4	35	0	0	134.6	75.7	130.4	180.1	1.8	3.8	3.4	42.3
95	4	40	1	0	208.0	119.2	118.3	180.1	4.0	3.2	3.4	29.6
96	4	41	0	0	89.1	43.6	94.9	180.1	-	2.7	3.4	-
97	4	128	0	1	134.0	117.6	84.1	180.1	2.6	3.2	3.4	44.4
98	4	127	0	2	101.4	118.6	88.3	180.1	2.3	2.6	3.4	51.8
99	4	81	0	1	34.5	21.7	102.8	180.1	4.0	2.8	3.4	5.4
100	4	42	0	0	17.9	140.0	115.7	180.1	1.6	2.6	3.4	89.0
101	4	43	0	1	36.0	116.0	133.8	180.1	3.6	3.0	3.4	32.2
102	5	133	1	0	70.0	182.5	134.2	225.4	1.5	2.3	3.7	122.5
103	5	44	1	1	173.6	208.8	154.4	225.4	4.2	2.8	3.7	49.7
104	5	45	0	0	50.7	23.7	198.5	225.4	0.6	3.0	3.7	39.5
105	5	82	2	0	128.0	240.9	167.6	225.4	4.2	3.3	3.7	57.7

Table G.3 continued

Order	DU	SS Body	Amalg L	Amalg V	Width (m) M	Width (m) True	Width (m) MA	Width (m) DU Ave	Thickness (m) M	Thickness (m) MA	Thickness (m) DU Ave	W/T
106	5	126	1	2	156.1	336.7	149.6	225.4	4.3	3.3	3.7	78.6
107	5	131	1	0	17.0	27.7	190.2	225.4	3.2	3.9	3.7	8.7
108	5	129	0	1	233.7	118.9	166.6	225.4	4.5	3.8	3.7	26.6
109	5	48	0	1	48.3	226.8	113.5	225.4	3.1	3.6	3.7	72.1
110	5	83	0	0	19.2	122.9	254.6	225.4	4.1	4.1	3.7	30.1
111	5	46	0	0	55.9	71.0	251.9	225.4	3.2	3.8	3.7	22.3
112	5	47	1	2	11.1	733.5	221.2	225.4	5.4	3.9	3.7	135.2
113	5	130	0	0	119.7	105.6	257.7	225.4	3.0	4.3	3.7	35.2
114	5	49	2	2	32.8	72.9	263.9	225.4	-	4.1	3.7	-
115	5	50	1	2	14.7	305.6	185.2	225.4	5.5	4.1	3.7	55.3
116	5	53	1	1	17.2	101.7	205.6	225.4	2.5	4.3	3.7	40.4
117	5	51	2	2	91.0	340.2	316.6	225.4	5.2	4.4	3.7	65.4
118	5	84	0	1	50.9	207.6	276.7	225.4	4.0	4.1	3.7	52.0
119	5	85	1	2	24.0	628.0	261.0	225.4	4.6	4.1	3.7	138.0
120	5	86	0	1	66.5	106.0	234.6	225.4	-	4.1	3.7	-
121	5	54	0	1	114.6	23.0	331.8	225.4	2.8	4.1	3.7	8.3
122	5	55	1	2	40.3	208.2	220.6	225.4	5.0	3.7	3.7	41.9
123	5	52	1	2	34.4	693.9	215.0	225.4	4.0	3.5	3.7	171.9
124	5	56	1	2	23.5	72.1	236.1	225.4	2.9	4.2	3.7	24.8
125	6	57	1	2	65.5	77.6	249.8	191.0	3.0	3.8	3.5	25.7
126	6	58	1	2	75.9	128.9	140.9	191.0	5.9	3.8	3.5	22.0
127	6	223	2	2	173.4	276.6	181.3	191.0	3.0	4.3	3.5	91.2
128	6	219	2	2	309.3	149.1	238.0	191.0	4.2	4.1	3.5	35.2
129	6	220	2	2	207.9	274.5	249.5	191.0	5.5	3.9	3.5	49.8
130	6	59	2	1	44.6	360.9	228.0	191.0	1.9	3.8	3.5	194.7
131	6	63	2	2	23.6	186.4	215.1	191.0	4.9	3.3	3.5	38.3
132	6	221	2	2	223.2	168.9	211.4	191.0	2.4	2.6	3.5	71.5
133	6	222	2	2	120.2	85.0	181.1	191.0	1.7	3.3	3.5	51.0
134	6	60	2	2	98.9	256.1	167.6	191.0	2.0	2.7	3.5	126.8
135	6	61	2	2	100.3	209.0	167.2	191.0	5.6	2.5	3.5	37.1
136	6	62	2	2	78.2	118.9	194.7	191.0	1.9	2.8	3.5	63.9

Table G.4

Projected Channel Centers

Order	SS Body	DU	Parallel		Parallel Rotated		Perpendicular		Perpendicular Rotated	
			X	Y	X	Y	X	Y	X	Y
1	210	0	1980.01	1418.76	2023.60	1355.86	1672.64	1418.77	1716.38	1365.53
2	201	0	1879.72	1426.06	1923.58	1366.32	1573.93	1426.07	1617.95	1375.93
3	200	0	1706.37	1430.63	1750.47	1376.33	1404.49	1430.64	1448.74	1385.82
4	211	1	2173.65	1441.35	2217.85	1372.37	1914.96	1441.36	1959.29	1380.50
5	199	1	1555.24	1436.97	2091.02	1378.87	1290.92	1436.98	1850.33	1386.44
6	216	1	1670.10	1438.90	1714.48	1385.73	1394.81	1438.91	1439.32	1394.39
7	213	1	2046.67	1443.87	1599.61	1387.41	1805.87	1443.88	1335.42	1395.72
8	203	1	1407.07	1441.28	1451.65	1396.37	1168.30	1441.28	1213.00	1403.88
9	212	2	2171.64	1448.56	2216.07	1379.63	1937.22	1448.57	1981.77	1387.00
10	95	2	1179.59	1440.46	1967.70	1391.26	947.43	1440.47	1782.65	1397.08
11	109	2	1152.88	1444.81	2172.47	1399.05	929.16	1444.82	1960.10	1405.73
12	88	2	944.62	1441.91	1418.69	1400.88	727.38	1441.92	1578.94	1407.51
13	204	2	1373.98	1444.75	1768.11	1401.56	1127.34	1444.76	1172.16	1408.64
14	206	2	1370.06	1447.69	1595.26	1402.55	1127.02	1447.69	1395.32	1408.84
15	205	2	1393.35	1447.65	1224.25	1402.70	1182.87	1447.66	1227.76	1409.79
16	208	2	1309.03	1455.72	1438.13	1403.17	1135.53	1455.72	992.21	1410.00
17	187	2	1923.02	1452.38	1414.85	1403.94	1737.89	1452.38	1657.62	1410.55
18	193	2	1550.42	1451.96	1849.13	1404.53	1350.38	1451.97	1171.93	1411.58
19	186	2	1723.21	1456.40	2170.14	1406.67	1533.95	1456.41	1425.78	1412.89
20	185	2	1804.10	1461.92	1589.28	1407.75	1612.49	1461.92	1964.01	1413.15
21	94	2	1039.45	1443.88	1197.70	1407.88	825.52	1443.88	1759.46	1414.48
22	87	2	831.85	1446.79	1934.74	1408.96	630.32	1446.76	974.09	1414.92
23	207	2	1305.76	1451.55	1516.12	1409.01	1098.24	1451.55	1318.21	1415.24

Table G.4 continued

Order	SS Body	DU	Parallel		Parallel Rotated	
			X	Y	X	Y
24	93	2	1035.48	1445.26	1350.71	1409.82
25	108	2	1097.43	1446.60	1084.29	1410.51
26	184	2	2127.45	1466.60	1142.32	1411.41
27	183	2	2124.88	1474.14	1702.90	1411.44
28	182	2	1968.57	1474.57	989.44	1411.53
29	191	2	1544.28	1456.97	1192.61	1411.87
30	181	2	1889.53	1469.04	2013.91	1412.00
31	179	2	1657.73	1464.24	1080.37	1412.02
32	180	2	1749.63	1468.32	1794.89	1412.64
33	192	2	1471.11	1455.94	1354.11	1413.88
34	107	2	1147.67	1448.64	1071.12	1416.24
35	92	2	1026.10	1449.19	1038.98	1416.34
36	90	2	993.98	1448.27	897.00	1419.04
37	1	2	851.99	1446.52	876.88	1419.95
38	209	3	1340.42	1457.72	1071.83	1414.65
39	111	3	1117.69	1452.00	1385.54	1414.89
40	112	3	1155.44	1453.50	1162.75	1416.17
41	105	3	1072.57	1452.91	1200.53	1416.49
42	96	3	1026.86	1447.62	1117.68	1418.51
43	4	3	770.65	1456.59	816.02	1431.66
44	9	3	889.23	1463.11	934.75	1434.46
45	8	3	576.60	1458.93	2075.88	1438.66
46	119	3	1261.77	1481.59	622.14	1440.10
47	118	3	1148.81	1479.24	1307.68	1441.23
48	171	3	2029.67	1503.16	1736.01	1441.41

Perpendicular		Perpendicular Rotated	
X	Y	X	Y
822.54	1445.26	1143.29	1416.34
888.90	1446.60	1527.47	1416.96
1914.97	1466.61	1850.70	1417.14
1918.66	1474.15	870.47	1417.24
1805.27	1474.57	933.90	1417.97
1380.69	1456.98	1625.91	1418.00
1714.16	1469.05	986.38	1418.36
1482.21	1464.24	772.31	1418.36
1577.43	1468.32	867.53	1418.71
1273.10	1455.94	1180.69	1419.34
941.34	1448.64	861.39	1422.84
816.28	1449.19	831.52	1422.86
786.42	1448.28	696.10	1425.36
650.99	1446.52	675.46	1426.25
1148.66	1457.72	873.53	1420.89
916.89	1452.00	1193.89	1420.92
955.96	1453.51	962.05	1422.49
879.18	1452.92	1001.15	1422.76
828.47	1447.62	924.38	1424.59
593.42	1456.59	638.88	1437.23
726.42	1463.12	772.02	1439.58
418.15	1458.93	1912.25	1443.81
1105.10	1481.60	463.77	1445.08
995.27	1479.25	1151.09	1446.15
1865.96	1503.17	1584.15	1446.19

Table G.4 continued

Order	SS Body	DU	Parallel		Parallel Rotated	
			X	Y	X	Y
75	75	4	972.99	1517.36	1266.28	1489.28
76	24	4	732.56	1513.60	1074.76	1489.84
77	76	4	1027.44	1522.86	779.74	1489.84
78	224	4	1146.67	1524.61	1958.45	1491.92
79	124	4	1277.91	1529.33	1081.63	1495.85
80	123	4	1218.87	1528.32	713.14	1497.72
81	29	4	665.74	1519.38	1216.16	1497.86
82	30	4	862.19	1526.37	909.71	1498.53
83	31	4	878.67	1529.22	1947.41	1499.25
84	77	4	1034.11	1529.09	1312.20	1499.28
85	80	4	1168.51	1535.32	926.27	1500.86
86	125	4	1264.46	1539.76	1837.67	1502.70
87	78	4	941.38	1534.96	989.13	1504.63
88	32	4	622.26	1527.92	669.95	1507.62
89	225	4	1043.30	1541.65	1091.21	1508.12
90	79	4	988.45	1542.29	430.75	1509.49
91	33	4	734.32	1537.50	1036.41	1510.48
92	34	4	383.13	1522.27	709.04	1511.70
93	39	4	661.21	1533.23	782.26	1513.67
94	35	4	400.21	1532.99	448.17	1519.67
95	40	4	637.94	1543.30	686.10	1522.50
96	41	4	779.25	1553.08	1331.54	1526.13
97	128	4	1282.94	1567.21	758.06	1527.60
98	127	4	1269.50	1570.29	827.65	1527.84
99	81	4	916.68	1558.41	965.18	1528.85

Perpendicular		Perpendicular Rotated	
X	Y	X	X
887.47	1517.37	985.54	1492.64
640.57	1513.60	1159.13	1492.65
938.17	1522.86	687.80	1492.74
1049.27	1524.61	1843.10	1495.55
1170.25	1529.33	1000.15	1498.42
1111.67	1528.32	632.14	1500.27
584.71	1519.39	1125.70	1500.71
783.27	1526.37	830.83	1501.02
804.39	1529.22	1212.65	1502.41
952.59	1529.09	1835.28	1502.78
1078.01	1535.32	852.03	1503.20
1164.86	1539.76	1740.51	1505.76
866.88	1534.96	914.67	1506.97
557.30	1527.92	605.02	1509.66
971.84	1541.65	1019.79	1510.37
916.49	1542.29	365.81	1511.53
660.31	1537.50	964.49	1512.74
318.15	1522.28	638.79	1513.91
590.92	1533.23	708.27	1516.00
346.53	1532.99	394.51	1521.35
579.62	1543.30	627.81	1524.33
718.71	1553.08	1255.22	1528.53
1206.59	1567.21	693.50	1529.63
1193.29	1570.30	767.14	1529.74
857.62	1558.41	906.14	1530.70

Table G.4 continued

Order	SS Body	DU	Parallel		Parallel Rotated	
			X	Y	X	Y
100	42	4	709.70	1550.65	1318.20	1529.64
101	43	4	432.97	1547.22	481.36	1532.86
102	133	5	1463.69	1579.83	1087.26	1529.78
103	44	5	429.30	1556.50	1343.82	1531.93
104	45	5	760.61	1563.08	1512.59	1533.08
105	82	5	1038.67	1563.17	476.19	1535.00
106	126	5	1295.04	1573.39	1426.09	1537.14
107	131	5	1465.45	1586.45	1115.74	1537.68
108	129	5	1377.11	1581.18	809.33	1538.41
109	48	5	271.43	1558.04	1514.55	1539.63
110	83	5	1066.89	1571.97	902.03	1547.82
111	46	5	852.97	1575.39	320.24	1548.75
112	47	5	671.40	1571.59	720.44	1549.73
113	130	5	1473.79	1602.13	1027.66	1550.72
114	49	5	119.93	1561.71	799.44	1552.02
115	50	5	296.94	1564.64	582.37	1554.08
116	53	5	533.27	1571.60	345.94	1554.54
117	51	5	282.41	1569.77	1523.39	1555.05
118	84	5	978.44	1582.23	1229.03	1555.13
119	85	5	1179.58	1592.97	168.93	1557.17
120	86	5	1108.90	1592.97	1158.39	1557.35
121	54	5	750.30	1576.37	843.75	1557.96
122	55	5	794.40	1583.70	331.58	1560.13
123	52	5	449.08	1577.10	498.40	1562.22
124	56	5	773.86	1589.56	823.40	1564.47

Perpendicular		Perpendicular Rotated	
X	Y	X	Y
645.11	1550.66	1242.02	1532.04
390.17	1547.22	1027.24	1531.67
1401.34	1579.84	1271.93	1534.19
583.32	1556.50	438.57	1534.20
700.57	1563.08	1450.27	1535.04
978.62	1563.18	631.92	1537.41
1223.11	1573.39	1361.03	1539.19
1405.84	1586.45	1057.78	1539.51
1312.02	1581.18	749.32	1540.30
245.02	1558.04	1454.98	1541.51
1008.90	1571.97	857.11	1549.23
808.03	1575.39	293.84	1549.58
624.59	1571.59	1028.74	1550.68
1423.84	1602.13	673.65	1551.20
110.33	1561.71	747.87	1553.64
271.05	1564.64	557.79	1554.85
508.67	1571.60	320.07	1555.35
261.76	1569.77	1473.46	1556.62
979.52	1582.23	1170.78	1556.96
1121.30	1592.97	159.33	1557.47
1063.40	1592.97	1112.91	1558.78
698.70	1576.37	797.86	1559.41
748.48	1583.70	310.94	1560.77
425.59	1577.10	474.92	1562.95
728.52	1589.56	778.09	1565.89

Table G.4 continued

Order	SS Body	DU	Parallel		Parallel Rotated		Perpendicular		Perpendicular Rotated	
			X	Y	X	Y	X	Y	X	Y
125	57	6	805.09	1592.49	1383.15	1566.06	765.34	1592.49	814.98	1567.67
126	58	6	729.00	1593.96	854.72	1566.42	683.05	1593.96	1330.04	1567.73
127	223	6	1333.28	1608.73	778.71	1570.27	1280.14	1608.73	732.78	1571.72
128	219	6	1399.31	1616.38	1405.08	1570.62	1355.36	1616.38	1405.46	1573.01
129	220	6	1355.05	1613.98	1449.39	1571.62	1305.67	1616.98	990.50	1573.15
130	59	6	544.55	1592.13	1028.27	1571.96	532.33	1592.13	582.07	1574.62
131	63	6	978.39	1603.49	594.29	1574.24	940.60	1603.49	1355.82	1575.17
132	221	6	1391.00	1620.00	1441.20	1575.50	1347.63	1620.00	654.08	1576.39
133	222	6	1428.92	1623.21	671.27	1575.85	1390.47	1623.22	1397.85	1576.87
134	60	6	621.44	1596.16	860.58	1576.13	604.24	1596.16	830.16	1577.09
135	61	6	810.64	1602.39	1479.20	1577.53	780.21	1602.39	1440.77	1578.74
136	62	6	797.78	1607.09	847.86	1581.24	765.04	1607.09	815.14	1582.27
137	218	7	1354.04	1623.72	1404.37	1580.39	1305.69	1623.72	1356.05	1581.91

REFERENCES

Aalto, R., Maurice-Bourgoin, L., Dunne, T., Montgomery, D. R., Nittrouer, C. A., Guyot, J. L., 2003, Episodic sediment accumulation on Amazonian flood plains influenced by El Niño/Southern Oscillation: Nature, v. 425, p. 493-497.

Allen, J. L., 2009, Transgressive-regressive cycles in the John Henry Member, Straight Cliffs Formation, Southern Utah, U.S.A. [PhD thesis]: University of Utah, 188 p.

Allen, J. L., and Johnson, C. L., 2010, Sedimentary facies, paleoenvironments, and relative sea level changes in the John Henry Member, Cretaceous Straight Cliffs Formation, Southern Utah, U.S.A.: *in* Carney, S. M., Tabet, D. E., and Johnson, C. L., eds., Utah Geological Association Geology of South-Central Utah, v. 39, p. 225-247.

Allen, J. L., and Johnson, C. L., 2011, Architecture and formation of transgressive-regressive cycles in marginal marine strata of the John Henry Member, Straight Cliffs Formation, Upper Cretaceous of Southern Utah, U.S.A.: Sedimentology, v. 58, no. 6, p. 1486-1513.

Allen, J. R. L., 1966, On bed forms and paleocurrents: Sedimentology, v. 6, p. 153-190.

Allen, J. R. L., 1978, Studies in fluviatile sedimentation: An exploratory quantitative model for the architecture of avulsion-controlled alluvial suites: Sedimentary Geology, v. 21, p. 129–147.

Armitage, J. J., Duller, A. C., Whittaker, A. C., and Allen, P. A., 2011, Transformation of tectonic and climatic signals from source to sedimentary archive: Nature Geoscience, v. 4, p. 231-235.

Blum, M. D., and Törnqvist, T., 2000, Fluvial responce to climate and sea-level change: a review and look forward: Sedimentology, v. 47, Suppl. 1, p. 2-48.

Blum, M. D., and Aslan, A., 2006, Signatures of climate vs. sea-level change within incised valley-fill successions: quaternary examples from the Texas Gulf Coast: Sedimentary Geology, v. 190, no. 1-4, p. 177-211.

Bobb, M. C., 1991, The Calico bed, Upper Cretaceous, southern Utah: a fluvial sheet deposit in the western interior foreland basin and its relationship to eustacy and tectonics [M.S. thesis]: University of Colorado, 166 p.

Bridge, J. S., 2003, Rivers and floodplains: forms, processes, and the sedimentary record: Oxford, Blackwell Science Ltd, 491 p.

Bridge, J. S., and Tye, R. S., 2000, Interpreting the dimensions of ancient fluvial channel bars, channels, and channel belts from wireline-logs and core: American Association of Petroleum Geologists Bulletin, v. 84, no. 8, p. 1205-1228.

Bromley, R. G., Pemberton, S. G., and Rahmani, R. A., 1984, A Cretaceous woodground: the *Teredolites* ichnofacies: Journal of Paleontology, v. 58, no. 2, p. 488-498.

Burns, B. A., Heller, P. L., Marzo, M., and Paola, C., 1997, Fluvial responce in a sequence stratigraphic framework: example from the Montserrat fan delta, Spain: Journal of Sedimentary Research, v. 64, no. 2, p. 311-321.

Castelltort, S., and Van Den Driessche, J., 2003, How plausible are high-frequency sediment supply-driven cycles in the stratigraphic record?: Sedimentary Geology, v. 157, no. 1-2, p. 3-13.

Chitale, S. V., 1973, Theories and relationships of river channel patterns: Journal of Hydrology, v. 19, p. 285-308.

Christensen, A. E., 2005, Sequence stratigraphy, sedimentology and provenance of the Drip Tank Member of the Straight Cliffs Formation, Kaiparowits Formation, southern Utah [M.S. thesis]: New Mexico State University, 96 p.

Collinson, J.D., 1969, The sedimentology of the Grindslow Shales and the Kinderscout Grit: a deltaic complex in the Namurian of northern England: Journal of Sedimentary Petrology, v. 149, p. 194-221.

Corbett, M. J., Fielding, C. R., and Birgenheier, L. P., 2011, Stratigraphy of a Cretaceous coastal-plain fluvial succession: the Campanian Masuk Formation, Henry Mountains syncline, Utah, U.S.A: Journal of Sedimentary Research, v. 81, no. 2, p. 80-96.

Cotter, E., 1978, The evolution of fluvial style, with special reference to the central Appalacian Paleozoic, *in* Miall, A. D., de., Fluvial sedimentaology: Canadian Society of Petrolium Geologists Memoir, v. 5, p. 361-383.

Currie, B. S., 1997, Sequence stratigraphy of nonmarine Jurassic-Cretaceous rocks, central Cordilleran foreland-basin system: Geological Society of America Bulletin, v. 109, no. 9, p. 1206-1222.

Dalrymple, M., 2001, Fluvial reservoir architecture in the Statfjord Formation (northern North Sea) augmented by outcrop analogue statistics: Petroleum Geoscience, v. 7, p. 115-122.

Dalrymple, R. W., and Choi, K., 2007, Morphologic and facies trends through the fluvial–marine transition in tide-dominated depositional systems: A schematic framework for environmental and sequence-stratigraphic interpretation: Earth-Science Reviews, v. 81, no. 3-4, p. 135-174.

Davies, R., Howell, J., Boyd, R., Flint, S., and Diessel, C., 2006, High-resolution sequence-stratigraphic correlation between shallow-marine and terrestrial strata: examples from the Sunnyside Member of the Cretaceous Blackhawk Formation, Book Cliffs, eastern Utah: American Association of Petroleum Geologists Bulletin, v. 90, no. 7, p. 1121-1140.

DeCelles, P. G., 2004, Late Jurassic to Eocene evolution of the Cordilleran thrust belt and foreland basin system, western U.S.A.: American Journal of Science, v. 304, p. 105-168.

DeCelles, P.G., Lawton, T.F., and Mitra, G., 1995, Thrust timing, growth of structural culminations, and synorogenic sedimentation in the type Sevier orogenic belt, western U.S.A.: Geology, v. 23, p. 699–702.

DeCelles, P. G., and Giles, K. A., 1996, Foreland basin systems: Basin Research, v. 8, p. 105-123.

DeCelles, P.G., and Coogan, J.C., 2006, Regional structure and kinematic history of the Sevier fold-and-thrust belt, central Utah: Geological Society of America Bulletin, v. 118, p. 841-864.

Deissel, C., Boyd, R., Wadsworth, J., Leckie, D., and Chalmers, G., 2000, On balanced and unbalanced accommodation/peat accumulation ratios in the Cretaceous coals from Gates Formation, Western Canada, and their sequence-stratigraphic significance: International Journal of Coal Geology, v. 43, p. 143-186.

Dickinson, W. R., 1985, Interpreting provenance relations from detrital modes of sandstones, *in* Zuffa, G. G., ed., Provenance of Arenites: Dordrecht, Reidel Publishing, p. 333–361.

Dickinson, W. R., and Suczek, C. A., 1979, Plate tectonics and sandstone composition: American Association of Petroleum Geologists Bulletin, v. 63, no. 12, p. 2164-2182.

Doelling, H. H., 1967, Kaiparowits Plateau, Garfield County, Utah, Escalante-Upper Valley coal area: Utah Geological and Mineralogical Survey Special Studies, v. 20, 16 p.

Doelling, H. H., 1968, Carcass Canyon coal area in the Kaiparowits Plateau, Garfield and Kane County, Utah: Geological and Mineralogical Survey Special Studies, v. 20, 42 p.

Doelling, H. H., and Graham, R. L., 1972, Southwestern Utah coal fields: Alton, Plateau, and Kolob-Harmony: Utah Geological and Mineralogical Survey Monograph Series, v. 1, 333 p.

Doelling, H. H., and Willis, G.C., 1999, Interim geologic map of the Escalante and parts of the Loa and Hite Crossing 30' x 60' quadrangles, Garfield and Kane Counties, Utah: Utah Geological Survey, Open-File Report 368, scale 1:100,000.

Doelling, H. H., Blackett, R. E., Hamblin, A. H., Powell, J. D., and Pollock, G. L., 2000, Geology of Grand Staircase-Escalante National Monument, Utah, *in* Sprinkel, D. A., Chidsey, T. C., and Andreson, P. B., eds., Geology of Utah's Parks and Monuments, Utah Geological Association Publication, v. 28, p. 1-43.

Doelling, H.H., and Willis, G.C., 2006, Geologic map of the Smoky Mountain 30' x 60' quadrangle, Kane and San Juan Counties, Utah and Coconino County, Arizona: Utah Geological Survey, map 213, scale 1:100,000.

Dooling, P. R., in prep, Tidal facies, stratigraphic architecture, and along-strike variability of a high energy, transgressive shoreline, Upper Cretaceous, Kaiparowits Plateau, southern Utah [M.S. thesis]: University of Utah.

Dreyer, T., Falt, L. M., Hoy, T., Knarud, R., Steel, R., and Cuevas, J. L., 1993, Sedimentary architecture of field analogues for reservoir information (SAFARI): a case study of fluvial Escanilla Formation, Sapanish Pyrenees *in* Flint, S. S., and Bryant, I. D., eds., The geological modelling of hydrocarbon resevoirs and outcrop analogues, International Association of Sedimentologists Special Publication, v. 15, p. 57-80.

Driese, S. G., Ludvigson, G. A., Roberts, J. A., Fowle, D. A., Gonzalez, L. A., Smith, J. J., Vulava, V. M., and McKay, L. D., 2010, Micromorphology and stable-isotope geochemistry of historical pedogenic siderite formed in PAH-contaminated alluvial clay soils, Tennessee, U.S.A.: Journal of Sedimentary Research, v. 80, no. 11, p. 943-954.

Eaton, J. G., 1987, The Campanian-Maastrichtian boundary in the Western Interior of North America: Newsletters on Stratigraphy, v. 18, no. 1, p. 31-39.

Eaton, J. G., 1991, Biostratigraphic framework for the upper Cretaceous rocks of the Kaiparowits Plateau, southern Utah, *in* Nations, J. D., and Eaton, J. G., eds., Stratigraphy, depositional environments, and sedimentary tectonics of the western margin, Cretaceous Western Interior Seaway: Geological Society of America Special Paper, v. 260, p. 47-64.

Eaton, J. G., and Nations, J. D., 1991, Introduction; tectonic setting along the margin of the Cretaceous Western Interior Seaway, southwestern Utah and northern Arizona, *in* Nations, J. D., and Eaton, J. G., eds., Stratigraphy, depositional environments, and sedimentary tectonics of the western margin, Cretaceous Western Interior Seaway: Geological Society of America Special Paper, v. 260, p. 2-8.

Ethridge, F. G., 2011, Interpretation of ancient fluvial channel deposits: review and recommendations, *in* Davidson, S.L., and North, C.P. eds., From river to rock record: SEPM Special Publication, v. 97, p. 6-32.

Fabuel-Perez, I., Hodgetts, D., and Redfern, J., 2009, A new approach for outcrop characterization and geostatistical analysis of a low-sinuosity fluvial-dominated succession using digital outcrop models: Upper Triassic Oukaimeden Sandstone Formation, central High Atlas, Morocco: American Association of Petroleum Geologists Bulletin, v. 93, no. 6, p. 795-827.

Fielding, C. R., 1984, Upper delta plain lacustrine and fluviolacustrine facies from the Westphalian of the Durham coalfield, NE England: Sedimentology, v. 31, no. 4, p. 547-567.

Fillmore, R. P., 1991, Tectonic influence on sedimentation in the southern Sevier foreland, Iron Springs Formation (Upper Cretaceous), southwestern Utah, Geological Society of America Special Paper, v. 260, p. 9-26.

Fisk, H. N., 1944, Geological investigation of the alluvial valley of the lower Mississippi River: Army Corps of Engineers, Mississippi River Commission, 79 p.

Flemings, P. B., and Jordan, T. E., 1989, A synthetic stratigraphic model of foreland basin development: Journal of Geophysical Research, v. 94, no. B4, p. 3851-3866.

Flemings, P. B., and Jordan, T. E., 1990, Stratigraphic modeling of foreland basins: interpreting thrust deformation and lithosphere rheology: Geology, v. 18, no. 5, p. 430-434.

Flores, R. M., 1983, Basin facies analysis of coal rich fluvial deposits, northern Powder River Basin, Montana and Wyoming: International Association of Sedimentologists Special Publication, v. 6, p. 501-515.

Fürsich, F. T., and Mayr, H., 1981, Non-marine *Rhizocorallium* (trace fossil) from the Upper Freshwater Molasse (Upper Miocene) of southern Germany: Neues Jahrbuch für Geologie und Paläontologie, v. 6, p. 321-333.

Gallin, W. N., 2010, Fluvial stratigraphic architecture of the John Henry Member of the Straight Cliffs Formation, Kaiparowits Plateau, Utah, U.S.A. [M.S. thesis]: University of Utah, 255 p.

Gallin, W. N., Johnson, C. L., and Allen, J. L., 2010, Fluvial and marginal marine architecture of the John Henry Member, Straight Cliffs Formation, Kelly Grade of the Kaiparowits Plateau, South-Central Utah, *in* Carney, S. M., Tabet, D. E., and Johnson, C. L., eds., Utah Geological Association, Geology of South-Central Utah, v. 39, p. 248-279.

Gibling, M. R., 2006, Width and thickness of fluvial channel bodies and valley fills in the geological record: a literature compilation and classification: Journal of Sedimentary Research, v. 76, no. 5, p. 731-770.

Gibling, M. R., Fielding, C. R., and Sinha, R., 2011, Alluvial valleys and alluvial sequences: toward a geomorphic assessment: SEPM Special Publication, no. 97, p. 423-447.

Goldstrand, P. M., 1992, Evolution of Late Cretaceous and Early Tertiary basins of southwest Utah based on clastic petrology: Journal of Sedimentary Petrology, v. 62, no. 3, p. 495-507.

Goldstrand, P. M., 1994, Tectonic development of Upper Cretaceous to Eocene strata of southwestern Utah: Geological Society of America Bulletin, v. 106, no. 1, p. 145-154.

Goodbred, S. L., 2003, Response of the Ganges dispersal system to climate change: a source-to-sink view since the last interstade: Sedimentary Geology, v. 162, no. 1-2, p. 83-104.

Gooley, J., 2010, Alluvial architecture and predictive modeling of the late Cretaceous John Henry Member, Straight Cliffs Formation, southern Utah [M.S. thesis]: University of Utah, 376 p.

Gregory, H. E., and Moore, R. C., 1931, The Kaiparowits Region: a geographic and geologic reconnaissance of parts of Utah and Arazona: U.S. Geologic Survey Professional Paper, v. 164, 161 p.

Hajek, E. A., Heller, P. L., and Sheets, B. A., 2010, Significance of channel-belt clustering in alluvial basins: Geology, v. 38, no. 6, p. 535-538.

Hajek, E. A., and Wolinsky, M. A., 2012, Simplified process modeling of river avulsion and alluvial architecture: connecting models and field data: Sedimentary Geology, v. 257-260, p. 1-30.

Hampson, G. J., Royhan Gani, M., Sahoo, H., Rittersbacher, A., Irfan, N., Ranson, A., Jewell, T. O., Gani, N. D. S., Howell, J. A., Buckley, S. J., and Bracken, B., 2012, Controls on large-scale patterns of fluvial sandbody distribution in alluvial to coastal plain strata: Upper Cretaceous Blackhawk Formation, Wasatch Plateau, central Utah, U.S.A.: Sedimentology, v. 59, no. 6 p. 1-33.

Hartley, A. J., Weissmann, G. S., Nichols, G. J., and Warwick, G. L., 2010, Large distributive fluvial systems: characteristics, distribution, and controls on development: Journal of Sedimentary Research, v. 80, no. 2, p. 167-183.

Haq, B. U., Hardenbol, J., and Vail, P. R., 1987, Chronology of fluctuating sea levels since the Triassic: Science, v. 235, no. 4793, p. 1156-1167.

Haq, B. U., Hardenbol, J., and Vail, P. R., 1988, Mesozoic and Cenozoic chronostratigraphy and cycles of sea-level change, *in* Wilgus, C. K., Hastings, B. S., Kendall, C. G. St. C., Posamentier, H. W., Ross, C. A., and Van Wagoner, J. C., eds., Sea level changes: an integrated approach: SEPM Special Publication, v. 42, p. 71–108.

Heller, P. L., Angevine, C. L., Winslow, N. S., and Paola, C., 1988, Two-phase stratigraphic model for foreland-basin sequences: Geology, v. 16, p. 501-504.

Heller, P. L., and Paola, C., 1996, Downstream changes in alluvial architecture: an exploration of controls on channel-stacking patterns: Journal of Sedimentary Research, v. 66, no. 2, p. 297-307.

Hettinger, R. D., 1995, Sedimentological descriptions and depositional interpretation, in sequence stratigraphic context, of two 300-meter cores from the Upper Cretaceous Straight Cliffs Formation, Kaiparowits Plateau, Kane County, Utah: U.S. Geological Survey Bulletin, Report 2115-A, p. A1-A32.

Hettinger, R. D., 2000, A summary of coal distribution and geology in the Kaiparowits Platea, Utah, *in* Krischbaum, M. A., Roberts, L. N. R., and Biewick, L. R. H., eds., Geologic assessment of coal in the Colorado Plateau: Arizona, Colorado, New Mexico, and Utah, p. J1-J17.

Hettinger, R. D., McCabe, P. J., and Shanley, K. W., 1993, Detailed facies anatomy of transgressive and highstand systems tracts from the Upper Cretaceous of southern Utah, U.S.A.: Chapter 9: Recent applications of siliciclastic sequence stratigraphy, American Association of Petroleum Geologists Memoir 58, p. 235-257.

Hirst, J. P. P., 1991, Variations in alluvial architecture across the Oligo-Miocene Huesca fluvial system, Ebro Basin, Spain, *in* Miall, A. D., and Tyler, N., eds., The three-dimensional facies architecture of terrigenous clastic sediments and its implications for hydrocarbon discovery and recovery: SEPM Concepts in Sedimentology and Paleontology 3, p. 111-121.

Holbrook, J., Scott, S. W., and Oboh-Ikuenobe, F. A., 2006, Base-level buffers and buttresses: a model for upstream versus downstream control on fluvial geometry and architecture within sequences: Journal of Sedimentary Research, v. 76, no. 1, p. 162-174.

Horne, J. C., Ferm, J. C., Caruccio, F. T., and Baganz, B. P., 1978, Depositional models in coal exploration and mine planning in Appalachian region, American Association of Petroleum Geologists Bulletin, v. 62, p. 2379-2411.

Ingersoll, R. V., Bullard, T. F., Ford, J. P., Grimm, J. P., Pickle, J. D., and Sares, S. W., 1984, The effects of grain size on detrital modes: a test of the Gazzi-Dickinson point-counting method: Journal of Sedimentary Petrology, v. 54, no. 1, p. 0103-0116.

Jackson II, R. G., 1981, Sedimentology of muddy fine-grained channel deposits in meandering streams of the American Middle West: Journal of Sedimentary Petrology, v. 51, p. 1169–1192.

Jerolmack, D. J., and Swenson, J. B., 2007. Scaling relationships and evolution of distributary networks on wave-influenced deltas: Geophysical Research Letters, v. 34, L23402, 5 p.

Kauffman, E. G., 1977, Geological and biological overview: Western Interior Cretaceous Basin: The Mountain Geologist, v. 14, no. 3-4, p. 75-99.

Kauffman, E. G., 1984, Paleobiogeographic and evolutionary response dynamic in the Cretaceous Western Interior Seaway of North America, *in* Westermann, G. E. G., ed., Jurassic-Cretaceous Biochronology and paleogeography of North America: Geological Association of Canada Special Paper, v. 27, p. 273-306.

Kauffman, E. G., and Caldwell, W. G. E., 1993, The Western Interior Basin in space and time, *in* Caldwell, W. G. E., and Kauffman, E. G., eds., Evolution of the Western Interior Basin: Geological Association of Canada Special Paper, v. 39, p. 1-30.

Kern, J. P., and Warme, J. E., 1974, Trace fossil and bathymetry of the upper Cretaceous Point Loma: Geological Society of America Bulletin, v. 85, p. 893-900.

Kjemperud, A. V., Schomacker, E. R., and Cross, T. A., 2008, Architecture and stratigraphy of alluvial deposits, Morrison Formation (Upper Jurassic), Utah: American Association of Petroleum Geologists Bulletin, v. 92, no. 8, p. 1055-1076.

Kleinhans, M. G., 2010, Sorting out river channel patterns: Progress in Physical Geography, v. 34, no. 3, p. 287-326.

Kosters, E. C., and Suter, J. R., 1993, Facies relationships and systems tracts in the Late Holocene Mississippi delta plain: Journal of Sedimentary Petrology, v. 63, p. 727–733.

Kreisa, R. D., and Moiola, R. J., 1986, Sigmoidal tidal bundles and other tide-generated sedimentary structures of the Curtis Formation, Utah: Geological Society of America Bulletin, v. 97, p. 381-387.

Kvale, E. P., and Mastalerz, M., 1998, Evidence of ancient freshwater tidal deposits. *in* Alexander, C. R., Davis, R. A., Henry, V. J. eds., Tidalites: processes and products. SEPM Special Publication, v. 61, pp. 95–107.

Lawton, T. F., Pollock, S. L., and Robinson, R. A. J., 2003, Integrating sandstone petrology and nonmarine sequence stratigraphy: application to the late Cretaceous fluvial systems of southwestern Utah, U.S.A.: Journal of Sedimentary Research, v. 73, no. 3, p. 389-406.

Leclair, S. F., and Bridge, J. S., 2001, Quantitative interpretation of sedimentary structures formed by river dunes: Journal of Sedimentary Research, v. 71, no. 5, p. 713-716.

Legarreta, L., and Uliana, M. A., 1998, Anatomy of hinterland depositional sequences: Upper Cretaceous fluvial strata, Neuquen Basin, west-central Argentina, relative role of eustacy, climate, and tectonism in continental rocks: SEPM Special Publication, v. 59, p. 83-92.

Little, W. W., 1995, The influence of tectonics and eustacy on alluvial architecture, middle Coniacian through Campanian strata of the Kaiparowits Basin, Utah [M.S. thesis]: Brigham Young University, 327 p.

Little, W. W., 1997, Tectonic and eustatic controls on cyclical fluvial patterns, Upper Cretaceous strata of the Kaiparowits Basin, Utah, *in* Hill, L. M., ed., Learning from the land: Grand Staircase – Escalante National Monument science symposium proceedings: Salt Lake City, Utah, Bureau of Land Management, p. 489-504.

Liu, S., Nummedal, D., and Liu, L., 2011, Migration of dynamic subsidence across the Late Cretaceous United States Western Interior Basin in response to Farallon plate subduction: Geology, v. 39, no. 6, p. 555-558.

Mack, G. H., 1984, Exceptions to the relationship between plate tectonics and sandstone composition: Journal of Sedimentary Petrology, v. 54, no. 1, p. 0212-0220.

MacKey, S., and Bridge, J. S., 1995, Three-dimensional model of alluvial stratigraphy: theory and application: Journal of Sedimentary Research, v. B65, no. 1, p. 7-31.

Martin, J., Cantelli, A., Paola, C., Blum, M., and Wolinsky, M., 2010, Quantitative modeling of the evolution and geometry of incised valleys: Journal of Sedimentary Research, v. 81, no. 1, p. 64-79.

McCabe, P. J., and Parrish, J. T., 1992, Tectonic and climatic controls on the distribution and quality of Cretaceous coals, *in* McCabe, P. J., and Parrish, J. T., eds., Controls on the distribution and quality of Cretaceous coals: Geological Society of America Special Paper, v. 267, p. 1-15.

Miall, A. D., 1974, Paleocurrent analysis of alluvial sediments; a discussion of directional variance and vector magnitude: Journal of Sedimentary Research, v. 44, no. 1174-1185.

Miall, A. D., 1977, A review of the braided-river depositional environment: Earth-Science Reviews, v. 13, p. 1–62.

Miall, A. D., 1978, Lithofacies types and vertical profile models in braided river deposits: a summary, *in* Miall, A. D., eds., Fluvial Sedimentology, Canadian Society of Petroleum Geology Memoir, no. 5, p. 597-604.

Miall, A. D., 1985, Architectural-element analysis: a new method of facies analysis applied to fluvial deposits: Earth-Science Reviews, v. 22, p. 261–308.

Miall, A. D., 1996, The geology of fluvial deposits: sedimentary facies, basin analysis and petroleum geology: Heidelberg, Springer-Verlag, 582 p.

Miall, A. D., 2000, Principles of sedimentary basin analysis: Heidelberg, Springer-Verlag, 616 p.

Miller, K. G., Kominz, M. A., Browning, J. V., Wright, J. D., Mountain, G. S., Katz, M. E., Sugarman, P. J., Cramer, B. S., Christie-Blick, N., and Pekar, S. F., 2005, The Phanerozoic record of global sea-level change: Science, v. 310, no. 5752, p. 1293-1298.

Morton, R. A., and Suter, J. R., 1996, Sequence stratigraphy and composition of Late Quaternary shelf-margin deltas, northern Gulf of Mexico: American Association of Petroleum Geologists Bulletin, v. 80, no. 4, p. 505-530.

Nadon, G. C., 1994, The genesis and recognition of anastomosed fluvial deposits; data from the St. Mary River Formation, southwestern Alberta, Canada: Journal of Sedimentary Research, v. 64, no. 4b, p. 451-463.

Olsen, T., Steel, R. J., Hogseth, K., Skar, T., and Roe, S., 1995, Sequential architecture in fluvial succession; sequence stratigraphy in the upper Cretaceous Mesaverde Group, Price Canyon, Utah: Journal of Sedimentary Research, v. B65, no. 2, p. 265-280.

Ouchi, S., 1985, Response of rivers to slow active tectonic movement: Geologic Society of America Bulletin, v. 95, p. 504-515.

Page, K. J., Nanson, G. C., and Frazier, P. S., 2003. Floodplain formation and sediment stratigraphy resulting from oblique accretion on the Murrumbidgee River, Australia: Journal of Sedimentary Research, v. 73, p. 5–14.

Pang, M., and Nummedal, D., 1995, Flexural subsidence and basement tectonics of the Cretaceous Western Interior basin, United States: Geology, v. 23, p. 173-176.

Paola, C., 1988, Subsidence and gravel transport in alluvial basins, *in* Kleinspehn, K. L., and Paola, C., eds., New perspectives in basin analysis, Springer-Verlag, p. 231-243.

Paola, C., Heller, P. L., and Angevine, C. L., 1992, The large-scale dynamics of grain-size variation in alluvial basins. 1: theory: Basin Research, v. 4, p. 73-90.

Paola, C., and Mohrig, D., 1996, Palaeohydraulics revisited: palaeoslope estimation in coarse-grained braided rivers: Basin Research, v. 8, p. 243-254.

Paola, C., Straub, K., Mohrig, D., and Reinhardt, L., 2009, The "unreasonable effectiveness" of stratigraphic and geomorphic experiments: Earth-Science Reviews, v. 97, no. 1-4, p. 1-43.

Parker, G., (E-book) 1D sediment transport morphodynamics with applications to rivers and turbidity currents: University of Illinois, http://vtchl.uiuc.edu/people/parkerg (Accessed February 2012).

Peterson, F., 1969a, Cretaceous sedimentaion and tectonism in the southeastern Kaiparowits region, Utah: U.S. Geologic Survey Open-file Report, no. 60-167, 258 p.

Peterson, F., 1969b, Four new members of the upper Cretaceous Straight Cliffs Formation in the southeastern Kaiparowits region, Kane County, Utah: U.S. Geological Survey Bulletin, no. 1274-J, p. J1-J28.

Peterson, F., and Waldrop, H. A., 1965, Jurassic and Cretaceous stratigraphy of south-central Kaiparowits Plateau, Utah: Guidebook to the Geology of Utah, v. 19, p. 47-69.

Petter, A. L., 2010, Stratigraphic implications of the spatial and temporal variability in sediment transport in rivers, deltas, and shelf margins [PhD thesis]: University of Texas at Austin, 205 p.

Pettijohn, F. J., 1975, Sedimentary Rocks, 3rd edition: New York, Harper and Row Publishers, 628 p.

Pranter, M. J., and Sommer, N. K., 2011, Static connectivity of fluvial sandstones in a lower coastal-plain setting: an example from the Upper Cretaceous lower Williams Fork Formation, Piceance Basin, Colorado: American Association of Petroleum Geologists Bulletin, v. 95, no. 6, p. 899-923.

Putnam, P. E., 1982, Fluvial channel sandstones within Upper Mannville (Albian) of Lloydminster area, Canada - geometry, petrography, and paleogeographic implications: American Association of Petroleum Geologists Bulletin, v. 66, no. 4, p. 436-459.

Richards, M. T., 1996, Fluvial systems, *in* Emery, D., and Myers, K. J., eds., Sequence Stratigraphy: Oxford, Blackwell Science, p. 111-133.

Roberts, L. N. R., and Kirschbaum, M. A., 1995, Paleogeography of the Late Cretaceous of the Western Interior of Middle North America - coal distribution and sediment accumulation: U.S. Geological Survey Professional Paper, no. 1561, p. 115.

Robison, R. A., 1963, A reconnaissance survey of coal resources of southwestern Utah, Utah Geological and Mineralogical Survey Special Studies, v. 3, 24 p.

Robison, R. A. ,1964, Geology and coal resources of southwestern Utah, Utah Geological and Mineralogical Survey Special Studies, v. 7, 27 p.

Robison, R. A., 1966, Geology and coal resources of the Tropic area, Garfield County, Utah: Utah Geological and Mineralogical Survey Special Studies, v. 18, 47 p.

Ryer, T. A., 1977, Patterns of Cretaceous shallow-marine sedimentation, Coalville and Rockport areas, Utah: Geological Society of America Bulletin, v. 88, p. 177-188.

Ryer, T. A., 1993, Speculation on the origins of Mid-Cretaceous clastic wedges, central Rocky Mountains region, United States: Geologic Association of Canada Special Publication, v. 39, p. 189-198.

Schumm, S. A., and Khan, H. R., 1972, Experimental study of channel patterns: Geological Society of America Bulletin, v. 83, p. 1755-1770.

Selley, R. C., 1968, Classification of paleocurrent models: Journal of Geology, v. 76, p. 99-110.

Semple, I. L., 2011, Sedimentary geology and geoscience education: a combined study of sequence stratigraphy and spatial visualization using outcrop examples from the Cretaceous Tertiary of Utah [M.S. thesis]: University of Utah, 183 p.

Shanley, K. W., 1991, Sequence stratigraphic relationships and facies architecture of Turonian-Cenomanian strata, Kaiparowits Plateau, south central Utah [PhD thesis]: Colorado School of Mines, 390 p.

Shanley, K. W., and McCabe, P. J., 1991, Predicting facies architecture through sequence stratigraphy - an example from the Kaiparowits Plateau, Utah: Geology, v. 19, p. 742-745.

Shanley, K. W., McCabe, P. J., and Hettinger, R. D., 1992, Tidal influence in Cretaceous fluvial strata from Utah, U.S.A.: a key sequence stratigraphic interpretation: Sedimentology, v. 39, p. 905-930.

Shanley, K. W., and McCabe, P. J., 1993, Alluvial architecture in a sequence stratigraphic framework: a case history from the Upper Cretaceous of southern Utah, U.S.A.: Special Publication of the International Association of Sedimentologists, v. 15, p. 21-56.

Shanley, K. W., and McCabe, P. J., 1994, Perspectives on the sequence stratigraphy of continental strata: American Association of Petroleum Geologists Bulletin, v. 78, no. 4, p. 544-568.

Shanley, K. W., and McCabe, P. J., 1995, Sequence stratigraphy of Turonian-Santonian strata, Kaiparowits Plateau, southern Utah, U.S.A.: implications for regional correlation and foreland basin evolution: American Association of Petroleum Geologists Memoir, v. 64, p. 103-136.

Shanley, K. W., McCabe, P. J., and Hettinger, R. D., 1992, Tidal influence in Cretaceous fluvial strata from Utah, U.S.A.: a key sequence stratigraphic interpretation: Sedimentology, v. 39, p. 905-930.

Sheets, B. A., Paola, C., and Kelberer, J. M., 2007, Creation and preservation of channel-form sand bodies in an experimental alluvial system, sedimentary processes, environments and basins: International Association of Sedimentologists Special Publication, v. 38, p. 555-567.

Slingerland, R. L., and Snow, R. S., 1988, Stability analysis of a rejuvenated fluvial system: Zeitschrift für Geomorphologie, v. 67, p. 93-102.

Smith, D. G., and Smith, N. S., 1980, Sedimentation in anastomosing river systems: examples from Alluvial Valley near Banff, Alberta: Journal of Sedimentary Petrology, v. 50, no. 1, p. 157-164.

Stephen, K. D., and Dalrymple, M., 2002, Reservoir simulation developed from an outcrop of incised valley fill strata: American Association of Petroleum Geologists Bulletin, v. 86, no. 5, p. 797-822.

Straub, K. M., Paola, C., Mohrig, D., Wolinsky, M. A., and George, T., 2009, Compensational stacking of channelized sedimentary deposits: Journal of Sedimentary Research, v. 79, no. 9, p. 673-688.

Suarez, M. B., Gonzalez, L. A., and Ludvigson, G. A., 2010, Estimating the oxygen isotopic composition of equatorial precipitation during the mid-Cretaceous: Journal of Sedimentary Research, v. 80, no. 5, p. 480-491.

Takano, O., and Waseda, A., 2003, Sequence stratigraphic architecture of a differentially subsiding bay to fluvial basin: the Eocene Ishikari Group, Ishikari Coal Field, Hokkaido, Japan: Sedimentary Geology, v. 160, no. 1-3, p. 131-158.

Thomas, L. P., 2002, Coal geology: West Success, England, Wiley, 384 p.

Thomas, R. G., Smith, D. G., Wood, J. M., Visser, J., Calverley-Range, E. A., and Koster, E. H., 1987, Inclined heterolithic stratification - terminology, description, interpretation and significance: Sedimentary Geology, v. 53, p. 123-179.

Thornton, R. C. N., 1979, Regional stratigraphic analysis of the Gidgealpa Group, Southern Cooper Basin, Australia: Geological Survey of South Australia Bulletin, v. 49, p. 140.

Tilton, T. L., 1991, Upper Cretaceous stratigraphy of the southern Paunsagunt Plateau, Kane County, Utah: University of Utah, 162 p.

Törnqvist, T., 1993, Holocene alternation of meandering and anastomosing fluvial systems in the Rhine–Meuse Delta (central Netherlands) controlled by sea-level rise and subsoil erodibility: Journal of Sedimentary Research, v. 63, p. 683-693.

Tye, R. S., 2004, Geomorphology: an approach to determining subsurface reservoir dimensions: American Association of Petroleum Geologists Bulletin, v. 88, no. 8, p. 1123-1147.

Vaninetti, G. E., 1979, Coal stratigraphy of the John Henry Member of the Straight Cliffs Formation, Kaiparowits Plateau, Utah [M.S. thesis]: University of Utah, 274 p.

Van Heijst, M. W. I. M., and Postma, G., 2001, Fluvial response to sea-level changes: a quantitative analogue, experimental approach: Basin Research, v. 13, p. 269-292.

Van Sickel, W. A., Kominz, M. A., Miller, K. G., and Browning, J. V., 2004, Late Cretaceous and Cenozoic sea-level estimates: backstripping analysis of borehole data, onshore New Jersey: Basin Research, v. 16, no. 4, p. 451-465.

Visser, J. M., 1980, Neap-spring cycles reflected in Holocene subtidal large-scale bedform deposits: a preliminary note: Geology, v. 8, p. 543-546.

Wadsworth, J., Boyd, R., Diessel, C., Leckie, D., and Zaitlin, B. A., 2002, Stratigraphic style of coal and non-marine strata in a tectonically influenced intermediate accommodation setting: the Mannville Group of the Western Canadian Sedimentary Basin, south-central Alberta: Bulletin of Canadian Petroleum Geology, v. 50, no. 4, p. 507-541.

Weimer, R. J., 1988, Record of relative sea-level changes, Cretaceous of Western Interior, U.S.A.: SEPM Special Publication, v. 42, p. 285-288.

Weissmann, G. S., Hartley, A. J., Nichols, G. J., Scuderi, L. A., Olson, M. E., Buehler, H. A., and Massengill, L. C., 2010, Alluvial facies distribution in continental sedimentary basins - distributive fluvial systems: SEPM Special Publication, v. 97, p. 227-355.

Wolfe, J. A., and Upchurch, J., G. R., 1987, North American nonmarine climates and vegetation during the Late Cretaceous: Palaeogeography, Palaeoclimatology, Palaeoecology, v. 61, p. 33-77.

Wright, V. P., and Mariott, S. B., 1993, The sequence stratigraphy of fluvial depositional systems: the role of sediment storage: Sedimentary Geology, v. 86, p. 203-210.

Ziegler, P. A., Raymond, A. L., Gierlowski, T. C., Horell, M. A., Rowley, D. B., and Lottes, A. L., 1987, Coal, climate and terrestrial productivity: the present and early Cretaceous compared: Geological Society of London Special Publication, v. 32, p. 25-49.

Zuffa, G. G., 1985, Optical analysis of arenites: influence of methodology on compositional results, *in* Zuffa, G. G., ed., Provenance of Arenites: Dordrecht, Reidel, North Atlantic Treaty Organization, Advanced Study Institute Series, v. 148, p. 165–189.